SACLANTCEN Conference Proceedings No. 17 Part 4

SACLANTCEN
Conference Proceedings No. 17

PART 4
SEA BOTTOM

SACLANT ASW
RESEARCH CENTRE

OCEANIC ACOUSTIC MODELLING

Proceedings of a Conference held at SACLANTCEN
on 8-11 September 1975

Organized by

WOLFGANG BACHMANN and ROBERT BRUCE WILLIAMS

15 OCTOBER 1975

NORTH
ATLANTIC
TREATY
ORGANIZATION

VIALE SAN BARTOLOMEO 400
I - 19026 - LA SPEZIA, ITALY

Compiled and Published by

SACLANTCEN

SACLANTCEN
CONFERENCE PROCEEDINGS NO. 17

NORTH ATLANTIC TREATY ORGANIZATION
SACLANT ASW Research Centre
Viale San Bartolomeo 400
I 19026 - La Spezia, Italy

OCEANIC ACOUSTIC MODELLING

Proceedings of a Conference held at SACLANTCEN
on 8-11 September 1975

In eight parts
Part 4: Sea Bottom

Organized by
Wolfgang Bachmann and Robert Bruce Williams

15 October 1975

PAPERS PRESENTED AT CONFERENCE

Pt 1: Noise (and Introductory Matter)

1. A.W. Pryce, "Keynote address: Underwater acoustics — modelling".
2. P. Wille, "Noise sources in the ocean, Pt I".
3. M. Daintith, "Noise sources in the ocean, Pt II".
4. H. Cox, "Acoustic noise models".

Pt 2: Bubbles

5. B. Williams & L. Foster, "Gas bubbles in the sea: A review and model proposals".
6. H. Medwin, "Acoustical probing for microbubbles at sea".

Pt 3: Sea surface

7. C.R. Ward, "A spectral ocean wave model".
8. H. Schwarze, "A theoretical model for doppler spread of backscattered sound from a composite-roughness sea surface".
9. O.I. Diachok, "Effects of sea-ice ridges on sound propagation in the Arctic Ocean".
10. J. Siebert, "Low-frequency acoustic measurements in a shallow-water area with a rough sea surface".
11. P.A. Crowther, "Surface wave spectra".
12. H. Trinkaus, "Scattering and reflection of sound from the sea surface".

Pt 4: Sea bottom

13. F.M. Phelan, B. Williams & F.H. Fisher, "Highlights of bottom topography inferred from received depression and bearing angles".
14. S.R. Santaniello & F.R. Dinapoli, "Ocean-bottom reflectivity (a point of view)".
15. W.A. Kuperman & F. Ingenito, "Relative contribution of surface roughness and bottom attenuation to propagation loss in shallow water".
16. R.E. Christiensen & W.H. Geddes, "Refraction of sound in the sea floor".
17. J.A. Desanto, "Scattering from a random interface".
18. E.L. Hamilton, "Acoustic properties of the sea floor".
19. H. Bucker & H. Morris, "Reflection of sound from a layered ocean bottom".
20. B. Hurdle, K.D. Flowers & J.A. Desanto, "Acoustic scattering from rough surfaces".

Pt 5: Macro-scale phenomena

21. W. Munk, "Acoustic scintillations of acoustic waves".
22. S. Flatté, "Intensity and phase fluctuations in low-frequency acoustic transmission through internal waves".
23. T.H. Bell, Jr., J.M. Bergin, J.P. Dougan, Z.C.B. Hamilton, W.D. Morris, B.S. Okawa, E.E. Rudd & J. Witting, "Two-dimensional internal-wave spectra".
24. I.M. Blatstein, "Ocean-basin reverberation from large underwater explosions, Pt I: Source-level and propagation-loss modelling".
25. J.A. Goertner, "Ocean-basin reverberation from large underwater explosions, Pt II: Computer model for reverberation".
26. J.D. Shaffer, R.M. Fitzgerald & A.N. Guthrie, "Some effects of large-scale oceanography on acoustic propagation".
27. H.H. Essen, "Influence of internal waves on sound propagation in the SOFAR channel".
28. O.M. Johannessen, "A review of oceanic fronts".
29. R. Mellen & D.G. Browning, "Some acoustic effects of internal macrostructure".

Pt 6: Micro-scale phenomena

30. D.R. Del Balzo & W.B. Moseley, "Random temperature structure as a factor in long-range propagation".
31. J.J. McCoy, "Beam spreading and loss of spatial coherence in an inhomogeneous and fluctuating ocean".
32. R. Tait, "Internal oceanographic microstructure phenomena".
33. D. Mintzer, "Acoustic effects of internal microstructure".

Pt 7: Field calculations

34. S.N. Wolf, "Measurements of normal-mode amplitude functions in a nearly-stratified medium".
35. R.D. Graves, A. Nagl, H. Uberall, A.J. Haug & G.L. Zarur, "Range-dependent normal modes in underwater sound propagation".
36. J.A. Desanto, "Inverse wave propagation in an inhomogeneous waveguide".
37. A. Gille & D. Odero, "A solution of the wave sound equation in shallow water for real-speed profiles and solid bottom under-sediment".
38. D.J. Ramsdale, "A wave-theoretic method for estimating the effects of internal tides on acoustic wave transmission".
39. J.G. Schothorst, "Effect of ship motion on sonar detection performance".
40. C.W. Spofford & H. Garon, "Deterministic methods of sound-field computation".
41. R. Goodman, "Stochastic methods of sound-field computation".

Pt 8: Sonar models

42. B.B. Adams & G.R. Giellis, "A technique of comparative analysis of underwater-sound-transmission loss curves".
43. J.A. Desanto, "Connection between the solution of the Helmholtz and parabolic equations for sound propagation".
44. F. Dinapoli, "Computer models for underwater-sound propagation".
45. D. Wood, "Assessment techniques for computer models of sound propagation".

TABLE OF CONTENTS

Pt 4: Sea Bottom

(Total number of printed pages in this document: 223)

HIGHLIGHTS OF BOTTOM TOPOGRAPHY INFERRED FROM RECEIVED DEPRESSION AND BEARING ANGLES

by

F.M. Phelan, R.B. Williams* and F.H. Fisher
University of California, San Diego
Marine Physical Laboratory of the
Scripps Institution of Oceanography
San Diego, California, U.S.A.

ABSTRACT

Statistical properties of the acoustic reflection from the ocean floor have been studied for a variety of bottom types including deep, smooth, flat topography to rough, jagged bottom in shallower ($\approx$ 1 km) depths. Explosive sources are used with ranges from 4 to 20 km, while the receiver array is mounted on a moored stable platform (Marine Physical Laboratory's FLIP). High coherence is found from the first part of the return, and degradation in the coherence is noted as more of the return is processed. A simple empirical model is offered for this coherence versus signal processed. Due to the initial high coherence, 3-D coordinates of the bottom bounce point can be calculated, and fine features (highlights) of the bottom can be deduced.

* *Now at NATO SACLANT ASW Research Centre*
La Spezia, Italy

INTRODUCTION

The statistical modelling of bottom reflection phenomena is in an infant stage at the present time. Many basic questions need attention before an adequate basis can be formed upon which these models can proceed. Over the last several years, our group at the Marine Physical Laboratory of the University of California at San Diego have been involved in studies of reflected signals from various bottom topography. Part of our study has addressed itself to a few of these "basis building" questions: what is the level of coherence of the bottom reflected return, and under what conditions or with what processing procedures can the coherence be enhanced? Is the energy reflected from a small fraction of the bottom surface with well defined regions (highlights), or is there energy reflected from most of the bottom (reverberation)? Under what conditions can we expect highlights or reverberation? If there are highlights, are they well enough defined to apply pattern recognition techniques? How may we model the distribution of highlights, if they do indeed exist? At present, the study is far from having clear answers to these questions, but some results are emerging, and as the study proceeds we are hopeful that further knowledge will be forthcoming. This paper sets down our knowledge of these questions to date, and the procedure we have used.

Our work thus far has covered several types of bottoms off of the coast of California and near Hawaii. Those near California include deep (4 km), smooth, flat bottoms, rougher bottoms with average slopes up to 5 degrees, and very rough bottoms with average slopes up to 20 degrees and depths from 700 to 1400 meters. The Hawaii area studied varied in bottom type from rough volcanic to smooth hard bottoms with depths from 600 to 1100 meters. In this paper, we will present results from the Hawaii areas, pointing out similarities to the California areas also studied.

1. INSTRUMENTATION AND EXPERIMENTAL SET-UP

While the receiver vessel, FLIP, was stationary over the bottom in a three-point moor, the source ship opened range from 4 up to 20 km, setting off SUS mark-61 explosive "shots" every 200 meters. Many different runs were made thus, each time the source ship's beginning point was offset perpendicular to the run direction by 200 meters, forming a grid of "shot" positions 200 by 200 meters. A trailing hydrophone at the source ship connected to a radio link to FLIP allowed a precise measure (taking into account the delay from the shot to the trailing hydrophone) of the acoustic travel time to FLIP. Using a precise sound velocimeter, the range of the shot could be measured to a relative accuracy of a few meters.

Mounted aboard FLIP was an array of four hydrophones; two at a 90 meter depth horizontally separated by 13.5 meters, and another pair at 85 meter depth with the same horizontal separation. All four

hydrophones were in a plane roughly perpendicular to the sound path, and optically surveyed to a position accuracy better than 1 cm. In addition, a fifth or "sync" hydrophone was situated on a 5 m mast projecting toward the source ship so as to receive the sound before the others. The "sync" hydrophone signal was used for initiating data sampling and data validation described below.

Profiles of sound speed and temperature were made from FLIP by lowering a f.m. multiplexed system of sensors developed at the Marine Physical Laboratory (MPL). The package consisted of a Lockheed sound-speed sensor, an MPL-developed f.m. thermometer, and a vibrating-wire depth sensor. The various separated signals were fed into a multi-channel f.m.-to-digital converter, which is a component of an MPL computer system centered around a Hewlett Packard 2116B computer. The hydrophone signals were sent up cables aboard FLIP, analog high-passed at 300 Hz and fed into a multi-channel analog-to-digital converter capable of digitizing eight signals simultaneously, up to a rate of 50 kHz. This unit is also a component of the MPL computer system: the selection of one of eight sets of the eight signals to be digitized, and the rate of digitization are dynamically set by the computer program. A radio link signal described above was also used for facilitating data collection described below, and validating data. Fluctuations in the radio link due to the equipment were about two milliseconds.

2. DATA COLLECTION PROCEDURES

Data collection was performed under computer control, valid data being stored on digital magnetic tapes. Rather elaborate procedures were used to collect the data, in anticipation of competing signals from other ships in the area, energy received from our own shots by unwanted paths, and biological noise. The procedure taken was based on using as much information of our signal as possible: knowledge of when the pulse was initiated (via radio link information), the range (computed from the previous valid signal or weighted information of previous signals), length and character of the signal and the repetition rate of the shots were all used.

The computer was instructed to "look" for a radio link signal and then wait for a time based on the range calculated from a previous signal (originally estimated by the computer operator at the beginning of a run). At that time, minus a small safety factor, the computer then repeatedly sampled at a 10 kHz rate, the signal energy of the "sync" hydrophone. When this energy rose above a threshold dynamically set by the program, digitization at a 50 kHz rate of the hydrophone signals took place for about 10 ms. This data thus gathered was temporarily stored in the core of the computer. Inspection of the gathered data by the program was then done to see if the signal received was of proper character to be a direct (water-borne) signal. This procedure guards against short noise pulses of biological origin previously encountered, or confusion resulting from missing the direct signal. If the signal was not

long enough to be valid the data was ignored and the "sync" energy sampling was reinstated. If the signal was "good", a time was set before "looking" for the bottom-reflected signal, based on the current range, water depth and sound speed profile. When the reflected signal arrived and was validated by the above procedure, all of the data were logged on magnetic tape, real-time analysis was performed, a new expected time for receipt of the next signal was calculated, and the cycle reinitiated. If valid data were not received in a set "window period", a new expected time was calculated, the "window" widened somewhat and the process reinitiated.

3. REAL-TIME ANALYSIS

Between shots (90 seconds for most runs), analysis of the data took place and various displays and calculations were made. The digitized data of the different hydrophones were presented on a scope display to show personnel aboard FLIP whether or not proper sampling was taking place. Due to a lead time from the sync hydrophone, sampling of the data signals took place about one or two milliseconds before actual receipt of the signal, guaranteeing a sampling of the beginning of the signal and also obtaining a sample of the noise for signal-to-noise analysis. Correlations between the various signals were made and, using an iterative routine, approximate bottom-bounce coordinates were calculated. However, refinements to the procedure were made at a later time, and more exact solutions were obtained.

4. BOTTOM REFLECTION POINT COORDINATE CALCULATIONS

In order to obtain a solution for the three coordinates (x,y,z) of the (effective) reflection point on the bottom, the following information is needed: (1) horizontal and vertical arrival angles of the received wavefront with respect to FLIP for both the water-borne (direct) and bottom-reflected signals, (2) the precise travel time of both types of signals, (3) the sound speed profile, and (4) FLIP's orientation in space. Due to the refraction effects, the equations for (x,y,z) are non-linear. We have used an iterative technique for the solution, starting the iteration with the solution without refraction, and find that convergence of the solution is always possible provided the input data are reasonable. Studies of the approximate sensitivity of the various input values on the solution have been done. [See, for example, Fig. 4, showing uncertainty in (x,z) by estimating uncertainties in the input values]. However, a more extensive study of this is presently underway.

5. SOME RESULTS AND DISCUSSION

Figure 1 is characteristic of vertical-arrival angle data in "rough" and "semi-rough" topographies. This particular data was from a "semi-rough" area 100 miles from the coast of California. An interesting feature of this data is the existence of plateaus, such that the arrival angle at the receiver is constant even though the source to receiver range is opening. This feature has been interpreted by us to mean that a small part of the bottom surface is responsible for reflections for several different ranges. As the range is opened further, the reflection points shifts to the next "highlight". Note also that sometimes two arrival angles are seen, corresponding to reflections from two "highlights" simultaneously. This is manifested by two peaks in the vertical correlation function.

Figure 2 shows a plot of X vs Z coordinates of the calculated bottom bounce points for a run in the same area. This "side view" is a result of connecting the bottom bounce points by straight lines, and then projecting the resulting line (in 3D space) onto a vertical plane roughly parallel to the propagation of sound. The vertical exaggeration is ten to one. The X value does not always increase as the source range increases, but sometimes doubles back, depending on the topography (for example, the loop near X = 8 km).

The plan view (X vs Y) of the results of several runs made near Hawaii (Fig. 3) illustrates features of rough and smooth areas. Toward the east, the topography has high average slopes and is much rougher than to the west, where more gentle slopes are found. Note that the bottom bounce points tend to cluster in the rough regions. In fact, the radius of some clusters is within the uncertainty of our measurements. In the smoother bottom areas, the bottom-bounce points form more of a line (with slight deviations), as would be expected of reflections from a plane. These slight deviations can be correlated with known bottom topographic features such as valleys with as little as a meter or two of depression in a depth of 700 meters.

As mentioned earlier, coherence between pairs of hydrophone signals is degraded as more of the reflected signal is used. We believe this is due to the increase of the number of reflections that are received simultaneously as time increases. We have attempted to describe this in a single mathematical model that fits our data. A two parameter formula which is consistent with our result is

$$ccc(t) = b + (1 - b)e^{-t/a} \qquad \text{[Eq. 1]}$$

where t is the length of signal processed starting from the initial reception of the signal, a and b are constants that depend on the statistics of the bottom. At this time, we feel it is premature to put forth a physical argument for this, but merely offer it as an empirical result. Figure 4 shows some data from Hawaii in the rough and smooth areas, with Eq. 1. Typical values for a are about 2 ms, while b ranges from 0.7 to 0.9.

CONCLUSIONS

High correlations (> 0.95) were found between receiver signals spaced 5 and 13.5 meters apart when the first 0.5 ms of the bottom-reflected signal was processed. This high correlation is believed due to reflection from a single small area (highlight) of the bottom topography. As more of the received signal is processed, the correlation is degraded, which is consistent with the simultaneous reception of reflections from other highlights. The degradation of the correlation can be summarized in a empirical model:

$$ccc(t) = b + (1 - b)e^{-t/a}$$

where ccc is the correlation coefficient between receiver signals, t is the length of signal processed and a and b are constants that depend on the statistics of the bottom topography. Typical values are $a = 2$ ms and $b = 0.90$ for the vertical receiver separation, $b = 0.80$ for horizontal receiver separation.

For some topography one distinct highlight dominated the reflection signal: whereas the source receiver was varied such that for a flat bottom, the reflection point would be expected to cover an area of 800×800 m , the measured reflection points were concentrated in a 50 m radius. In all rough and semi-rough bottom topography measured to date, single reflection points could be well discerned. The distribution of these highlights was not uniform over the bottom, but formed clusters. In contrast, the smooth bottoms showed a distribution much closer to being uniform.

There is other information regarding the bottom topography that can be extracted from the data. It is possible at a bottom-bounce point to calculate the two components of the slope vector, and thus generate slope statistics. We believe that the data is also good enough for some runs to identify the coordinates of several highlights from one shot. These are some of the specific aspects of our future work.

ACKNOWLEDGMENTS

The authors wish to thank the crews of FLIP and the Rig Pusher for their dedicated efforts in making these experiments possible. This work was sponsored by Office of Naval Research, Contract N00014-69-A-0200.

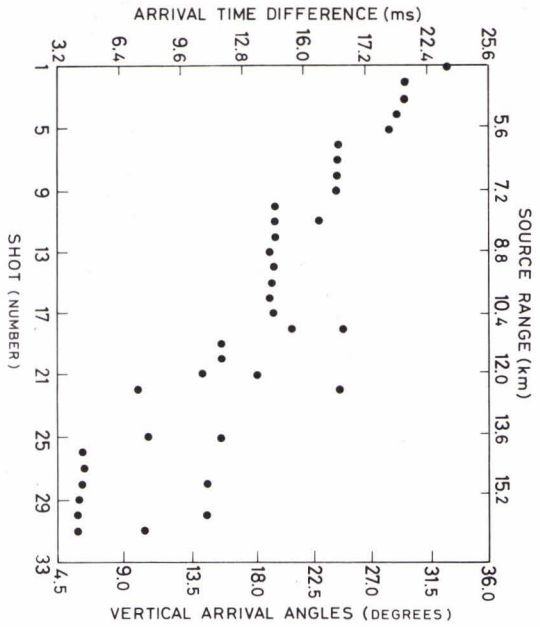

FIG. 1 VERTICAL DELAY TIMES

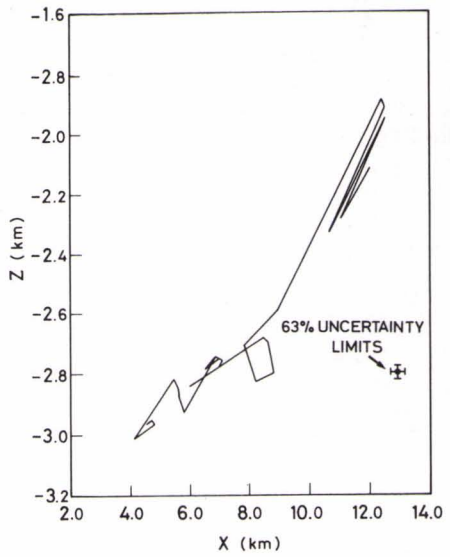

FIG. 2 BOTTOM BOUNCE COORDINATES SIDE VIEW

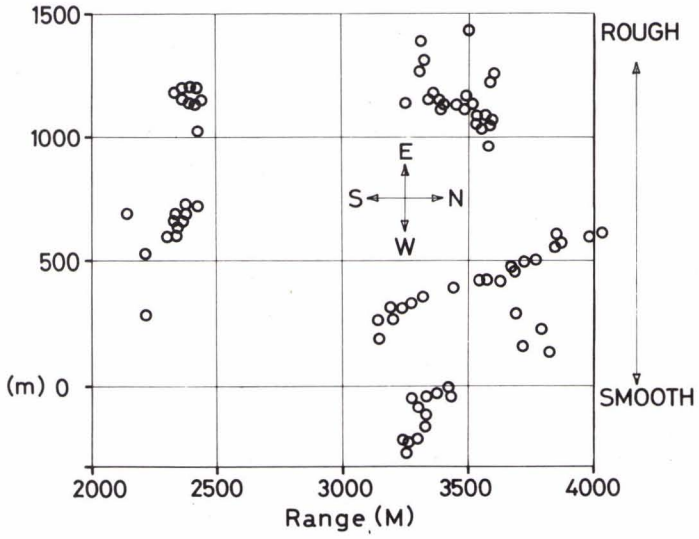

FIG. 3 BOTTOM BOUNCE POINTS PLAN VIEW

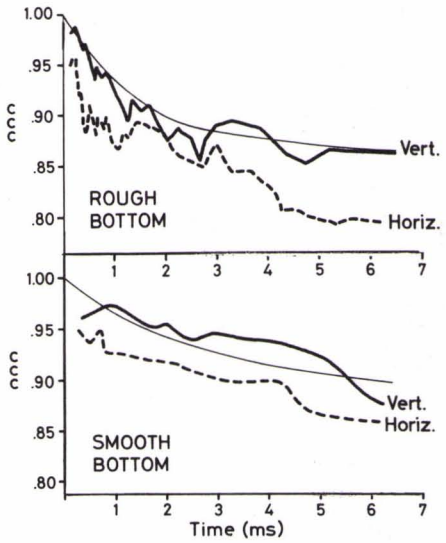

FIG. 4 CORRELATION COEFFICIENT VS SIGNAL PROCESSED

OCEAN BOTTOM REFLECTIVITY (A POINT OF VIEW)

S.R. Santaniello and F.R. DiNapoli

Naval Underwater Systems Center
New London Laboratory
New London, Connecticut 06320

ABSTRACT

The analysis procedures for extracting bottom loss values from pulsed-acoustic signals that have interacted only with the ocean bottom do not inherently consider sub-bottom refraction and reflection of sound, which are important effects at low frequencies (i.e., < 500 Hz). Sound returning from the sub-bottom can constructively interact with sound reflected from the water-sediment interface, yielding "negative bottom loss" results. To support this premise a Fast Field Program (FFP) time domain model simulation of a bottom loss measurement was performed in which the lateral wave was the only additional arrival interacting with the bottom reflected wave arrival. The simulation demonstrates a plausible cause for anomalous bottom loss results and suggests that propagation models must accommodate the environmental description of both the water column and ocean bottom.

INTRODUCTION

To acquire an understanding of the transmission of low frequency sound through the ocean, it is mandatory that propagation models be designed to account for the refraction of acoustic energy by the ocean bottom. To accomplish this the model must be capable of accommodating the complete environmental description of the water column and ocean bottom. Studies at the Naval Underwater Systems Center (NUSC) indicate that developing this type of model to predict low frequency propagation loss is more meaningful than extending high frequency measurement and analysis techniques to obtain bottom loss values for use with less complete propagation models. The reasoning behind this viewpoint is presented in this paper.

DISCUSSION

In general, acousticians describe an acoustic signal's interaction with the ocean bottom in terms of a single function, i.e., the reflection coefficient. A typical geo-acoustic model that yields the plane-wave reflection coefficient as a function of angle and frequency is shown in figure 1. This model considers an infinite single-frequency plane-wave to be incident at only one angle with

the ocean bottom. The bottom is assumed to have smooth parallel boundaries where the layer thickness, density, sound speed, sound-speed gradient, and attenuation are the input parameters. The coefficient may be defined as the ratio of reflected-to-incident acoustic intensities and the logarithm of the coefficient is termed the "bottom-reflection loss." To measure bottom-reflection loss within the constraints of this definition is virtually impossible so, in practice, it is estimated through an indirect approach that requires interpretation.

The approach illustrated in figure 2 is to first measure the propagation loss of an acoustic pulse that has traversed the medium from source-to-receiver via the acoustic path that has enabled the pulse to interact once with only the ocean bottom. Then the water-column propagation loss for only the bottom-reflection path is calculated by assuming a flat, single-interface bottom having a reflection coefficient of one. The final step is to compare the measured and calculated propagation losses; the difference is known as "bottom loss."

However, because of water-region multipaths, considerable care and interpretation is required (especially for low grazing angle data) to determine the propagation loss for the energy that has interacted only with the ocean bottom. At low frequencies additional factors, such as low-frequency noise and knowledge of the exact source level for each detonation of an explosive can affect results. When experiments are conducted in deep water it is possible to minimize multipath and source level effects.

By laterally separating an explosive source and a hydrophone and positioning them well away from the ocean boundaries as shown in figure 3, the time separation

between water-region arrivals can become sufficient to perform a relative bottom loss measurement for grazing angles below 5 deg. For this acquisition method, the bottom loss calculation reduces to the difference between two ratios (presented in logarithmic form in the figure). The first ratio accounts for the difference between the energies of the direct and bottom-reflected arrivals; the second accounts for the difference between the calculated propagation losses for the two acoustic paths. Although source level, processing, and prediction errors are minimized, interpretation is still required (especially at low frequencies when sub-bottom refraction and reflection of acoustic energy occurs).

Consider an ideal Rayleigh plane-wave reflection curve having a critical angle caused by the sediment sound speed being greater than that of the water column (this is a realistic premise at low frequencies). Consider also an omnidirectional impulsive point source and an acoustic path where energy impinges on the bottom at a relatively low grazing angle θ_1 (see figure 4). Based on the ideal plane-wave reflection curve, all this energy will be reflected. When acoustic energy impinges on the ocean bottom at a higher grazing angle θ_2 (figure 4), energy will penetrate the sediment. If a positive sound-speed gradient exists in the sediment, this energy will be refracted and returned to the water at a considerable distance down range. If the travel time of the reflected energy is equal to the travel time of the refracted energy at some point in the medium, the arrival <u>interpreted</u> as being <u>only</u> a bottom-reflected arrival will actually contain additional interfering energy. In such a case bottom loss results will not be good estimates of the bottom-reflection loss.

To support the premise that time coincident bottom reflected and refracted arrivals cause anomalous low frequency bottom loss values, we will discuss results of one of our experiments. These results are not unique; similar anomalies have been observed during other experiments by NUSC personnel and by other investigators.

The experimental configuration was optimized to ensure that the bottom interacting energy could be isolated at low grazing angles. A sample of a sequence of acoustic arrivals in which the single-point grazing angle was determined to be 11.4 deg is shown in figure 5. Bottom loss data were obtained under the constraints of the previously discussed relative measurement approach. The data were processed over a two-octave band centered at the spectrum peak for the explosive used.

Seventeen values between 9 and 15 deg form a transition into and out of a region which, for lack of a better expression, has become known as the negative bottom-loss region (see figure 6). Although we recognize these results are representative of the particular experimental configuration, we also realize that because of the relative measurement approach experimental error was insignificant; therefore, all values are real. The negative values are consistently calculated over a considerable coverage of angles because more energy was received for the signal identified as the bottom reflected arrival than could be accounted for by the water-column propagation loss model, which assumes that only a single bottom-reflected signal is involved in the reflection process. It is hypothesized that during the actual measurements, energy penetrated the ocean bottom at relatively high grazing angles, was refracted back into the water column, and arrived at the hydrophone coincident in time with the low grazing angle reflected

energy. Evidence supporting this hypothesis will be presented in the remaining portion of the paper.

During all of NUSC's recent experiments the Lamont-Doherty Geological Observatory has conducted wide-angle seismic reflectivity measurements to provide estimates of the thickness, interval sound speed, and sound-speed gradient of the sediment. Thus, the sediment sound-speed profile could be combined with the profile of the water column to produce ray-tracing diagrams, one of which is presented in figure 7. This ray diagram is of interest simply because it demonstrates a concept found in current texts, i.e., the focusing of acoustic energy by the ocean bottom because of refracted acoustic waves. The formation of a caustic is evident. Furthermore, as the figure illustrates, there is a possibility that multiple refracted arrivals could overlap in time with reflected arrivals over a considerable volume of the water column.

Quantitative evidence in support of the above hypothesis is obtained by considering the simplest environmental description involving acoustic interaction at a single boundary (see figure 8). Such a description consists of two semi-infinite ideal fluids having constant but different sound speeds and densities. The process is to treat only the reflected and lateral wave interaction at the boundary. A point source emitting 100-msec, 50-Hz sinusoidal pulses is situated in the lower speed water, 305 m above the higher speed bottom; the receiver is located 610 m above the bottom. The total field can be expressed in terms of three integrals, one associated with the direct wave, one with the bottom-reflected wave, and one with the lateral wave. Asymptotic methods are usually invoked in the lateral wave solution and provide results that can be physically interpreted only when the grazing angle is not close to the critical angle. For angles

close to critical, uniform asymptotic methods must be used and, unfortunately, it becomes impossible to interpret results in terms of either the reflected or lateral wave. To demonstrate the difficulty in physical interpretation we have simulated the exact total field in the time domain for the model shown here, using the Fast Field Program (FFP) technique.[1]

Figure 9 outlines the mathamatical process; detailing it would be time consuming and beyond the scope of this paper. The time domain solution for the pressure field is obtained by convolving the transfer function of the medium with the frequency spectrum of the input waveform, as shown in equation 1. The transfer function, given in terms of the Fourier Bessel Transform shown in equation 2, takes into account the Rayleigh plane-wave reflection coefficient. The branch point singularity of the coefficient at the critical angle is one of the reasons one must resort to asymptotic methods in the analytical evaluation of the integral. However, the integral can be evaluated directly with the aid of the Fast Fourier Transform. If the Hankel function is approximated by the first term in the asymptotic expansion, the field integral can be considered as a Fourier Transform. The transfer function can then be written as the discrete Fourier Transform shown in equation 3. This equation was evaluated at 1024 discrete frequencies and the previously described convolution procedure yielded a time history for the 100-msec, 50-Hz sinusoidal pulse pressure waveform at many ranges.

The waveform at the left of figure 10 is for a near range where the grazing angle is greater than the critical angle and there is no contribution caused by the lateral wave. The amplitude of the waveform agrees well with the amplitude of the 20 log (R) ray-theory prediction. (Agreement is denoted by

the lines above and below the waveforms.) The middle waveform is for a range, close to where the critical angle would occur and the lateral wave is excited. There is a significant difference between the amplitude of the waveform and that of the ray theory prediction. Ray theory is in error because it cannot account for the effect of the lateral wave. The waveform at the right of the figure is for a far range where the angle is less than critical. There is no time coincident contribution from the lateral wave arrival and, therefore, there is agreement between amplitudes. Simulated waveforms for a considerable coverage in range were processed in a manner analogous to the relative bottom loss measurement approach.

As expected for the higher grazing angles the bottom loss curve agrees well with the bottom-reflection loss curve obtained using the Rayleigh reflection coefficient (see figure 11). Between roughly 20 and 35 deg, the bottom loss curve differs significantly from the Rayleigh curve. This is also expected because they differ over precisely the angular region in which the reflected and lateral wave signals are coincident in time. Anomalous values occur in both the negative and positive direction. The bottom loss curve and the Rayleigh bottom-reflection loss curve are each correct but, in the final analysis, one is not truly representative of the other. Although this example is over-simplified, it clearly demonstrates why anomalous values can occur when determining bottom loss.

SUMMARY

We have shown that, theoretically, there is a plausible cause for anomalous bottom loss values, specifically, low-frequency negative bottom loss values.

The ocean bottom can redirect into the water column both reflected and refracted acoustic waves that interact in either a destructive or constructive manner. The interaction of time coincident acoustic waves influencing the measured data cannot be accounted for under the constraints of accepted experimental procedures and manifests itself through anomalous values when extracting bottom loss. To overcome this difficulty, it is suggested that a propagation loss model be constructed to accommodate the environmental description of both the water column and the ocean bottom. Comparing measured and predicted propagation losses would then become a measure of the accuracy of the propagation model and not of the magnitude of bottom loss. This causes us to suggest the eventual abandonment of extracting bottom loss from measured propagation loss data.

Current research efforts at NUSC are consequently oriented toward determining if seismic reflectivity information is suitable as model input information for accurate low-frequency propagation loss prediction. Such an effort requires the expertise of geologists and acousticians; an association we believe will be increasing necessary to enhance our knowledge of underwater acoustics. To aid in the prediction of low frequency bottom loss in an ocean area, all that may be required in the future is ocean bottom seismic data (in conjunction with water column environmental data) of the type acquired on a regular basis by many oceanographic and geological institutions.

REFERENCES

1. F.R. DiNapoli, Fast Field Program for Multilayered Media, NUSC TR 4103, 26 August 1971.

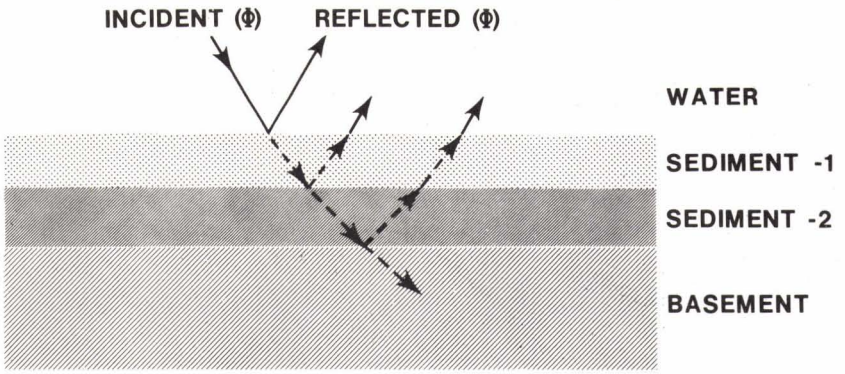

FIG. 1
PLANE-WAVE GEO-ACOUSTIC MODEL

MODEL OUTPUT PARAMETERS

$$\text{BOTTOM-REFLECTION COEFFICIENT } (R) = \frac{\text{REFLECTED } (\Phi)}{\text{INCIDENT } (\Phi)}$$

$$\text{BOTTOM-REFLECTION LOSS} = -10 \log (R)$$

1 MEASURE PROPAGATION LOSS OF BOTTOM-REFLECTION PATH ONLY $(PL)_B$

EXPERIMENTAL GEOMETRY

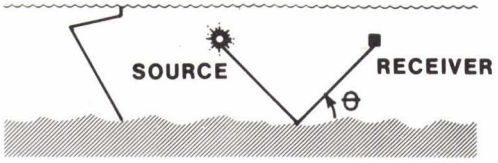

2 CALCULATE WATER-COLUMN PROPAGATION LOSS $(WPL)_B$ OF REFLECTED ACOUSTIC RAY ONLY

WATER-COLUMN PROPAGATION LOSS MODEL

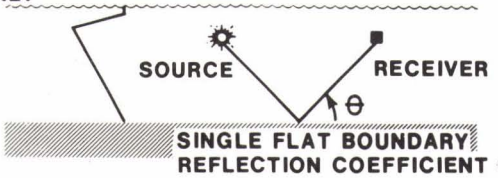

3 DETERMINE BOTTOM LOSS

$$\text{BOTTOM LOSS (BL)} = \text{MEASURED } (PL)_B - \text{CALCULATED } (WPL)_B$$

FIG. 2
BASIC APPROACH TO DETERMINE BOTTOM LOSS

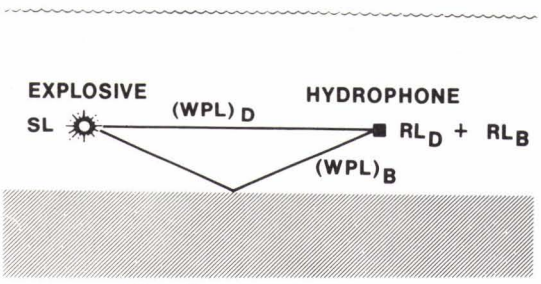

FIG. 3
RELATIVE MEASUREMENT (SELF-CALIBRATION) METHODOLOGY

$$BL = (PL)_B - (WPL)_B$$

$$(PL)_B = SL - RL_B \qquad SL = RL_D + (WPL)_D$$

$$BL = \left[RL_D - RL_B\right] + \left[(WPL)_D - (WPL)_B\right]$$

- SL ERRORS OVERCOME
- PROCESSING ERRORS MINIMIZED
- INTERPRETATION STILL REQUIRED

- PREDICTION ERRORS MINIMIZED (DIFFERENCE BETWEEN TWO SIMILAR PREDICTIONS WHERE $(WPL)_D$ IS VERIFIABLE)

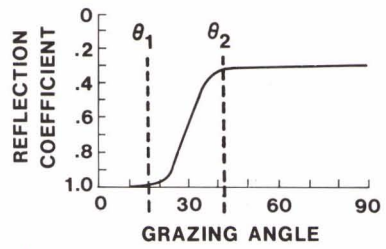

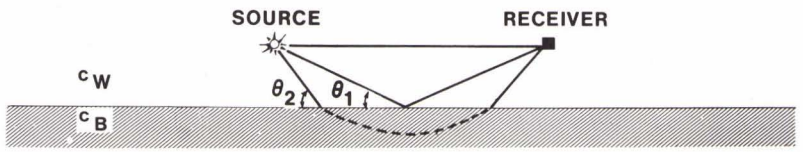

FIG. 4 TIME COINCIDENT BOTTOM REFLECTION AND REFRACTION (IDEAL RAYLEIGH REFLECTION CURVE FOR $C_B > C_W$)

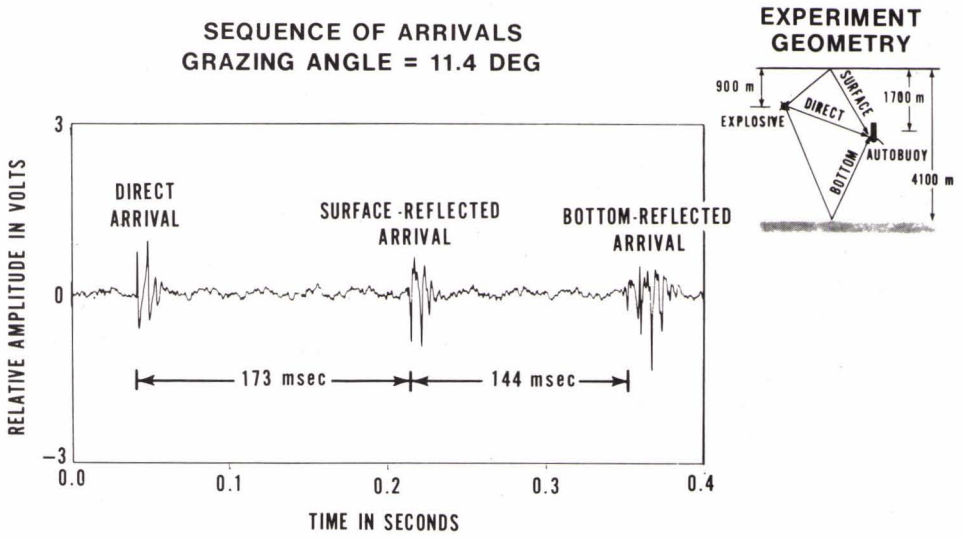

FIG. 5 EXAMPLE OF NUSC BOTTOM LOSS MEASUREMENTS RESULT

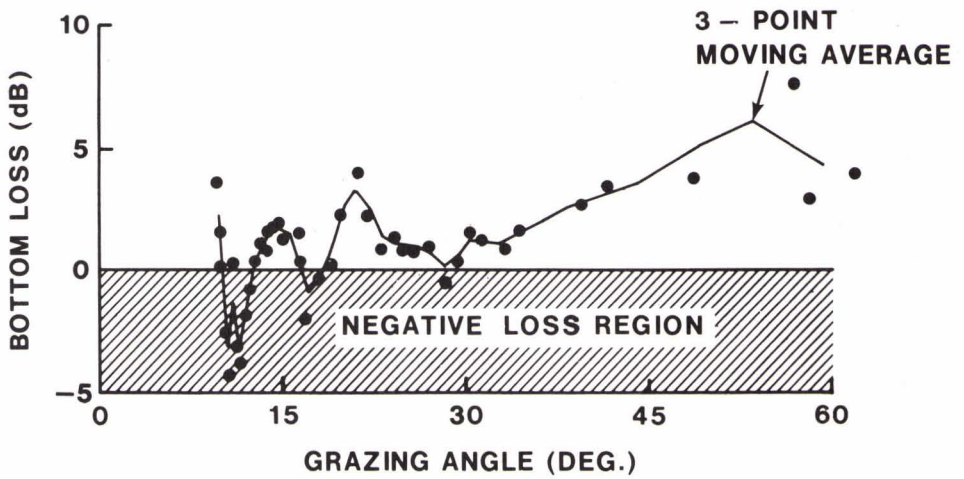

FIG. 6 NUSC BOTTOM LOSS RESULTS (80–320 Hz BAND)

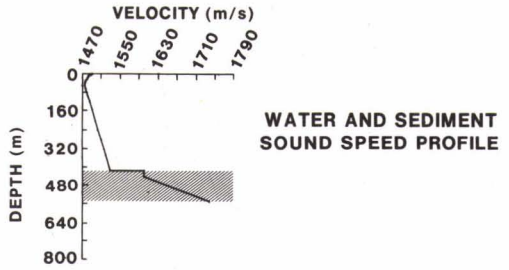

FIG. 7
RAY DIAGRAM
(FORMATION OF A CAUSTIC DUE TO REFRACTION)

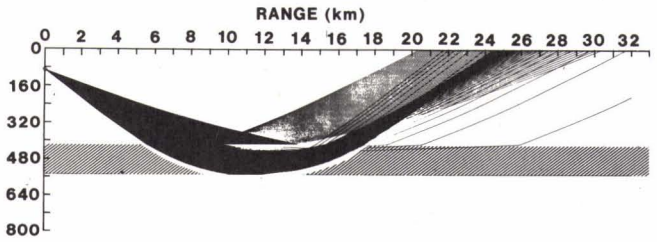

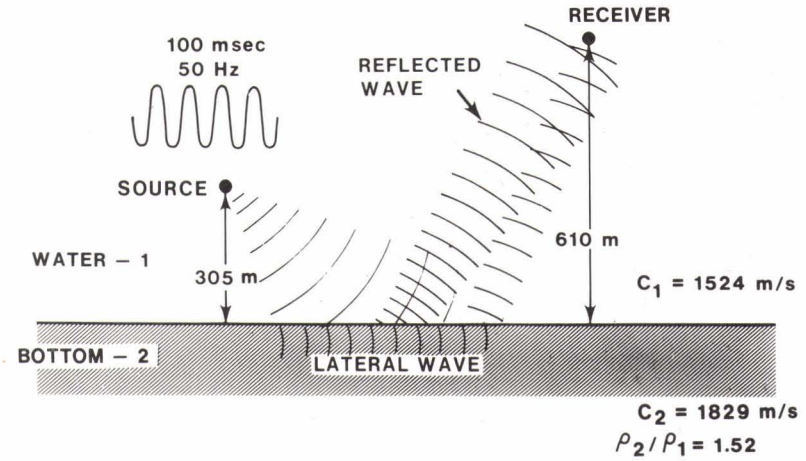

FIG. 8
TWO SEMI-INFINITE FLUIDS WITH POINT SOURCE

FIG. 9
MATHEMATICAL PROCESS

TIME DOMAIN PRESSURE FIELD

$$\tilde{P}(r,z,t) = -i2\pi\rho \int_{-\infty}^{\infty} \underbrace{\mathcal{F}(f)\,\mathcal{H}(r,z,f)}_{\text{SPECTRUM (INPUT WAVEFORM)}} e^{-i2\pi ft}\,df \qquad (1)$$

TRANSFER FUNCTION

$$\mathcal{H}(r,z,f) = \underbrace{\frac{e^{ikR}}{R}}_{\text{DIRECT PATH}} + \underbrace{\frac{i}{2}\int_{-\infty}^{\infty} \frac{\overbrace{V(\xi)}^{\text{REFLECTION COEFFICIENT}} e^{i(z+z_0)\beta_1}}{\beta_1} \overbrace{H_0^{(1)}(\xi r)}^{\text{HANKEL FUNCTION}} \xi\,d\xi}_{\text{BOTTOM-INTERACTION PATHS}} \qquad (2)$$

WHERE:

$$H_0^{(1)}(\xi r) \approx \sqrt{\frac{2}{\pi}}\frac{e^{-i\pi/4}}{\sqrt{\xi r}}\, e^{i\xi r}$$

AND LET $\xi_m = \xi_0 + m\,\Delta\xi$ $r_n = r_0 + n\,\Delta r$, $\Delta\xi\Delta r = 2\pi/M$

DISCRETE TRANSFER FUNCTION

$$\mathcal{H}(z, r_n, f_p) \approx \frac{e^{ikR}}{R} + A_n \sum_{m=0}^{M-1} (E_m, p)\, e^{i2\pi mn/M} \qquad (3)$$

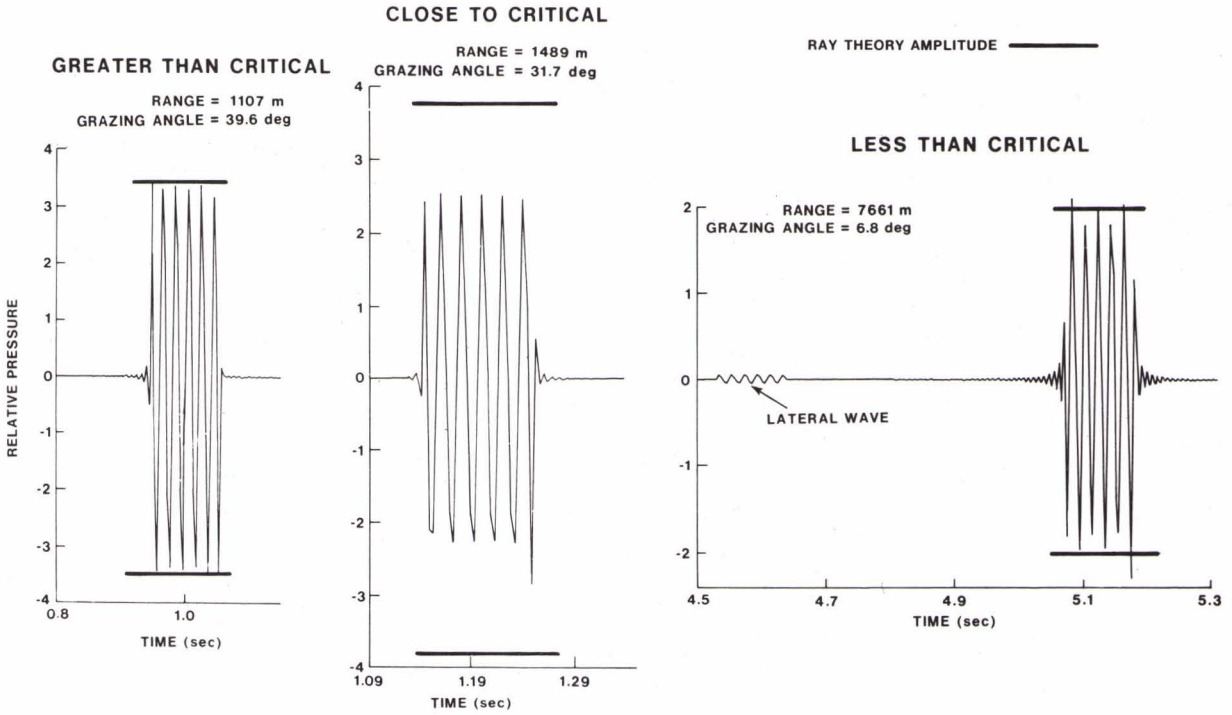

FIG. 10 RECEIVED WAVEFORMS FOR VARIOUS GRAZING ANGLES

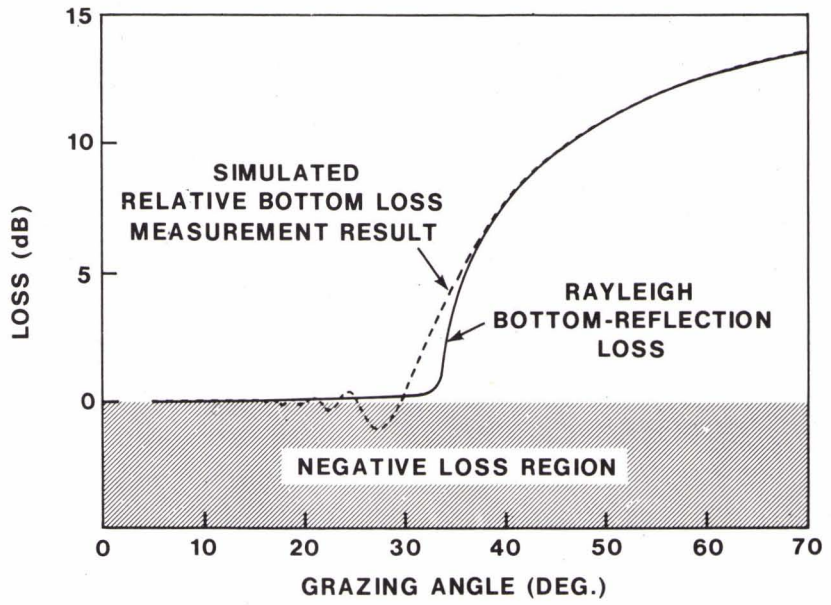

FIG. 11 EFFECT OF LATERAL WAVE

RELATIVE CONTRIBUTION OF SURFACE ROUGHNESS AND BOTTOM ATTENUATION TO PROPAGATION LOSS IN SHALLOW WATER

W. A. Kuperman

F. Ingenito

Naval Research Laboratory, Washington, D. C. 20375

Abstract

A simulation study has been performed to investigate the relative importance of the contributions of surface roughness and bottom attenuation to propagation loss under differing environmental conditions. The NRL normal mode model, which was used in the calculations, is restricted to range independent environments but can accommodate a sound velocity profile in the water layer which varies arbitrarily with depth. The bottom sediment is treated as a fluid of constant density and sound velocity with a small frequency dependent attenuation coefficient. The surface of the water layer is allowed to be rough and by using an ocean surface wave spectrum model, the roughness is characrerized by a wind speed and wind direction. Modal attenuation coefficients have been calculated as a function of frequency and parameterized according to bottom sediment type, velocity profile and wind direction. Propagation loss at a given range has been calculated as a function of wind velocity, where frequency, sediment type and velocity profile were varied. The results show that for isovelocity and downward refracting profiles the contribution of surface roughness to the total propagation loss is important when the wind speed exceeds a threshold value, the latter depending upon the environmental conditions. Surface roughness can be the major attenuation mechanism for upward refracting profiles above a certain windspeed.

INTRODUCTION

Aside from cylindrical spreading, the major contributions to propagation loss in shallow water are bottom attenuation and boundary roughness. In this study we theoretically investigate the relative importance of bottom loss and surface roughness in different shallow water acoustic environments using a normal mode model.[1] In a duct where there are no loss mechanisms (other than geometric spreading) the eigenvalues associated with a normal mode solution are real. The introduction of loss mechanisms results in complex eigenvalues, the imaginary parts of which can be interpreted as attenuation coefficients of the individual normal modes. Rather than directly solve a complex eigenvalue problem, expressions for attenuation coefficients due to bottom loss can be derived which relate the imaginary parts of the eigenvalues to the solutions of the lossless normal mode problem.[2] For the rough surface case, an impedance boundary condition[3] which has been derived earlier can be used to calculate the resulting imaginary parts of the eigenvalues. In the next section we outline the derivation of these attenuation coefficients. In Section II we present some calculated results using a wind driven model of a fully developed sea to describe the surface roughness and some empirical results on ocean bottom sediments to describe the bottom loss.

I. THEORY

Figure 1 illustrates the geometry. A harmonic point source of unit source strength is located on the z axis at depth z_0 and it is desired to calculate the sound field at the point (x,y,z). If $\phi(x,y,z)$ is the velocity potential then we must have (a time dependence of $\exp(-i\omega t)$ is assumed)

$$\nabla^2\phi(x,y,z) + \left[\omega^2/c^2(z)\right]\ \phi(x,y,z) = -\ \delta^2(\vec{r})\delta(z-z_0), \tag{1}$$

where $\vec{r}$ is a transverse vector to the point (x,y). The boundary conditions associated with Eq. 1 are that ϕ vanishes at the surface and that the pressure and particle velocity are continuous at the ocean bottom water-sediment interface. It is convenient to solve Eq. 1 using a Fourier transform method with

$$\phi(\vec{r},z) = \frac{1}{2\pi}\int d\vec{\eta}\ e^{i\vec{\eta}\cdot\vec{r}}\ v(\vec{\eta},z), \tag{2}$$

where $\vec{\eta}$ is the two dimensional Fourier conjugate vector of $\vec{r}$ and $v(\vec{\eta},z)$ satisfies the inhomogeneous differential equation

$$\frac{d^2v}{dz^2} + \left[\omega^2/c^2(z) - \eta^2\right]\ v = -\ \frac{1}{2\pi}\ \delta(z-z_0). \tag{3}$$

We seek the normal mode solution of Eq. 3 in terms of the eigenfunctions, v_n, and the eigenvalues, k_n, of the homogeneous form of Eq. 3,

$$\frac{d^2v_n}{dz^2} + \left[k^2(z)-k_n^2\right]\ v_n = 0, \tag{4}$$

where $k^2(z) = \omega^2/c^2(z)$. The solution to Eq. 1, neglecting the continuous modes, is then given by

$$\phi(\vec{r},z) = \frac{-\rho_1}{(2\pi)^2} \sum_n \int d\vec{\eta} \; \frac{v_n(z_0)v_n(z)}{k_n^2 - \eta^2} \; e^{i\vec{\eta}\cdot\vec{r}} \tag{5}$$

The contour is appropriately chosen to give outgoing waves. Note that the poles in the integrand correspond to a summation of integral representations of Hankel functions. When no attenuation mechanisms are present, the k_n's are real and hence the poles are located on the real axis. When loss is introduced, the eigenfunctions and eigenvalues become complex. In particular, $k_n \rightarrow k_n + i\delta_n$ and the dominant effect on Eq. 5 is to shift the poles off the real axis. The asymptotic form of the Hankel function is proportional to $\exp(ik_n r)$ and hence, when k_n has an imaginary part, each term in the normal mode expansion will contain an attenuation coefficient $\exp(-\delta_n r)$.

The complex conjugates of v_n and k_n, v_n^* and k_n^*, satisfy the complex conjugated version of Eq. 4. By manipulating Eq. 4 and its complex conjugate it has been shown[3] that one can (under reasonable assumptions) derive an expression for δ_n without going through the formal solution of a complex eigenvalue problem.

When the sole attenuation mechanism is bottom attenuation and the propagation constant of a plane wave in the bottom can be written as a complex number of the form $\omega/c_2+i\varepsilon$ where c_2 is the velocity of sound in the bottom, then the imaginary parts of the normal mode eigenvalues (the attenuation coefficients) are given by[2]

$$\delta_n^B \approx \varepsilon\gamma_n, \tag{6}$$

where

$$\gamma_n = \frac{\omega\rho_2}{c_2 k_n} \int_H^\infty |v_n(z)|^2 \, dz. \tag{7}$$

If the ocean surface is rough, an additional loss mechanism for the mean acoustic field is introduced. For random roughness of the ocean surface we can replace the pressure release condition at the actual surface $z=\alpha(\vec{r})$ where α is a random function by an effective impedance boundary condition at the mean surface $z=0$.[3] This new boundary condition for the mean field is

$$v = i\,\langle\alpha^2\rangle\, a(\vec{\eta})\, \frac{\partial v}{\partial z}, \tag{8}$$

where

$$a(\vec{\eta}) = \frac{1}{2\pi} \int d\vec{\xi} \; \sqrt{k^2(0) - \xi^2} \; P(\vec{\eta}-\vec{\xi}). \tag{9}$$

$P(\vec{\lambda})$ is the normalized power spectrum of the ocean surface, i.e., the Fourier transform of the autocorrelation function of the ocean surface.

Using a method similar to that used for the bottom loss case, we can again derive expressions for the imaginary parts of the eigenvalues without going through a formal solution of a complex eigenvalue problem. The derivation will be given elsewhere; below we give the result:

$$\delta_n^s(\vec{\eta}) = -(4ik_nA_n)^{-1} \left| v_n^1(0) \right|^2 \left[\frac{v_n^*(0)}{v_n^{*\prime}} - \frac{v_n(0)}{v_n'(0)} \right], \tag{10}$$

with the prime denoting the z derivative and where A_n is a normalization integral,

$$A_n = \int_0^\infty dz\rho(z) \left| v_n(z) \right|^2. \tag{11}$$

The values of the logarithmic derivatives of the velocity potentials are given by Eq. 8 and its complex conjugate. Returning to the dispersion expression in the denominator of Eq. 5 we see that the poles now occur at

$$\eta = k_n + i\delta_n^s(\eta) \approx k_n + i\delta_n^s(k_n), \tag{12}$$

the last approximation resulting from the fact that δ_n^s is of the order α^2 which is our perturbation expansion parameter. The attenuation coefficient due to surface roughness is therefore given by

$$\delta_n^s = \frac{<\alpha^2>}{2k_nA_n} \left| v_n'(0) \right|^2 \mathrm{Re}\left\{ a(k_n) \right\} \tag{13}$$

Finally, the normal mode attenuation coefficient resulting from both bottom loss and surface scattering is given by the sum of the two individual coefficients,

$$\delta_n = \delta_n^B + \delta_n^s. \tag{14}$$

II. SAMPLE CALCULATIONS

In this section we present some computer results using different environmental inputs to calculate transmission loss (TL). If we carry out the integration in Eq. 5 and insert the asymptotic form of the Hankel function into the expression we get that the acoustic pressure is given by

$$P \approx \frac{\omega\rho_1}{\sqrt{8\pi r}} \sum_{n=1}^{N} \frac{v_n(z_0)v_n(z)}{\sqrt{k_n}} \exp(ik_n r) \exp(-\delta_n r) \tag{15}$$

where δ_n is given by Eq. 14. The acoustic field at a receiver is, of course, a function of receiver depth. Since we are concerned here with attenuation we can average out the effect of receiver depth by defining our transmission loss as follows:

$$TL = 10 \log \left\{ \frac{1}{M} \sum_{m=1}^{M} P_m^2 \right\}, \tag{16}$$

where P_m is the pressure at the m-th receiver and M is the number of receivers; for the cases that follow we will take M=10 with the receivers equally spaced throughout the water column. Finally, as a measure of attenuation we define the function Γ at range R to be

$$\Gamma = R^{-1} \left[TL \text{ (windspeed} \neq 0) - TL \text{ (windspeed} = 0) \right] . \tag{17}$$

Γ will be expressed in dB/km and is a function of surface roughness; Γ is a measure of attenuation due to surface loss with geometric spreading loss and bottom loss eliminated. It is, unfortunately, a range dependent quantity but at a given range, it is indicative of the importance of surface loss.

We now present some numerical calculations of this Γ function for different shallow water environments. Below are the three bottom types used which were taken from Hamilton's work.[4,5]

PROPERTIES OF THE THREE BOTTOM SEDIMENTS

	SOUND SPEED RATIO (C_2/C_1)	DENSITY (ρ_2)	K
A. COARSE SAND	1.201	2.03	0.46
B. SILTY SAND	1.096	1.83	0.65
C. SAND-SILT-CLAY	1.032	1.58	0.2

K is defined in Hamilton's paper[4] by the relation α(dB/m) = Kf(kHz) where α is the attenuation constant for a plane wave traveling through the bottom sediment.

Three generic sound speed profiles chosen for the calculations are shown in Fig. 2. Note that the depth of water was taken to be 100 meters in all the cases.

We mentioned earlier that Γ is range dependent. We show this range dependence for a typical case in Fig. 3. The Pierson-Moskowitz[5] spectrum for a wind generated fully developed sea is used as our model for the ocean surface roughness. The calculations were done for three different source depths. In the following examples we present some sample results using 50 meters as the source depth and 25 km as the range.

Figures 4 and 5 are samples of the results at 50 Hz. Note that cases II are for negative profiles. Case IIA and IIB indicate a saturation effect after a certain wind velocity is reached. Cases IIA and IIB have four and three normal modes, respectively, of which only one in each case is trapped below the thermocline. Because the other modes that interact with the surface are stripped away we are just left with the trapped modes which do not interact with the surface. Hence, we have this saturation effect. Case IIC only has one mode that is barely trapped below the thermocline and therefore no surface loss should be observed.

Figure 5 illustrates the results for an upward refracting profile. Note that there is no saturation effect. Case C is significantly different than cases A and B indicating the importance of bottom type when calculating surface loss.

Figures 6 through 11 are sample results at 500 Hz. These figures include the effect of wind direction relative to the direction of acoustic propagation. The calculated results indicate a larger surface loss along the direction of the wind.

Figures 8 and 9 are for negative profiles and again we see the saturation effect. However, saturation occurs at a lower windspeed and at a significantly higher level than at 50 Hz. No saturation effects are predicted in Figs. 6 and 7 which are for isovelocity or Figs.10 and 11 which are for an upward refracting profile. For all these cases the surface loss is significant as compared to bottom loss. The transmission loss with bottom attenuation was of the order of 70 dB with 5 to 10 dB being attributed to bottom loss. For the isovelocity case for windspeeds greater than about 10 m/sec the contribution to transmission loss begins to exceed 5 dB at this 25 km range. For the upward refracting case, the surface loss is much larger.

A few general conclusions can be made from this limited sample of results. For negative gradient profiles we see a saturation effect. The fact that Γ climbs very rapidly to its saturated value indicates that a simple surface scattering model could be used in some transmission loss programs for negative gradient cases which is certainly typical of many areas of the world. This model would be a threshold model putting in no surface loss below a certain windspeed and a constant value above this critical windspeed. For the positive gradient cases both at 50 and 500 Hz, surface loss was a significant contribution to the total transmission loss being of the order of the bottom loss in the 50 Hz case and the dominating loss mechanism for 500 Hz. Finally, we have seen examples when the bottom type has a significant effect on surface loss.

An important caveat must be mentioned. These results are for a Pierson-Moskowitz model of a wind driven fully developed sea. Calculations must be made for more realistic ocean surfaces and work is continuing along that direction together with doing more calculations for higher frequency cases.

The work is being supported by NAVSEA 06H1-4 and the Office of Naval Research.

REFERENCES

1. J. F. Miller and F. Ingenito, "Normal Mode FORTRAN Program for Calculating Sound Propagation in the Ocean," NRL Memo Report 3071, June 1975.

2. F. Ingenito, J. Acoust. Soc. Am. 53, 858 (1973).

3. W. A. Kuperman, J. Acoust. Soc. Am. 58, 365 (1975).

4. E. L. Hamilton, Geophysics 37, 620 (1972).

5. E. L. Hamilton, J. Geophys, Res. 23, 4423 (1970).

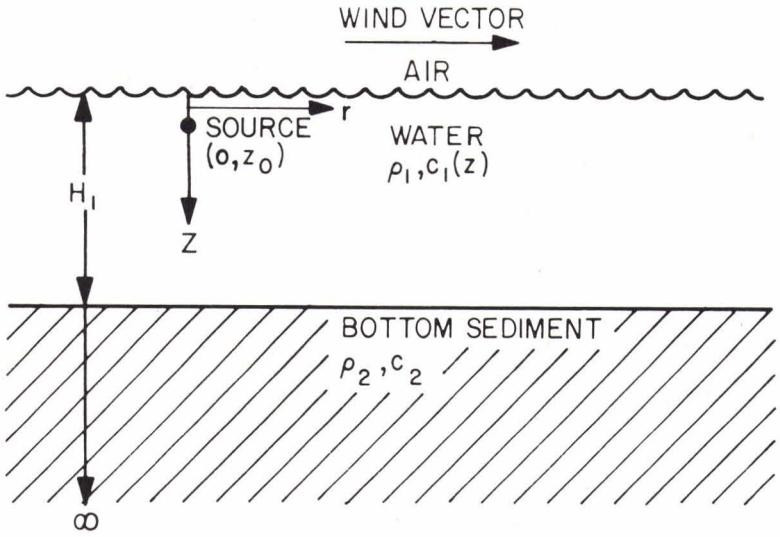

FIG. 1

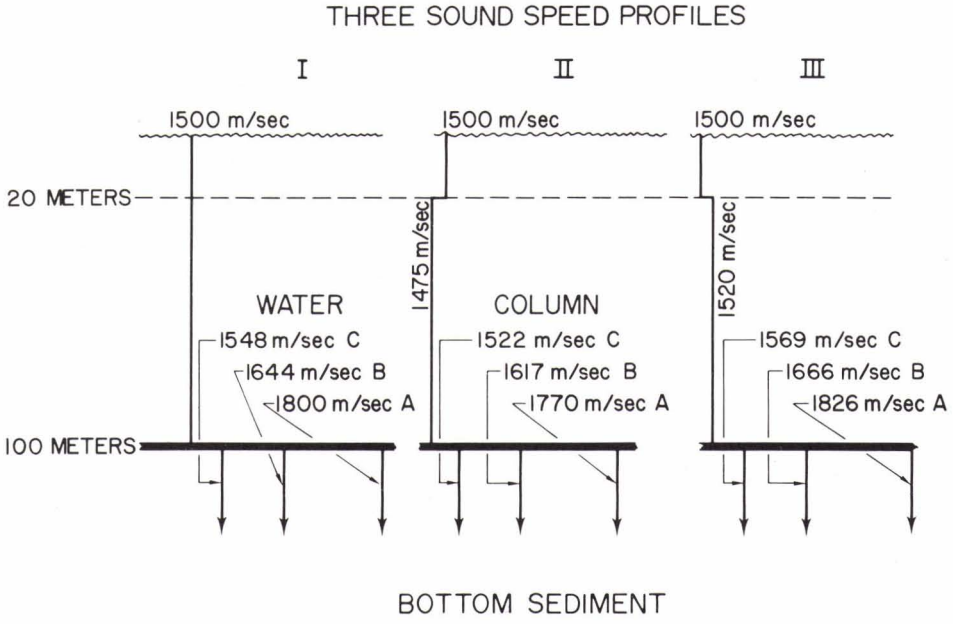

FIG. 2

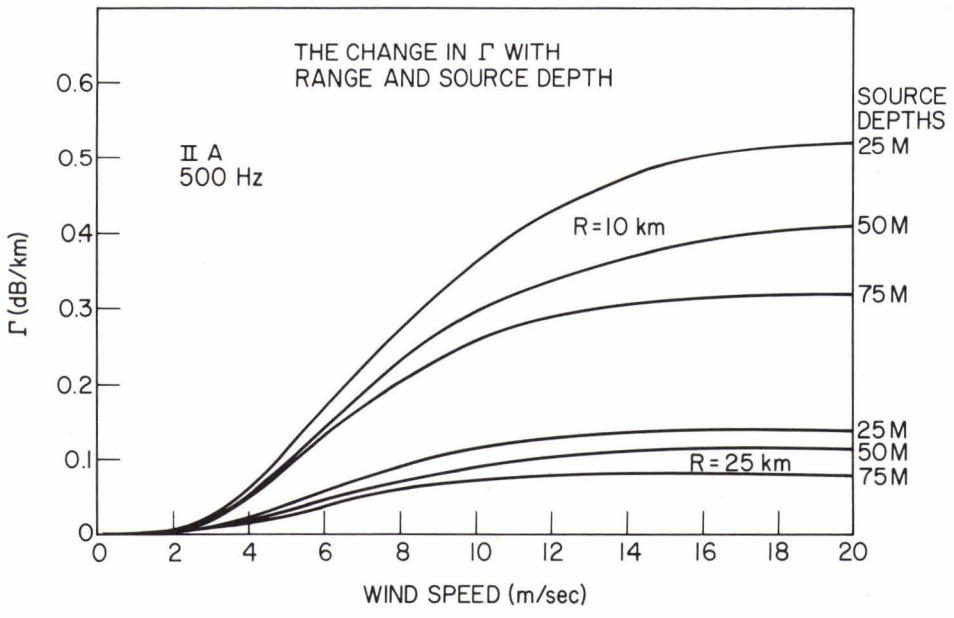

FIG. 3

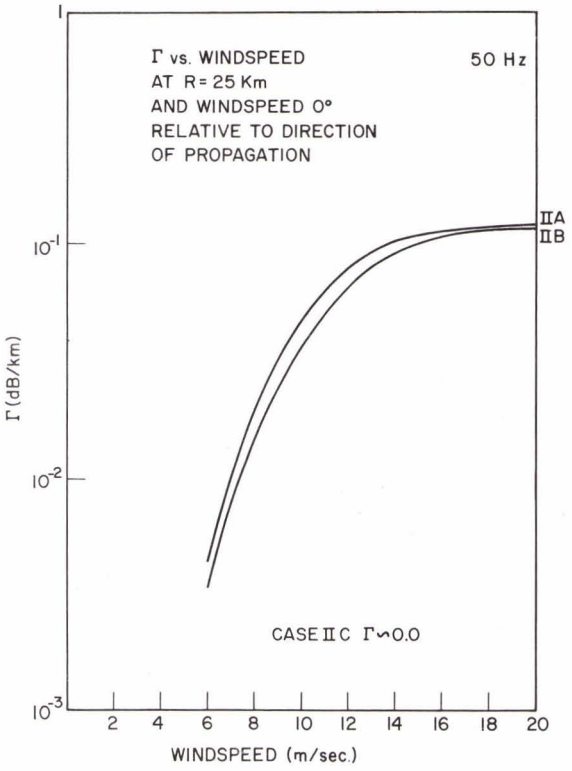

FIG. 4

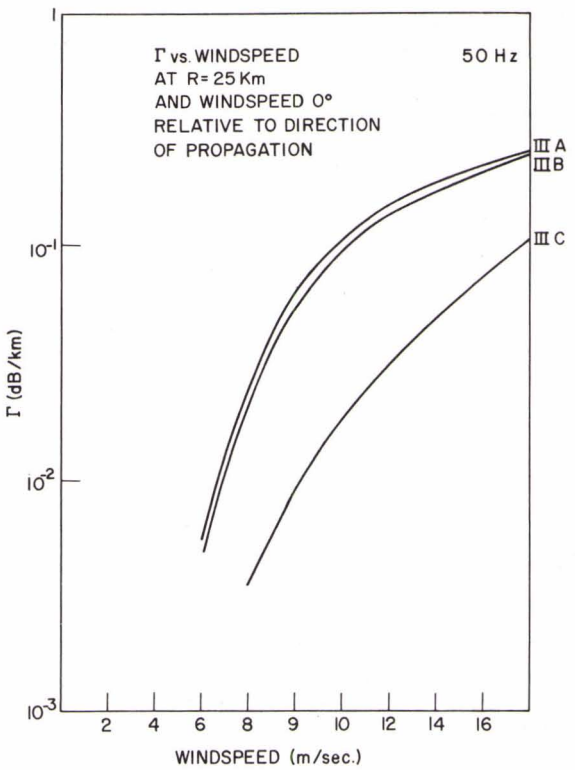

FIG. 5

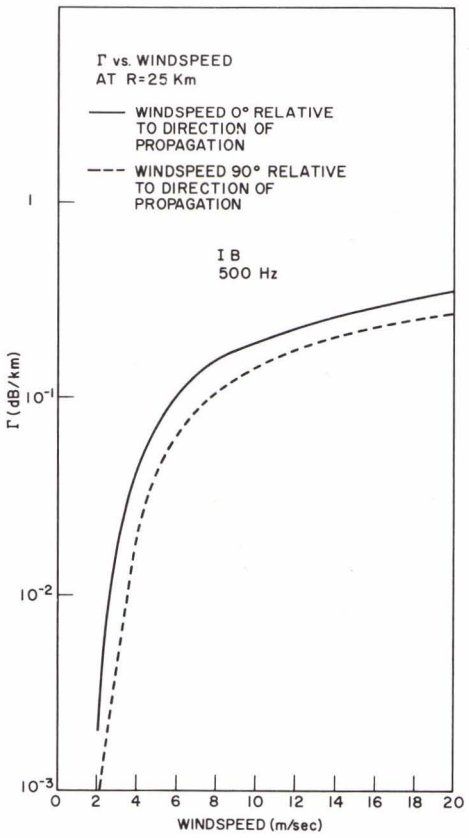

FIG. 6

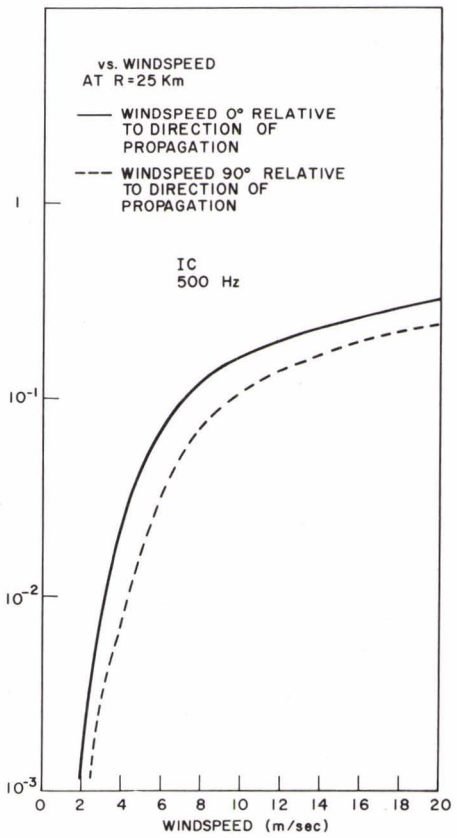

FIG. 7

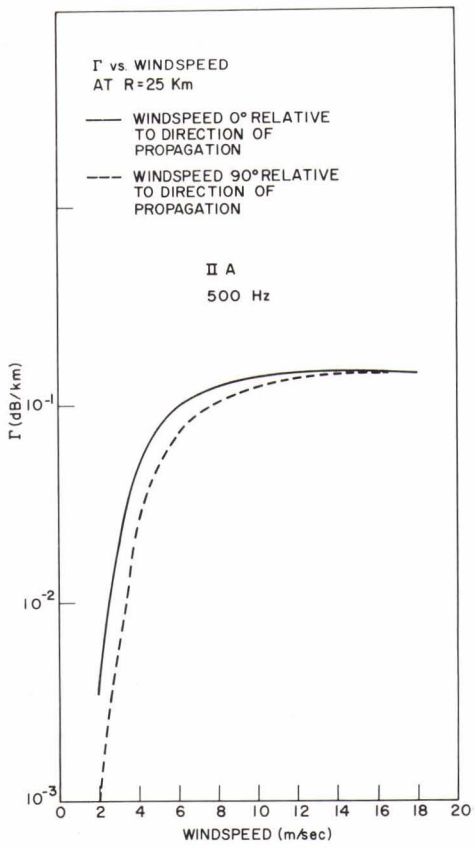

FIG. 8

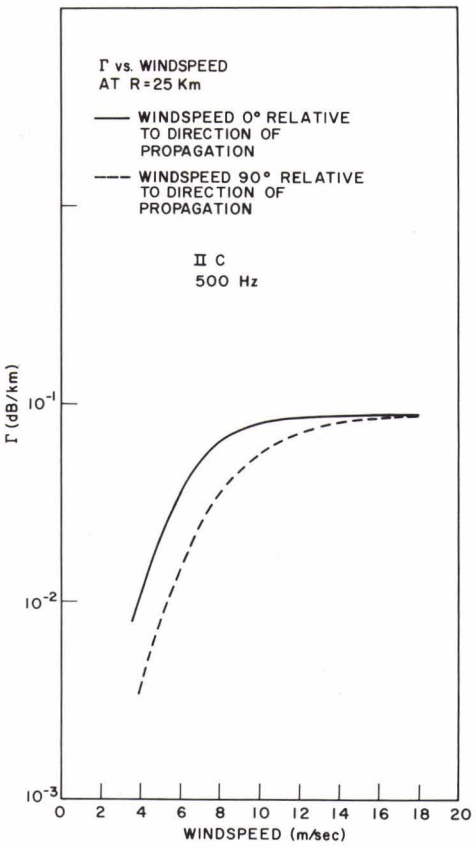

FIG. 9

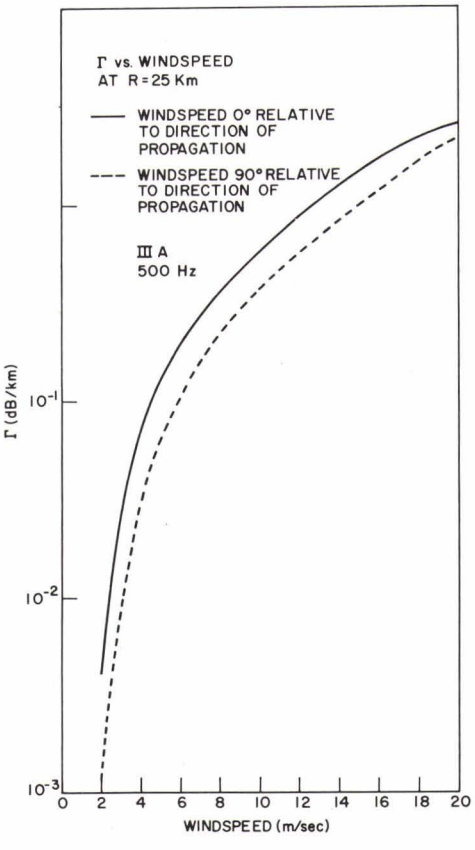

FIG. 10

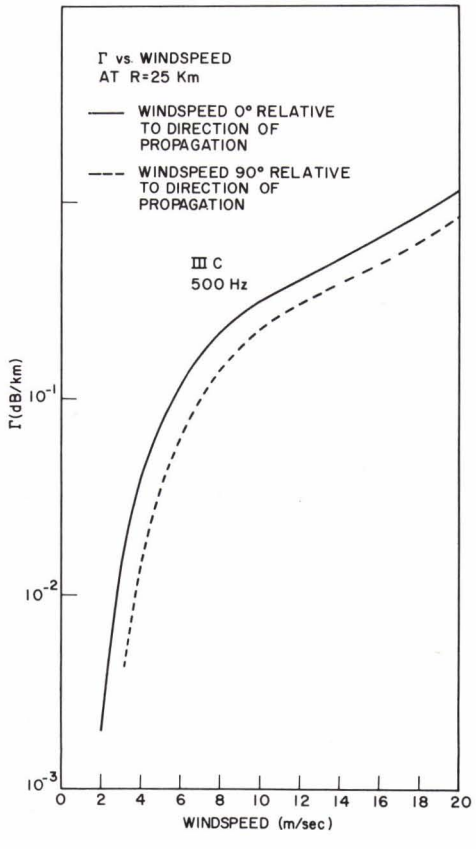

FIG. 11

REFRACTION OF SOUND IN THE SEA FLOOR

by

R. E. Christensen
W. H. Geddes

U.S. Naval Oceanographic Office
Washington, D.C.

Abstract

A major mode of propagation of acoustic energy at low frequencies is a shallow refracted path through unconsolidated sediments of the sea floor. Successful modelling of the bottom-refracted mode of propagation requires knowledge of the sediment thickness, sound velocity, and acoustic attenuation in the sediments. Unconsolidated sediments may be considered an extension of the water column with the acoustic floor of the ocean being the base of the unconsolidated sediments. Observed bottom loss results from two Pacific Ocean sites of differing sediment thickness are discussed. Lower losses noted at the low grazing angles from the thick sediment station are attributed to added acoustic energy that is received from shallow bottom-refracted arrivals. Lower losses noted at the high grazing angles from the thin sediment station, on the other hand, are attributed to added acoustic energy that is received from subbottom reflections occuring at the base of the unconsolidated sediments.

INTRODUCTION

Development of a low frequency acoustic propagation model requires a more complicated physical concept of the sea floor than is required for a high frequency acoustic propagation model. The attenuation of high frequency sound energy in bottom sediments precludes its propagation through the sediments for long distances. However, low frequency acoustic energy can be both reflected at the sea floor boundary (or subbottom boundaries) and refracted through the sediments. Experiments are being conducted by the U.S. Naval Oceanographic Office to study the effects of sediment layering on acoustic propagation results.

Refraction of sound energy through sea floor sediments was first described by Hill (1952). Geophysicists have since used the bottom-refracted arrival as a tool to estimate sound velocity characteristics of bottom sediments. Recently, as more emphasis was placed on long range propagation, acousticians have studied the effect of bottom-refracted arrival on low frequency propagation loss results (Morris, 1970; Hanna, 1973; Christensen, Geddes, and Frank, 1975).

Some of our recent work indicates that considerable low frequency acoustic energy is received by way of shallow bottom-refracted paths through the unconsolidated sediments of the sea floor. In an attempt to test this hypothesis, bottom loss surveys were conducted over areas of various sediment thickness in the eastern North Pacific Ocean. The results from these surveys and the relationship between low frequency bottom loss values and sediment thickness will be discussed in the paper.

DATA COLLECTION AND PROCESSING TECHNIQUES

Two ships were used to obtain quantitative measurements of bottom loss as a function of grazing angle and total propagation loss as a function of horizontal range. The USNS BENT was outfitted as the receiving ship and an AGOR class ship was outfitted as the shooting ship. The receiving ship remained stationary while the shooting ship proceeded along a designated shooting course, dropping about 50 MK 61 SUS sound sources at selected intervals, out to a horizontal range of approximately 30 miles (figure 1). The bottom-returned signal was received by a hydrophone (suspended from the receiving ship), amplified, and recorded broadband on a magnetic tape recorder. The hydrophone was calibrated by the Underwater Sound Reference Division (USRD), Orlando, Florida. An internal calibration, which consists of generating a known voltage through the system, was also incorporated in order to calibrate the remaining components of the acoustic system. During the conduct of the station a sound speed profile was obtained to accurately determine the amount of acoustic energy dispersed due to refraction of the ray paths in the water. Horizontal distances between ships were measured by a ship-to-ship electro-magnetic ranging system. Other pieces of vital information included bathymetry and sub-bottom profiles obtained along the shooting track by the shooting ship.

The magnetic tapes were played back in the laboratory and the data were processed utilizing the Fourier Acoustic Measurement and Analysis System (FAMAS) developed at NAVOCEANO (Hansen, 1975). The main component of this system is a Hewlett-Packard 5451 fourier analyzer. Bottom loss data were computed using

total energy processing techniques by:

$$BL = SL - RL - PL - 6$$

where: BL = Bottom loss in dB,

SL = Source level in dB re 1 erg-sec/cm^2 @ 1 yd.,

RL = Received level in dB, re 1 erg-sec/cm^2 , and

PL = Propagation loss in the water in dB re 1 yd.

In addition to the bottom path, acoustic energy is also received via the surface paths. Since the signal from all four paths were integrated a 6 dB correction was required in the above equation. As a check on the receiving system, values of source levels (SL) were measured independently and compared to historical values (Christian, 1967; Gaspin and Schuler, 1971). Received levels (RL) for a given frequency were calculated by algebraically summing the hydrophone sensitivity level, gain level, and recorded level of the bottom return. The propagation loss term (PL) was obtained from a computer program. Inputs to the bottom loss computer program included values of source level, component values of received level, source depth, receiver depth, water depth, horizontal range, and values of sound velocity as a function of water depth. Outputs from the program included tabulated values of bottom loss versus grazing angle and total propagation loss as function of horizontal range for standard 1/3 octave frequencies from 63 Hz to 3150 Hz. The program also provided plots of the above information. Values of bottom loss and propagation loss for each station are stored on a master digital magnetic tape.

ANALYSIS PROCEDURES

In some of our earlier work (Christensen, Frank, and Geddes, 1975) an arrival was identified at the lower frequencies (20 to 200 Hz) that was not present at the higher frequencies (2000 to 20,000 Hz). We concluded that by treating the unconsolidated sediments of the sea floor as a fluid and considering the sediment sound velcoity as an extension of the water column sound velocity, two basic bottom paths should exist as shown in figure 2. Energy at all frequencies would be expected to be received at point, R, from a source, S, via (A) the bottom-reflected path. In addition, low frequency acoustic energy could be expected to be received via (B) the bottom-refracted path. High frequency acoustic energy could reasonably be expected not to be received via (B) the bottom-refracted path due to high attenuation within the sediments (Hamilton, 1972).

Furthermore, the bottom-refracted path was found to decrease very rapidly with an increase in horizontal range (decrease in grazing angle) between source and receiver. This resulted in rapid decrease in propagation loss (bottom loss) at a range of about 16 kiloyards or 25° bottom grazing angle.

In an effort to further study the effects of the bottom-refracted arrival, two stations were selected on the basis of the thickness of the unconsolidated sediment layers. Selection of initial sites were based on a sediment thickness study preformed by the Lamont-Doherty Geolological Observatory (Ewing, 1968). Refined estimates of thickness were obtained from seismic profiles taken either along the shot run or in the nearby vicinity of the

station. To minimize the effects of bathymetry, stations with similar bottom roughness characteristics were chosen. The stations were also conducted over ares of similar sediments to discount any differences in bottom loss due to differences in sediment type. Piston cores nearby each site were obtained and analyzed. These, along with seismic profiles, were used to tie in long cores obtained by the JOIDES project (McManus, et.al., 1970). Distances between the selected station and JOIDES holes ranged between 100 miles for station A and 170 miles for station B. Sediments at all sites were found to consist of clays and oozes with virtually little or no silt-size or sand-size material.

RESULTS AND DISCUSSION

The results from two stations, stations A and B, are shown in figures 3 through 7. Bathymetric and subbottom profiles along each shot run are shown in figures 3 and 5. Only the subbottom termed "basement" was plotted. Basement as defined here is interpreted to be the base of the unconsolidated sediment layer. All depths are based on water and sediment sound velocities of 4,800 feet per second.

A graph showing bottom loss as a function of grazing angle is shown beneath the bathymetric and subbottom profiles for each station. Bottom loss data at 80 Hz (1/3 octave bandwidth) was selected because it is representative of other low frequency data from 63 Hz to 315 Hz. Selected low frequency (20-300 Hz) traces from Stations A and B are shown in figures 4 and 6, respectively. A summary of bottom loss results for all frequencies is presented in figure 7 where mean values for grazing angle bands of 90°-20° and 20° to 0° are shown. Discussion of figures 3 through 7 follows.

Station A

Station A is located near the seaward edge of a deep-sea fan. Sediments are 1,000 feet thick near the start of the shot run to about 650 feet thick at 45,000 yards horizontal range (figure 3a). The average sediment thickness under the reflecting points of each shot (half the horizontal range) is equal to approximately 900 feet. Sediments from an eight-foot core, obtained 45 miles from the shot run, consist of clays and silty clays (mean grain size from .0009 to .0015 mm. with 78% porosity. The sediments from a 1000-foot JOIDES core, about a 100 miles from station A, were identified as siliceous-fossil ooze and mud.

Bottom loss values at 80 Hz are 8 dB at near-normal incidence (figure 3b) and increase to 11.5 dB at 21° grazing. A marked decrease in bottom loss is noted at 20° grazing angle and values drop to 2.8 dB; from 20° to 5°, bottom values continue to decrease to about 0 dB. The observed rapid decrease of about 9 dB in bottom loss corresponds to the onset of the shallow bottom-refracted arrival noted previously (Christensen, Frank, and Geddes, 1975). The bottom returns from station A were reprocessed using a low frequency wide-band filter (20 Hz to 300 Hz) for purposes of locating the bottom-refracted arrival. Refracted arrivals were identified at grazing angles less than 20° (figure 4). The reflected arrival from the water-sediment interface is designated by the letter "A" and was determined from high frequency oscillographic trace (not shown). As can be seen in the low frequency traces (figure 4), 4), negligible energy is received at the water-sediment interface whereas considerable energy is received from the bottom-refracted

arrival (designated by the letter "B"). Subsequent high amplitude traces are from surface paths of the bottom-refracted arrival (e.g., about 200 and 300 milliseconds at 17.2°).

Station B

Station B is located in the vast abyssal hills province of the eastern North Pacific Ocean. Sediment thicknessess were relatively constant and averaged about 250 feet along the reflecting point portion (0.5 to 2.5 kiloyards) of the shot run (figure 5a). Unfortunately, the nearest piston core is about 450 nautical miles from station B. However, the core is from the abyssal hills region and probably typifies sediment characteristics on the acoustic station. Sediments consist of silty clays with a porosity of 72%. Average sediment sound velocity values, measured along the eight-foot core, average 4938 ft/sec, or 148 ft/sec less than the bottom water sound velocity. The sediment from a JOIDES core located about 170 miles from the station, consists of brown clays with basalt (basement) encountered at 110 feet.

Bottom loss values at 80 Hz (figure 5b) average about 7 dB in the 90° to 40° grazing angle band, and about 5 dB in the 40° to 10° grazing angle band. An increase in bottom loss values is observed at grazing angles less than 10°. Upon comparison with station A (figure 3b), the sharp decrease in bottom loss values noted at grazing angles less than

20° in the station A results does not appear in the station B results. This suggests the absence of the shallow bottom-refracted arrival noted in the bottom returns from Station A. Indeed, the low frequency record traces from the wide-band filter (20 to 300 Hz) showed no indication of refracted arrivals for any of the bottom returns.

However, it should also be noted that the overall bottom loss values from 90° to 20° (figure 5b) for station B are significantly less than bottom loss values over the same grazing angle band for station A. The largest difference is noted from about 50° to 20°, where bottom losses from station B average 5.5 dB less than values obtained from station A. Where the unconsolidated sediments are relatively thin, such as station B, considerable energy at the higher grazing angle is apparently reflected from basement rock. Inspection of the low-frequency (20-300 Hz) records indiates this to be the case. As shown in Figure 6, the dominant arrival from a record trace obtained at 87.2° is not from the water-sediment interface, but occurs from a subbottom reflection occuring 80 milliseconds later. This travel time difference corresponds to time differences between the sediment surface and basement as identified on our seismic records (figure 5b). On the other hand, over areas of relatively thick sediments, such as station A, the basement is too deep to contribute much energy as a subbottom reflector. Consequently, reflections occur predominantly from, or near, the water-sediment interface. Since the sediments have very low sound velocities, high losses near the angle of intromission

would be expected (Kinsler and Frey, 1962). This is the probable explanation for slightly higher losses observed in the 50° to 20° range (figure 5b). Before losses become too high, however, low frequency is received from the bottom-refracted arrival at grazing angles less than 20° as noted earlier.

Bottom Loss Vs. Frequency

Bottom loss values were averaged over two grazing angle bands for comparison of results ranging from 63 Hz to 3150 Hz from the two stations. Mean values for the 90° to 20° grazing angle band are shown in figure 7a; whereas, mean values for the 20° to 0° grazing angle band are shown in figure 7b.

Very little freqeuncy dependency is noted in figure 7a for station A (thick sediment layer). However, for station B (thin sediment layer), an increase of about 2 dB per octave is observed from 3150 Hz to 315 Hz while no frequency dependency is noted between 315 Hz and 63 Hz. Higher standard deviations are noted for station A than station B suggesting a greater grazing angle dependency. This is consistent with our findings at 80 Hz (compare figure 3b with 5b). Even more variability is noted at the higher frequencies (500 Hz to 3150 Hz) which can be attributable to a greater effect of the angle of intromission noted on station A bottom loss results.

In the high and mid-grazing angle bands (figure 7a), slightly higher average losses are observed at the higher frequencies for station B than for station A but significantly lower losses are

noted at the lower frequencies. Greatest differences in mean values occur between 63 Hz and 500 Hz with station B results averaging about 4 dB less than station A. As noted in the discussion at 80 Hz, this decrease in low frequency bottom loss in the 90° to 20° grazing angle band can be attributed to subbottom-refracted energy received from the basement rock.

A decrease in mean bottom loss values in the 0° to 20° grazing angle band (figure 7b) with decreasing frequency is observed on station B with about a 1.5 dB per octave slope. On the other hand, station A shows little frequency dependency between 1,000 and 3150 Hz, but shows a sharp decrease in bottom loss (almost 4 dB per octave) between 1000 Hz and 250 Hz. Below 250 Hz, the slope on station A decreases to about 1.5 dB per octave.

In the 20° to 0° grazing angle band (figure 7b), the opposite results are observed from that shown in the 90° to 20° grazing angle band (figure 7a) for frequencies less than 1250 Hz; that is, station A bottom loss values are lower than station B bottom loss values, throughout the frequency spectrum. Furthermore, the biggest differences occur at the lower frequencies with values ranging from 5 dB at 63 Hz to 3 dB at 315 Hz. This decrease in low frequency bottom loss at the lower grazing angles is attributed to added energy being received via shallow refracted paths through the relatively thick sediment layer of station A.

CONCLUSIONS AND SUMMARY

Over the area of relatively thick unconsolidated sediments (≅ 900 feet thick), the dominant mechanism for returning acoustic energy at the lower grazing angles and lower frequencies is from refractions through the sediment layer. For example, at 80 Hz, bottom loss values in the 20° to 0° grazing angle band averaged 10 dB less than bottom loss values in 50° to 20° grazing angle band. The most dominant effects of the bottom-refracted arrival are observed in the 63 Hz to 315 Hz frequency range.

Over an area of relatively thin layer of unconsolidated sediments (≅ 250 feet thick), the dominant mechanism for returning acoustic energy at all frequencies and grazing angle are reflections from the bottom and subbottoms. Furthermore, considerable energy does seem to be returned via subbottom reflections from basement rock. This is most pronounced at lower frequencies and higher grazing angles. Also, the effects of the bottom-refracted arrival were not observed over the area of thin sediments and virtually no grazing angle dependency was noted throughout the frequency spectrum of 63 Hz to 3150 Hz.

A comparison of low frequency acoustic results from the thin sediment station to results from the thick sediment station shows: (1) lower bottom loss results in the high and mid-grazing angle bands and, (2) higher bottom loss results in the low grazing angle band. For example, in the 90° to 20° grazing angle band, bottom losses averaged 4 dB less for the thin sediment station than for the thick sediment station at frequencies from 63 Hz to 500 Hz. In the 20° to 0° grazing angle band, however, bottom losses averaged 5 to 3 dB more for the thin sediment station than for the thick sediment

station at frequencies from 63 Hz to 315 Hz. The lower losses observed at the higher grazing angles are due to added low frequency energy that is received via subbottom reflections from basement rock. The higher losses observed at the lower grazing angles (when compared to a thick sediment area) occur because no energy is received from shallow bottom-refracted arrivals through the sediment layer. It is concluded that the sediment layer is not thick enough to provide the sound velcoity excess (from the sound velocity gradient within the sediment) to support a bottom-refracted path. The sediment thickness cut-off for the area studied appears to lie between 250 feet and 900 feet, or more accurately, between 0.1 and 0.37 seconds of two-way travel time from the water-sediment interface to the base of the unconsolidated sediments.

More work is required to develop a comprehensive relationship between low frequency bottom loss results and sediment thickness. More sophisticated statistical analyses requiring additional acoustic data may provide greater insight into the problem. Certainly more information on sediment thickness, sediment sound velocities, and attenuation of sound energy through the sediments are needed.

ACKNOWLEDGEMENTS

The authors wish to thank Mr. Luther Little and Mr. Allen Lowrie, of the U.S. Naval Oceanographic Office, for their assistance in the determination of sediment thickness.

REFERENCES

R. E. Christensen, J. A. Frank, and W. H. Geddes, "Low-Frequency Propagation via Shallow Refracted Paths through Deep Ocean Unconsolidated Sediments", J. Acoust. Soc. Am. 57, 1421-1426 (1975).

E. A. Christian, "Source Levels for Deep Underwater Explosions," J. Acous. Soc. Am. 42, 905-908 (1967).

J. Ewing, M. Ewing, T. Aitken, and W. J. Ludwig, "North Pacific Sediment Layers Measured by Seismic Profiling", in The Crust and Upper Mantle of the Pacific Area, Knopoff, Drake and Hart, Am. Geophys. Union Monograph 12, William Byrd Press, 147-173 (1968).

J. B. Gaspin, and V. K. Shuler, "Source Levels of Shallow Under Explosions," Naval Ordnance Laboratory, LTR 71-160 (1971).

E. L. Hamilton, "Compressional-Wave Attenuation in Marine Sediments," Geophys. 37, 620-646 (1972).

J. S. Hanna, "Short-Range Transmission Loss and the Evidence for Bottom-Refracted Energy," J. Acoust. Soc. Am. 53, 1686-1690 (1973).

G. A. Hansen, "FAMAS; Fourier Acoustic Measurement and Analysis System", NAVOCEANO Tech. Note No. 6220-5-75 (unpublished) (1975).

M. N. Hill, "Seismic Refraction Shooting in an Area of the Eastern Atlantic," Phil. Trans, Ray, Soc. London, A, 244, 561-569 (1952).

L. E. Kinsler and A. R. Frey, Fundamentals of Acoustics, J. Wiley and Sons, New York, p. 145 (1962).

D. A. McManus, et. al., Initial Reports of the Deep Sea Drilling Projects, Washington, D.C. (U.S. Government Printing Office), Vol. V, (1970).

H. E. Morris, "Bottom-Reflection-Loss Model with a Velocity Gradient," J. Acoust. Soc. Am. 48, 1198-1202 (1970).

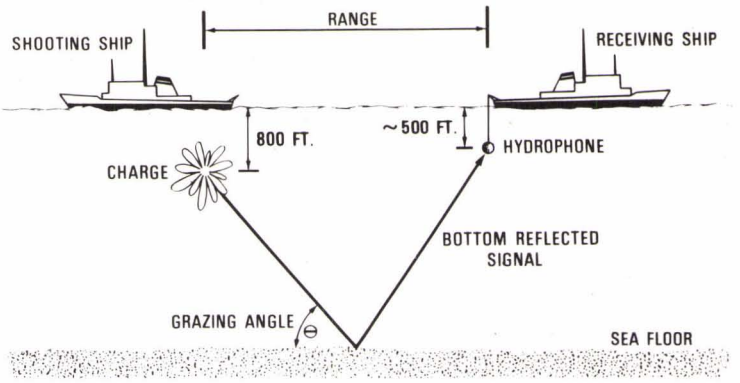

FIG. 1
GEOMETRY OF AT-SEA EXPERIMENT

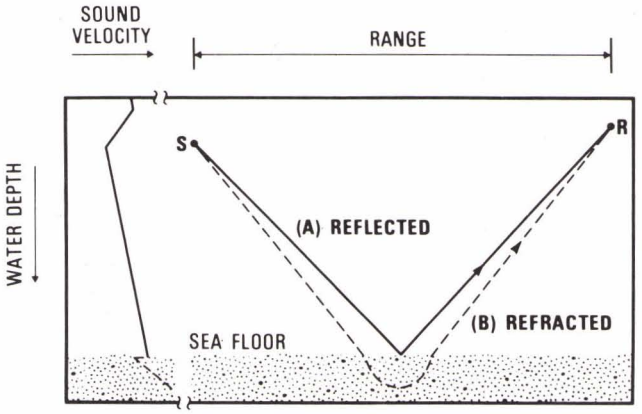

FIG. 2
SCHEMATIC SHOWING (A) THE BOTTOM-REFLECTED ARRIVAL AND (B) THE BOTTOM-REFRACTED ARRIVAL BASED ON A COMBINED WATER-SEDIMENT SOUND VELOCITY PROFILE

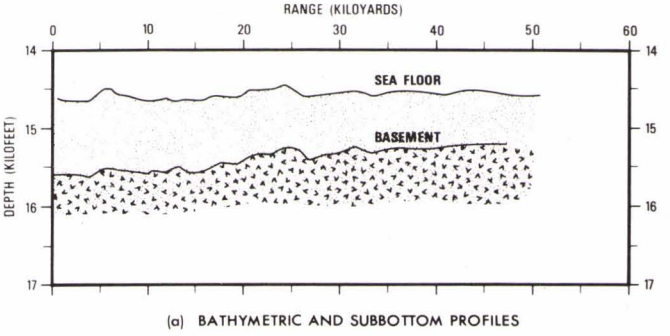

(a) BATHYMETRIC AND SUBBOTTOM PROFILES

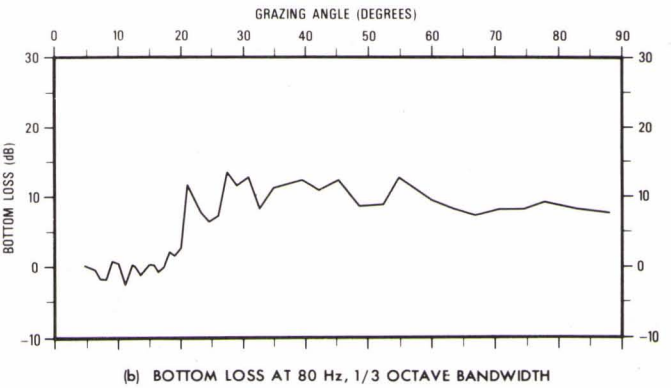

(b) BOTTOM LOSS AT 80 Hz, 1/3 OCTAVE BANDWIDTH

FIG. 3
ACOUSTIC RESULTS ON STATION A.
NOTE THE RELATIVELY THICK LAYER OF UNCONSOLIDATED SEDIMENT ALONG SHOT RUN (a).

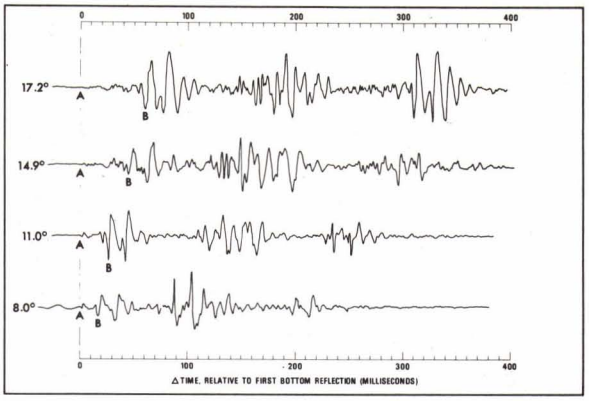

FIG. 4
REPRODUCTION OF LOW FREQUENCY (20–200 Hz) OSCILLOGRAPHIC TRACES FROM FOUR SHOTS AT VARIOUS GRAZING ANGLES (θ) ON STATION A. FIRST BOTTOM-REFLECTED ARRIVAL IS NOTED BY THE LETTER "A" AND THE BOTTOM-REFRACTED ARRIVAL IS NOTED BT THE LETTER "B"

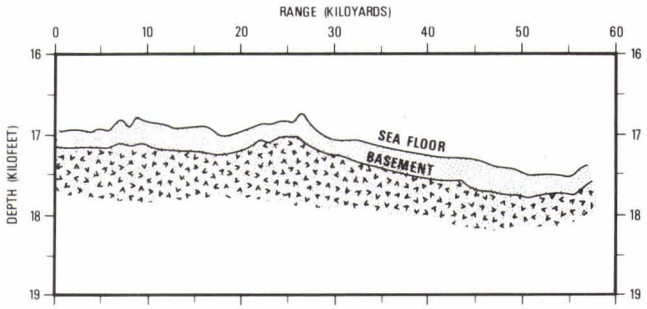

(a) BATHYMETRIC AND SUBBOTTOM PROFILES

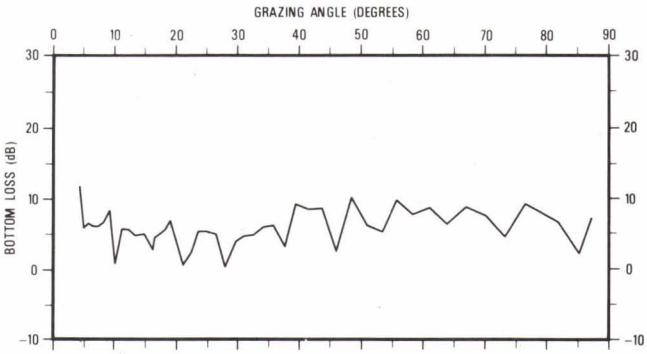

(b) BOTTOM LOSS AT 80 Hz, 1/3 OCTAVE BANDWIDTH

FIG 5
ACOUSTIC RESULTS ON STATION B. NOTE THE RELATIVELY THIN LAYER OF UNCONSOLIDATED SEDIMENT ALONG SHOT RUN (a)

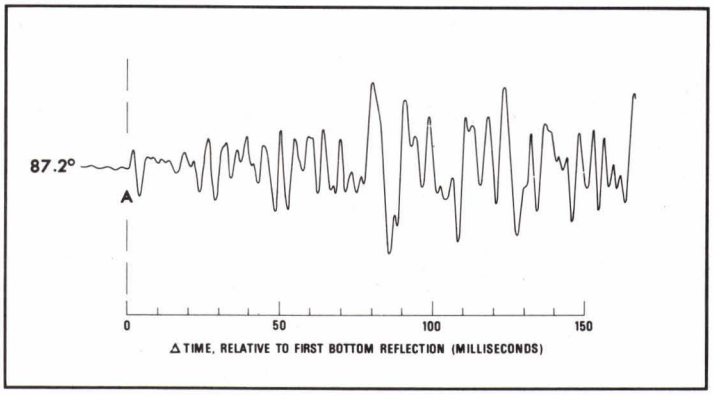

FIG. 6
REPRODUCTION OF LOW FREQUENCY (20–300 Hz) OSCILLOGRAPHIC TRACE FROM A NEAR-NORMAL INCIDENCE SHOT ON STATION B. NOTE THAT THE MAXIMUM ARRIVAL APPEARS 80 MILLISECONDS AFTER THE FIRST BOTTOM-REFLECTED ARRIVAL (DESIGNATED BY THE LETTER "A")

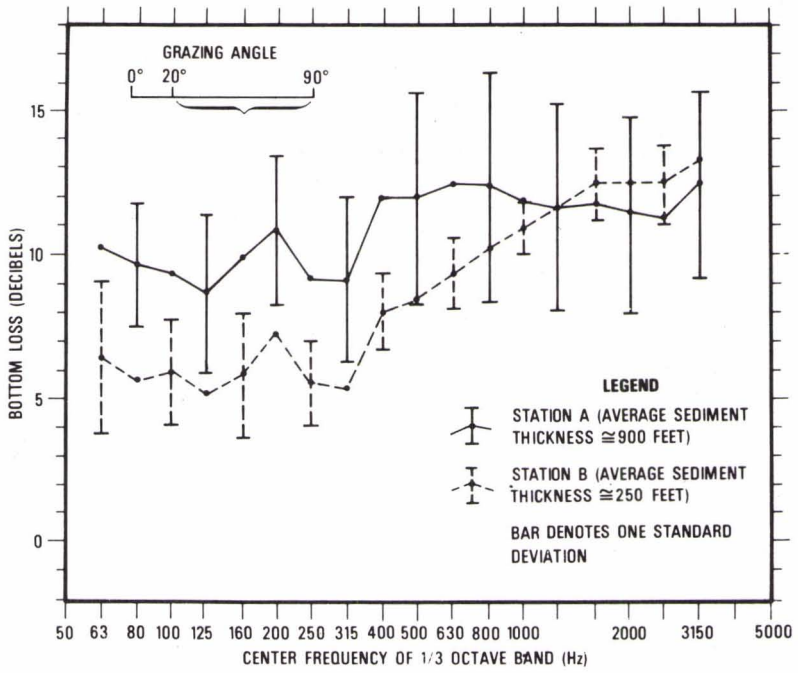

FIG. 7 (a) COMPARISON OF STATIONS A AND B SHOWING FREQUENCY VERSUS MEAN BOTTOM LOSS IN A 20 TO 90 GRAZING ANGLE BAND

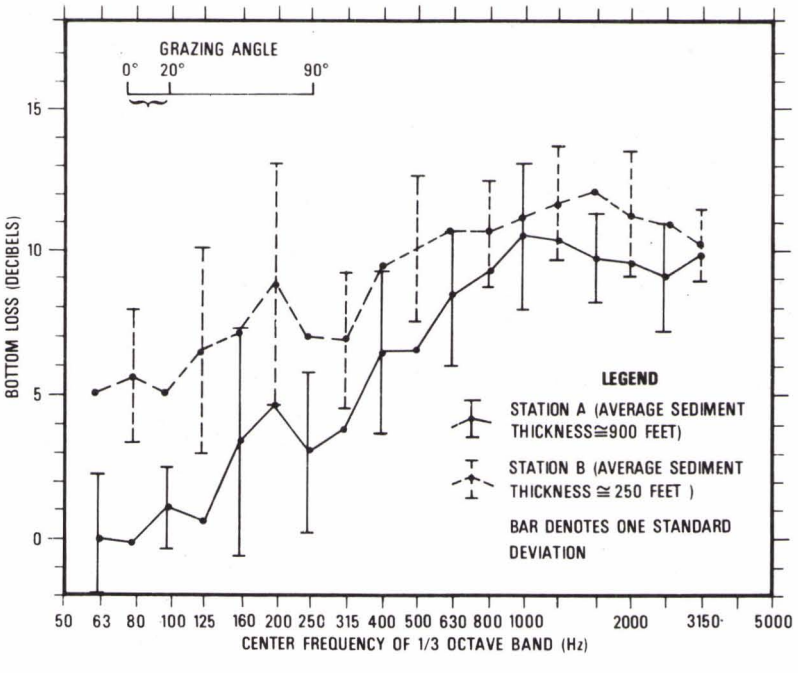

FIG. 7 (b) COMPARISON OF STATIONS A AND B SHOWING FREQUENCY VERSUS MEAN BOTTOM LOSS IN A 0 TO 20 GRAZING ANGLE BAND

SCATTERING FROM A RANDOM INTERFACE

by

John A. DeSanto
Naval Research Laboratory
Washington, D.C.
and
Admiralty Research Laboratory
Teddington, England, U.K.

ABSTRACT

The problem of scattering from a random interface separating two fluids with different densities and sound speeds is considered. The method is to write coupled integral equations in coordinate space connecting the surface and volume values of the Green's function for the deterministic problem. In Fourier transform space the equations simplify, and it is possible to write a single integral equation for the Fourier transform of the surface value of the Green's function. Feynman-diagram methods can be used to aid the construction of both the Dyson equation for the mean of this Green's function and the Bethe-Salpeter equation for the mean of its second moment. These are derived assuming a Gaussian distribution of surface heights and using the accompanying cluster decomposition. As an example, a simple integral equation for the scattering amplitude corresponding to multiple scattering using the Kirchhoff approximation is also derived. It is analogous to the smoothing approximation used in random volume scattering theory. Its numerical solution for the special case of a Neumann surface is presented and, for large values of the Rayleigh roughness parameter, yields more coherent specular intensity than the Kirchhoff approximation. Other examples and the relation of our formalism to other methods are also discussed. In the limiting cases the general formalism reduces to the standard results. In particular, in the flat surface limit we get the result in Officer's book.

1. Introduction and Notation

We describe the scattering of a scalar wave from a random two fluid interface in Fig. 1. Regions V_1 and V_2 are semi-infinite fluids with sound speeds, wavenumbers, and densities given by c_1, k_1, ρ_1 and c_2, k_2, ρ_2 respectively. Coordinate three-vectors are specified by $\underset{\sim}{x} = (x,y,z) = (x_\perp, z)$ and the random interface by $z = h(x_\perp)$. The latter is assumed to be a Gaussian distributed random variable. A three-vector on the surface is $\underset{\sim}{x}_s = (x_\perp, h(x_\perp))$. The method is to derive integral equations for the Green's function of the problem, which is composed of two parts, G_1 defined in V_1, and G_2 defined in V_2. They satisfy the equations ($x \in V_j$)

$$(\partial_m \partial_m + k_{1,2}^2) G_{1,2}(\underset{\sim}{x}, \underset{\sim}{x}'') = -\delta(\underset{\sim}{x} - \underset{\sim}{x}'') \tag{1}$$

where $\partial_m = \partial/\partial x_m$ is the derivative (repeated subscripts are summed from 1 to 3), appropriate radiation conditions for large $|\underset{\sim}{x}|$, and continuity conditions at the interface. The free-space Green's functions $G_j^{o\pm}(\underset{\sim}{x}, \underset{\sim}{x}'')$ ($j = 1,2$) satisfy similar equations except that $\underset{\sim}{x}$ is in all space. Explicitly they are

$$G_j^{o\pm}(\underset{\sim}{x}, \underset{\sim}{x}'') = [4\pi|\underset{\sim}{x}-\underset{\sim}{x}''|]^{-1} \exp[\pm ik_j|\underset{\sim}{x}-\underset{\sim}{x}''|] \tag{2}$$

where the $\pm$ indicate the radiation condition. We now drop this $\pm$ notation for simplicity, resurrecting it only when necessary.

Next, apply Green's theorem to G_1 and G_2^o in V_1 and to G_2 and G_2^o in V_2, that is use the same free space Green's function in both regions. The results are evaluated in V_1 and combined to yield

$$\begin{aligned} &G_1(\underset{\sim}{x}', \underset{\sim}{x}'')\theta(z' - h(x_\perp')) \\ &= G_2^o(\underset{\sim}{x}', \underset{\sim}{x}'') + (k_1^2 - k_2^2)\int G_2^o(\underset{\sim}{x}', \underset{\sim}{x}) G_1(\underset{\sim}{x}, \underset{\sim}{x}'')\theta(z - h(x_\perp))\, d\underset{\sim}{x} \\ &\quad + \int \partial_m' G_2^o(\underset{\sim}{x}', \underset{\sim}{x}_s) n_m(x_\perp) [G_2(\underset{\sim}{x}_s, \underset{\sim}{x}'') - G_1(\underset{\sim}{x}_s, \underset{\sim}{x}'')]\, dx_\perp \end{aligned} \tag{3}$$

where the step function

$$\theta(z - h(x_\perp)) = \begin{cases} 1 & z > h(x_\perp) \\ 0 & z < h(x_\perp) \end{cases} \tag{4}$$

is used to explicitly indicate the discontinuous nature of the l.h.s. of (3), and the normal is $n_m(x_\perp) = \delta_{m3} - \partial_{m\perp} h(x_\perp)$ with δ_{m3} the Kronecker delta. In order to derive (3) we have used a continuity condition on the normal derivative of the Green's function

$$\partial_m G_2(\underset{\sim}{x}_s, \underset{\sim}{x}'') n_m(x_\perp) = \partial_m G_1(\underset{\sim}{x}_s, \underset{\sim}{x}'') n_m(x_\perp). \tag{5}$$

A further continuity condition is necessary on the Green's function and we express it generally as

$$G_2(\underset{\sim}{x}_s, \underset{\sim}{x}'') = a(x_\perp) G_1(\underset{\sim}{x}_s, \underset{\sim}{x}'') \tag{6}$$

The explicit form for a is derived from the flat surface limit of the theory in the Appendix and it is shown to be a constant. For the moment we keep it general.

Using (6) in (4), defining the "field" Green's function G_1^D and the "surface" Green's function G^S as

$$G_1^D(\underset{\sim}{x}, \underset{\sim}{x}'') = G_1(\underset{\sim}{x}, \underset{\sim}{x}'') \theta(z - h(x_\perp)) \tag{7}$$

$$G^S(\underset{\sim}{x}_s, \underset{\sim}{x}'') = 1/2\,[1 + a(x_\perp)]\, G_1(\underset{\sim}{x}_s, \underset{\sim}{x}'') \tag{8}$$

yields the result

$$G_1^D(\underset{\sim}{x}', \underset{\sim}{x}'') = G_2^o(\underset{\sim}{x}', \underset{\sim}{x}'') + (k_1^2 - k_2^2) \int G_2^o(\underset{\sim}{x}', \underset{\sim}{x}) G_1^D(\underset{\sim}{x}, \underset{\sim}{x}'') d\underset{\sim}{x} \tag{9}$$

$$-2 \int \partial'_m G_2^o(\underset{\sim}{x}', \underset{\sim}{x}_s) n_m(x_\perp) r(x_\perp) G^s(\underset{\sim}{x}_s, \underset{\sim}{x}'') dx_\perp$$

with

$$r(x_\perp) = [1 - a(x_\perp)] / [1 + a(x_\perp)] . \tag{10}$$

Letting $\underset{\sim}{x}' \to \underset{\sim}{x}'_s$ through positive z' values in (9) yields

$$G^s(\underset{\sim}{x}_s', \underset{\sim}{x}'') = G_2^o(\underset{\sim}{x}_s', \underset{\sim}{x}'')+(k_1^2-k_2^2)\int G_2^o(\underset{\sim}{x}_s', \underset{\sim}{x})G_1^D(\underset{\sim}{x}, \underset{\sim}{x}'')d\underset{\sim}{x} \qquad (11)$$

$$- \int P_m^{(2)}(\underset{\sim}{x}_s', \underset{\sim}{x}_s)n_m(x_\perp)r(x_\perp)G^s(\underset{\sim}{x}_s, \underset{\sim}{x}'')dx_\perp$$

where

$$P_m^{(2)}(\underset{\sim}{x}_s', \underset{\sim}{x}_s) = (2\pi)^{-3}\int d\underset{\sim}{k} \exp\left[i\underset{\sim}{k}\cdot(\underset{\sim}{x}_s'-\underset{\sim}{x}_s)\right] G_2^o(k)\ P_m^{(2)}(\underset{\sim}{k}) \qquad (12)$$

With $G_2^o(k)$ the Fourier transform of $G_2^o(x)$ and

$$P_m^{(2)}(\underset{\sim}{k}) = 2i\left\{ k_{m\perp} + \delta_{m3}P\ \frac{k_2^2 - k_\perp^2}{k_z} \right\} . \qquad (13)$$

Here P in (13) stands for the Cauchy principle value. These functions were previously calculated when we discussed scattering from a random Neumann surface[1]. Equations (9) and (11) can be thought of as coupled surface-volume integral equations for the Green's function of the problem. Their utility is realised under Fourier transformation.

2. Fourier Transformation

Introducing Fourier transforms of the form

$$G_1^D(\underset{\sim}{x}', \underset{\sim}{x}'') = (2\pi)^{-6}\iint d\underset{\sim}{k}'d\underset{\sim}{k}''\exp\left\{ i(\underset{\sim}{k}'\cdot\underset{\sim}{x}' - \underset{\sim}{k}''\cdot\underset{\sim}{x}'')\right\} G_1^D(\underset{\sim}{k}', \underset{\sim}{k}'') \qquad (14)$$

and analogous functions for G^s and G_2^o in (9) and (11), then setting the resulting integrands to zero using a gauge condition argument previously discussed[1] yields two equations which can be combined. The most elegent way to define the result is to first define singularity free Green's functions Γ_1^D and Γ^s via

$$G_1^{D,S}(\underset{\sim}{k}',\underset{\sim}{k}'') = (2\pi)^3\,\delta(\underset{\sim}{k}'-\underset{\sim}{k}'')\ G_1^o(k')$$

$$+ (2\pi)^3 G_1^o(k')\ \Gamma_1^{D,S}(\underset{\sim}{k}', \underset{\sim}{k}'')\ G_1^o(k'') \qquad (15)$$

Note that we now have G_1^o rather than G_2^o occurring. This arises naturally from the algebra. Then we can derive an integral relation for Γ_1^D

$$\Gamma_1^D(\underset{\sim}{k}',\underset{\sim}{k}'') = B^o(\underset{\sim}{k}',\underset{\sim}{k}'') + \int B^o(\underset{\sim}{k}', \underset{\sim}{k})G_1^o(k)\,\Gamma^s(\underset{\sim}{k}, \underset{\sim}{k}'')d\underset{\sim}{k} \tag{16}$$

where

$$B^o(\underset{\sim}{k}',\underset{\sim}{k}'') = -2i(2\pi)^{-3}k_m' r_m(\underset{\sim}{k}' - \underset{\sim}{k}'') \tag{17}$$

and

$$r_m(\underset{\sim}{k}) = \int \exp(-i\underset{\sim}{k}\cdot\underset{\sim}{x}_s)n_m(x_\perp)r(x_\perp)dx_\perp, \tag{18}$$

and an integral equation for Γ^s

$$\Gamma^s(\underset{\sim}{k}',\underset{\sim}{k}'') = W(\underset{\sim}{k}', \underset{\sim}{k}'') + \int W(\underset{\sim}{k}', \underset{\sim}{k})G_1^o(k)\Gamma^s(\underset{\sim}{k}, \underset{\sim}{k}'')d\underset{\sim}{k} \tag{19}$$

where

$$W(\underset{\sim}{k}',\underset{\sim}{k}'') = V_m(\underset{\sim}{k}')r_m(\underset{\sim}{k}' - \underset{\sim}{k}'') \tag{20}$$

and

$$V_m(\underset{\sim}{k}) = -\frac{2i}{(2\pi)^3}G_2^o(k)\left\{(k_1^2-k_2^2)k_m+(k^2-k_1^2)\left[k_{m\perp} + \delta_{m3}P\ \frac{k_2^2-k_\perp^2}{k_z}\right]\right\} \tag{21}$$

Note that if we set $k_2^2 - k_\perp^2 = k_z^2$ in the principle value part of (21) (called the "on-shell" or "0" condition) then

$$V_m(\underset{\sim}{k}')\Big|_o = k_m' \tag{22}$$

so that

$$\Gamma^s(\underset{\sim}{k}', \underset{\sim}{k}'')\Big|_o = \Gamma_1^D(\underset{\sim}{k}', \underset{\sim}{k}'') \tag{23}$$

Hence we have an integral equation for Γ^s and an algebraic procedure for calculating Γ_1^D from it. The latter is intimately related to scattering as we point out in the next section. Our results here reduce to the analogous results for the Neumann problem[1] when $r(x_\perp) = 1$ and $k_1 = k_2$.

3. Reduction

To point out the relation between Γ_1^D and the scattering problem we note that we can write the outgoing scattered field ψ^o in terms of the incident field ψ^i by using the Fourier transform of the Γ_1^D part of (15). The result is

$$\psi^o(\underset{\sim}{x}') = (2\pi)^3 \iint G_1^o(\underset{\sim}{x}', \underset{\sim}{x}_1)\, \Gamma_1^D(\underset{\sim}{x}_1, \underset{\sim}{x}_2)\, \psi^i(\underset{\sim}{x}_2)\, d\underset{\sim}{x}_1\, d\underset{\sim}{x}_2 \tag{24}$$

Each of these fields can be further decomposed into plane wave fields ϕ^o and ϕ^i via

$$\psi^o(\underset{\sim}{x}) = \int \exp(i\underset{\sim}{k}\cdot\underset{\sim}{x})\phi^o(k_\perp)\, dk_\perp \qquad k_z = (k_1^2 - k_\perp^2)^{\frac{1}{2}} = K_1 \tag{25}$$

$$\psi^i(\underset{\sim}{x}) = \int \exp(i\underset{\sim}{k}\cdot\underset{\sim}{x})\phi^i(k_\perp)\, dk_\perp \qquad k_z = -K_1 \tag{26}$$

and the plane wave fields related via

$$\phi^{o+}(k_\perp) = \int T(k_\perp, k_\perp')\phi^{i+}(k_\perp')\, dk_\perp' \tag{27}$$

where

$$T(k_\perp, k_\perp') = \left\{(\pi i/k_z)\, \Gamma_1^{D+}(\underset{\sim}{k}, \underset{\sim}{k}')\right\}\Bigg|_{\substack{k_z = K_1 \\ k_z' = -K_1'}} \tag{28}$$

The various conditions on the z-components of the wave numbers describe asymptotic conditions necessary to ensure that we have appropriate incoming and outgoing waves. It is interesting and useful to note that, using these conditions, we can again algebraically relate Γ_1^D and Γ^s

$$\Gamma_1^{D+}(\underset{\sim}{k}, \underset{\sim}{k}') = \Gamma^s(\underset{\sim}{k}, \underset{\sim}{k}') \quad \text{if } k_z = K_1 \text{ , } k_z' = -K_1' \tag{29}$$

Similarly complex conjugate fields can be defined and the scattered intensity $I(k_\perp)$ given by

$$I(k_\perp)\delta(k_\perp - k_\perp') = \phi^{o+}(k_\perp)\left\{\phi^{o+}(k_\perp')\right\}^*$$

$$= (\pi^2/K_1^2)\int \Gamma^{s+}(k_\perp, K_1;\ k_\perp'', -K_1'')\,\phi^{i+}(k_\perp'')dk_\perp''.$$

$$\int \left\{\Gamma^{s+}(k_\perp', K_1';\ k_\perp''', -K_1''')\,\phi^{i+}(k_\perp''')\right\}^* dk_\perp''' \qquad (30)$$

For single plane wave incidence

$$\phi^i(k_\perp) = \delta(k_\perp - k_\perp^i) \qquad (31)$$

(30) considerably simplifies. Note that we've used the functions Γ^s in the calculations via (29).

4. Random Surface

Up to now we have been describing a deterministic problem. In this section we write down the integral equations for the first two moments of Γ^s without going into detail about their derivation. Details can be found in the references. We consider the surface to be Gaussian distributed. Note that the only place $h(x_\perp)$ occurs explicitly in (19) is in the r_m integral which is part of the function W. Integration of r_m by parts reduces the problem to taking the ensemble average of an exponential function. If we were to write an iterative solution of (19), then take the ensemble of the result term by term and resum the result it is necessary to consider ensemble averages of products of the r_m. This can be simplified using the characteristic function

$$\left\langle \prod_{j=1}^{n} \exp\left[-ik_z^{(j)} h(x_\perp^{(j)})\right] \right\rangle$$

$$= \exp\left\{ -\tfrac{1}{2}\gamma(0) \sum_{j=1}^{n}\left[k_z^{(j)}\right] - \sum_{\substack{i,j=1 \\ i<j}}^{n} \gamma(x_\perp^{(i)} - x_\perp^{(j)} k_z^{(i)} k_z^{(j)}) \right\} \qquad (33)$$

where

$$\gamma(x_{\perp}^{(i)} - x_{\perp}^{(j)}) = \langle h(x_{\perp}^{(i)})\, h(x_{\perp}^{(j)}) \rangle \tag{34}$$

is the two-point correlation function. Equation (33) follows from Gaussian statistics. In addition the products of r_m are cluster decomposed using methods previously discussed[1,2].

Using these properties we can write the integral equation for the first moment of Γ^s, the Dyson equation, as

$$\langle \Gamma^{s+}(\underset{\sim}{k}', \underset{\sim}{k}'') \rangle = M(\underset{\sim}{k}', \underset{\sim}{k}'') + \int M(\underset{\sim}{k}', \underset{\sim}{k})\, G_1^{o+}(k) \langle \Gamma^{s+}(\underset{\sim}{k}, \underset{\sim}{k}'') \rangle \, d\underset{\sim}{k} \tag{35}$$

where the function M is called the mass operator in analogy with random volume scattering theory[3]. Although three-dimensional, the integral equation (35) appears simple. This is deceiving since M is an infinite series of successively more complicated terms involving multiple integrals. It cannot be summed, although each term can be formally written down quite easily using diagram techniques.[1,3] Solutions for this first moment describe coherent scattering.

The integral equation for the second moment is a Bethe-Salpeter type equation and is

$$\begin{aligned}
&\langle \Gamma^{s+}(\underset{\sim}{k}, \underset{\sim}{k}_a)\, \Gamma^{s-}(\underset{\sim}{k}', \underset{\sim}{k}_a') \rangle \\
&\quad = \langle \Gamma^{s+}(\underset{\sim}{k}, \underset{\sim}{k}_a) \rangle \langle \Gamma^{s-}(\underset{\sim}{k}', \underset{\sim}{k}_a') \rangle + L(\underset{\sim}{k}, \underset{\sim}{k}_a;\ \underset{\sim}{k}', \underset{\sim}{k}_a') \\
&\quad + \int L(\underset{\sim}{k}, \underset{\sim}{k}'';\ \underset{\sim}{k}', \underset{\sim}{k}_a') G_1^{o+}(k'')\ \Gamma^{s+}(\underset{\sim}{k}'', \underset{\sim}{k}_a)\ d\underset{\sim}{k}'' \\
&\quad + \int L(\underset{\sim}{k}, \underset{\sim}{k}_a;\ \underset{\sim}{k}', \underset{\sim}{k}'')\, G_1^{o-}(k'')\ \Gamma^{s-}(\underset{\sim}{k}'', \underset{\sim}{k}_a')\ d\underset{\sim}{k}'' \\
&\quad + \iint L(\underset{\sim}{k}, \underset{\sim}{k}'';\ \underset{\sim}{k}', \underset{\sim}{k}''') G_1^{o+}(k'') G_1^{o-}(k''') \cdot \\
&\qquad \cdot \langle \Gamma^{s+}(\underset{\sim}{k}', \underset{\sim}{k}_a)\, \Gamma^{s-}(\underset{\sim}{k}''', \underset{\sim}{k}_a') \rangle \, d\underset{\sim}{k}''\, d\underset{\sim}{k}'''
\end{aligned} \tag{36}$$

Where the intensity operator L is again an infinite series of terms also most easily written down using diagram techniques. The solution of (36) yields the incoherent intensity. Writing down higher order moment equations is also possible.

We have presented the above as examples of what can be done using this general method of approach. The problem can be considered formally in a very straightforward way. But the general cases of (35) and (36) are too complicated to be solved as yet. What is available however is a simple example of (35) which can be solved. If we approximate M as the first term in its series expansion it is possible to write an approximation to the coherent specular intensity for plane wave incidence (at angle θ_i) as

$$I_C(k_\perp) = R^2(\rho, N, \theta_i) \left| V^+(Ki, -Ki) \right|^2 \delta(k_\perp - ki_\perp) \tag{37}$$

where

$$\begin{aligned} \rho &= \rho_1/\rho_2 \\ N &= k_1/k_2 \\ ki &= k_1 \sin\theta_i \\ Ki &= (k_1^2 - k_\perp^{i2})^{\frac{1}{2}} \end{aligned} \tag{38}$$

and where R is the plane wave reflection coefficient (see the Appendix)

$$R(\rho, N, \theta_i) = \frac{(1 - N^2\sin^2\theta_i)^{\frac{1}{2}} - \rho\cos\theta_i}{(1 - N^2\sin^2\theta_i)^{\frac{1}{2}} + \rho\cos\theta_i} \tag{39}$$

Here V^+ satisfies a one-dimensional integral equation of the form

$$T^+(\xi', \xi'') = C_0(\xi' - \xi'') \tag{40}$$

$$+ \frac{R(\rho, N, \theta_i)}{\pi i} \int_{-\infty}^{\infty} \frac{C_0(\xi' - \xi)}{\xi^2 - 1 - i\epsilon} P\left(\frac{1}{\xi}\right) T^+(\xi, \xi'')\, d\xi$$

where $$C_0(\xi) = \exp(-\tfrac{1}{2}\xi^2\Sigma^2) \tag{41}$$

and $$\Sigma = k_1\sigma \cos\theta_i \tag{42}$$

with σ is the rms height of the surface, Σ the Rayleigh roughness parameter, and the definition

$$V^+(K^i\xi, -K^i\xi') = T^+(\xi, \xi') \tag{43}$$

If we further approximate V^+ by the C_0 term in (40) we get the Kirchhoff result. The full equation (41) can be interpreted as a lowest order (in the mass operator) multiple Kirchhoff expansion. Numerical solutions of (41) for the Neumann surface ($R = 1$) have been presented[4] and are shown in Fig. 2. For $\Sigma < 1$ the result agrees with the Kirchhoff approximation but for $\Sigma > 1$ the multiple scattering yields more coherent specular intensity than that expected from the Kirchhoff result. This effect has been experimentally observed in diverse scattering problems and explained using various theoretical models.[5] A comparison of our results with others will be discussed elsewhere.[6]

5. Summary

We have presented rather briefly an outline of our method of approach to scattering from a random interface. It is based on using only a single free-space Green's function in deriving the coordinate-space integral equations, the use of Fourier transform methods, and cluster decomposition methods similar to those used in statistical mechanics. Once the general method is understood it is straightforward to write down moment equations as in Sec. 4. A program to investigate the general properties of these equations as well as numerical solutions of specific examples is under way. Early results indicate the necessity of considering multiple scattering in problems of this type.

Appendix - Flat Surface Limit

We have already pointed out that the formalism reduces to the Neumann case when $r(x_\perp) = 1$, but have not shown how to derive $r(x_\perp)$, or equivalently $a(x_\perp)$, which we used in the boundary condition (6). We do this here. For a flat surface, $h(x_\perp) = 0$, and

$$r_m(\underset{\sim}{k}) = \delta_{m3}\,\tilde{r}\,(k_\perp) \tag{A.1}$$

where $$\tilde{r}(k_\perp) = \int dx_\perp \exp(-ik_\perp \cdot x_\perp) r(x_\perp) \tag{A.2}$$

and thus $$W(\underset{\sim}{k}', \underset{\sim}{k}'') = V_3(\underset{\sim}{k}')\,\tilde{r}\,(k_\perp' - k_\perp''). \tag{A.3}$$

Substituting (A.3) into (19) it is easy to show that

$$\Gamma^s(\underset{\sim}{k}', \underset{\sim}{k}'') = V_3(\underset{\sim}{k}')\,\tilde{r}\,(k_\perp' - k_\perp''). \tag{A.4}$$

Similarly (16) yields

$$\Gamma_1^D(\underset{\sim}{k}', \underset{\sim}{k}'') = -2i(2\pi)^{-3} k_z'\,\tilde{r}\,(k_\perp' - k_\perp'') \tag{A.5}$$

for a flat surface. Substituting (A.5) into (15), Fourier transforming the result, carrying out the integrals and defining

$$\tilde{r}(k_\perp' - k_\perp'') = (2\pi)^2 \delta(k_\perp' - k_\perp'') R(k_\perp') \tag{A.6}$$

where $R(k_\perp)$ is the same plane wave reflection coefficient defined in (39), yields the result

$$G_1^D(\underset{\sim}{x}', \underset{\sim}{x}'') = (2\pi)^{-2} \int \exp\left\{ik_\perp' \cdot (x_\perp' - x_\perp'')\right\} G_1(z', z'')\,dk' \tag{A.7}$$

$$G_1(z', z'') = \frac{\exp(iK_1' z'')}{-2iK_1'} \left[\exp(-iK_1' z') + R(k_\perp)\exp(iK_1' z')\right] \tag{A.8}$$

which is the one-dimensional Green's function for the flat interface. Similarly, results can be derived for the transmitted field. If we set $k_\perp'' = 0$ in (A.6) we can solve for $\tilde{r}(k_\perp)$, $r(x_\perp)$ by Fourier inversion using (A.2), and hence $a(x_\perp)$ to yield

$$a(x_\perp) = \rho_1/\rho_2 \qquad (A.9)$$

just the ratio of densities of the two media. Thus starting with a general form for a we are led to a coordinate independent result via the flat surface limit. Several equations in the paper are thus simplified.

Footnotes

1. G. G. Zipfel and J. A. De Santo - J Math Phys 13, 1903 (1972)
2. K. Huang, Statistical Mechanics (Wiley, N.Y., 1963) Chap. 14
3. U. Frisch, "Wave Propagation in Random Media", in Probabilistic Methods in Applied Mathematics, ed by A T Bharucha-Reid (Academic, N.Y., 1968)
4. J. A. DeSanto and O. Shisha - J Comp Phys 15, 286 (1974) and J. A. DeSanto, J Acoust Soc Am 57S, 17(1975)
5. See, for example; C. S. Clay, H. Medwin and W. M. Wright - J Acoust Soc Am 53, 1677 (1973), M. L. Boyd and R. L. Deavenport - J Acoust Soc Am 53, 791 (1973), H. Medwin, R. A. Helbig and J. D. Hagy - J Acoust Soc Am 54, 99(1973), P. J. Lynch and R. J. Wagner - J Math Phys 11, 3032 (1971) and W. A. Kuperman, "Attenuation From Boundary Scattering In Shallow Waters", in Sound Propagation in Shallow Water II. Unclassified Papers, SACLANTCEN Conf Proc No 14 (15 Nov 1974)
6. J. A. DeSanto - "Multiple Scattering From a Random Interface", Invited Paper for Special Underwater Acoustics Session on Scattering From Rough Surfaces, Acoustical Society of America, San Francisco meeting, 4-7 November 1975

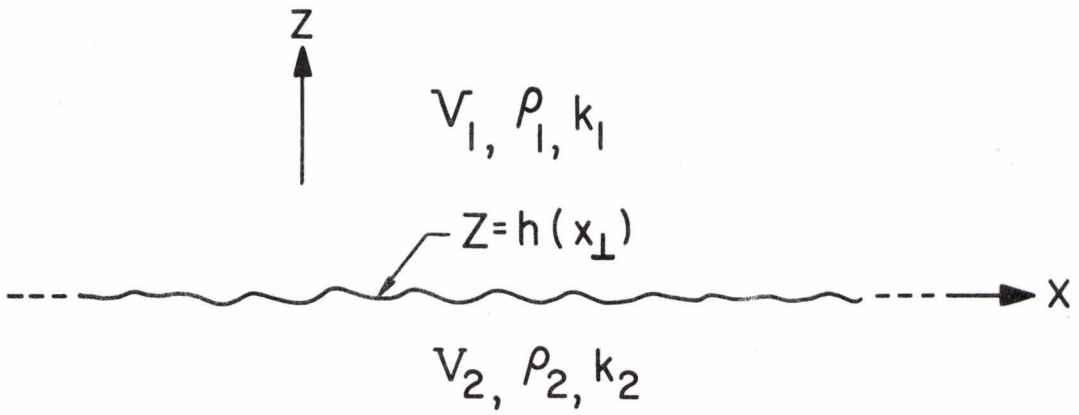

FIG. 1 SECTION OF A RANDOM INTERFACE $z = h(x_1)$ SEPARATING TWO SEMI-INFINITE FLUIDS (REGIONS V_1 AND V_2) HAVING DIFFERENT DENSITIES ρ AND WAVENUMBERS k

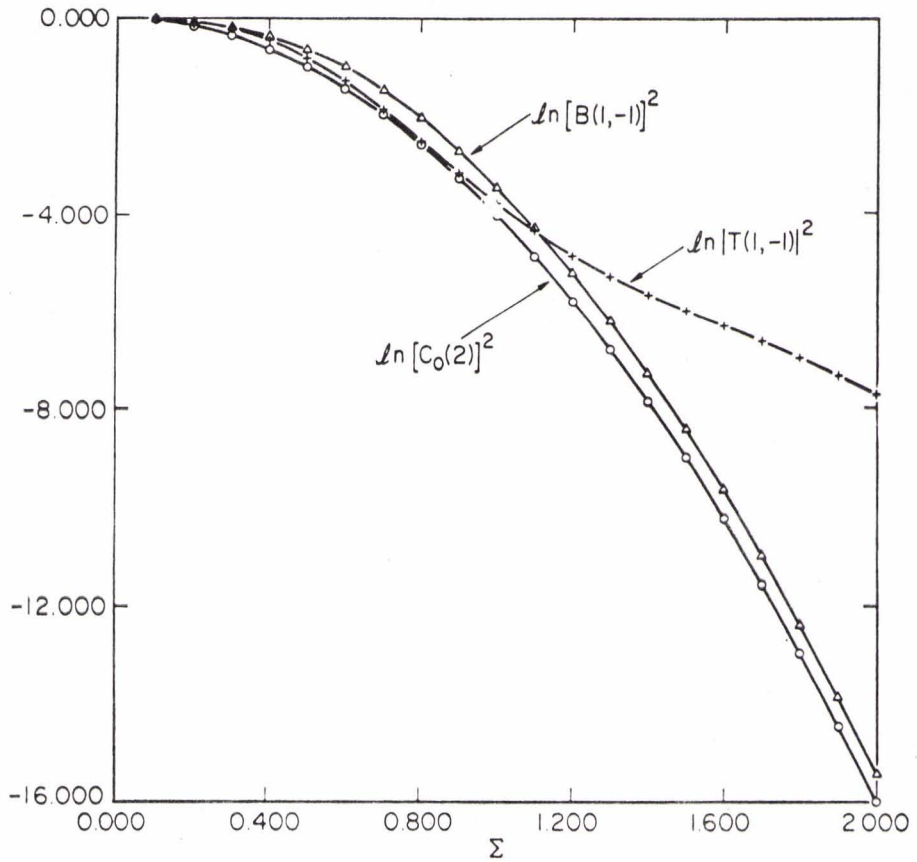

FIG. 2 COHERENT SPECULAR SCATTERING FROM A RANDOM NEUMANN SURFACE (Ref. 4) PLOTTED VERSUS $\sum = k_1 \sigma \cos \theta_i$, THE RAYLEIGH ROUGHNESS PARAMETER. $C_o(2) = \exp(-2 \sum^2)$ IS THE KIRCHHOFF RESULT, B(1, -1) ANOTHER SINGLE SCATTER RESULT INVOLVING COMBINATIONS OF EXPONENTIALS AND T(1, -1) THE MULTIPLE SCATTERING SOLUTION OF Eq. (41) HERE FOR $R = 1$

REVIEW PAPERS

ACOUSTIC PROPERTIES OF THE SEA FLOOR: A REVIEW

by

Edwin L. Hamilton
Naval Undersea Center
San Diego, California, 92132
U.S.A.

(No Abstract received)

INTRODUCTION

Geologists and geophysicists have two basic roles in underwater acoustics and, especially, in oceanic acoustic modeling. They must study all properties of the sea floor of interest in underwater acoustics, and synthesize these data in order to furnish quantitative information to the acoustician concerned with sound interactions with the sea floor. When data are not available, reasonable predictions may be required. Because of the state of the art, there is insufficient data; therefore, the second important role of the geologist-geophysicist is to make measurements and conduct research in the field of acoustically relevant properties of the sea floor.

At higher sound frequencies, the acoustician may be interested in only the first few meters, or tens of meters of sediments. At lower frequencies, information must be provided on the whole sediment column and on properties of the underlying rock. This information should be provided in the form of geoacoustic models of the sea floor.

A "geoacoustic model" is defined as a model of the real sea floor with emphasis on measured, extrapolated, and predicted values of those properties important in underwater acoustics, and those aspects of geophysics involving sound transmission. In general, a geoacoustic model details the true thicknesses and properties of the sediment and rock layers in the sea floor.

Geoacoustic models are important to the acoustician studying sound interactions with the sea floor in several critical aspects: to guide theoretical studies, to reconcile experiments at sea with theory, and to be able to predict the effects of the sea floor on sound propagation.

The information required for a complete geoacoustic model should include the following for each layer; in some cases, the state of the art allows only rough estimates, in others, information may be non-existent.

1. Properties of the overlying water mass from Nansen casts and velocimeter lowerings.
2. Sediment information (from cores, drilling, or geologic extrapolation): sediment types, grain-size distributions, densities, porosities, compressional and shear wave attenuations and velocities, and other elastic properties. Gradients of these properties with depth; for example, velocity gradients and interval velocities from sonobuoy measurements.
3. Thicknesses of sediment layers (in time) determined at various frequencies by continuous reflection profiling.
4. Locations, thicknesses, and properties of reflectors within the sediment body as seen at various frequencies.
5. Properties of rock layers. Those at or near the sea floor are of special importance to the underwater acoustician.
6. Details of bottom topography, roughness, relief, and slope; for examples, as seen by underwater cameras, and deep-towed equipment.

Among the above properties and information, the basic, minimum information required for most current work in sound propagation is layer thickness, compressional (sound) wave velocity and its attenuation and gradient, and density. Some models require elastic properties such as Lamé's constants. It is the responsibility of the geologist-geophysicist in this field to coordinate his efforts withthose of acousticians in order to supply them with pertinent data, but also to anticipate their future needs.

In 1973, the writer reviewed the present state of the art in acquiring and presenting much of theabove information (Hamilton, 1974a,b). Therefore, some of the following is redundant, or is repeated from the earlier reviews. However, additional, unpublished studies have been done on density and porosity

gradients in the sea floor, on shear wave variations with depth in marine sediments, on sound attenuation versus depth in the sea floor, and on the attenuation of shear waves. Additionally, older figures on sound attenuation are revised, and some new figures are presented on sound velocity gradients based on sonobuoy results. Some new measurements of sediment properties are also presented in partially revised tables.

In the general sections which follow, the information required to form geoacoustic models will be discussed, and, finally, the methods of model construction will be noted.

DISCUSSION OF INFORMATION REQUIRED TO FORM GEOACOUSTIC MODELS

Introduction

The methods used in the field and laboratory to acquire the necessary data for geoacoustic models have been described and discussed in previous reports and in the references in these reports (Hamilton, 1970b, 1971a,b, 1972; Hamilton et al., 1970, 1974). These reports contain, also, numerous references to the results of others, and no attempt is made herein to compile an exhaustive bibliography.

In the discussions which follow, frequent references will be made to the three general environments (Figure 1): the continental terrace (shelf and slope), the abyssal hill environment, and the abyssal plain environment. These environments and associated sediments were discussed in more detail in Hamilton (1971b).

Sediment nomenclature on the continental terrace follows that of Shepard (1954), except that within the sand sizes, the various grades of sand follow the Wentworth scale (noted in Appendix B). In the deep sea, pelagic clay contains less than 30 percent siliceous or calcareous material. Calcareous ooze contains more than 30 percent calcium carbonate, and siliceous ooze more

than 30 percent silica in the form of Radiolaria or diatoms. The Shepard (1954) size grades are shown in these deep-sea sediment types in order to show the effects of grain size.

The averaged results of the writer's measurements and computations to July 1975 are listed in Tables 1 through 6. These tables are revised, in part, from measurements taken since 1973. These data are for the upper 30 cm in the continental terrace where measurements were made in situ with probes, from diver-taken samples, and from cores and other samplers. In deep sea pelagic clay the upper 30 cm of gravity cores and deeper depths in piston cores furnished sediment for measurements. All velocity values are corrected to 23° C and 1 atmosphere pressure (Hamilton, 1971b), using tables for the speed of sound in sea water.

Recent reviews by the writer have bibliographies to about 1973. In the special field of acoustic properties of the sea floor, the reader is also directed to reports in two volumes from Office of Naval Research symposia (Inderbitzen, 1974; Hampton, 1974), and a report by Morton (1975); others are referenced in appropriate, special sections.

Density-Porosity Relationships

General. The equation linking density, porosity, pore-water density, and bulk density of mineral solids in a gas-free system is

$$\rho_{sat} = n\rho_w + (1 - n)\rho_s \qquad (1)$$

where

ρ_{sat} is saturated bulk density

n is fractional porosity (volume of voids/total volume)

ρ_w is density of pore water

ρ_s is bulk density of mineral solids

When sea water is evaporated from sediments during laboratory measurements, dried salts remain with the dried mineral residues. A 'salt correction' should be made to eliminate the false increment to the weight of dried minerals; otherwise, porosity, water content, and bulk grain density values are incorrect. Methods of making a salt correction were detailed by Hamilton (1971b). All values in the tables have been so corrected.

Density of pore water. In computations involving pore-water density, it can be assumed that pore-water and bottom-water salinities are approximately the same. Values for the laboratory density of sea water can be obtained from Sigma-T tables (e.g., NAVOCEANO, 1966). For almost all deep-sea sed-

iments, a laboratory value at 23° C of 1.024 g/cm^3 will be within 0.002 g/cm^3 of any other density at reasonable 'room temperatures'. This value is recommended for laboratory computations. In situ values of water density can be computed from NAVOCEANO tables (1966); such values would vary little (when rounded off) in deep water from those given in Hamilton (1971b) for the Central Pacific.

Density of mineral solids. The bulk density of mineral solids in sediments varies widely because the mineral species present depend on mineralogy and nearness of source areas for terrigenous components, on pelagic particles deposited from the water, and on diagenetic changes in mineralogy in the sea floor.

The geographic variation in pelagic organisms such as diatoms and Radiolaria (silica) and Foraminifera (calcium carbonate) have marked effects on grain density. An average value for grain densities in diatomaceous sediments of the Bering and Okhotsk Seas (Table 2a) is 2.46 g/cm^3, whereas in the open Pacific to the south, the deep-sea clays have average grain density values between 2.68 and 2.78 g/cm^3 (avg. 2.74 g/cm^3).

The averages (g/cm^3) of all samples in each of the three environments (not including diatomaceous and calcareous sediments) are: terrace-2.680, abyssal-hill 'red' clay-2.735 abyssal plain (mostly fine-grained)-2.652. The overall average of the above is 2.693 g/cm^3. Keller and Bennett (1970) report an average for terrigeneous materials of 2.67 g/cm^3, and for the Pacific, 2.71 g/cm^3. Cernock (1970), for the Gulf

of Mexico, reports 2.637 g/cm^3. Akal (1972) reports a general value of 2.66 g/cm^3. In soil mechanics computations a value of about 2.65 g/cm^3 is used for sands and silts when the value is unknown (e.g., Wu, 1966). Thus, there is enough information at hand to predict, with confidence, grain densities for general sediment types.

The conclusion is that the following grain densities be predicted and used in computations when no data is available.

Sediment Type	Avg. Bulk Density of Minerals, g/cm^3
Terrigeneous	2.67
Deep-sea (red clay)	2.72
Calcareous ooze	2.71
Diatomaceous ooze	2.45

Saturated bulk density (or unit wet weight). Averaged values of saturated bulk density for each sediment type within each environment are listed in Tables 1b and 2b. The relationships of saturated bulk density to porosity (Equation 1), not illustrated, are indicated for these data in regression equations in Appendix A. Previous illustrations and discussions indicate the small errors for most sediments when either property is used as an index to the other (Hamilton et al., 1956, 1970b).

In the two deep-water environments, the least saturated bulk density was 1.16 g/cm^3 from the Okhotsk Sea, and the

highest was 1.65 g/cm^3 in a silty layer in Japan Basin turbidites.

In predicting density without any sediment data, one can enter the tables for the appropriate environment and sediment type. In both the abyssal plain and abyssal hill environments, silty clay is the dominant sediment type; there is no significant difference between average densities in these two environments in silty clay: plains-1.333 g/cm^3, and hills-1.344 g/cm^3.

If mean grain size, M_z, is known, a value of density can be derived by entering the diagram or regression equation relating M_z to density (Figure 2).

There is a small (and probably insignificant) correction of laboratory values of sediment saturated density to in situ values. This correction involves an increment to density resulting from more dense water in sediment pore spaces in the sea floor. Laboratory values can usually be used as in situ values, but the correction can be easily made by computing saturated bulk density with equation (1), using in situ density of sea water. The increment to density for most high-porosity sediments varies with water depth, but is only about 0.02 to -.03 g/cm^3 to 6000 m water depth.

Porosity. The amount of pore space in a sediment is the result of a number of complex, interrelated factors; most important are the mineral sizes, shapes, and distributions, mineralogy, sediment structure, and packing of solid grains.

This subject has been previously discussed with many references (Hamilton, 1970b). The interrelated effects of the above factors usually result in a general decrease in porosity with increasing grain size (Figure 3). There is much scatter in the data because of the factors cited above.

The marked effect of mineralogy and environmental control in porosity-density can be seen in the tables and figures: the diatomaceous sediments of the Okhotsk and Bering Seas have significantly higher porosities and lower densities than do similar sediments of the same grain size. Silty clay in diatomaceous ooze has average densities of 1.214 g/cm^3 and porosities averaging 86.8 percent, whereas this sediment type in abyssal hills and other plains have densities around 1.33 g/cm^3 and porosities around 81 percent.

In predicting porosity or density, given the other property (or deriving it by using mean grain size), one can enter density vs. porosity equations or diagrams, but it is usually better procedure to assume values of grain density and pore-water density (laboratory or in situ) and compute the missing property with Equation (1).

Density and porosity versus depth in sediments.- At present it is possible to predict within reasonable limits the density and porosity of sediments at the surface of the sea floor (Hamilton, 1971b), but not at depths greater than can be reached by gravity or piston corers (usually a maximum of about 10 to 20 m). In recent years the Deep Sea Drilling Project has drilled hundreds of holes in the sea floor, and density and porosity measurements have been made

on the cored sediments and rocks. Unfortunately, these measurements cannot account for the increase in volume ("rebound") caused by the removal of the samples from the pressures of overlying sediments ("overburden pressure"). In addition, these density measurements are subject to various errors and must be used with caution.

In an unpublished report (Hamilton, 1975a), special laboratory measurements of density and porosity were combined with other studies to estimate the volumetric increases in sediments removed from boreholes. These data were then used to estimate and illustrate in situ variations of density and porosity with depth in the various important deep-sea sediment types: calcareous ooze, siliceous oozes (diatomaceous and radiolarian oozes), pelagic clay, and deep-water sediments from nearby land sources (terrigenous sediments).

In general, the procedures followed in developing the final profiles and density gradient information were as follows. The best laboratory measurements of density and porosity on Deep Sea Drilling Project (DSDP) samples were selected for the principle sediment types. The volumetric increases, or rebound, in these samples caused by removal from the overburden pressures in the boreholes were estimated from consolidation (compression) tests on similar marine sediments. The in situ porosity profiles were then constructed by subtracting the estimated rebound in porosity from laboratory porosity at various pressures which were converted to depths. In situ density profiles and gradients were then computed from the porosity data.

In Figures 4 and 5, the laboratory and in situ curves of porosity versus depth in the sea floor are illustrated for calcareous ooze and terrigenous sediments. In Figure 6, the variations of density with depth are illustrated for the 5 major deep-sea sediment types. These are generalized examples for the sediment types and no attempt is made to show the scatter of the data. Fine-grained, shallow-water sediments would have a profile similar to the curve for terrigenous sediments.

Some of the other general conclusions of this unpublished study are as follows. There is less reduction of porosity with depth in the first 100 m in these deep-water sediments than previously supposed: 8 to 9 percent in pelagic clay, calcareous and terrigenous sediments, and only 4 to 5 percent in the siliceous sediments. From depths of 300 m the most rebound is in pelagic clay (about 7 percent), and the least in diatomaceous ooze (about 2 percent); calcareous ooze and terrigenous sediment should rebound from 300 m about 4 to 5 percent. Terrigenous sediment, from depths of 1000 m to the surface, probably rebounds a maximum of about 9 percent.

Given profiles of in situ porosity vs. depth in sediments, it is possible to approximate the amounts or volumes of original sediments which have been compressed to present thicknesses by overburden pressures (Hamilton, 1959). This was done for the principle sediment types. To compress to present-day thicknesses of 300 m (the 0 to 300 m interval), it would have required an original thickness of about 420 m of terrigenous sediments, 430 m of calcareous ooze, 440 m of diatomaceous ooze, and 500 m of pelagic clay. Slightly over 2000 m of original sediments would have been required for compression to a present-day thickness of 1000 m of terrigenous sediments.

To estimate the density of a deep sediment layer, the recommended method is to enter (with depths) the density vs. depth curve (Figure 6) for the probable or known sediment type. Determine the density at the top and bottom of the layer and average for a mean density.

The velocity of a deep rock layer is often available from reflection and refraction surveys. To get the mean density of these layers (given velocity) the recommended method is to enter curves relating density and velocity for rocks. At present, the recommended curves are those of Christensen and Salisbury (1975, table 9), Nafe and Drake (1967), and Dortman and Magid (1969).

Compressional Wave (Sound) Velocity

General.- In this section, the better empirical relationships between sound velocity and other properties, and velocity gradients, will be discussed. The empirical relationships are important in predicting sound velocity, but it should be emphasized that wave velocities are elastic properties of the sediment mass. Properties such as porosity and grain size affect sound velocity only in the effects they have on elasticity of the sediment (discussed in Hamilton, 1971a).

Sound velocity and porosity-density relationships. The relationships between sound velocity and porosity have received much attention in the literature because porosity is an easily measured or computed property likely to yield predictable relations with sound velocity. This is because porosity is the volume of water-filled pore space in a unit volume of sediment, and compressional-wave speed is largely determined by the compressibility of pore water, especially in high-porosity silt-clays.

Many studies have emphasized the relationships between sound velocity and porosity over the full range of porosity (Hamilton, 1956, 1970b; Hamilton et al., 1956; Sutton et al., 1957; Laughton, 1957; Nafe and Drake, 1957, 1963; Horn et al., 1968, 1969; Schreiber, 1968; McCann and McCann, 1969; Kermabon et al., 1969; Cernock, 1970; Buchan et al., 1972; McCann, 1972; Akal, 1972;). These studies have included sediments for all of the world's major oceans. The latest data of the writer is illustrated in Figures 7 and 8.

The relationships between sound velocity and density are similar to those for sound velocity and porosity because of the linear relationship between porosity and density.

Sound velocity and grain-size relationships. Grain-size analyses in the laboratory usually include percentages

of sand, silt, and clay, mean and median diameters of mineral grains, and other statistical parameters. The relationships between grain-size and velocity (Figures 9, 10, 11) are in accord with previous studies (Hamilton et al., 1956; Hamilton, 1970b; Sutton et al., 1957; Shumway, 1960; Horn et al., 1968; Schreiber, 1968). Empirically, mean grain size and percent clay size (Figure 11), or percent sand and silt, are important indices to velocity. This is important because size analyses can be made on wet or dry material; and, frequently, size analyses are all the data available in published reports.

Discussion of velocity indices. The information currently available indicates that the higher-porosity silt-clays in the deep basins of the world's oceans have velocities within 1 to 2 percent at any given porosity above about 65 to 70 percent (excluding special types such as diatom and calcareous ooze), at the same temperature and pressure. It is difficult to compare velocity measurements when all have not been corrected to a common temperature, or where temperature is not reported for velocity measurements. Variations in 'room temperature' can easily cause velocity variations on the order of 20 to 30 m/sec (about 1 to 2 percent); variations are much greater if measurements are made in sediment soon after coring or removal from a refrigerator. Temperature measurements should always be made with velocity measurements because temperature variations can cause velocity changes which obscure, and can be greater than,

environmental differences, or differences between sediment types.

If abyssal plain and abyssal hill measurements are lumped together, velocity, at a porosity of 80 percent, from the Mediterranean (Horn et al., 1967; Kermabon et al., 1969), North Atlantic, Caribbean, and Gulf of Mexico (Horn et al., 1968; Schreiber, 1968; Cernock, 1970; McCann, 1972; Akal, 1972), and Pacific and Indian Oceans (Hamilton, this report) averages about 1500 ± 25 m/sec. The lumping of data from various environments and unknown temperatures of measurement is not advised, but the results indicate the small velocity variations in high-porosity sediments of the world's oceans.

As discussed in previous reports, general curves covering the full range of porosity, density, or grain size, wherein data from all environments and sediment types is lumped, should be abandoned in favor of those for particular environments and/or geographic areas or sediment types. In other words, enough data is at hand to quit lumping and start splitting. Examples of this are illustrated in the velocity vs. porosity ~~[velocity-density]~~ diagrams (Figures 7,8). These figures and the tables indicate that at porosities around 80 percent that abyssal-hill silt-clays have lower velocities than do abyssal plain or terrace sediments. The diatomaceous sediments of the Bering Abyssal Plain have significantly higher velocities at higher porosities and

lower densities than either abyssal hill or other terrigeneous abyssal plain sediments (Figure 8).

A resume" of velocity vs. mean or median grain size data indicates that in the various ocean basins, deep-sea sediments of the same mean grain size are apt to have about the same velocities. At a mean grain size of 9.5 phi, the range of velocities from the Pacific and Indian Oceans and adjacent areas (Hamilton, this report), the Gulf of Mexico (Cernock, 1970), the Atlantic, Caribbean, and Mediterranean (Horn et al., 1968, 1969; Schreiber, 1968; is about one percent (about 1495 to about 1510 m/sec).
This is remarkably close considering the lack of temperature control and geographic range. However, as previously discussed in the cases of porosity and density vs. velocity, such lumping should be discouraged. An example, again, is the siliceous sediment of the Bering and Okhotsk Seas. At any given grain size between 8 and 10 phi, these diatomaceous sediments have higher velocities than do the other deep-water sediments (Figure 10).

In the figures, sea-water velocity, if plotted, would be at about 1530 m/sec at 23° C and 1 atmosphere pressure. In the tables, the "Velocity Ratio" (velocity in sediment/velocity in sea water) indicates, quantitatively, the sediment velocity in relation to water velocity. Inspection of the velocity vs. porosity diagrams (Figures 7 and 8), and Tables 1b and 2b, indicate that almost all high-porosity silt-clays from the sediment surface have velocities less than in sea water. This is true in the laboratory and in situ because

the velocity ratio is the same in the laboratory as it is in situ. This interesting relationship results in a small sound channel between the sediment surface and some depth in the sediments depending on the velocity gradient (Hamilton, 1970c).

Prediction of in situ sound velocity at the sediment surface.-

There are three general ways to predict in situ sound velocity at the sediment surface: (1) correct the laboratory velocity from 1 atmosphere pressure and temperature of measurement to the in situ temperature and pressure, using tables for the speed of sound in sea water, (2) multiply the laboratory velocity ratio (sediment velocity/sea-water velocity at 1 atmos., temperature of sediment, and bottom-water salinity) by the bottom-water velocity, or (3) in the absence of sediment data, enter a table (e.g., Table 2b) and select a velocity or ratio for the particular environment and most common sediment type, and then correct to in situ as in (1) or (2), above. The ratio method, (2), is the easiest to apply because the ratio remains the same in the laboratory or in situ, and all one needs for in situ computations is a curve of sound velocity vs. depth in the water mass. These methods were discussed at length (with a numerical example) in a special report concerned with prediction of in situ properties (Hamilton, 1971b).

Compressional Velocity Gradients and Layer Thicknesses

General.- Reflection profiling has become an important tool in geologic, geophysical, and engineering studies. Reflection records indicate sound travel time between impedance mismatches within the sediment or rock layers of the sea floor. To derive the true thicknesses of these layers, it is necessary to measure or predict the interval or mean layer velocity, or to use a measured or predicted sediment surface velocity and a velocity gradient in the sediment body. True thicknesses of layers is a critically important requirement in studies of sound propagation in the sea floor, and in various geological and geophysical investigations. At the present time, the simplest method of measuring layer interval velocities involves the use of expendable sonobuoys. These sonobuoy measurements also provide the basic data for determining velocity profiles and gradients in the sea floor.

The techniques of sediment velocity measurements at sea with expendable sonobuoys, and subsequent data reduction, were developed during the late 1960's (Clay and Rona, 1965; LePichon et al., 1968; Houtz et al., 1968). The results of sonobuoy measurements in the Atlantic, Gulf of Mexico, and Pacific were reported by Houtz et al. (1968). Sonobuoy measurements in the Pacific by Lamont-Doherty scientists have been summarized by M. Ewing et al. (1969) and J. Ewing et al. (1970) for the South Pacific and Coral Sea. Measurements in the North Pacific and Bering Sea have been made by Houtz et al. (1970) and Ludwig et al. (1971); in the Japan Sea (Ludwig et al., 1975a); in the Caribbean Sea (Ludwig et al., 1975b). Measurements have been reported from the Pacific and Indian Oceans, and the Japan and Bering Sea by Hamilton et al. (1974); an example is shown in Figure 12 from the Bay of Bengal. A summary article covering the main ocean basins was published by Houtz (1974). Other references can be found within the cited references, above.

In the discussion in this section, several velocities are involved: (a) instantaneous velocity, V, is the velocity of a compressional wave at any given depth or travel time within the sediment body, (b) mean velocity, or interval velocity, $\overline{V}$, is the average velocity for an interval or layer, and (c) sediment-surface velocity, V_0, is compressional-wave velocity in the sediment just below the water-sediment interface.

Velocity-gradient data for the sea floor are usually produced in the form of linear or non-linear curves based on plots of instantaneous and mean velocity vs. one-way travel time in the sediment or rock layer (e.g., Figure 12).

Velocity gradients. Velocity gradients are usually expressed as an increase in velocity per linear increase in depth, m/sec/m, or sec^{-1}. In the upper levels of deep-water marine sediments these gradients are normally positive, and usually between 0.5 and 2.0 sec^{-1} (Ewing and Nafe, 1963; Houtz et al. 1968; Hamilton et al. 1974). However, most velocity gradients are non-linear if followed to sufficient depths within the sediment body (e.g., Figure 12; Houtz et al., 1968, 1970).

When the velocity gradient, a, is linear, the instantaneous velocity, V, at depth, h, is (Houtz and Ewing, 1963):

$$V = V_0 + ah \qquad (2)$$

At any depth within sediment layers, an average linear gradient, a, can be determined from the parabolic equations for V and $\overline{V}$ vs. t (Houtz et al., 1968, equation 3) by

$$a = (V - V_0)/h \qquad (3)$$

where

V = instantaneous velocity at time t

V_0 = velocity at sediment surface ($t = 0$)

h = layer thickness at time $t = \bar{V}t$

In most sediment sections, the linear velocity gradient decreases with increasing depths, or travel times. The average linear velocity gradient was computed with Equation (3) at increments of 0.1 sec (from 0 to 0.5 sec) for each of 13 areas of mostly turbidite deposition: 4 from Lamont-Doherty investigations (Atlantic, Gulf of Mexico, Aleutian Trench, and Bering Sea-thin), and 9 from Hamilton et al. (1974). The values at each 0.1 sec interval were averaged and plotted in Figure 13. These averaged gradients decreased from about 1.31 sec^{-1} at $t = 0$, to 0.77 sec^{-1} at $t = 0.5$ sec.

As discussed in the next section, such average values can be used to compute a predicted true sediment thickness in many areas where no interval velocity data are available.

The best published data for pelagic, calcareous sediments are summarized in the equations for the Pacific Equatorial Zone (Houtz et al., 1970). Velocity gradients in these thick calcareous sections appear to be higher than the average for turbidite sections: about 1.83 sec^{-1} in the upper levels.

From the same areas, Figure 14 illustrates instantaneous and mean velocity versus one-way travel time of sound in the sediments. From these data one can construct curves of instantaneous velocity versus depth in the sea floor (Figure 15).

In contrast to silt-clays and turbidites, laboratory measurements of compressional wave velocities in water-saturated sands indicates that there is a relatively small, positive gradient with increasing pressure or depth. In computations or predictions of compressional wave velocity versus depth in sands, it is recommended that velocity be increased with the 0.015 power of depth (Hamilton, 1975c).

Thickness computations.- There are three usual alternatives when computing true sediment thicknesses for an area where no interval velocities have been measured: (1) use an equation or curve for mean velocity vs. travel time from a similar area, (2) use a predicted linear gradient and a predicted V_o (discussed below), or (3) assume an interval velocity.

There is now sufficient, published data to show that most areas of turbidites have reasonably close velocity gradients in the upper, unlithified layers. For example, at a one-way travel time of t = 0.2 sec, the computed thickness of a layer using the Atlantic and Gulf of Mexico equations of Houtz et al., (1968), and those for the Central Bengal Fan and Kamchatka Basin (Hamilton et al., 1974) are respectively, 347 m, 341 m,

351 m, and 343 m: a variation of less than 3 percent. Thus, if one is computing sediment layer thicknesses for an area of turbidites where no measurements have been made, the use of equations for the most similar area will probably yield reasonable results. If the sediment type is calcareous ooze, the equations for the Pacific Equatorial Zone (Houtz et al., 1970) are recommended.

Given a linear gradient, a, the sediment surface velocity, V_0, and one-way travel time, t, the thickness of a layer can be computed (Houtz and Ewing, 1963) by

$$h = V_0(e^{at} - 1)/a \qquad (4)$$

where e is the base of natural logarithms

This is a very useful equation because V_0 can be closely estimated (Hamilton, 1971b) and one-way travel time in a layer can be measured from a reflection record; and, as discussed in the preceding section, the velocity gradient can usually be reasonably estimated (Figure 13).

In summary, the following steps are recommended when computing layer thicknesses with Equation (4): (1) measure one-way travel time, t, in the sediment layer from a reflection record; when possible, the measurement should be to 0.001 sec, (2) predict the in situ sediment surface velocity, V_0, using the method discussed by Hamilton (1971b), (3) select a linear velocity gradient for the section depending on one-way travel time (Figure 13); for example, if one-way travel time was 0.25 sec, the assumed gradient

would be 1.0 sec^{-1}, and (4) compute layer thickness, h, with Equation (4).

The third, most popular and least accurate, method for computing layer thicknesses is to measure travel time from a reflection record and assume an interval velocity. These various methods and errors which might be encountered are further discussed in Hamilton et al. (1974).

Attenuation of Compressional (Sound) Waves

Attenuation versus Frequency.

Hamilton (1972) reported the results of in situ measurements of sound velocity and attenuation in various sediments off San Diego. These measurements and others from the literature, allowed analyses of the relationships between attenuation and frequency, and other physical properties. It was concluded that attenuation in dB/ unit length is approximately dependent on the first power of frequency, and that velocity dispersion is negligible or absent in water-saturated sediments. The report also discussed the causes of attenuation, its prediction (given grain size or porosity), and appropriate viscoelastic models which can be applied to sediments. In this section, additional data since 1972 will be noted and briefly discussed.

Figure 16 illustrates a large collection of data on attenuation versus frequency in marine sediments and sedimentary rocks. This figure has been revised from previous publications (Hamilton, 1972, 1974b). The new data include measurements of Meissner (1965), Berzon et al. (1967), Buchan et al. (1971), and Neprochnov (1971). All of the newly-added measurements are indicated with open symbols or dashed lines to indicate the impact of the newer data.

The line labelled "f^1" in Figure 16 indicates the slope of any line representing a first power dependence of attenuation on frequency. It can be

seen that most of the data are consistent with a first power dependence of attenuation on frequency over a frequency range from below 10 Hz to one MHz. The upper and lower bounds of the data plot probably define the area in which most natural marine sediments and sedimentary rocks will lie. With regard to sediment type, the silt-clays, or "mud",(squares) lie in a narrow band along the lower side of the data plot, and the sands (circles), and mixtures such as silty sand, sandy silt, etc., (triangles), lie along the top. These different sediment types are shown on the same plot for convenience. There is no significant difference between sediment types in regard to the relationship between attenuation and frequency. It is interesting to note that Neprochnov (1971) in his summary of a great deal of Soviet data on attenuation in thick layers in the sea floor, remarked that as a rule, a linear relationship was found between attenuation and frequency in the frequency range from 20 to 400 Hz.

In summary, the experimental evidence indicates that the dependence of attenuation on frequency in mud, sand, and marine sedimentary strata, is close to f^1, and does not support any theory calling for a dependence of attenuation on $f^{1/2}$ or f^2 for either (or both) sediment types or mixtures. These data are enough to show that dependence of attenuation on frequency is more nearly f^1 than $f^{1/2}$ or f^2 (but is not enough to verify an exact dependence) for the following: silt-clays, or muds, from a few Hz to at least one MHz, from about 1 kHz to at least one MHz for most sands, and from 150 Hz to one MHz for mixed types. More information is needed for attenuation in pure sands at frequencies below 1 kHz.

Attenuation versus sediment porosity.- The relationships between attenuation and frequency were expressed (Hamilton, 1972) in the form

$$\alpha = kf^n \qquad (5)$$

where

α is attenuation of compressional waves in db/m

k is a constant

f is frequency in kHz

n is the exponent of frequency

The case was made in the preceding section that attenuation is dependent, approximately, on the first power of frequency. If n in Equation (5) is taken as one, the only variable in the equation for various sediments is the constant k. This constant is useful in relating attenuation to other sediment properties such as mean grain size and porosity. The relationships between k and common physical properties give an insight into causes of attenuation, and allow prediction of attenuation.

Assuming that linear attenuation is dependent on the first power of frequency, values of k can be easily computed by dividing attenuation by frequency. This was done for all measurements by the writer and for those in the literature in natural saturated sediments. These values of k were then plotted versus mean grain size and porosity (Hamilton, 1972). Some new data has been added to the figure for sediment porosity vs. k (Figure 17). These measurements are: Tyce (1975): silty clays in the San Diego Trough, and calcareous sediments on the Carnegie Ridge; Muir and Adair (1972): fine sand; Buchan et al. (1971): average of 11 cores in the North Atlantic with less than 5 percent $CaCO_3$; and Igarashi (1973): silty sand off Santa Barbara, California.

The causes of the variations of k (or attenuation) with porosity, as in Figure 17, and with mean grain size, were discussed at length in the original report (Hamilton, 1972, p. 635-643) and will not be repeated here. In general, it was concluded that internal friction between mineral particles was by far the dominant cause of energy losses, and that internal friction varied with the size of grains, the number and kind of grain contacts, and with surface areas of grains in sands, and with cohesion and friction between fine silt and clay particles. In the sands (at porosities less than about 50 %) as grains become smaller, there is a rapid increase in the number of grains per unit volume between porosities of about 45 and 50 percent; additionally the grains become more angular, and there is a marked increase in surface areas in contact. All of these factors result in increased friction between grains which in turn results in greater attenuation of energy from any compressional or shear wave passing through the material. In the mixed sediment types (e.g., silty sand, sandy silt), between porosities of 50 to 55 percent, attenuation reaches a maximum, and with the admixture of finer-grained silt and clay particles, as porosity increases, the larger grains become separated and there is less inter-grain friction. At porosities above about 65 percent, attenuation depends on friction between clay and silt particles, and on cohesion between particles. It is interesting to note that dynamic rigidity varies in the same was as attenuation, as it should if both are mostly caused by friction between grains (Hamilton, 1970a, 1972, 1974a).

The relations between sediment porosity and the constant k (Figure 17) furnish a simple method for predicting attenuation in surficial sediments. The diagram, or regression equations (in Hamilton, 1972, figure 5), can be entered with measured or predicted porosity, and a value of k can be obtained which, when placed in Equation 5, yields an equation useable at

any frequency. A similar figure relating mean grain size and k is in the original report. The values of k so obtained are approximations, but it is predicted that most future measurements of attenuation in marine sediments will result in k values which fall within or near the indicated "envelope." In predicting attenuation, one can use the central (heavy line) values (for which there are regression equations) as "most probable", and the upper and lower dashed lines as indicating "probable maximum" and "probable minimum."

Attenuation versus depth in the sea floor.- For various computations in underwater acoustic and marine geophysics it is necessary to know, or approximate, the average value of attenuation of an interval or layer, or to approximate the gradient of attenuation with depth. Consequently, a collection has been made of available published data on attenuation at the surface and at depth in marine sediments and rocks (Hamilton, 1975b).

As briefly discussed in the preceding section, the relations between the constant k in Equation (5) and sediment physical properties have furnished a useful means of extrapolating measurements and predicting attenuation. The constant k will be used in this section to study the variations of attenuation with depth in the sea floor.

Figure 18 illustrates the available published data (listed and referenced in Hamilton, 1972, 1974b, 1975b, and this report) on the variations of attenuation (expressed as k) at the surface and at depth in silt-clays, turbidites, sedimentary rocks, and basalts in the sea floor. Not shown in Figure 18 are all the values of k for sands and mixed sands and silts; values of k in these materials usually range from about 0.3 to about 0.9 (see Figure 17). Sand bodies in the sea floor are usually relatively thin compared to thick silt-clay and turbidite sections, and the gradients of attenuation in sands are

better known than in silt-clays. All data were recomputed, if necessary, into the form of Equation (5), and then k was computed. Where attenuation was given for an interval or layer, the value is plotted at 1/2 the interval thickness for the first layer, or to the midpoint of a lower layer. As a result, the data in Figure 18 form curves of "instantaneous attenuation" versus depth in the sea floor.

Neprochnov (1971, p. 711) presented attenuation data for thick sediment and rock layers, in the frequency range of 20 to 200 Hz, for 7 areas in the Indian Ocean, Black Sea, and Japan Sea. In Figure 18, the Soviet data are given special symbols. The first layers, which should all be unlithified sediments, are indicated by triangles; the second layers, dominantly sedimentary rock (probably mudstone), are indicated by squares; and the third layers, indicated by diamonds, are sedimentary rock and basalt. These layer identifications are based on Deep Sea Drilling Project sites in the various areas.

Experimental work on attenuation of shear and compressional waves versus pressure in sediments has been largely confined to sands. In these studies, both shear and compressional wave attenuation decreased at about the same rate with increasing pressure. The best data (e.g., Gardner et al., 1964) indicate that attenuation decreases with about the -1/6 power of effective overburden pressure in sands. Curve "B" shown in part in Figure 18, was computed for a fine sand using an average value of k (0.45, off the figure to the right, for 4 stations off San Diego; Hamilton, 1972) at one meter depth and assuming a decrease in k with the -1/6 power of depth. Curve B indicates very rapid decreases in attenuation to about 10 meters, and a less rapid decrease to 150 m (where the computations stopped).

In silt-clays there is probably a distinctly different reaction of attenuation with depth or overburden pressure in the sea floor. The data indicate a probability that attenuation increases with depth from the sediment surface

to some depth where the pressure effect becomes dominant over reduction in porosity. If so, this is a previously unreported finding.

High-porosity silt-clays at or near the sediment surface usually have porosities from about 70 to 90 percent, and k values from about 0.05 to 0.1 (Figure 17). When these sediments are placed under overburden pressures there is a reduction in porosity which would cause an increase in attenuation (Figure 17) as grains are forced closer together and there is more grain contact. At the same time, pressure increases on the mineral frame cause attenuation to decrease as internal friction between grains decreases (grains in harder contact). Thus,under increasing overburden pressure, there should be a progressive increase in attenuation due to reduction in porosity, and a progressive decrease in attenuation due to pressure on the mineral frame. From the appearance of the data plot (Figure 18) it is predicted that the balance of effects is such that attenuation increases with depth in high-porosity silt-clays until a null point is reached. Thereafter, pressure becomes the dominant effect, and attenuation decreases with depth and overburden pressure.

Values and gradients of attenuation in layers in the sea floor can be approximated as follows:

In sands, determine the attenuation at the surface, or predict it from its porosity and Figure 17, and compute the reduction in attenuation at various depths, assuming a -1/6 power-of-depth relationship. If the material is silt-clay, attenuation should increase from a value at the surface to about 100 to 200 m depth (parallel to Curve A in Figure 18) and thereafter decrease gradually with depth as with Curve C.

For sedimentary rocks below about 400 m, use Curve C to establish

values of k. For basalt layers below the sea floor, use a value of k established from laboratory and field experiments: 0.02 to 0.05; a value of 0.03 is recommended (full references in Hamilton, 1975b).

Impedance

The characteristic impedance of a medium is the product of density, ρ, and velocity, V_p (impedance = ρV_p, $g/cm^2 sec$); it is an important property of any material. The amount of energy reflected (or lost) when sound passes from one medium into another of greater impedance is largely determined by impedance difference, or "mismatches" (e.g., Kinsler and Frey, 1962). In the field of marine geophysics, echo-sounding and continuous-reflection-profiling records indicate the travel-time of sound between impedance mismatches at the particular power and frequencies involved in the sound source, and in amplifying and filter systems. Most deep-water surficial sea-floor sediments have sound velocities less than that in the overlying bottom water, but the echo-sounder records strong reflections in these areas because sediment densities are so much greater than water densities that a sufficient impedance mismatch is created.

Average impedances were computed for the sediments of this study (Tables 3 and 4), using the averaged, measured values of sediment density and velocity in Tables 1b and 2b. Figures and regression equations in Hamilton (1970b,d) illustrate the relationships between impedance and porosity and density.

Laboratory impedances require corrections to in situ values. The methods of correcting laboratory density and velocity to in situ values were noted above; the in situ impedance is merely the product of the corrected values.

Rayleigh Reflection Coefficients and Bottom Losses at Normal Incidence

The computations of Rayleigh reflection coefficients and bottom losses at normal incidence, herein discussed, are a simple, straightforward procedure, given accurate values of density and velocity for sediment and water. Comparisons of such computations with actual measurements at sea (Hamilton, 1970d) by Breslau (1965, 1967) and Fry and Raitt (1961), and the measurements and computations of Hastrup (1970, p. 183-184, figure 5) demonstrate that the method is valid and yields realistic predicted values for acoustic bottom losses (dB) at the water-sediment interface given certain restricted conditions.

The whole subject of reflection, refraction, and energy losses of sound incident on the sea floor is too complex for simple statements and is the subject of other papers in this symposium. The reader is cautioned against attempted use of Rayleigh reflection coefficients and bottom losses except under very restricted conditions of bottom sediment layering, sound energy levels, and frequency. In general, the Rayleigh fluid/fluid model is valid only when, for various reasons, any second or other layers in the sea floor cannot reflect sound which interferes with that reflected from the water-sediment interface (see Cole, 1965 for discussion). As discussed in the paper by Bucker and Morris (this symposium) more sophisticated models of reflectivity and bottom loss involve layers and varying layer properties (Bucker, 1964; Bucker et al., 1965; Cole, 1965; Morris, 1970; Hastrup, 1970; Hanna, 1973).

Rayleigh reflection coefficients and bottom losses at normal incidence were illustrated by Hamilton et al. (1956) and are the subject of a separate paper (Hamilton, 1970d). For the present report, the values of Rayleigh reflection coefficients and bottom losses (Tables 3 and 4) were computed using average density and velocity values in Tables 1b and 2b, plus values of water density and velocity, and appropriate salinity, at 23° C; the normal-incidence equations under Table 3 were used in these computations. As discussed in the

1970d report, laboratory values of reflection coefficients and bottom losses at normal incidence are so close to corrected, in situ, values, that laboratory values can be used as in situ values in generalized studies.

Figures in Hamilton (1970d) illustrate the empirical relationships between porosity and density and Rayleigh reflection coefficients and bottom losses at normal incidence; regression equations are included in the cited report.

Elastic and Viscoelastic Models for Marine Sediments

The subjects of elastic and viscoelastic models for water-saturated porous media, and measurements and computations of elastic constants in marine sediments have been discussed in six recent reports (Hamilton, 1971a,b, 1972, 1974a,b; Hamilton et al., 1970). Some general conclusions are noted below, but the reader should consult, especially, the 1971a, and 1972 reports for fuller discussions, supporting data and detail, and numerous references to the literature on the subject, and the work and opinions of others. Other references are in the symposium volume edited by Hampton (1974).

In soil mechanics and foundation engineering, and in some fields of physics and geophysics, the Hookean model and equations are commonly used in studies of wave velocities and the elastic constants in sediments and rocks. Although the Hookean equations adequately account for wave velocities in most earth materials, they do not provide for wave-energy losses. To account for both wave velocities and energy losses, various anelastic models have been studied or proposed.

In older literature it was possible to consider such models as the Maxwell or Kelvin-Voigt viscoelastic models and others, for wave propagation in earth materials, where the sparse data were made to fit models by use of arbitrary constants. In the past decade there has been enough research in earth materials to indicate restrictive parameters for any anaelastic model.

Given macroscopic isotropy, small, sinusoidal stresses, wave lengths much greater than grain size, and frequencies from a few Hertz to at least several hundred kHz (and probably in the MHz range for most natural sediments), the restrictive parameters for any elastic, 'nearly elastic', or viscoelastic model for marine sediments can be summarized as follows: (1) almost no marine sediments can be considered suspensions, (2) almost all have non-spherical mineral particles which form structures which have sufficient rigidity to transmit shear waves, (3) Poiseuille flow (through small tubes) probably does not hold for relatively impermeable silt-clays nor for natural sands, (4) velocity dispersion is absent or negligibly present, and (5) the dependence of attenuation on frequency is close to f^1. Some relative movement of pore water and mineral frame cannot be excluded on the basis of present evidence, although the above parameters indicate that, if present, it should be small.

The model proposed below is within, or accounts for, the above restrictions, and has several advantages. It is a good working model which does not specify the mechanics of attenuation. It is an anelastic model which includes provision for velocity dispersion and non-linear dependence of attenuation on frequency; the user is thus not committed, a priori, to no-velocity-dispersion or to any particular f^n relationship. The model also indicates clearly those factors involving velocity dispersion and non-linear attenuation which, if negligible, can be dropped. It indicates clearly under what conditions Hookean elastic equations can be used to in-

terrelate wave velocities and other elastic moduli. And interestingly, this model has been widely used in studies of rocks and the earth's crust, as well as in the properties of polymers, and in some soil mechanics studies.

It should be emphasized that other models are not excluded if they are within the above stated parameters. The whole subject merits much more experimental and theoretical study.

A model and concomitant equations within the parameters noted above is a case of linear viscoelasticity. The basic equations of linear viscoelasticity have been summarized in an excellent treatise by Ferry (1961). For the model recommended in this paper, the basic equations (Adler, Sawyer, and Ferry, 1949) have been discussed in different form, including neglect of negligible factors, by Nolle and Sieck (1952), Ferry (1961, p. 93-94), Krizek (1964), White (1965), Krizek and Franklin (1968), Hamilton et al. (1970), and others.

In the above model, the Lamé elastic moduli μ and λ are replaced by complex moduli, $(\mu + i\mu')$ and $(\lambda + i\lambda')$, in which μ,λ, and density govern wave velocity and the imaginary moduli, $i\mu'$ and $i\lambda'$ govern energy damping. The following (Ferry, 1961, p. 11-13) illustrates the stress-strain relations in this model. For a sinusoidal wave, if the viscoelastic behavior is linear, the strain will be out of phase with stress.

The stress can be vectorially decomposed into two components: one in phase with strain and one 90° out of phase. For a shear wave, the complex stress/strain ratio is $\mu^* = \mu + i\mu'$. The phase angle, Φ, which expresses energy damping is, in this case: $\tan \Phi = \mu'/\mu$.

The basic derivations of the above model are in Ferry (1961) and White (1965) and will not be repeated here. Without assumptions as to negligible factors, the equations of the model in the form of Bucker (in Hamilton et al., 1970, p. 4046), or in Ferry (1961, p. 94, 419), reduce to the following for both compressional and shear waves (with some changes in notation).

$$\frac{1}{Q} = \frac{aV}{\pi f - \frac{a^2V^2}{4\pi f}} \qquad (6)$$

where

1/Q is the specific attenuation factor, or specific dissipation function

a is the attenuation coefficient

V is wave velocity

f is frequency (circular frequency, $\omega = 2\pi f$)

Subscripts (p or s) can be inserted into Equation (6) when referring to compressional or shear waves.

When energy damping is small (i.e., $\lambda' \ll \lambda$ and $\mu' \ll \mu$: White, 1965, p. 95; Ferry, 1961, p. 123: $r \ll 1$, where $r = aV/2\pi f$), the term in the denominator of Equation (6), $a^2V^2/4\pi f$, is negligible and can be dropped. This leaves the more familiar expression (e.g., Knopoff and Macdonald, 1958; White, 1965; Bradley and Fort, 1966; Attwell and Ramana, 1966):

$$\frac{1}{Q} = \frac{aV}{\pi f} \qquad (7)$$

$$\frac{1}{Q} = \frac{2aV}{\omega} = \frac{\Delta}{\pi} = \tan \phi \tag{8}$$

$$\Delta = aV/f, \text{ or } a = \Delta f/V \tag{9}$$

Additionally

$$\frac{1}{Q_p} = \tan \phi_p = \frac{\lambda' + 2\mu'}{\lambda + 2\mu} \tag{10}$$

$$\frac{1}{Q_s} = \tan \phi_s = \frac{\mu'}{\mu} \tag{11}$$

$$\frac{\Delta E}{E} = \frac{2\pi}{Q} \tag{12}$$

$$\alpha = 8.686a \tag{13}$$

Where (in addition to those symbols already defined)

Δ is the logarithmic decrement (natural log of the ratio of two successive amplitudes in an exponentially decaying sinusoidal wave)

$\tan \phi$ is the loss angle

$\Delta E/E$ is fraction of strain energy lost per stress cycle

α is attenuation in dB/linear measure (e.g., dB/cm)

Equations involving compressional - and shear-wave velocities in Hamilton et al. (1970), or in Ferry (1961), are (in Ferry's notation)

$$(\lambda + 2\mu) = \rho V_p^2 (1 - r^2)/(1 + r^2)^2 \tag{14}$$

$$\mu = \rho V_s^2 (1 - r^2)/(1 + r^2)^2 \tag{15}$$

where

$r = aV/2\pi f$, λ = Lame´'s constant, μ = rigidity, ρ = density

In Equations (14) and (15), the term, $(1 - r^2)/(1 + r^2)^2$, indicates the degree of velocity dispersion for linear viscoelastic media. When damping is small (defined above), this term is negligible, and can be dropped, as implied by Ferry (1961, p. 94). This leaves the more familiar Hookean equations

$$(\lambda + 2\mu) = \rho V_p^2 \tag{16}$$

$$\mu = \rho V_s^2 \tag{17}$$

This means that if the factor $(1 - r^2)/(1 + r^2)^2$ in Equations (14) and (15), and the term in the denominator of Equation (6), $a^2V^2/4\pi f$, are considered negligible and dropped, that wave velocity, 1/Q, and the log decrement are independent of frequency, and linear attenuation is proportional to the first power of frequency.

Computations with the data of Hamilton (1972), and from the literature, indicate that most water-saturated rocks and sediments qualify under the above definitions as media with 'small damping'. For example, computations from Hamilton (1972, table 1) indicate that the factor $(1 - r^2)/(1 + r^2)^2$ for compressional waves at 14 kHz is 0.9992 in fine sand, and an average of 0.9997 for 4 silty clays; in Pierre shale (McDonal et al., 1958), the factor for shear waves is about 0.992. Equations (7) through (13), (16) and (17) should apply to both water-saturated sediments and rocks.

Those investigators who wish to include velocity dispersion and 1/Q or a log decrement dependent on frequency, and linear attenuation not proportional to the first power of frequency, can consider Equations (6), (14), and (15). The results of computations involving wave velocities, densities, and associated elastic constants will be negligibly different if one uses viscoelastic Equations (6), (14), and (15), or the classic Hookean elastic Equations (e.g., Equations 16 and 17.).

→ Computations of Elastic Constants →

The computation of elastic constants for saturated sedi-

ments was discussed at length in Hamilton (1971a), and was reviewed in Hamilton (1971b, 1974). The general subject will only be briefly noted in this section.

To compute elastic constants in saturated sediments using Hookean elastic equations, as justified in the preceding section, requires values of density, and any two other constants. Density and compressional velocity are easily measured or can be reasonably predicted for most common sediment types (Hamilton, 1971a,b,1974). One more elastic constant is required to compute the others. The third constant selected (Hamilton, 1971a) to use in computations was the bulk modulus (incompressibility). The theoretical basis of this computation follows Gassmann (1951).

Gassmann (1951) formulated a 'closed system' in which pore water does not move significantly relative to the mineral frame (no movement of water in or out of a unit volume), the effective density of the medium is the sum of the mass of water and solids in a unit volume, wave velocity and energy damping (e.g., 1/Q) are independent of frequency, and Hookean elastic equations can be used in studying wave velocities unless energy damping is to be considered. The closed system as a special case in the elasticity or viscoelasticity of saturated, porous media, has been noted in many studies (references in Hamilton, 1972).

The bulk modulus was selected as the third constant to use in computing the other elastic constants because it appears possible to compute a valid bulk modulus from its com-

ponents. The equation used in this computation (Gassmann, 1951) is

$$K = K_s \frac{K_f + Q}{K_s + Q} \qquad Q = \frac{K_w(K_s - K_f)}{n(K_s - K_w)} \qquad (18)$$

where,

K_s = aggretate bulk modulus of mineral solids

K_f = frame bulk modulus ("skeletal" bulk modulus of Gassmann, 1951)

K_w = bulk modulus of pore water

n = decimal-fractional porosity of sediment.

Good values for the bulk modulus of distilled and sea water, K_w, and most of the common minerals of sediments, K_s, have been established in recent years. This leaves only a value for the frame bulk modulus, K_f, needed to compute a bulk modulus for the water-mineral system.

A contribution of Hamilton (1971a) was in derivation of a relationship between sediment porosity and the dynamic frame bulk modulus. Using this relationship, the frame bulk modulus was derived for each sample, and used with the bulk moduli of pore water and minerals to compute the system bulk modulus with Equation (18). The expectable excellent relations between porosity and the bulk modulus are shown in Figure 19.

The computed bulk modulus, and measured density and compressional-wave velocity were then used to compute the other elastic constants. Those equations using these three constants were favored. The equations are

$$\text{Compressibility, } \beta = \frac{1}{\kappa} \tag{19}$$

$$\text{Lamé's constant, } \lambda = \frac{3\kappa - \rho V_p^2}{2} \tag{20}$$

$$\text{Poisson's ratio, } \sigma = \frac{3\kappa - \rho V_p^2}{3\kappa + \rho V_p^2} \tag{21}$$

$$\text{Rigidity (Shear) Modulus, } \mu = (\rho V_p^2 - \kappa)3/4 \tag{22}$$

$$\text{Velocity of shear wave, } V_s = (\mu/\rho)^{1/2} \tag{23}$$

Tables of measured and computed elastic constants for various sediment types are in Hamilton (1971a); up-dated tables are in Hamilton (1974a) and in this report (Tables 5, 6). The decimal places do not indicate accuracy, but are merely listed for comparisons. The values of the elastic properties listed should be regarded as approximations and predictions for comparison with future measurements.

The values for the elastic constants in the tables and figures are for 23° C and 1 atmosphere pressure. These can be used in some basic studies, but cannot be used as in situ values because density, velocity, and the bulk modulus all require corrections from laboratory to in situ. Such corrections with a numerical example are in Hamilton (1971b).

Shear Wave Velocities, Gradients, and Attenuation

Near-surface velocities of shear waves.- The bulk moduli, k, of the deep-water sediments are plotted against density X (velocity)^2, or ρV_p^2, in Figure 20. When a material lakcs rigidity, k = ρV_p^2. A line representing k = ρV_p^2 is also plotted in Figure 20. Assuming these are true values of k, the consistent divergence of the data from the line indicates the presence and approximate values of rigidity, μ ($\rho V_p^2 = k + 4/3\mu$). In Figure 8 (porosity vs. velocity), almost all points are well above Wood's equation for a suspension, which also indicates the presence of appreciable rigidity. The conclusion that almost all natural marine sediments have enough rigidity to transmit shear waves is supported by such laboratory measurements and computations, and by actual in situ measurements.

The computed values of shear wave velocities for the various sediments are listed in Tables 5 and 6. The least values of shear velocity (170 to 190 m/sec) are in deep-water clays in the abyssal plain and abyssal hill environments, and the highest values (470 m/sec) in continental terrace fine sands.

The computed values in the tables are comparable to values measured in situ. A survey of the literature indicates that near-surface shear wave velocities in water-saturated sands vary from 50 to over 500 m/sec (e.g., Cunny and Fry, 1973; Hamilton et al., 1970; White and Sengbush, 1953; Shima et al., 1968; Kawasumi et al., 1966; Barnes et al., 1973). Some measured, in situ, near-surface shear wave velocities in silt-clays ("muds"), include: 30 m/sec in a tidal mud flat near Monterey, California (Lasswell, 1970); 90 m/sec in San Francisco Bay mud (Warrick, 1974); 50 to 190 m/sec in deep-sea pelagic sediments in the Indian Ocean (Davies, 1965); 137 m/sec in silty clay on land (Cunny and Fry, 1973); 100 to 300 m/sec in silt in Japan (Kudo and Shima, 1970; Shima et al., 1968).

Shear wave velocity versus depth in marine sediments.- A recent, unpublished report (Hamilton, 1975c) reviewed the available data concerning the variations of shear wave velocity with depth in sands and in silt-clays.

The shear wave velocity measurements in sands included 29 selected in situ values at depths to 12 m (Figure 21). The regression equation for these data is $V_s = 128(D)^{0.28}$, where V_s is shear wave velocity in m/sec, and depth, D, in m. The data from field and laboratory studies indicates that shear wave velocity is proportional to the 1/3 to 1/6 power of pressure or depth in sands; that the 1/6 power is not reached until very high pressures are applied; and that for most sands, the velocity of shear waves is proportional to the 3/10 to 1/4 power of depth or pressure. The use of a depth exponent of 0.25 is recommended for prediction of shear velocity vs. depth in sands.

The shear velocity measurements in silt-clays and turbidites included 47 selected, in situ measurements to depths of 650 m (Figure 22). The shear velocity gradient in the upper 40 m ($4.65\ sec^{-1}$) is 4 to 5 times greater than is the compressional velocity in comparable sediments. At deeper depths, shear velocity and compressional velocity gradients are comparable.

Attenuation of shear waves (general).- There is an interesting approximation of the relations between attenuation and velocity which has been derived from Equations (10) and (11) with the assumption that bulk viscosity, k' ($k' = \lambda' + 2/3\mu'$) is zero; resulting in: $\lambda' = -2/3\mu'$ (Kolsky, 1963; Vasil'ev and Gurevich, 1962; De Bremaecker et al., 1966). Substituting for λ' in Equation (10), and then substituting $\mu' = \mu/Q_s$ (Equation, 11), $\mu = \rho V_s^2$, and $(\lambda + 2u) = \rho V_p^2$, yields

$$\frac{Q_p}{Q_s} = 0.75 \frac{V_p^2}{V_s^2} \qquad (24)$$

All of the cited authors, above, noted that Equation (24) is not in accord with the sparse experimental data.

De Bremaecker et al. (1966) set $\lambda' = 0$ for sedimentary rocks, which leads to

$$\frac{Q_p}{Q_s} = 0.50 \frac{V_p^2}{V_s^2} \tag{25}$$

which these authors believed more in accord with the experimental data.

The few available values (measured and computed) for the numerical coefficient in Equations (24) and (25), for saturated marine sediments, indicate it to be much less than 0.75 or 0.50; more in the range of 0.03 to 0.2.

Because of the many uncertainties and assumptions involved in computing shear wave energy losses using Equations (24) or (25) (or variations thereof), it is considered a better method at this time, in the absence of measurements, to use logarithmic decrements, Δ_s, and the ratio of compressional wave decrement to shear wave decrements, Δ_p / Δ_s to approximate values of shear wave attenuation. The relationships between the logarithmic decrement and the attenuation coefficient are shown in Equations (8) and (9).

Logarithmic decrement of shear waves (sands).- Literature values of the logarithmic decrement of shear waves in sands range mostly from 0.1 to 0.6 for laboratory and in situ studies; most values lie between 0.2 and 0.4. There are very few measurements of Δ_p / Δ_s. One of the best in situ studies using shear waves, was that of Kudo and Shima (1970) who derived a logarithmic decrement value of 0.39 for diluvial sand in Tokyo. Kudo and Shima (1970) also found that the attenuation of shear waves was approximately proportional to the first power of frequency, and that there was no velocity dispersion in the range of 30 to 80 Hz. Meissner (1965) measured Δ_s as 0.125 to 0.325 (avg. 0.25) in situ in diluvial sand and clay. Barkan (1962) reported damping ratio, D, values which convert to values of Δ_s between 0.3 and 0.4 ($\Delta_s \approx 2\pi D$). Both Seed and Idriss (1970) and Whitman and Richart (1967) have used

damping ratios equivalent to $\Delta_s = 0.31$ for sands and other sediments. In summary, if values of shear wave energy losses in sands are required for computations, a value of $\Delta_s = 0.3$ can be assumed and used with shear wave lengths to derive values of attenuation (e.g., with Equations 8, 9, and 13).

Logarithmic decrements of shear waves (silt-clays).- Values of logarithmic decrement in silt-clays vary from about 0.1 to 0.6, as in sands. The best values are probably in the range of 0.1 to 0.3 (Molotova, 1966; Zhadin, in Vasil'ev and Gurevich, 1962; Richart et al., 1970; Barkan, 1962; Kudo and Shima, 1970). Whitman and Richart (1967) and Seed and Idriss (1970) have used damping ratios of 0.05 ($\Delta_s = 0.31$) for silt-clay soils. The few literature values of Δ_p / Δ_s are about 0.2 to 0.3. When computing values of shear wave attenuation in water-saturated clay, Berzon et al. (1967) chose a value of 0.3 for Δ_p / Δ_s. It is recommended that if approximate values of attenuation of shear waves are desired for silt-clays, that a value of $\Delta_p / \Delta_s = 0.3$ be assumed, and Δ_s computed after reducing measured or predicted compressional wave attenuation to Δ_p using Equations (13) and (9). After Δ_s is derived, shear wave attenuation can be computed from Equations (9) and (13).

Shear wave attenuation in shale and mudstone.- Very little information is available for in situ shear wave attenuation in shales and mudstones. The two best known to the writer are studies of compressional and shear waves in the Pierre shale (f = 20 to 125 Hz) and in mudstone in Japan (15 to 90 Hz). McDonal et al. (1958) measured the following in Pierre shale:

$\Delta_p \approx 0.087$, $\Delta_s \approx 0.324$, and $\Delta_p / \Delta_s \approx 0.27$.

Shear wave attenuation in dB/m in Pierre shale is about 10 times greater than compressional wave attenuation. Kudo and Shima (1970) measured shear wave velocity and attenuation in Tertiary mudstone in Tokyo. These values were $V_s = 420$ m/sec, $Q_s = 6.5$, and $\Delta_s = 0.48$.

Shear wave attenuation versus frequency.- The little information presently available indicates that shear wave attenuation, as compressional wave attenuation, is dependent on the first power of frequency (e.g., Kudo and Shima, 1970; McDonal et al., 1958). Some of the shear wave energy-loss data previously referenced can be placed in the form of Equation (5), where the attenuation of shear waves, α_s is in dB/m, and frequency, f, is in kHz. Examples computed by the writer are:

Material	Equation	Reference
Diluvial sand	$\alpha_s = 13.2f$	Kudo and Shima (1970)
Diluvial sand and clay	$\alpha_s = 4.8f$	Meissner (1965)
Alluvial silt	$\alpha_s = 13.4f$	Kudo and Shima (1970)
Water-saturated clay	$\alpha_s = 15.2f$	Molotova (1966)
Tertiary mudstone	$\alpha_s = 10.1f$	Kudo and Shima (1970)
Pierre shale	$\alpha_s = 3.4f$	McDonal et al. (1958)

Comparisons of the attenuation of compressional and shear waves (in dB/m) indicate that, in the few cases available, shear wave attenuation is on the order of 10 to 20 times greater than compressional wave attenuation.

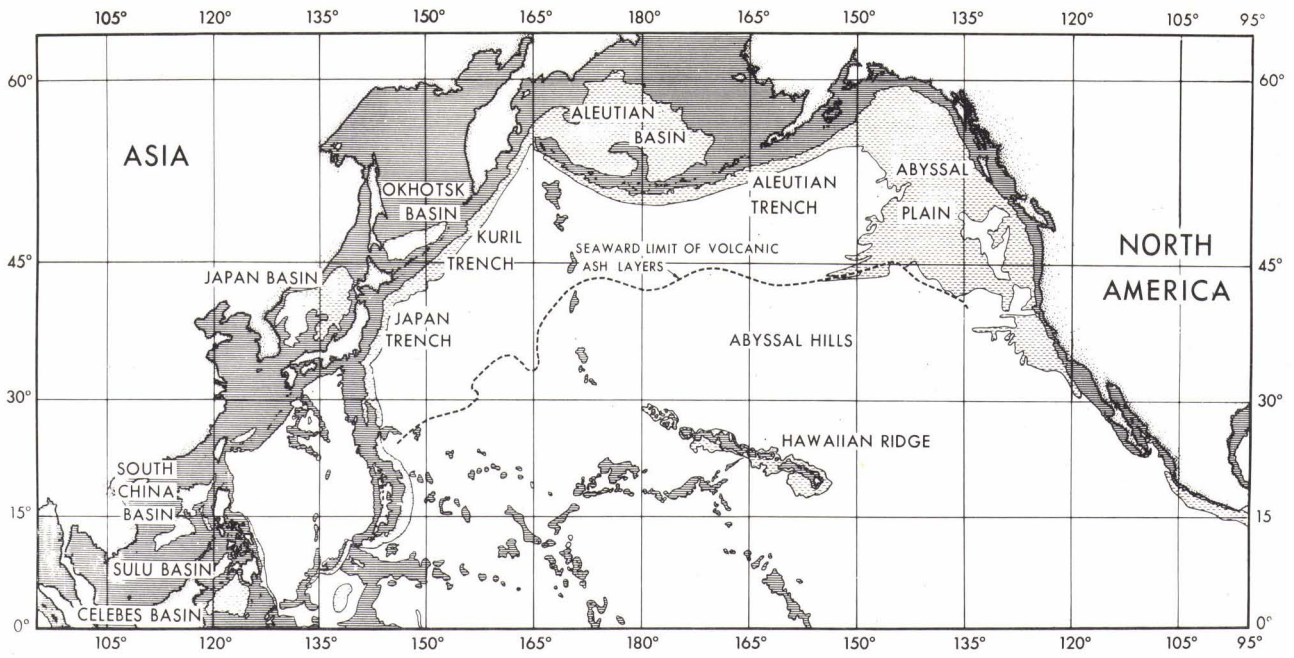

FIG. 1 PHYSIOGRAPHIC PROVINCES AND RELATED ENVIRONMENTS, NORTH PACIFIC AND ADJACENT AREAS. SEAWARD LIMIT OF VOLCANIC ASH LAYERS FROM HORN ET AL (1969). THE THREE GENERAL ENVIRONMENTS ARE CONTINENTAL TERRACE (SHELF AND SLOPE): SOLID, HORIZONTAL LINES; ABYSSAL PLAIN (TURBIDITE): HORIZONTAL, DASHED LINES; AND ABYSSAL HILL (PELAGIC): WHITE AREAS.

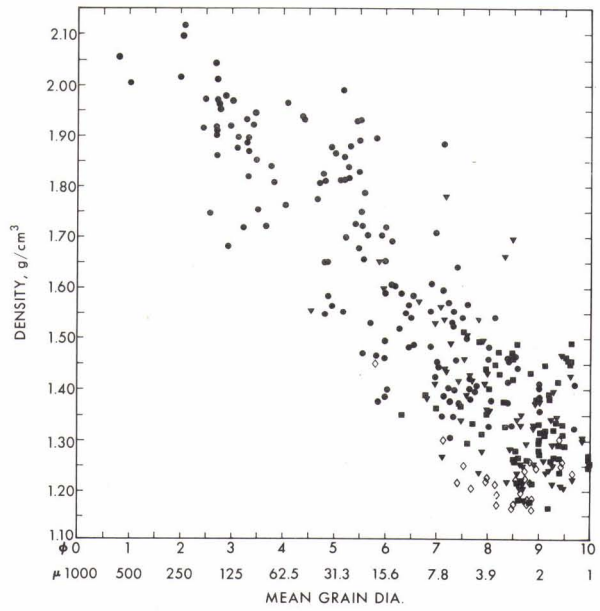

FIG. 2 MEAN DIAMETER OF MINERAL GRAINS VERSUS DENSITY. ROUND DOTS ARE CONTINENTAL TERRACE (SHELF AND SLOPE) SAMPLES; SQUARES ARE ABYSSAL HILL SAMPLES; TRIANGLES ARE ABYSSAL PLAIN SAMPLES; OPEN DIAMONDS ARE DIATOMACEOUS SAMPLES FROM THE BERING AND OKHOTSK SEAS.

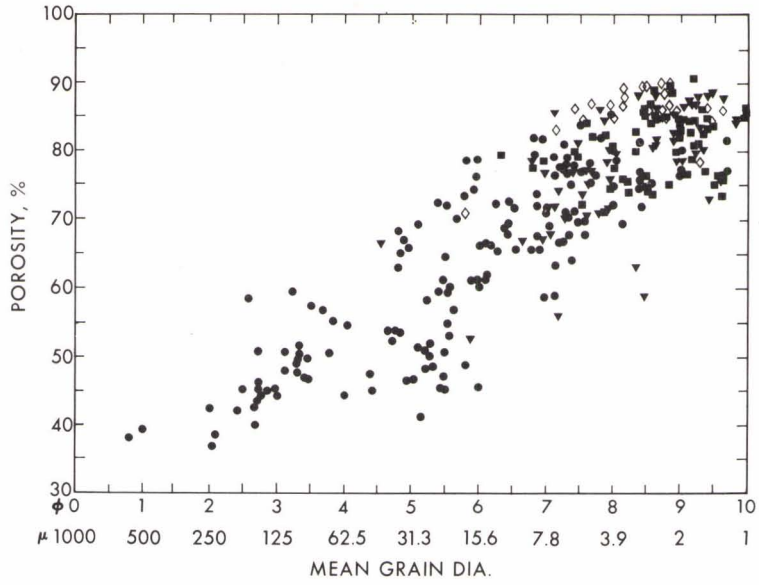

FIG. 3
MEAN DIAMETER OF MINERAL GRAINS VERSUS POROSITY, ALL ENVIRONMENTS; SYMBOLS AS IN FIGURE 2.

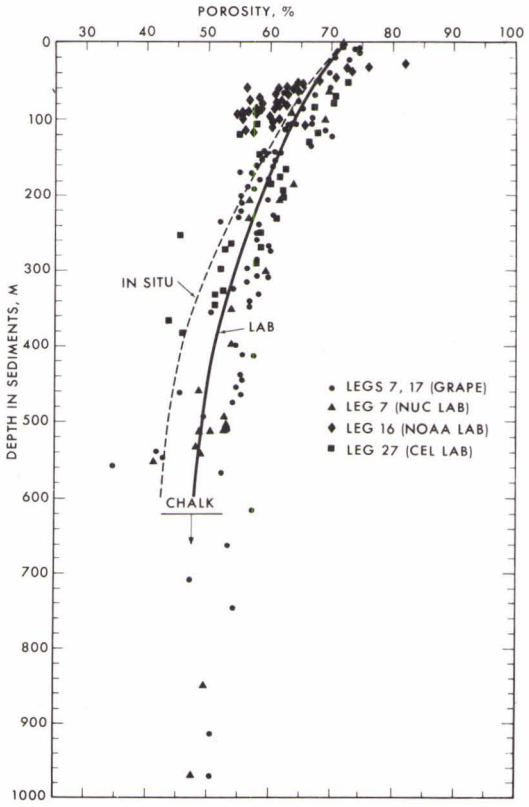

FIG. 4
POROSITY VERSUS DEPTH IN CALCAREOUS SEDIMENTS, CENTRAL PACIFIC. SYMBOLS ARE LABORATORY VALUES FROM THE DEEP SEA DRILLING PROJECT. DERIVATION OF THE IN SITU CURVE EXPLAINED IN THE TEXT.

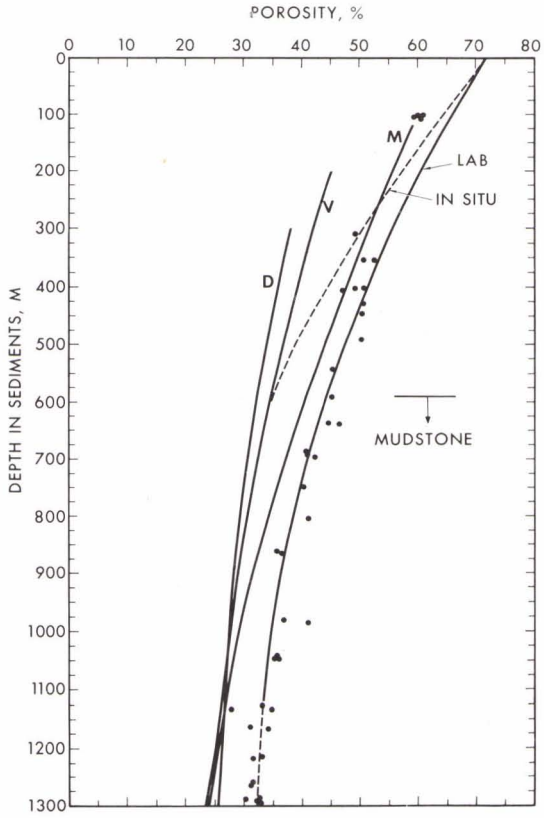

FIG. 5
POROSITY VERSUS DEPTH IN TERRIGENOUS SEDIMENTS. DOTS ARE LABORATORY VALUES FROM DEEP SEA DRILLING PROJECT SIZE 222 IN THE ARABIAN SEA. CURVE "D": GULF COAST SHALE (DICKINSON, 1953); CURVE "V" IS SHALE FROM VASSOEVICH (IN RIEKE AND CHILINGARIAN, 1974, p. 40, Fig. 16); CURVE "M": MUDSTONE IN JAPAN (MAGARA, 1968).

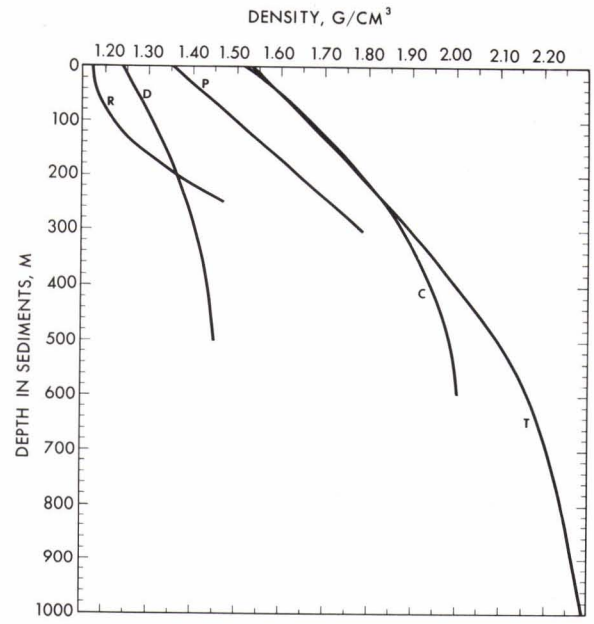

FIG. 6
IN SITU DENSITY OF VARIOUS MARINE SEDIMENTS VERSUS DEPTH IN THE SEA FLOOR. LETTERS INDICATE SEDIMENT TYPE: R IS RADIOLARIAN OOZE; D IS DIATOMACEOUS OOZE; P IS PELAGIC CLAY; C IS CALCAREOUS SEDIMENT; T IS TERRIGENOUS SEDIMENT.

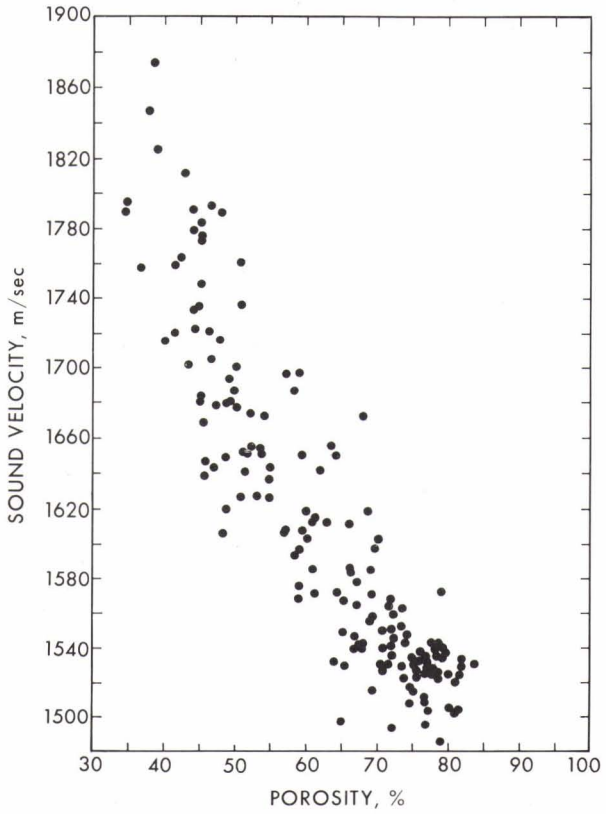

FIG. 7
SEDIMENT POROSITY VERSUS SOUND VELOCITY, CONTINENTAL TERRACE.

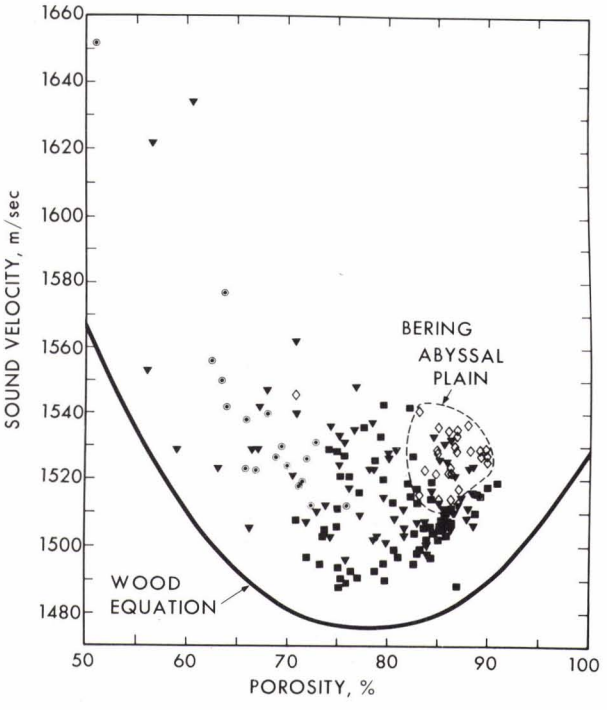

FIG. 8
SEDIMENT POROSITY VERSUS SOUND VELOCITY, ABYSSAL HILL AND ABYSSAL PLAIN ENVIRONMENTS; SYMBOLS AS IN FIGURE 2, EXCEPT CIRCLED DOTS ARE CALCAREOUS SAMPLES.

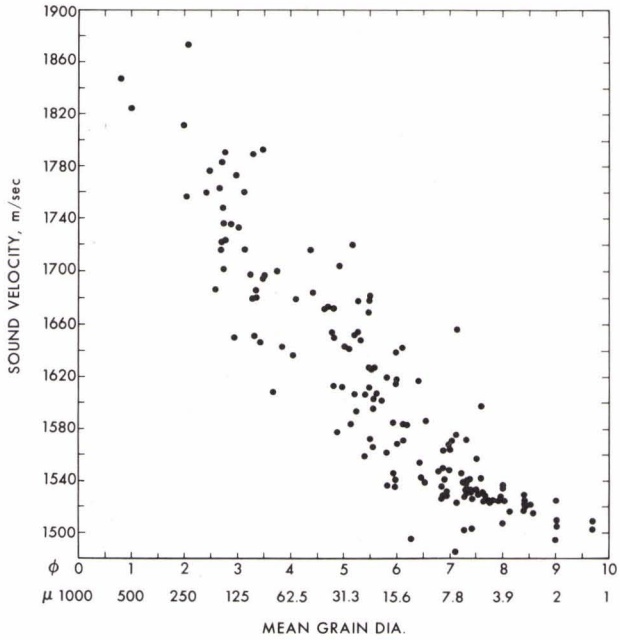

FIG. 9
MEAN DIAMETER OF MINERAL GRAINS VERSUS SOUND VELOCITY, CONTINENTAL TERRACE (SHELF AND SLOPE).

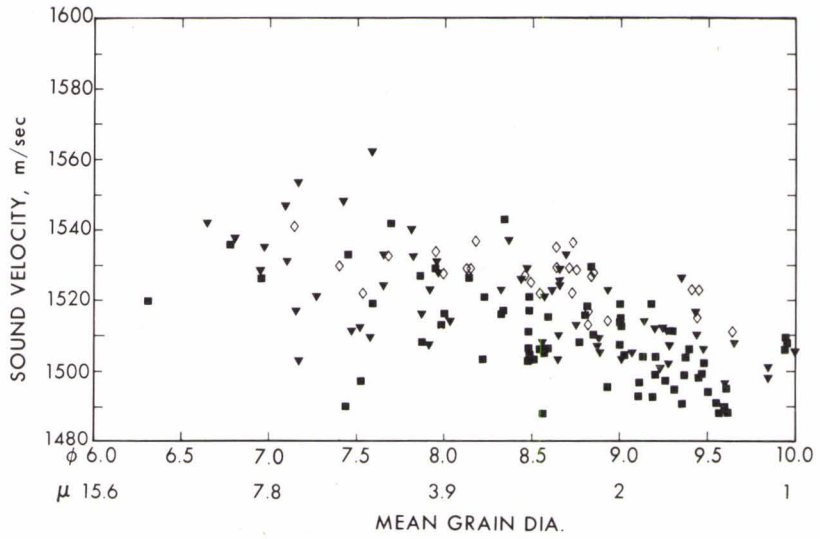

FIG. 10 MEAN DIAMETER OF MINERAL GRAINS VERSUS SOUND VELOCITY, ABYSSAL HILL AND ABYSSAL PLAIN ENVIRONMENTS; SYMBOLS AS IN FIG. 2.

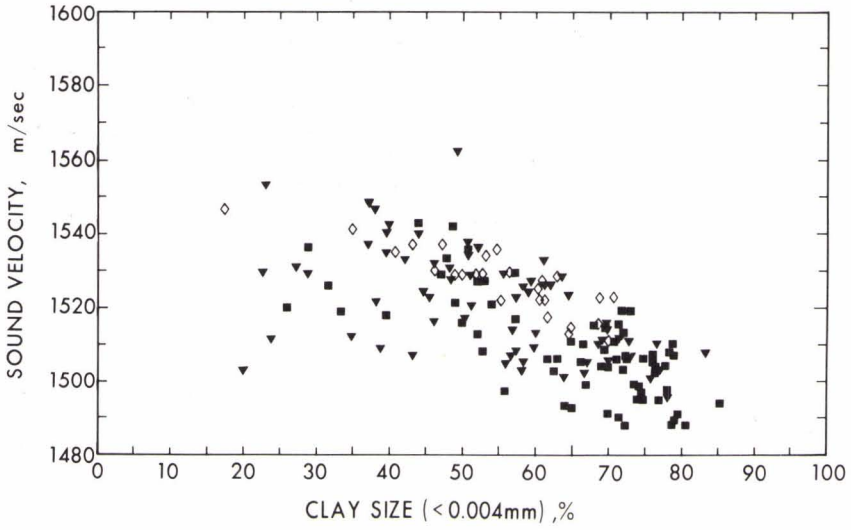

FIG. 11 PERCENT CLAY SIZE VERSUS SOUND VELOCITY, ABYSSAL HILL AND ABYSSAL PLAIN ENVIRONMENTS; SYMBOLS AS IN FIGURE 2.

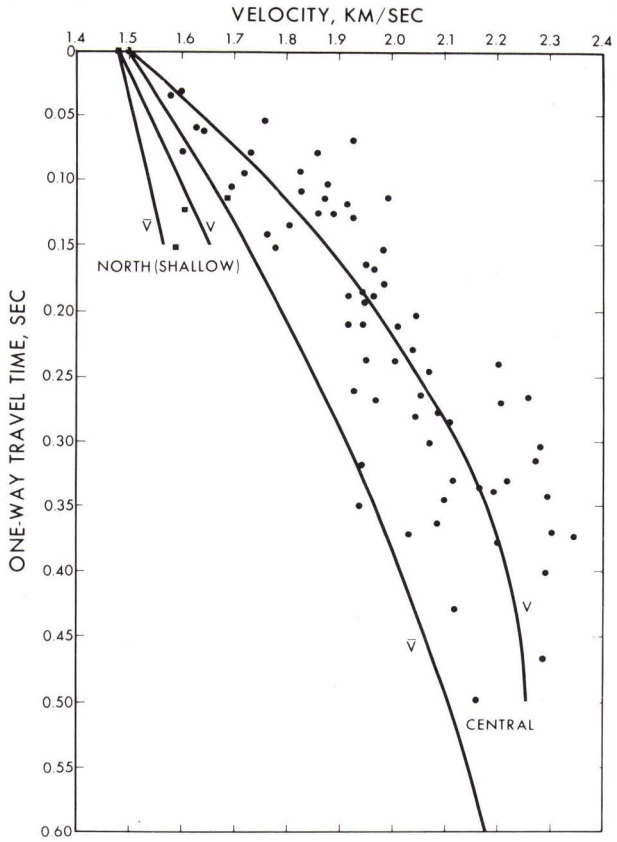

FIG. 12
INSTANTANEOUS VELOCITY, V, AND MEAN VELOCITY, $\bar{V}$, VERSUS ONE-WAY TRAVEL TIME IN THE CENTRAL (DOTS) AND NORTHERN (SQUARES) BENGAL FAN IN THE BAY OF BENGAL (FROM HAMILTON ET AL., 1974).

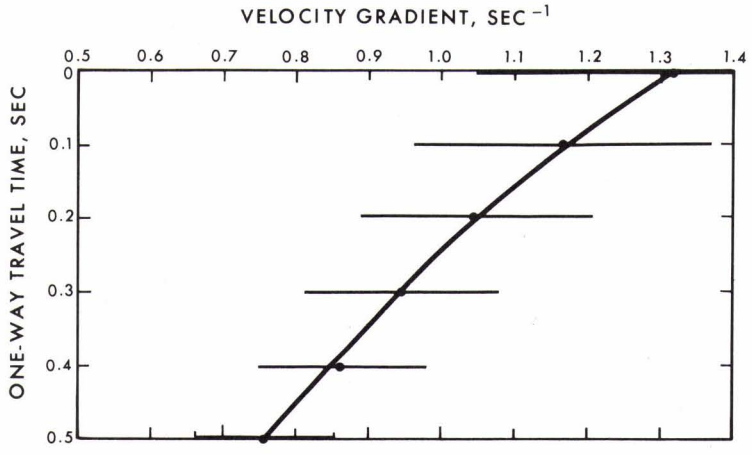

FIG. 13
AN AVERAGE LINEAR VELOCITY GRADIENT, IN METERS PER SECOND PER METER, OR SEC^{-1}, VERSUS ONE-WAY TRAVEL TIME OF SOUND IN THE SEA FLOOR. THE LINEAR GRADIENTS AT INCREMENTS OF 0.1 sec WERE AVERAGED FROM 13 AREAS IN WHICH THE SEDIMENTS WERE LARGELY TURBIDITES. THE HORIZONTAL BARS INDICATE 95 PERCENT CONFIDENCE LIMITS (REVISED FROM HAMILTON ET AL., 1974).

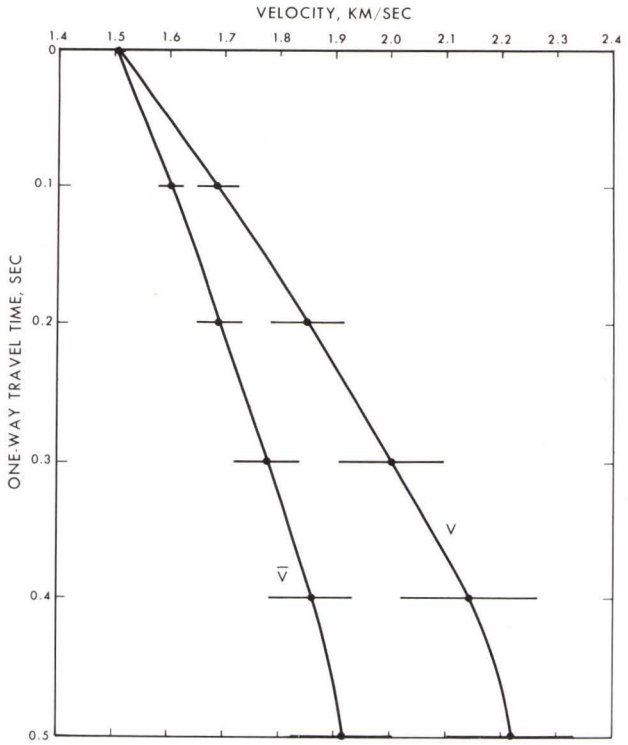

FIG. 14
INSTANTANEOUS VELOCITY, V, AND MEAN VELOCITY, $\bar{V}$, VERSUS ONE-WAY TRAVEL TIME IN THE SEA FLOOR. THE CURVES ARE AVERAGES FOR 13 AREAS IN WHICH THE SEDIMENTS ARE LARGELY TURBIDITES. THE HORIZONTAL BARS INDICATE 95 PERCENT CONFIDENCE LIMITS. SEE HAMILTON ET AL. (1974) FOR DISCUSSIONS.

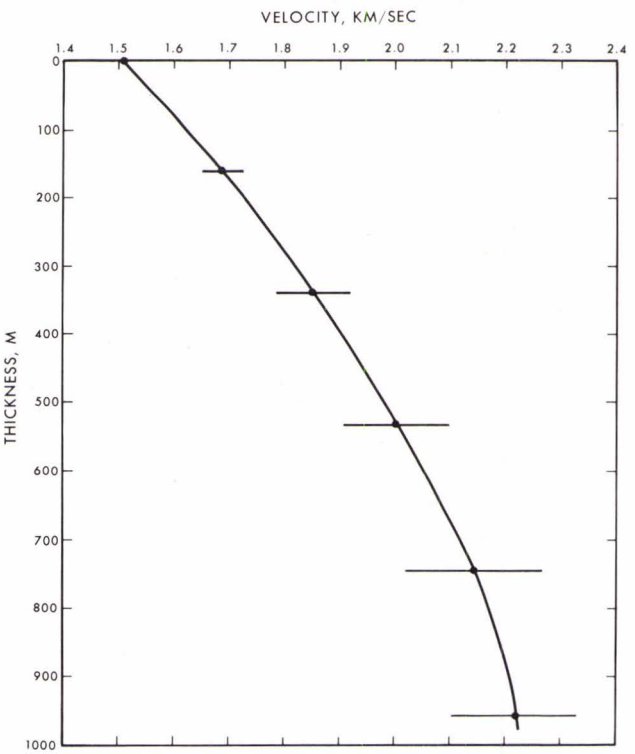

FIG. 15
INSTANTANEOUS SOUND VELOCITY VERSUS THICKNESS (OR DEPTH IN THE SEA FLOOR). THE CURVE IS AN AVERAGE FOR 13 AREAS IN WHICH THE SEDIMENTS ARE LARGELY TURBIDITES. THE HORIZONTAL BARS INDICATE 95 PERCENT CONFIDENCE LIMITS.

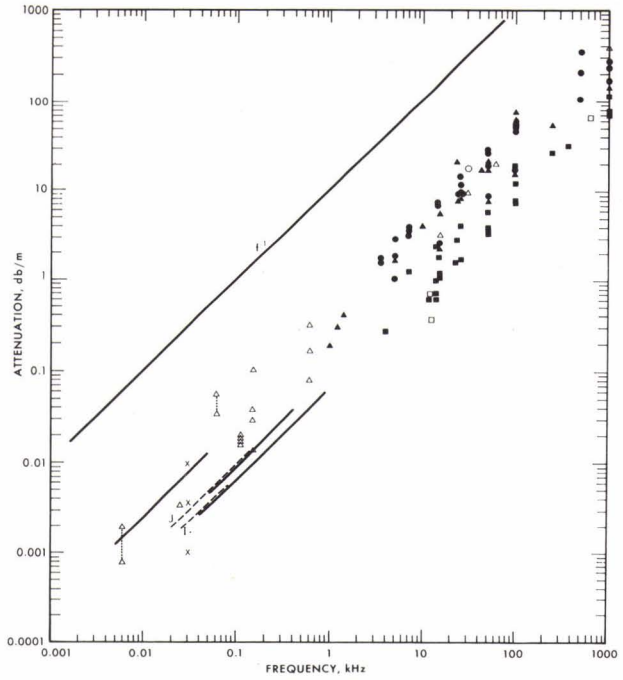

FIG. 16 ATTENUATION OF COMPRESSIONAL (SOUND) WAVES VERSUS FREQUENCY IN NATURAL, SATURATED SEDIMENTS AND SEDIMENTARY STRATA. SYMBOLS: CIRCLES–SANDS (ALL SIZES); SQUARES–CLAY–SILT (MUD); TRIANGLES– MIXED SIZES (e.g, SILTY SAND, SANDY SILT). THE SOLID LINES AND SYMBOLS ARE FROM HAMILTON (1972, Fig. 2); THE OPEN SYMBOLS AND DASHED LINES ARE NEWLY–ADDED DATA. THE LINES MARKED "J" AND "I" REPRESENT GENERAL EQUATIONS FOR THE JAPAN SEA AND INDIAN OCEAN CENTRAL BASIN (FROM NEPROCHNOV, 1971). THE VERTICAL, DASHED LINES INDICATE A RANGE OF ATTENUATION VALUES AT A SINGLE FREQUENCY. THE LINE LABELLED "f^1" INDICATES THE SLOPE OF ANY LINE HAVING A DEPENDENCE OF ATTENUATION ON THE FIRST POWER OF FREQUENCY.

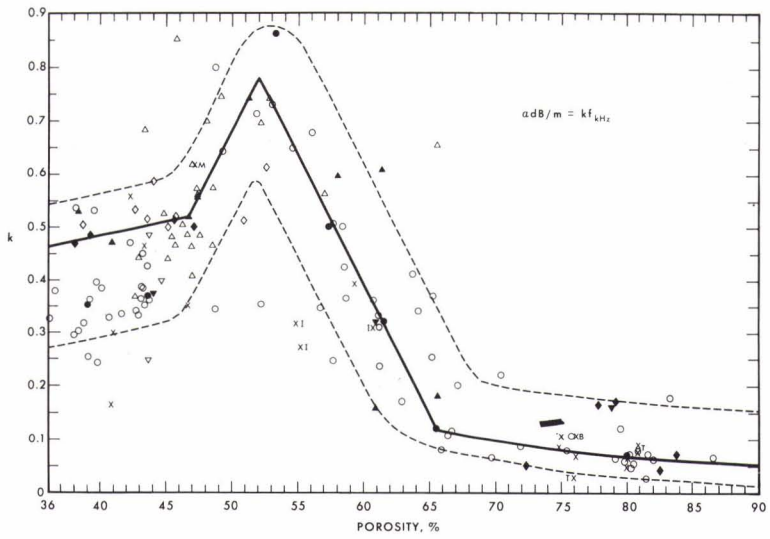

FIG. 17 ATTENUATION OF COMPRESSIONAL WAVES (EXPRESSED AS k IN: $\alpha_{dB/m} = kf_{kHz}$) VERSUS SEDIMENT POROSITY IN NATURAL, SATURATED SURFACE SEDIMENTS. SOLID SYMBOLS ARE AVERAGES AND OPEN SYMBOLS ARE THE AVERAGED DATA FROM MEASUREMENTS OFF SAN DIEGO; SOLID LINES ARE REGRESSIONS ON THE BEST DATA (See HAMILTON, 1972, for discussion); X INDICATES A VALUE FROM THE LITERATURE. THE DASHED LINES REPRESENT AREAS INTO WHICH IT IS PREDICTED MOST DATA WILL FALL. REGRESSION EQUATIONS ARE INCLUDED IN THE CAPTION TO THE ORIGINAL FIGURE (HAMILTON, 1972, Fig. 5) FOR THE SOLID LINES. NEWLY–ADDED DATA ARE THREE STATIONS IN SILTY SAND (IGARASHI, 1973) MARKED "I", AN AVERAGE OF 11 CORES OF PELAGIC CLAY (BUCHAN ET AL, 1971) MARKED "B", FINE SAND (MUIR AND ADAIR, 1972) MARKED "M", AND SILTY CLAY AND CALCAREOUS SEDIMENTS FROM TYCE (1975) MARKED "T".

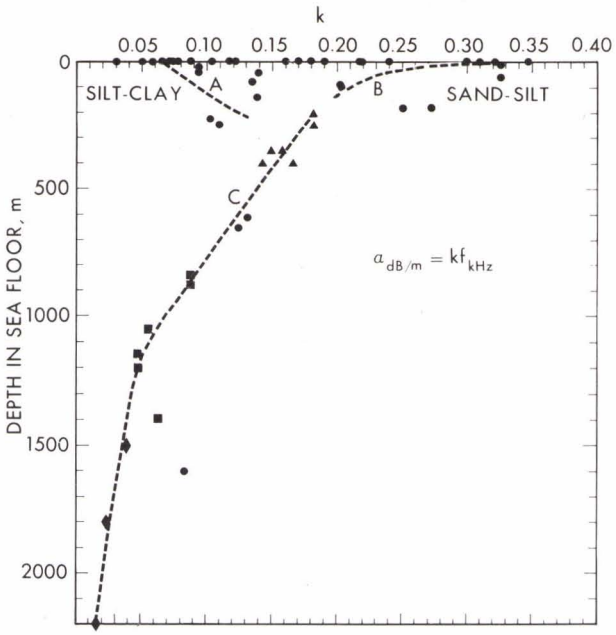

FIG. 18
ATTENUATION OF COMPRESSIONAL WAVES (EXPRESSED AS k IN : $\alpha = {}_{dB/m} = kf_{kHz}$) VERSUS DEPTH IN THE SEA FLOOR, OR IN SEDIMENTARY STRATA. SYMBOLS : CIRCLES–MEASUREMENTS FROM THE LITERATURE ; TRIANGLES, SQUARES, AND DIAMONDS REPRESENT THE FIRST, SECOND, AND THIRD LAYERS, RESPECTIVELY, IN THE SEA FLOOR IN 7 AREAS (FROM NEPROCHNOV, 1971). SEE TEXT FOR DISCUSSION OF THE LABELLED CURVES.

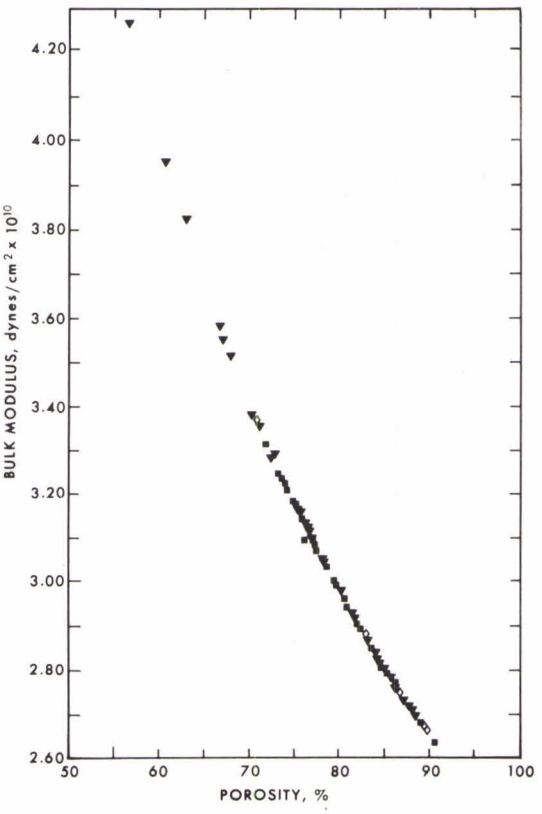

FIG. 19
SEDIMENT POROSITY VERSUS COMPUTED BULK MODULUS (23° C, 1 ATMOS.) FOR THE ABYSSAL HILL AND ABYSSAL PLAIN ENVIRONMENTS.

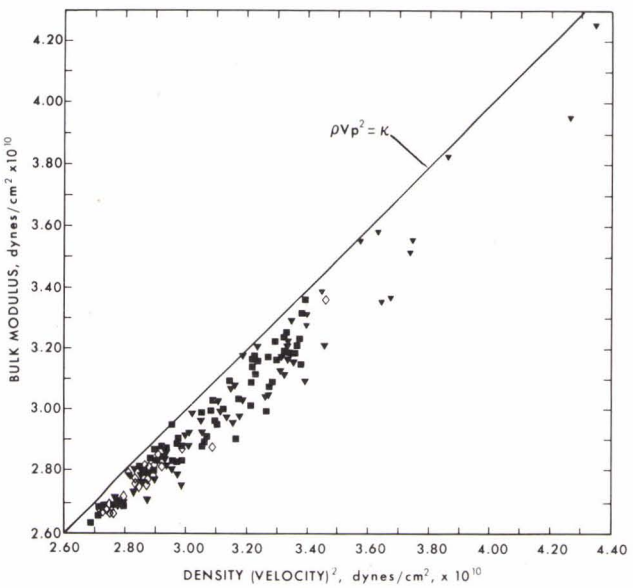

FIG. 20
DENSITY X (COMPRESSIONAL VELOCITY)^2 VERSUS COMPUTED BULK MODULUS OF SEDIMENT SAMPLES (23° C, 1 ATMOS.) IN THE ABYSSAL HILL AND ABYSSAL PLAIN ENVIRONMENTS. THE LINE LABELLED " $\rho V_p^2 = k$" INDICATES RELATIONSHIPS IF THE SAMPLES HAD NO RIGIDITY.

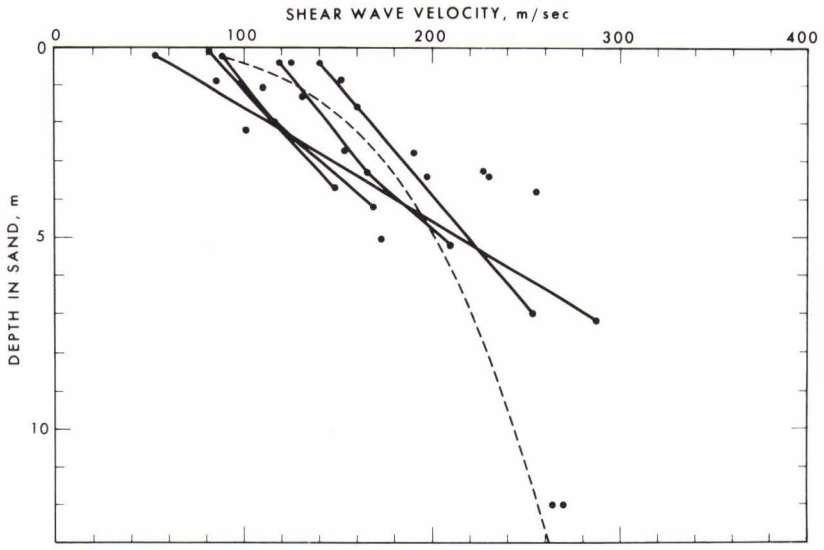

FIG. 21 SHEAR WAVE VELOCITY VERSUS DEPTH IN WATER-SATURATED SANDS. ALL MEASUREMENTS ARE IN SITU; MULTIPLE MEASUREMENTS AT THE SAME SITE ARE CONNECTED BY SOLID LINES. THE DASHED LINE IS THE REGRESSION EQUATION: $V_s = 128(D)^{0.28}$; V_s in m/sec, and D is depth in m.

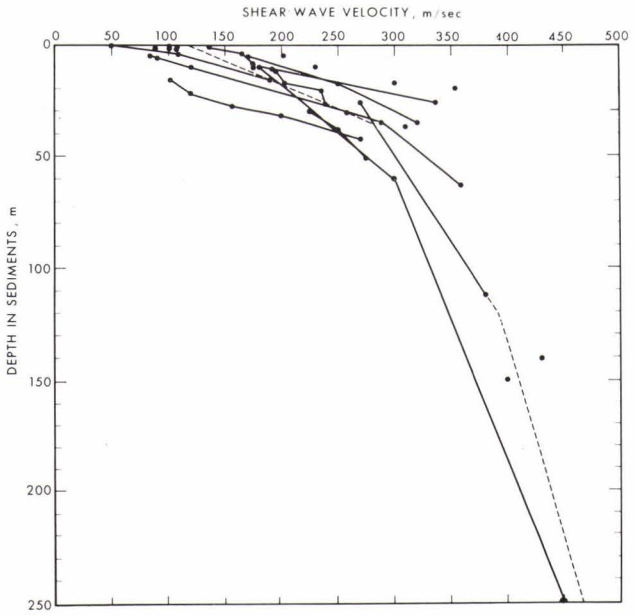

FIG. 22 SHEAR WAVE VELOCITY MEASURED IN SITU VERSUS DEPTH IN WATER-SATURATED SILT-CLAYS AND TURBIDITES. MULTIPLE MEASUREMENTS AT THE SAME SITE ARE CONNECTED BY SOLID LINES. THE DASHED LINES ARE THREE LINEAR REGRESSIONS. ONE MEASUREMENT (V_s = 700 m/sec at 650 m) IS NOT SHOWN.

TABLE 1a. Continental Terrace (Shelf and Slope) Environment; average sediment size analyses and bulk grain densities.

Sediment Type	No. Samples	Mean Grain Dia. mm	Mean Grain Dia. ϕ	Sand, %	Silt, %	Clay, %	Bulk Grain Density g/cm^3
Sand							
Coarse	2	0.5285	0.92	100.0	0.0	0.0	2.710
Fine	18	0.1638	2.61	92.4	4.2	3.4	2.708
Very fine	6	0.0915	3.45	84.2	10.1	5.7	2.693
Silty sand	14	0.0679	3.88	64.0	23.1	12.9	2.704
Sandy silt	17	0.0308	5.02	26.1	60.7	13.2	2.668
Silt	12	0.0213	5.55	6.3	80.6	13.1	2.645
Sand-silt-clay	20	0.0172	5.86	32.2	41.0	26.8	2.705
Clayey silt	60	0.0076	7.05	7.2	59.7	33.1	2.660
Silty Clay	19	0.0027	8.52	4.8	41.2	54.0	2.701

TABLE 1b. Continental Terrace (Shelf and Slope) Environment; sediment densities, porosities, sound velocities, and velocity ratios.

Sediment Type	Density, g/cm^3		Porosity, %		Velocity, m/sec		Velocity Ratio	
	Avg.	SE	Avg.	SE	Avg.	SE	Avg.	SE
Sand								
Coarse	2.034	—	38.6	—	1836	—	1.201	—
Fine	1.957	0.023	44.8	1.36	1753	11	1.147	0.007
Very fine	1.866	0.035	49.8	1.69	1697	32	1.111	0.021
Silty sand	1.806	0.026	53.8	1.60	1668	11	1.091	0.007
Sandy silt	1.787	0.044	52.5	2.44	1664	13	1.088	0.008
Silt	1.767	0.037	54.2	2.06	1623	8	1.062	0.005
Sand-silt-clay	1.590	0.026	66.8	1.46	1579	8	1.033	0.005
Clayey silt	1.488	0.016	71.6	0.87	1549	4	1.014	0.003
Silty clay	1.421	0.015	75.9	0.82	1520	3	0.994	0.002

Notes.

Laboratory values: 23° C, 1 atm; density: saturated bulk density; porosity: salt free; velocity ratio: velocity in sediment/velocity in sea water at 23° C, 1 atm, and salinity of sediment pore water. SE: Standard error of the mean.

TABLE 2a. Abyssal Plain and Abyssal Hill Environments; average sediment size analyses and bulk grain densities.

Environment Sediment Type	No. Samples	Mean Grain Dia. mm	Mean Grain Dia. ϕ	Sand, %	Silt, %	Clay, %	Bulk Grain Density, g/cm^3
Abyssal Plain							
Sandy silt	1	0.0170	5.88	19.4	65.0	15.6	2.461
Silt	3	0.0092	6.77	3.2	78.0	18.8	2.606
Sand-silt-clay	2	0.0208	5.59	35.2	33.3	31.5	2.653
Clayey silt	22	0.0053	7.57	4.5	55.3	40.2	2.650
Silty clay	40	0.0021	8.90	2.5	36.0	61.5	2.660
Clay	6	0.0014	9.53	0.0	22.2	77.8	2.663
Bering Sea and Okhotsk Sea (Diatomaceous)							
Silt	1	0.0179	5.80	6.5	76.3	17.2	2.474
Clayey silt	5	0.0049	7.68	8.1	49.1	42.8	2.466
Silty clay	23	0.0024	8.71	3.0	37.4	59.6	2.454
Abyssal Hill							
Deep-sea ("red") pelagic clay							
Clayey silt	17	0.0056	7.49	3.9	58.7	37.4	2.678
Silty clay	60	0.0023	8.76	2.1	32.2	65.7	2.717
Clay	45	0.0015	9.43	0.1	19.0	80.9	2.781
Calcareous ooze							
Sand-silt-clay	5	0.0146	6.10	27.3	42.8	29.9	2.609
Silt	1	0.0169	5.89	16.3	75.6	8.1	2.625
Clayey silt	15	0.0069	7.17	3.4	60.7	35.9	2.678
Silty clay	4	0.0056	7.48	3.9	39.9	56.2	2.683

TABLE 2b. Abyssal Plain and Abyssal Hill Environments; sediment densities, porosities, sound velocities, and velocity ratios.

Environment Sediment Type	Density, g/cm^3		Porosity, %		Velocity, m/sec		Velocity Ratio	
	Avg.	SE	Avg.	SE	Avg.	SE	Avg.	SE
Abyssal Plain								
Sandy silt	1.652	—	56.6	—	1622	—	1.061	—
Silt	1.604	—	63.6	—	1563	—	1.022	—
Sand-silt-clay	1.564	—	66.9	—	1536	—	1.004	—
Clayey silt	1.437	0.023	75.2	1.31	1526	3	0.998	0.002
Silty clay	1.333	0.019	81.4	1.03	1515	2	0.991	0.001
Clay	1.352	0.037	80.0	2.20	1503	2	0.983	0.001
Bering Sea and Okhotsk Sea (Diatomaceous)								
Silt	1.447	—	70.8	—	1546	—	1.011	—
Clayey silt	1.228	0.019	85.8	0.86	1534	2	1.003	0.001
Silty clay	1.214	0.008	86.8	0.43	1525	2	0.997	0.001
Abyssal Hill								
Deep-sea ("red") pelagic clay								
Clayey silt	1.347	0.020	81.3	0.95	1522	3	0.995	0.002
Silty clay	1.344	0.011	81.2	0.60	1508	2	0.986	0.001
Clay	1.414	0.012	77.7	0.64	1493	1	0.976	0.001
Calcareous ooze								
Sand-silt-clay	1.400	0.013	76.3	0.90	1581	8	1.034	0.005
Silt	1.725	—	56.2	—	1565	—	1.023	—
Clayey silt	1.573	0.020	66.8	1.22	1537	5	1.005	0.003
Silty clay	1.483	0.029	72.3	1.61	1524	7	0.996	0.005

Notes:

Laboratory values: 23° C, 1 atm; density: saturated bulk density; porosity: salt free; velocity ratio: velocity in sediment/velocity in sea water at 23° C, 1 atm, and salinity of sediment pore water. SE: Standard error of the mean.

TABLE 3. Continental Terrace (Shelf and Slope) Environment; average sediment impedances, density (velocity)^2, reflection coefficients, and bottom losses.

Sediment Type	$\rho_2 V_2$	$\rho_2 (V_2)^2$	R	BL
Sand				
Coarse	3.7344	6.8564	0.4098	7.7
Fine	3.4302	6.0125	0.3739	8.5
Very fine	3.1662	5.3725	0.3389	9.4
Silty sand	3.0129	5.0265	0.3168	10.0
Sandy silt	2.9732	4.9468	0.3108	10.1
Silt	2.8675	4.6534	0.2944	10.6
Sand-silt-clay	2.5106	3.9643	0.2326	12.7
Clayey silt	2.3049	3.5703	0.1917	14.3
Silty clay	2.1596	3.2822	0.1602	15.9

Notes.

Laboratory values: 23°C, 1 atmosphere.

$\rho_2 V_2$ = sediment impedance, g/cm^{2}sec x 10^5.

$\rho_2 (V_2)^2$ = sediment density X (velocity)^2, g/cmsec^2, or dynes/cm^2, x 10^{10}.

R = Rayleigh reflection coefficient at normal incidence = $\dfrac{\rho_2 V_2 - \rho_1 V_1}{\rho_2 V_2 + \rho_1 V_1}$

BL = -20 log R, bottom loss, dB.

ρ_1, V_1: sea-water density, velocity; ρ_2, V_2: sediment density, velocity.

TABLE 4. Abyssal Plain and Abyssal Hill Environments; average sediment impedances, density (velocity)^2, reflection coefficients, and bottom losses.*

Environment Sediment Type	$\rho_2 V_2$	$\rho_2 (V_2)^2$	R	BL
Abyssal Plain				
Sandy silt	2.6795	4.3462	0.2623	11.6
Silt	2.5071	3.9185	0.2311	12.7
Sand-silt-clay	2.4023	3.6899	0.2107	13.5
Clayey silt	2.1929	3.3463	0.1668	15.6
Silty clay	2.0195	3.0594	0.1265	18.0
Clay	2.0321	3.0542	0.1295	17.8
Bering Sea and Okhotsk Sea (Diatomaceous)				
Silt	2.2371	3.4585	0.1763	15.1
Clayey silt	1.8840	2.8904	0.0920	20.7
Silty clay	1.8514	2.8233	0.0833	21.6
Abyssal Hill				
Deep-sea ("red") pelagic clay				
Clayey silt	2.0501	3.1203	0.1339	17.5
Silty clay	2.0268	3.0563	0.1283	17.8
Clay	2.1111	3.1519	0.1482	16.6
Calcareous ooze				
Sand-silt-clay	2.2137	3.5003	0.1714	15.3
Silt	2.6996	4.2249	0.2658	11.5
Clayey silt	2.4175	3.7155	0.2138	13.4
Silty clay	2.2598	3.4435	0.1813	14.8

* See notes under Table 3.

TABLE 5. Continental Terrace (Shelf and Slope) Environment; computed elastic constants in sediments.

Sediment Type	κ Avg.	κ SE	σ Avg.	σ SE	μ Avg.	μ SE	V_s Avg.	V_s SE	No. Samples
Sand									
Coarse	6.6859	—	0.491	—	0.1289	—	250	—	2
Fine	5.5063	0.1638	0.466	0.005	0.3713	0.0509	417	37	15
Very fine	5.0243	0.3479	0.456	0.010	0.4501	0.1228	472	62	5
Silty sand	4.5017	0.1327	0.459	0.006	0.3716	0.0452	447	27	13
Sandy silt	4.4487	0.2137	0.469	0.007	0.2745	0.0613	363	47	13
Silt	4.3320	0.1631	0.484	0.003	0.1324	0.0187	270	27	9
Sand-silt-clay	3.5903	0.0907	0.463	0.003	0.2784	0.0223	412	17	18
Clayey silt	3.3173	0.0450	0.476	0.002	0.1687	0.0135	324	12	50
Silty clay	3.1459	0.0353	0.484	0.002	0.1026	0.0101	263	12	19

Notes.

Laboratory values: 23°C, 1 atmosphere pressure.

κ = bulk modulus, dynes/cm^2 x 10^{10}.

μ = rigidity (shear) modulus, dynes/cm^2 x 10^{10}.

σ = Poisson's Ratio.

V_s = velocity of shear wave, m/sec.

SE= Standard error of the mean. Data through 1973 in this table.

TABLE 6. Abyssal Plain and Abyssal Hill Environments; computed elastic constants in sediments.*

Environment / Sediment Type	κ Avg.	κ SE	σ Avg.	σ SE	μ Avg.	μ SE	V_s Avg.	V_s SE	No. Samples
Abyssal Plain									
Sandy silt	4.2572	—	0.492	—	0.0668	—	201	—	1
Silt	3.5798	—	0.484	—	0.1291	—	254	—	2
Sand-silt-clay	3.5670	—	0.488	—	0.0898	—	228	—	2
Clayey silt	3.1465	0.0479	0.480	0.002	0.1286	0.0126	292	16	21
Silty clay	2.8963	0.0391	0.487	0.001	0.0798	0.0078	238	11	34
Clay	3.0108	0.1048	0.493	0.001	0.0421	0.0079	173	20	5
Bering Sea and Okhotsk Sea (Diatomaceous)									
Silt	3.3610	—	0.489	—	0.0731	—	225	—	1
Clayey silt	2.7969	0.0222	0.488	0.004	0.0711	0.0247	224	41	5
Silty clay	2.7381	0.0191	0.488	0.002	0.0648	0.0079	225	12	22
Abyssal Hill									
Deep-sea ("red") pelagic clay									
Clayey silt	2.9955	0.0625	0.481	0.003	0.1165	0.0170	287	21	8
Silty clay	2.9455	0.0267	0.487	0.001	0.0759	0.0060	229	9	48
Clay	2.9474	0.0467	0.491	0.001	0.0512	0.0038	194	7	14
Calcareous ooze									
Sand-silt-clay	3.1370	0.0381	0.458	0.005	0.2730	0.0280	439	24	5
Clayey silt	3.5587	0.0529	0.488	0.001	0.0877	0.0077	234	10	14
Silty clay	3.3139	0.0779	0.485	0.002	0.0978	0.0137	255	17	4

* See notes under Table 5. Data through 1973 in this table

APPENDIX A: EQUATIONS FOR REGRESSION LINES AND CURVES

Regression lines and curves were computed for those illustrated sets of (x,y) data that constitute the best indices (x) to obtain desired properties (y). Separate equations are listed, where appropriate, for each of the three general evvironments, as follows: continental terrace (shelf and slope), (T); abyssal hill(pelagic), (H); abyssal plain (turbidite), (P). The equations are keyed by figure numbers to the related scatter diagrams in the main text. The Standard Errors of Estimate, σ, opposite each equation, are applicable only near the mean of the (x, y) values, and accuracy of the (y) values, given (x), falls off away from this region (Griffiths, 1967,p. 448). Grain sizes are shown in the logarithmic phi-scale ($\phi = -\log_2$ of grain diameter in millimeters).

It is important that the regression equations be used only between the limiting values of the index property (x values), as noted below. These equations are strictly empirical and apply only to the (x,y) data points involved. There was no attempt, for example, to force the curves expressed by the equations to pass through velocity values of minerals at zero porosity, or the velocity value of sea water at 100 percent porosity.

The limiting values of (x), in the equations below, are:

(1) Mean grain diameter, M_z,ϕ

(T) 1 to 9 ϕ

(H) and (P) 7 to 10 ϕ

(2) Porosity, n, percent

(T) 35 to 85 percent

(H) and (P) 70 to 90 percent

(3) Density, ρ, g/cm^3

(T) 1.25 to 2.10 g/cm^3

(H) 1.15 to 1.50 g/cm^3

(P) 1.15 to 1.70 g/cm^3

(4) Clay size grains, C, percent

(H) and (p) 20 to 85 percent

(5) Density × (Velocity)^2, ρV_p^2, dynes $/cm^2 \times 10^{10}$

(H) 2.7 to 3.4 dynes/$cm^2 \times 10^{10}$

(P) 2.7 to 3.8 dynes/$cm^2 \times 10^{10}$

Porosity, n (%) vs. Mean Grain Diameter, M_z (ϕ) Figure 3

(T) $n = 30.95 + 5.50(M_z)$ $\sigma = 6.8$

(H) $n = 82.42 - 0.29(M_z)$ $\sigma = 4.7$

(P) $n = 45.43 + 3.93(M_z)$ $\sigma = 6.5$

Density, p (g/cm^3) vs. Mean Grain Diameter, M_z (ϕ) Figure 2

(T) $p = 2.191 - 0.095(M_z)$ $\sigma = 0.12$

(H) $p = 1.327 + 0.005(M_z)$ $\sigma = 0.09$

(P) $p = 1.879 - 0.06(M_z)$ $\sigma = 0.11$

Sound Velocity, V_p (m/sec) vs. Mean Grain Diameter, M_z (ϕ) Figures 9,10

(T) $V_p = 1924.9 - 74.18(M_z) + 3.04(M_z)^2$ $\sigma = 33.6$

(H) $V_p = 1594.4 - 10.2(M_z)$ $\sigma = 11.6$

(P) $V_p = 1631.8 - 13.3(M_z)$ $\sigma = 18.3$

Sound Velocity, V_p (m/sec) vs. Porosity, n (%) Figures 7,8

(T) $V_p = 2467.3 - 22.13(n) + 0.129(n)^2$ $\sigma = 33.7$

(H) $V_p = 1410.8 + 1.175(n)$ $\sigma = 13.3$

(P) $V_p = 1630.8 - 1.402(n)$ $\sigma = 20.6$

Sound Velocity, V_p (m/sec) vs. Density, ρ (g/cm^3)

(T) $V_p = 2263.0 - 1164.8(\rho) + 458.8(\rho)^2$ $\sigma = 34.2$

(H) $V_p = 1591.7 - 63.5(\rho)$ $\sigma = 13.2$

(P) $V_p = 1430.6 + 65.2(\rho)$ $\sigma = 21.7$

Sound Velocity, V_p (m/sec) vs. Clay Size, C (%) Figure 11

(H) $V_p = 1549.4 - 0.66(C)$ $\sigma = 9.9$

(P) $V_p = 1568.8 - 0.89(C)$ $\sigma = 18.3$

Density, ρ (g/cm^3) vs. Porosity, n (%)

(T) $n = 156.0 - 56.8(\rho)$ $\sigma = 2.7$

(H) $n = 150.1 - 51.2(\rho)$ $\sigma = 1.2$

(P) $n = 159.6 - 58.9(\rho)$ $\sigma = 1.4$

Bulk Modulus, K (dynes/cm^2 $\times$ 10^{10}) vs. Porosity, n (%) Figures 19

(T) $K = 215.09467 - 133.1006\ (\log_e n) + 28.2872\ (\log_e n)^2 - 2.0446\ (\log_e n)^3$ $\sigma = 0.01146$

(H) and (P) $K = 128.9909 - 72.0478\ (\log_e n) + 13.8657\ (\log_e n)^2 - 0.9097\ (\log_e n)^3$ $\sigma = 0.0100$

Bulk Modulus, κ (dynes/cm^2 $\times$ 10^{10}) vs.

Density $\times$ (velocity)^2, ρV_p^2 (dynes/cm $\times$ 10^{10})

(H) $\kappa = 0.32039 + 0.862\ (\rho V_p^2)$ $\sigma = 0.049$

(P) $\kappa = 1.68823 + 0.134\ (\rho V_p^2)$ $\sigma = 0.069$

Note: The figures (numbers noted above) are from Hamilton (1974a). The regression equations include all new measurements to July 1975; these new data would not add significantly to the scatter diagrams.

APPENDIX B: CONTRUCTION OF GEOACOUSTIC MODELS

The acoustic properties of the sea floor for specific areas must be compiled into quantitative geoacoustic models to be of use to the acoustician. In 1973, the writer summarized and illustrated the methods used at the Naval Undersea Center to construct these models (Hamilton, 1974b). For the convenience of the reader, this information is reproduced in this Appendix. It should be noted that additional information can be supplied in those categories studied since 1973 (and, as yet, unpublished), and briefly discussed in appropriate sections of this report; namely: the profiles and gradients of density, porosity, and compressional wave attenuation with depth in the sea floor, and a suggested method for approximating the attenuation of shear waves.

DATA REQUIRED TO CONSTRUCT GEOACOUSTIC MODELS

Introduction

The real sea floor cannot be defined by any single geoacoustic model; therefore, it is important that acoustic and geophysical experiments at sea involving the sea floor be supported by a particular model of the area. However, it is possible to use geologic and geophysical judgment to extrapolate a general model over wider areas. A sufficient collection of models from diverse environments will allow predictions of bottom models in similar areas of the world's oceans.

A geoacoustic model should detail the real sea floor. It can then be used in studies of reflection and refraction of compressional and shear waves over a wide range of frequencies, in geologic studies of stratigraphy, sedimentology, and geologic history, and in various other studies in the field of geophysics (e.g., gravity computations).

The production of a geoacoustic model of the sea floor requires assembly of data from a wide variety of sources in the fields of oceanography, geology, and geophysics. A model thus brings into focus and utility, data from many scientific disciplines and operations at sea and in the laboratory. The gross layering may be all that is required in some geologic and geophysical studies, but the acoustician must be supplied sufficient detail to study insonified areas at various sound frequencies.

Data Required and Methods

In an ideal production of a geoacoustic model, the following data should be derived at sea and in the laboratory. In addition, associated information from all available sources, published and unpublished, should be sought and selectively used.

Data for a bathymetric chart. The first requisite of a geoacoustic model is a good bathymetric chart of the insonified (and adjacent) area. Data required includes: (1) all available sounding data from government sources and oceanographic institutions (published and unpublished), (2) a careful record of all ship's movements on station, (3) continuous echo sounding records, (4) a Nansen cast or other data which allows corrections from echo-sounder to true depths, (5) location by satellite navigation methods. In the laboratory, the smoothed ship's track is plotted with soundings, and all available data is used to produce a good contoured chart of the insonified and adjacent areas. It can rarely be assumed that any given, published chart of an area is valid. Very little of the sea floor has been charted properly, in detail.

Data to determine layer thicknesses and locations of reflectors. Continuous seismic reflection profiling determines travel time between impedance mismatches, or reflectors. Air-gun power sources can obtain data at low frequencies on the order of 20 to 50 Hz. Electric 'sparker' sources usually are operated between about 80 and 250 Hz. Layering

can be seen at 12 kHz by the normal echo sounder operating on a short ping to depths in silt-clay sediments on the order of 5 to 20 m. The 3.5 kHz system frequently shows reflectors in silt-clays to depths of 40 to 60 m.

Given travel time in a sediment layer, the true thickness can be derived if the interval velocity, or velocity gradient is known. At present, these data are usually acquired from wide-angle reflection measurements using expendable sonobuoys (LePichon et al., 1968; Houtz et al.,1968).

Water-Mass data. To predict in situ sediment surface properties, it is necessary to have information on the sound velocity, density, and salinity of the sea water at the water-sediment interface. These data can be derived from a normal Nansen cast; a curve showing sound velocity vs. water depth is particularly useful.

Data on sea-floor relief. Details of bottom topography, roughness, relief, and slope are required for some acoustic studies. These can be determined by surface echo sounders (especially those with narrow beams), underwater cameras, and deep-towed equipment.

Data on rock layers. Rock layers at or near the sea floor are important to the underwater acoustician or geophysicist. At low frequencies, all of the sediment column, and deeply buried rock layers can be important. Information is required on, at least, the density, compressional-wave velocity, and attenuation in these rock layers.

Data for sediment properties. Sediment samples from gravity and piston corers, box corers, or other samplers is required to obtain sediment physical properties. Sound velocities can be measured aboard ship, or the samples can be preserved under sea water in the refrigerator for velocity and other laboratory measurements.

In the laboratory, the minimum physical property measurements should include grain size analyses (mean grain size, and percentages of sand, silt, and clay), bulk grain density, saturated density, porosity, and additional sound velocity measurements. Other properties can be computed or predicted through these measured properties.

In shallow water, the best data can be obtained by in situ measurements for some properties (e.g., as in Hamilton et al.,1970; Hamilton, 1972).

If all of the above data are not available, or if there is no data at all, certain in situ predictions can be made following Hamilton (1971b). Predictions of layer thicknesses and attenuation (not included in the 1971 report) will be briefly noted below.

COMMON GEOACOUSTIC MODELS

Among an almost infinite variety of geoacoustic models there are four very common ones. Two of these are in the continental shelf and two in deep-sea areas. Actual gross models will illustrate these types.

Shallow-Water Geoacoustic Models

A common stratigraphy in continental shelves is a top layer of soft mud, or clay-silts, overlying harder silts and sands. This is common because during lowered sea levels of the Pleistocene, sand was deposited over wide areas of the shelf, and then covered with silt-clays as sea level rose. Figure B.1, from an actual station on the shallow Asiatic continental shelf, illustrates this model.

The other common shallow-water model is a layer of thick sand, usually overlying rock (Figure B.2). The sand usually forms a high-density, high-velocity (hence high-impedance) layer in which sound attenuation is also high. Subbottom layers are not usually acoustically seen in these areas.

Deep-Sea Geoacoustic Models

In the deep-sea there are two common models: one in abyssal plains and one in abyssal hills.

In abyssal hills, there is usually a single layer of pelagic silt-clays, with or without volcanic ash layers, over volcanic or sedimentary rock. The sediment layer may be quite thin as demonstrated in the Pacific by the Deep Sea Drilling Project, and by reflection surveys (e.g., Ewing et al., 1968). This type of geoacoustic model is illustrated in Figure B.3. The general area is the north central Pacific, west of the Aleutian Abyssal Plain. The area is in the volcanic ash zone as described by Horn et al. (1969).

As previously noted, when sedimentary layers are thin, or when frequencies are very low, the model must include properties of the rock layers. Much of the Pacific has a silt-clay layer (overlying basalt) in which one-way sound travel time is 0.05 sec or less (Ewing et al., 1968); these layers will usually be 50 to 100 m thick.

Rock velocities can usually be obtained from refraction surveys in or near the area of interest. For example, in the area represented by Figure B.3, the rock is basalt as determined by the Deep Sea Drilling Project, and an average velocity in the top of the basalt is 5.7 km/sec (Houtz et al., 1970). Given a rock velocity, the best procedure to get density, at present, is to enter diagrams relating density and velocity (e.g., Nafe and Drake, 1967; Christensen and Salisbury, 1975; Dortman and Magid, 1969). Approximate attenuation values for different rock types can usually be derived from the literature (e.g., Balakrishna and Ramana, 1968; Levykin, 1965).

The less common deep-sea geoacoustic model is from abyssal plains where turbidity currents have laid down alternating sequences of silt-clays and silt-sands (turbidites). These sediments over rock can vary in thickness from a few meters to over 2000 m. The section might comprise hundreds of layers. Most of these layers have been deposited by flows which top the natural levees of great undersea channels, and individual layers vary in thickness and cannot usually be correlated over appreciable distances. Only a few of these

layers are usually cored, and some deeper layers are seen as reflectors by echo sounders and reflection equipment. For the acoustician who requires a fully-layered model, the geologist-geophysicist should detail the layering (reflectors) as deep as he can from cores and reflection records, and then accept an alternation of probable 'average layers' to the full thickness of the sediment layer.

Figure B.4 represents the deep-water turbidite model; it is from the southern Japan Sea Abyssal Plain. The total thickness of the turbidite layer was determined by reflection profiling (to get sound-travel time in the sediment layer), and an interval velocity measurement using the sonobuoy technique developed at Lamont-Doherty Geological Observatory by Houtz and his colleagues (Houtz et al., 1968; Le Pichon et al., 1968). In the inset is a diagram from the 12 kHz echo sounder which shows detailed layering to about 10 meters. The first line (at 0 m) is the sea floor. About one m below the sea floor is a strong reflector. The corer dropped through a silty clay layer and stopped in a sand layer. Measurements in the cored sediment indicated that the first meter had a velocity a little more than one percent less than velocity in the bottom water. In situ layer velocities and densities were: first layer, 1467 m/sec and 1.23 g/cm^3; second layer, 1819 m/sec and 2.02 g/cm^3. The linear velocity gradient is from the sediment-surface velocity through the sonobuoy interval velocity.

DETAILED GEOACOUSTIC MODEL

General

The large, gross models illustrated and discussed above are of interest and utility, but for most studies of reflection and bottom loss, it has been determined that a fully-layered model must be used to reconcile experiment with theory; recent examples of this are in reports by Hastrup (1970) in the Mediterranean, and by Morris (1970) in the Pacific. For the acoustician who needs fully-layered models, all available data, estimates, and predictions are used to indicate probable layering and sediment properties down to and including the 'acoustic basement' (usually sedimentary or volcanic rock). In these estimates, available data from other sources are used: the general geologic and geophysical literature, Navy reports, unpublished data, data on similar sediments, and a certain amount of geologic 'intuition and judgment.'

At the Naval Undersea Center, our models include a gross figure such as described, plus a topographic chart of the area of the experiment, and slope and relief as seen by the echo sounder and lowered camera. The acoustician requires quantitative information. He should not have to try to measure it off figures or curves. Consequently, each model is accompanied by 5 tables and a general information sheet.

In the following section, the various tables and their headings are explained. The subsections are keyed by number to the tables, and explain the headings in each table with some explanatory discussion. The numbers in the tables are

examples and are part of the model represented by Figure B.3. Values not in parentheses were measured. The subject of predictive methods and corrections from laboratory to in situ properties was discussed in a recent report (Hamilton, 1971b).

A general information form sheet is furnished for each station; it accompanies the 5 tables. The general information sheet includes station location (Lat., Long.), maximum and minimum water depths in fathoms and meters (both echo-sounder and corrected depths), the general geographic area (e.g., the north-central Pacific), the geomorphic province (e.g., abyssal hills), and a brief description of the sea floor (topography, sediment distributions, stratigraphy, structure).

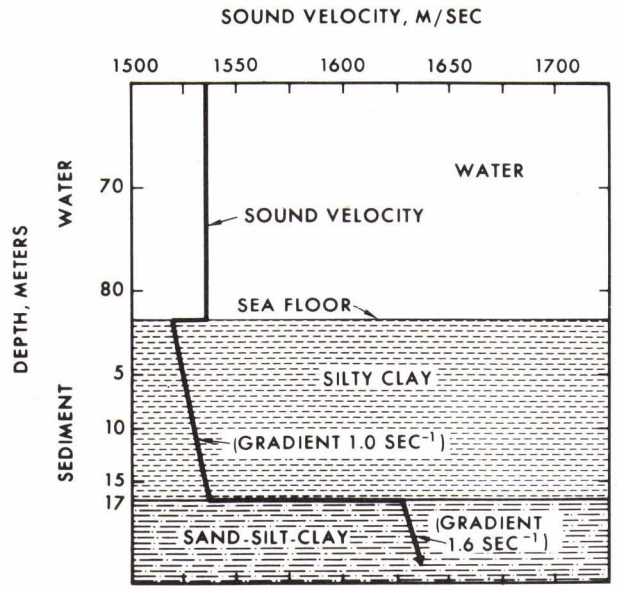

FIG. B.1 ONE OF TWO COMMON SHALLOW-WATER GEOACOUSTIC MODELS: MUD OVER SAND OR ROCK (SANDY SEDIMENTS IN THIS CASE). THE VELOCITY GRADIENT IS ASSUMED.

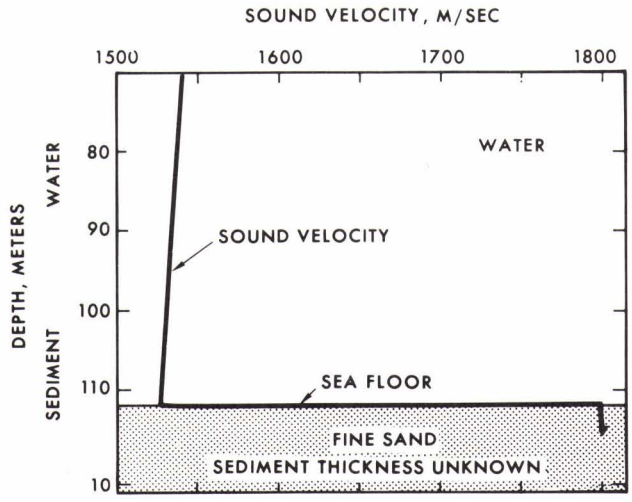

FIG. B.2 ONE OF TWO COMMON SHALLOW-WATER GEOACOUSTIC MODELS : A THICK LAYER OF HIGH-DENSITY, HIGH-VELOCITY SAND OVER ROCK. THE SLOPE OF THE GRADIENT LINE IN THE SAND HAS NO SIGNIFICANCE. SOUND VELOCITY IN SANDS INCREASES WITH ABOUT THE 0.015 POWER OF DEPTH.

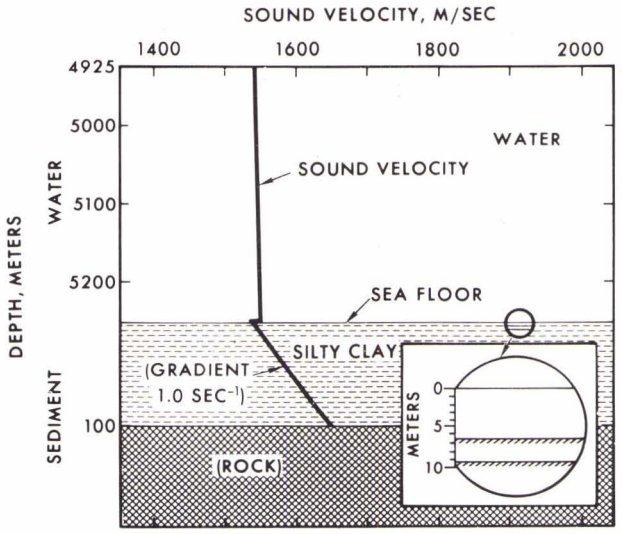

FIG. B.3 ONE OF TWO COMMON DEEP-SEA GEOACOUSTIC MODELS (ABYSSAL HILLS). THIS MODEL FROM THE NORTH PACIFIC ABYSSAL HILLS, REPRESENTS A THIN (100 m) LAYER OF PELAGIC DEEP-SEA CLAY OVERLYING BASALT. THE INSET FIGURE SHOWS REFLECTORS (AS SEEN ON 12 kHz RECORDS) WHICH ARE PROBABLY FORMED BY VOLCANIC ASH. APPENDIX B HAS FIVE TABLES WHICH ACCOMPANY THIS FIGURE, AND GIVE NUMERICAL DETAILS WHICH ARE DISCUSSED IN THE TEXT IN APPENDIX B.

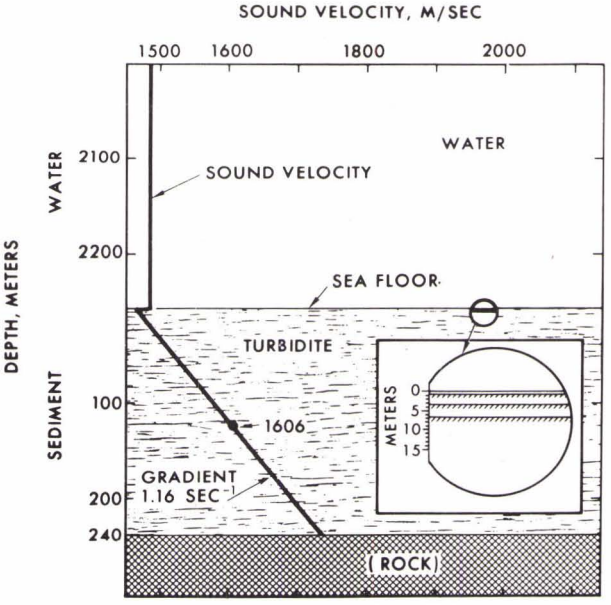

FIG. B.4 ONE OF TWO COMMON DEEP-WATER GEOACOUSTIC MODELS (ABYSSAL PLAINS). THIS MODEL, FROM THE JAPAN SEA ABYSSAL PLAIN, REPRESENT 240 m OF MULTI-LAYERED TURBIDITES OVERLYING ROCK. THE INTERVAL VELOCITY (1606 m/sec) WAS MEASURED BY THE SONOBUOY TECHNIQUE. THE LINEAR GRADIENT IS FROM THE SEDIMENT SURFACE VELOCITY (AS MEASURED IN A CORE AND CORRECTED TO IN SITU) THROUGH THE INTERVAL VELOCITY. THE INSET FIGURE SHOWS REFLECTORS AS SEEN IN 12 kHz RECORDS. A CORE IN THE AREA SHOWED THAT THE FIRST LAYER (ABOUT 1 m THICK) WAS SILTY CLAY AND THE SECOND LAYER (A STRONG REFLECTOR) WAS SAND.

Table B.1 In Situ Properties of Bottom Water

TRUE DEPTH was determined by correcting the echo-sounder depth to true depth. This additive correction is based on the velocity profile in the water mass derived from station Nansen casts. A small table supplied by the Acoustic Propagation Division, (Code 503, at NUC), is inset in the bathymetric chart (fig. 1 for each station) to indicate the value of these corrections and to permit correction of the echo-sounder depths on the contour charts to true depths. Such corrections can also be obtained from NAVOCEANO (1966).

TEMPERATURE, SALINITY, PRESSURE, and SOUND SPEED were derived from Nansen-cast data at the indicated true depth.

IMPEDANCE was computed by the formula: density x sound speed.

Table B.2 In Situ Physical Properties of Sediments (Other Than Acoustic)

The THICKNESSES of sediment layers were determined from cores, 12-kHz, and 3.5-kHz echo-sounder records, acoustic reflections (sparker), sonobuoys, and probabilities of layering (determined in similar sediments or taken from reports of other institutions for the area).

Below coring depths in the sediment, thicknesses of relatively thin layers between reflectors can be computed by measuring sound travel time between reflectors from an echo sounder record (12 or 3.5 kHz) and multiplying by a velocity extrapolated from layers above (using a velocity gradient, as

discussed in the main text). The true thicknesses of the reflecting layers (reflectors) can be estimated from the thicknesses of cored layers in probably similar sediments above or elsewhere. For example, Horn et al. (1969) reported that white volcanic ash in the northeast Pacific ranged in thickness from 1 to 29 cm (avg. 6.5 cm); the thicker sections would be those closest to sources of the ash; the mean grain size of these ashes was 5.42 phi. Similar information is usually available in the literature (e.g., Horn et al., 1971).

The alternatives when computing true thicknesses of relatively thick sediment and rock layers in areas where no interval velocities have been measured was discussed in the main text.

A growing and important source of information on sediment and rock layers, and their properties, are the Initial Reports of the Deep Sea Drilling Project. These reports should always be consulted when compiling geoacoustic models in deep-sea areas.

SEDIMENT TYPE, MEAN DIAMETER OF MINERAL GRAINS, and PERCENTAGES OF SAND, SILT, AND CLAY were determined from grain size analyses. These follow the nomenclature scheme discussed by Shepard, 1954; however, the Wentworth scale was used for sand sizes. The Wentworth scale is based on median diameter of mineral grains; very fine sand (0.062 to 0.125 mm); fine sand (0.125 to 0.250 mm); medium sand (0.250 to 0.500 mm); coarse sand (0.500 to 1.000 mm); silt (0.062 to 0.004 mm); and clay (less than 0.004 mm).

POROSITY is the volume of voids or pore space divided by the volume of the sample; this was determined from evaporation of pore water and corrected for dried salts (see Hamilton, 1971b for methods).

DENSITY OF SOLIDS, the bulk density of the mass of dried mineral grains (without salts evaporated from the pore water), was determined by the pycnometer method.

Total thickness of sediment over rock (in the footnote) was determined from one-way reflection time in the sediment and sediment interval velocity as discussed above.

Table B.3 In Situ Acoustic Properties of Sediments

SOUND VELOCITY was determined in the laboratory at approximately 200 kHz, and corrected to in situ values (Hamilton, 1971b); the values in parentheses are predictions. (See the following paragraphs for velocities in the lower layers.)

VELOCITY GRADIENT. The linear velocity gradient (in meters per second per meter, or sec^{-1}) shows the increase in velocity with depth in the sediments. At those stations where interval velocities were measured with sonobuoys, the overall linear gradient was established by using the sediment-surface velocity and the layer-interval velocity. The interval velocity is the actual velocity at a depth in the sediment of one-half the layer thickness. These gradients are smoothed, average gradients through the whole layer or layers, and do not reflect the various velocities in individual layers; consequently, only one gradient is usually given or estimated. Lacking actual measurements, a gradient is predicted (in par-

entheses); see main text, or Hamilton et al. (1974) for a discussion. These linear gradients usually vary between 0.5 and 2.0 sec^{-1}; a reasonable, over-all prediction is 1.0 sec^{-1}.

For many stations, the tables should indicate estimated properties for lower layers. The estimate is made by relating the properties to those in a higher layer or by predicting sediment type and properties from similar sediments.

The total thickness of sediments in models required by acousticians varies with frequency, energy, grazing angle, etc. Consequently, the known layering can be alternated, as previously indicated, to the sediment-rock interface to furnish a rational basis for geoacoustic models in areas where layered turbidites are present. The velocity gradient should then be used to correct (increase) velocity in each lower layer, a procedure which requires that the impedance also be corrected. For example, assume a velocity of 1500 m/sec and a gradient of 1.0 sec^{-1} in layer 1. A similar layer at a depth of 100 m in the sediment body will have a velocity of 1600 m/sec.

VELOCITY RATIO is computed by dividing the sediment velocity by the bottom-water velocity; it is the same in the laboratory as in situ (Hamilton, 1971b). At greater sediment depths, the ratio is not given or estimated. If computations are made for deeper layers, the velocity gradient in the sediment must

be considered (see previous paragraphs).

DENSITY is the saturated bulk density of a unit volume of sediment, in situ, as corrected from laboratory measurements. Densities at deeper depths can be estimated with the appropriate curve of density versus depth (Figure 6).

IMPEDANCE is the product of the in situ values of density and velocity.

Table B.4 Predicted Attenuation of Compressional (Sound) Waves

A study by Hamilton (1972) indicated that attenuation of sound in marine sediments was approximately dependent on the first power of frequency. In the equation $\alpha = kf^n$ (where attenuation, α, is in dB/m and frequency, f, in kHz), if the exponent "n" is taken as one, the only variable is the constant "k". Relationships between k and mean grain size and porosity (Hamilton, 1972, figs. 3-5) in the sediment layers have been used to derive a value of k. This value (and the probable maximum and minimum values) can be substituted into the equation above to derive an equation which can be used at any frequency. Attenuation at depth in thicker layers can be estimated from Figure 18 and associated text discussion.

Table B.5 In situ, Computed Elastic Constants of Sediments

All these values were computed by using the measured density, measured compressional (sound) velocity, and a computed value for the bulk modulus (corrected to in situ conditions) with Equations (19) to (23); as discussed in the first part, and in Hamilton (1971a, b.).

Table B.1 In situ properties of bottom water.*

True Depth, m	T, °C	S, ppt	P, kg/cm^2	Sound speed, m/sec	Density, g/cm^3	Impedance, g/cm^{2}sec x 10^5
5251	1.58	34.69	547.4	1546.6	1.05174	1.62662

* At location of model: coring site

Table B.2. In situ physical properties of sediments (other than acoustic).*

Layer No.	h, m	Sediment type	Mean Diam., mm	Sand, %	Silt, %	Clay, %	n, %	ρ_s, g/cm^3
1	6.2	Silty clay	0.004	9.8	39.0	51.2	76.3	2.65
2	0.1	(Volcanic ash)	—	—	—	—	(65.0)	(2.7)
3	3.0	(Silty clay)	—	—	—	—	(75.0)	(2.65)
4	0.2	(Volcanic ash)	—	—	—	—	(65.0	(2.7)
Rock	—	Basalt	—	—	—	—	—	—

Total thickness of sediment over rock: 100m

* At location of model: coring site.

Notes

(1) Column headings: h is thickness; n is porosity; ρ_s is density of solids.

(2) Values in parentheses are predicted.

(3) For a complete, estimated geoacoustic model, assume alternation of Layers 3 and 4 to full thickness of sediment (100m).

(4) Rock type (basalt) determined from velocity, acoustic reflection records (traced into seamounts), and Deep Sea Drilling Project in general area.

Table B.3 In situ acoustic properties of sediments.*

Layer No.	Sound velocity, m/sec	Velocity gradient, sec^{-1}	Velocity ratio	Density, g/cm^3	Impedance, $g/cm^2 sec \times 10^5$
1	1539	(1.0)	0.994	1.44	2.216
2	(1595)	——	(1 03)	(1.63)	(2.600)
3	(1545)	——	——	(1.45)	(2.240)
4	(1598)	——	——	(1.63)	(2.605)
Rock	(5700)	——	——	(2.8)	(15.96)

* At location of model: coring site,

Notes

(1) Values in parentheses are predicted. Velocity increased in lower layers by the amount indicated by the velocity gradient.

(2) For a complete, estimated geoacoustic model, assume alternation of Layers 3 and 4 to full thickness of sediment (100 m). See notes for this table in Appendix B.

(3) Velocity in basalt from an average for the general area from Houtz et al., 1970. Density in basalt from velocity-density relationship of Christensen and Salisbury, 1975, table 9: DSDP basalts at a pressure of 0.5 kb.

Table B.4. In situ, computed elastic constants of sediments.*

Layer No.	β	κ	σ	μ	λ	V_s
1	0.3055	3.2736	0.484	0.1028	3.2051	267
2	0.2623	3.8128	0.468	0.2505	3.6457	392
3	0.3003	3.3298	0.485	0.0986	3.2641	261
4	0.2623	3.8128	0.466	0.2622	3.6379	401
Rock (Basalt)	0.017	58.48	0.317	24.37	42.24	2950
(See note below for derivation of rock properties)						

*Compressibility, β, dynes/cm^2 X 10^{-10}
Bulk modulus, κ, dynes/cm^2 X 10^{10}
Poisson's Ratio, σ
Rigidity modulus, μ, dynes/cm^2 X 10^{10}
Lamé's Constant, λ, dynes/cm^2 X 10^{10}

Shear-wave velocity, V_s, m/sec

Data and the method used to compute elastic constants of sediments are in

Hamilton, E. L., 1971a, Elastic properties of marine sediments, JOUR. GEOPHYS. RES., v. 76, p. 579-604.

Hamilton, E. L., 1971b, Prediction of in-situ acoustic and elastic properties of marine sediments, GEOPHYSICS, v. 36, No. 2, p. 266-284.

Note: Properties of the basalt were computed from V_p from Houtz et al. (1970); density and V_s from Christensen and Salisbury, 1975: table 9: DSDP basalt at pressure of 0.5 kb; and Equations (19) to (23).

Table B.5. Predicted attenuation of compressional (sound) waves.*

Layer No.	k		
	Recommended	Probable Max.	Probable Min.
1	0.08	0.18	0.04
2	0.12	0.38	0.09
3	0.08	0.19	0.04
4	0.12	0.38	0.09
Rock (Basalt)	0.03	0.05	0.02

* To determine an equation which can be used at any frequency, substitute k into the equation

$$\alpha = kf^1$$

where

α is attenuation of compressional (sound) waves in dB/m
k is a constant
f is frequency in kHz

For deeper layers, alternate values shown for Layers 3 and 4 and as discussed in text with Figure 18.

Data and the method used to predict attenuation are in

Hamilton, E. L., 1972, Compressional-wave attenuation in marine sediments, GEOPHYSICS, v. 37, No. 4, p. 620-646.

Acknowledgments

This work was supported by the Naval Sea Systems Command (Code 06H14), by the Naval Electronic Systems Command (Code 320), and by the Office of Naval Research (Code 483). R.T. Bachman, P.H. Sherrer, and A.J. Brescia assisted in data analyses.

REFERENCES

ADLER, F.T., SAWYER, W.M., and FERRY, J.D. Propagation of transverse waves in viscoelastic media. Jnl. Applied Physics 20, 1949: 1036-1041.

AKAL, T. The relationship between the physical properties of underwater sediments that affect bottom reflection. Marine Geology 13, 1972: 251-266.

ATTWELL, P.B., and RAMANA, Y.V. Wave attenuation and internal friction as functions of frequency in rocks. Geophysics 31, 1966: 1049-1056.

BALARISHNA, S., and RAMANA, Y.V. Integrated studies of the elastic properties of some Indian rocks. In: KNOPOFF, L., et al (eds). The Crust and Upper Mantle of the Pacific Area, Geophysical Monograph No. 12. Washington, D.C., American Geophysical Union, 1968: pp 489-500.

BARKAN, D.D. Dynamics of Bases and Foundations. New York, McGraw-Hill, 1962.

BARNES, B.B., et al. Geophysics applied to geotechnical problems in a marine environment, a case study: Monterey Bay, California. In: Environmental Res. Labs., Annual Report 1972-1973. Washington, D.C., Nat. Oceanic and Atmos. Admin., 1973.

BERZON, I.S., RATNIKOVA, L.I., and MITRONOVA, V.A. Shear waves reflected from a thin high-speed layer. In: BERZON, I.S. (ed). Propagation in Real Media. (English trans.) New York, Consultants Bureau, 1969: 154-162. [Originally published Moscow, Nauka Press, 1967].

BRADLEY, J.J., and FORT, A.N. Internal friction in rocks. In: CLARK, S.P. (ed). Handbook of physical constants, Memoir 97. New York, Geological Society America, 1966: pp 175-194.

BRESLAU, L.R. Classification of sea-floor sediments with a shipborne acoustical system. In: Le Petrole et la Mer, Proceedings of Symposium, Sect. I, No. 132. Monaco, 1965: pp 1-9.
Also in: WHOI. Collected Reprints 1965, Pt 2, No. 1678. Woods Hole, Mass., Woods Hole Oceanographic Institution, 1966.

BRESLAU, L.R. The normally incident reflectivity of the sea floor at 12 Kc and its correlation with physical and geological properties of naturally-occurring sediments. WHOI Ref. 67-16. Woods Hole, Mass., Woods Hole Oceanographic Institution, 1967.

BUCHAN, S., et al. The Acoustic and Geotechnical Properties of North Atlantic Cores, Vols. 1 and 2. Menai Bridge, North Wales, Univ. College of North Wales Marine Science Lab., 1971.

BUCHAN, S., McCANN, D.M., and SMITH, D.T. Relations between the acoustic and geotechnical properties of marine sediments. Quarterly Jnl. Engineering Geology 5, 1972: 265-284.

BUCKER, H.P. Normal-mode sound propagation in shallow water. Jnl. Acoustical Society America 36, 1964: 251-258.

BUCKER, H.P., et al. Reflection of low-frequency sonar signals from a smooth ocean bottom. Jnl. Acoustical Society America 37, 1965: 1037-1051.

CERNOCK, P.J. Sound velocities in Gulf of Mexico sediments as related to physical properties and simulated overburden pressures. Tech. Rpt. 70-5-T. Austin, Texas., Texas A & M University Oceanographic Dept., 1970.

CHRISTENSEN, N.I., and SALISBURY, M.H. Structure and constitution of the lower oceanic crust. Review of Geophysics and Space Physics 13, 1975: 57-86.

CLAY, C.S., and RONA, P.A. Studies of seismic reflections from thin layers on the ocean bottom in the western North Atlantic. Jnl. Geophysical Research 70, 1965: 855-869.

COLE, B.F. Marine sediment attenuation and ocean-bottom-reflected sound. Jnl. Acoustical Society America 38, 1965: 291-297.

CUNNY, R.W., and FRY, Z.B. Vibratory in situ and laboratory soil moduli compared. Soil Mechanics and Foundation Engineering 99, 1973: 1055-1076.

DAVIES, D. Dispersed Stoneley waves on the ocean bottom. Bull. Seismological Society of America 55, 1965: 903-918.

DE BREMAECKER, J.C., GODSON, R.H., and WATKINS, J.S. Attenuation measurements in the field. Geophysics 31, 1966: 562-569.

DICKINSON, G. Geological aspects of abnormal reservoir pressures in Gulf Coast Louisiana. Bull. American Association of Petroleum Geologists 37, 1953: 410-432.

EWING, J.I., and NAFE, J.E. The unconsolidated sediments in the sea. In: HILL, M.N. (ed). The Sea; Ideas and Observations on Progress in the Study of the Seas, Vol. 3: The Earth beneath the Sea. New York, Interscience, 1963: pp 73-84.

EWING, J.I., et al. North Pacific sediment layers measured by seismic profiling. In: KNOPOFF, L., et al (eds). The Crust and Upper Mantle of the Pacific Area, Geophysical Monograph No. 12. Washington, D.C., American Geophysical Union, 1968: pp 147-173.

EWING, J.I., HOUTZ, R.E., and LUDWIG, W.J. Sediment distribution in the Coral Sea. Jnl. Geophysical Research 75, 1970: 1963-1972.

EWING, M., HOUTZ, R.E., and EWING, J. South Pacific sediment distribution. Jnl. Geophysical Research 74, 1969: 2477-2493.

FERRY, J.D. Viscoelastic Properties of Polymers. New York, John Wiley and Sons, 1961.

FRY, J.C., and RAITT, R.W. Sound velocities at the surface of deep sea sediments. Jnl. Geophysical Research 66, 1961: 589-597.

GARDNER, G.H.F., WYLLIE, M.R.J., and DROSCHAK, D.M. Effects of pressure and fluid saturation on the attenuation of elastic waves in sands. Jnl. Petroleum Technology 16, 1964: 189-198.

GASSMANN, F. Uber die Elastizitat Poroser Medien. Vierteljahresschrift der Naturforschenden Gesellschaft in Zurich 96, 1951: 1-23.

GRIFFITHS, J.C. Scientific Method in Analysis of Sediments. New York, McGraw-Hill, 1967.

HAMILTON, E.L. Low sound velocities in high-porosity sediments. Jnl. Acoustical Society America 28, 1956: 16-19.

HAMILTON, E.L. Thickness and consolidation of deep-sea sediments. Bull. Geological Society America 70, 1959: 1399-1424.

HAMILTON, E.L. Shear wave velocities in marine sediments (abstract). Trans. American Geophysical Union 51, 1970a: 333.

HAMILTON, E.L. Sound velocity and related properties of marine sediments, North Pacific. Jnl. Geophysical Research 75, 1970b: 4423-4446.

HAMILTON, E.L. Sound channels in surficial marine sediments. Jnl. Acoustical Society America 48, 1970c: 1296-1298.

HAMILTON, E.L. Reflection coefficients and bottom losses at normal incidence computed from Pacific sediment properties. Geophysics 35, 1970d: 995-1004.

HAMILTON, E.L. Elastic properties of marine sediments. Jnl. Geophysical Research 76, 1971a: 579-604.

HAMILTON, E.L. Prediction of in-situ acoustic and elastic properties of marine sediments. Geophysics 36, 1971b: 266-284.

HAMILTON, E.L. Compressional-wave attenuation in marine sediments. Geophysics 37, 1972: 620-646.

HAMILTON, E.L. Prediction of deep-sea sediment properties: state of the art. In: INDERBITZEN, A.L. (ed). Physical and Engineering Properties of Deep-Sea Sediments, Proceedings of a Symposium. New York, Plenum Press, 1974a: pp 1-43.

HAMILTON, E.L. Geoacoustic models of the sea floor. In: HAMPTON, L.D. (ed). Physics of Sound in Marine Sediments, Proceedings of a Symposium. New York, Plenum Press, 1974b: pp 181-221.

HAMILTON, E.L. Acoustic and related properties of the sea floor; density and porosity profiles and gradients, Tech. Pub. in press. San Diego, Calif., Naval Undersea Center, 1975a.

HAMILTON, E.L. Acoustic and related properties of the sea floor: sound attenuation versus depth, Tech. Pub. in press. San Diego, Calif., Naval Undersea Center, 1975b.

HAMILTON, E.L. Acoustic and related properties of the sea floor: shear wave profiles and gradients, Tech. Pub. in press. San Diego, Calif., Naval Undersea Center, 1975c.

HAMILTON, E.L., et al. Acoustic and other physical properties of shallow-water sediments off San Diego. Jnl. Acoustical Society America 28, 1956: 1-15.

HAMILTON, E.L., et al. Velocities of compressional and shear waves in marine sediments determined in situ from a research submersible. Jnl. Geophysical Research 75, 1970: 4039-4049.

HAMILTON, E.L., et al. Sediment velocities from sonobuoys: Bay of Bengal, Bering Sea, Japan Sea, and North Pacific. Jnl. Geophysical Research 79, 1974: 2653-2668.

HAMPTON, L. (ed). Physics of Sound in Marine Sediments. New York, Plenum Press, 1974.

HANNA, J.S. Short-range transmission loss and the evidence for bottom-refracted energy. Jnl. Acoustical Society America 53, 1973: 1686-1690.

HASTRUP, O.F. Digital analysis of acoustic reflectivity in the Tyrrhenian Abyssal Plain. Jnl. Acoustical Society America 70, 1970: 181-190.

HORN, D.R., HORN, B.M., and DELACH, M.N. Correlation between acoustical and other physical properties of Mediterranean deep-sea cores, Tech. Rpt. 2. Palisades, N.Y., Lamont Geological Observatory, 1967.

HORN, D.R., HORN, B.M., and DELACH, M.N. Correlation between acoustical and other physical properties of deep-sea cores. Jnl. Geophysical Research 73, 1968: 1939-1957.

HORN, D.R., DELACH, M.N., and HORN, B.M. Distribution of ash layers and turbidities in the North Pacific. Bull. Geological Society America 80, 1969: 1715-1724.

HORN, D.R., et al. Turbidities of the Hatteras and Sohm Abyssal Plains, western North Atlantic. Marine Geology 11, 1971: 287-323.

HOUTZ, R.E. Preliminary study of global sediment sound velocities from sonobuoy data. In: HAMPTON, L.D. (ed). Physics of Sound in Marine Sediments, Proceedings of a Symposium. New York, Plenum Press, 1974b: pp 519-535.

HOUTZ, R.E., and EWING, J.I. Detailed sedimentary velocities from seismic refraction profiles in the western north Atlantic. Jnl. Geophysical Research 68, 1963: 5233-5258.

HOUTZ, R.E., EWING, J.I., and LePICHON, X. Velocity of deep-sea sediments from sonobuoy data. Jnl. Geophysical Research 73, 1968: 2615-2641.

HOUTZ, R.E., EWING, J.I., and BUHL, P. Seismic data from sonobuoy stations in the northern and equatorial Pacific. Jnl. Geophysical Research 75, 1970: 5093-5111.

IGARASHI, Y. In situ high-frequency acoustic propagation measurements in marine sediments in the Santa Barbara shelf, California, Tech. Pub. 334. San Diego, Calif., Naval Undersea Center, 1973.

INDERBITZEN, A.L. (ed). Deep-Sea Sediments, Physical and Mechanical Properties. New York, Plenum Press, 1974.

KAWASUMI, H., et al. S-wave velocities of subsoil layers in Tokyo, 1. Bull. Earthquake Research Institute, Univ. of Tokyo 44, 1966: 731-747.

KELLER, G.H., and BENNETT, R.H. Variations in the mass physical properties of selected submarine sediments. Marine Geology 9, 1970: 215-223.

KERMABON, A., BLAVIER, C.G.P., and TONARELLI, B. Acoustic and other physical properties of deep-sea sediments in the Tyrrhenian Abyssal Plain. Marine Geology 7, 1969: 129-145.

KINSLER, L.E., and FREY, A.R. Fundamentals of Acoustics 2nd ed. New York, John Wiley and Sons, 1962.

KNOPOFF, L., and MacDONALD, G.J.F. Attenuation of small amplitude stress waves in solids. Reviews of Modern Physics 30, 1958: 1178-1192.

KOLSKY, H. Stress Waves in Solids. New York, Dover Publ. Co., 1963.

KRIZEK, R.J. Application of the one-sided Fourier transform to determine soil storage and dissipation characteristics. In: Soil Structure Interaction, Proceedings of a Symposium. Tuscon, Univ. of Arizona, 1964:

KRIZEK, R.J., and FRANKLIN, A.G. Energy dissipation in a soft clay. In: Wave Propagation and Dynamic Properties of Earth Materials, Proceedings of a Symposium. Albuquerque, N.M. Univ. of New Mexico Press, 1968: pp 797-807.

KUDO, K., and SHIMA, E. Attenuation of shear waves in soil. Bull. Earthquake Research Institute., Univ. of Tokyo 48, 1970: 145-158.

LASSWELL, J.B. A comparison of two methods for measuring rigidity of saturated marine sediments, MS Thesis. Monterey, California, U.S. Naval Postgraduate School, 1970.

LAUGHTON, A.S. Sound propagation in compacted ocean sediments. Geophysics 22, 1957: 233-260.

Le PICHON, X., EWING, J., and HOUTZ, R.E. Deep-sea sediment velocity determination made while reflection profiling. Jnl. Geophysical Research 73, 1968: 2597-2614.

LEVYKIN, A.I. Longitudinal and transverse wave absorption and velocity in rock specimens at multilateral pressures up to 4000 kg/cm . Academy of Sciences USSR Bull (Izvestya) Physics of the Solid Earth (English ed.) 2, 1965: 94-98.

LUDWIG, W.J., HOUTZ, R.E., and EWING, M. Sediment distribution in the Bering Sea: Bowers Ridge, Shirshov Ridge, and enclosed basins. Jnl. Geophysical Research 76, 1971: 6367-6375.

LUDWIG, W.J., MURAUCHI, S., and HOUTZ, R.E. Sediments and structure of the Japan Sea. Bull. Geological Society America 86, 1975a: 651-664.

LUDWIG, W.J., HOUTZ, R.E., and EWING, J.I. Profiler-sonobuoy measurements in Columbia and Venezuela Basins, Caribbean. Bull. American Assn. Petroleum Geologists 59, 1975b: 115-123.

MAGARA, K. Compaction and migration of fluids in Miocene mudstone, Nagaoka Plain, Japan. Bull. American Assn. Petroleum Geologists 52, 1968: 2466-2501.

McCANN, D.M. Measurement of the acoustic properties of marine sediments. Acustica 26, 1972: 55-66.

McCANN, C., and McCANN, D.M. The attenuation of compressional waves in marine sediments. Geophysics 34, 1969: 882-892.

McDONAL, F.J., et al. Attenuation of shear and compressional waves in Pierre shale. Geophysics 23, 1958: 421-439.

MEISSNER, R. P-and SV-waves from uphole shooting. Geophysical Prospecting 13, 1965: 433-459.

MOLOTOVA, L.V. Velocity dispersion of body waves in terrigenous rocks. Academy of Sciences USSR Bull. (Izvestiya) Physics of the Solid Earth (English ed.) 7, 1965: 500-506.

MORRIS, H.E. Bottom-reflection-loss model with a velocity gradient. Jnl. Acoustical Society America 48, 1970: 1198-1202.

MORTON, R.W. Sound velocity in carbonate sediments from the Whiting Basin, Puerto Rico. Marine Geology 19, 1975: 1-17.

MUIR, T.G., and ADAIR, R.S. Potential use of parametric sonar in marine archeology, unpublished manuscript. Austin, Texas, Applied Research Laboratory, 1972.

NAFE, J.E., and DRAKE, C.L. Variation with depth in shallow and deep water marine sediments of porosity, density and the velocities of compressional and shear waves. Geophysics 22, 1957: 523-552.

NAFE, J.E., and DRAKE, C.L. Physical properties of marine sediments. In: HILL, M.N. (ed). The Sea; Ideas and Observations on Progress in the Study of the Seas, Vol. 3: The Earth beneath the Sea. New York, Interscience, 1963: pp 794-815.

NAFE, J.E., and DRAKE, C.L. Physical properties of rocks of basaltic composition. In: HEES, H.H. and POLDERVAART, H. (eds). Basalts. New York, Interscience Publ., 1967: pp 483-502.

NAVOCEANO. Handbook of Oceanographic Tables, SP-68. Washington D.C., U.S. Naval Oceanographic Office, 1966.

NEPROCHNOV, Yu. P. Seismic studies of the crustal structure beneath the seas and oceans. Academy of Science USSR Oceanology (English ed.) 11, 1971: 709-715.

NOLLE, A.W., and SIECK, P.W. Longitudinal and transverse ultrasonic waves in synthetic rubber. Jnl. Applied Physics 23, 1952: 888-894.

RICHART, F.E., WOODS, R.D., and HALL, J.R. Vibrations of Soils and Foundations. New Jersey, Prentice-Hall, 1970.

RIEKE, H.H., and CHILINGARIAN, G.V. Compaction of Argillaceous Sediments. New York, Elsevier, 1974.

SCHREIBER, B.C. Sound velocity in deep-sea sediments. Jnl. Geophysical Research 73, 1968: 1259-1268.

SEED, B.H., and IDRISS, I.M. Analyses of ground motions at Union Bay, Seattle during earthquakes and distant nuclear blasts. Bull. Seismological Society America 60, 1970: 125-136.

SHEPARD, F.P. Nomenclature based on sand-silt-clay ratios. Jnl. Sedimentary Petrology 24, 1954: 151-158.

SHIMA, E., et al. S-wave velocities in subsoil layers in Tokyo. 3. Bull. Earthquake Research Institute, Univ. of Tokyo 46, 1968: 1301-1312.

SHUMWAY, G. Sound speed and absorption studies of marine sediments by a resonance method, Parts I & II. Geophysics 25, 1960: 451-467 and 659-682.

SUTTON, G.H., BERCKHEIMER, H., and NAFE, J.E. Physical analysis of deep-sea sediments. Geophysics 22, 1957: 779-812.

TYCE, R.C. Near-bottom observations of 4 kHz acoustic reflectivity and attenuation, in press. Geophysics, 1975.

VASSIL'EV, Y.I., and GUREVICH, G.I. On the ratio between attenuation decrements and propagation velocities of longitudinal and transverse waves. Academy of Sciences USSR Bull. (Izvestiya) Geophysics (English ed.) 12, 1962: 1061-1074.

WARRICK, R.E. Seismic investigation of a San Francisco Bay mud site. Bull. Seismological Society America 64, 1974: 375-385.

WHITE, J.E. Seismic Waves: Radiation, Transmission, and Attenuation. New York, McGraw-Hill, 1965.

WHITE, J.E., and SENGBUSH, R.L. Velocity measurements in near-surface formations. Geophysics 18, 1953: 54-69.

WHITMAN, R.V., and RICHART, F.E. Design procedures for dynamically loaded foundations. Soil Mechanics and Foundation Engineering 93, 1967: 169-193.

WU, T.H. Soil Mechanics. Boston, Allyn and Bacon, 1966.

REFLECTION OF SOUND FROM A LAYERED OCEAN BOTTOM

by

Homer P. Bucker and Halcyon E. Morris
US Naval Undersea Center
San Diego, California 92132
U.S.A.

(No Abstract received)

I. INTRODUCTION

This paper reviews the theory of how a horizontally stratified ocean bottom interacts with acoustic energy to effect sonar systems. At frequencies associated with active sonars ($\sim$ 2.5 to 15 kHz) the theory is well in hand although the bottom sediments may not be. That is, we are dealing only with the top 10 meters or so of sediment which may be somewhat variable.

In working with active sonar problems we usually use ray theory as shown in Fig. 1. The sound field is made up of contributions of rays that travel from the source to the receiver. On the right hand side of Fig. 1 we show two neighboring rays that bracket the receiver at range r. Thus there is an eigen-ray somewhere between these that travels precisely from the source to the receiver. Call this the n^{th} eigen-ray. The magnitude of the ray is A_n and its phase is θ_n. In the equations the terms that are not defined in the figure are R the reflection coefficient, ω the angular frequency, v the sound speed, $d\ell$ a path length along the ray, and m is the number of times the ray has touched a caustic. It is clear that the sediments interact with the sound field through the bottom reflection coefficient R, which is a complex number. The pressure carried by the ray is reduced by a factor equal to the modulus of R and the phase of the ray is advanced by the argument of R. In experimental work we can measure A_n and then determine $|R|$ from the equation for A_n.

In this paper we define R to be the plane wave reflection coefficient. As a matter of academic interest it could be argued that we should really be using a spherical reflection coefficient. This matter is discussed in Appendix A of the written paper. It is sufficient to say here that at high

frequencies the plane and spherical coefficients are essentially equal. At low frequencies the ray theory breaks down and we cannot separate the sound into packets that have a well defined trajectory. As shown in Appendix A we can write the direct and bottom reflected sound field at any frequency in terms of the plane wave reflection coefficient R.

The normal mode form of the wave theory representation, required for low frequency calculations, is shown in Fig. 2, (Bucker, 1970). The source is at depth z_0 and range zero and the receiver is at depth z and range r. The depth function U is a sum of linearly independent solutions of the z-separated part of the wave equation and k is the horizontal wave number. The k_n are those values of k for which U satisfies the boundary conditions. Consider the water near the bottom to have a constant sound speed v_b. Then the z-component solution for the layer can be written as a down-going plane wave $\exp(i\ell_b z)$ and an up-going plane wave $\exp(-i\ell_b z)$ multiplied by the plane wave reflection coefficient R. Small ℓ sub b, ℓ_b, is the vertical wave number. We can find the values of the coefficients A and B by requiring the usual interface conditions at depth z_p. These are that the pressure ($\rho\partial U/\partial t$) and the vertical component of particle velocity ($\partial U/\partial z$) must be continuous functions. We solve these two equations and take the limit $z_p \to z_b$ to obtain the values of A and B shown in Fig. 3. Note that the iso-speed layer has been removed from the problem as $z_p \to z_b$. However R remains in the solution in A and B.

Before proceeding to the models it should be noted that when working with active sonar systems we are sometimes interested in transient phenomena and need to know the time dependent response of the bottom. We will not cover these topics at this time but refer you to the excellent series of

papers by Ole Hastrup (Hastrup, 1966a, 1966b, 1968, 1969, 1970; Hastrup and Schunk, 1967) here at SACLANTCENTER. We will concentrate on plane wave sinusoidal solutions. Of course spherical waves can be formed by superposition of plane waves, and transient signals can be made up of sinusoidal signals.

II. PLANE WAVE REFLECTION COEFFICIENTS

A. Liquid

The most simple model of the bottom sediments is the Rayleigh model (Officer, 1958). The sediments are replaced by a liquid half-space. In Fig. 4 we have a velocity potential function $\phi(z_1)$, $-\infty < z_1 \leq 0$, that is the sum of a down-going plane wave $\exp i(\ell_0 z_1 + kx - \omega t)$ and a reflected up-going plane wave $R \exp i(-\ell_0 z_1 + kx - \omega t)$. Here k is the horizontal wave number, $k = (\omega/v_0) \cos \gamma_0$, where ω is the angular frequency, v_0 is the sound speed in the water half-space, and γ_0 is the grazing angle of the incident and reflected wave. Also, ℓ_0 is the vertical wave number, $\ell_0 = (\omega/v_0) \sin \gamma_0$, and R is the plane wave reflection coefficient. In the sediment half-space the velocity potential function $\phi(z_1)$, $0 \leq z_1 < \infty$ represents a down-going wave $T \exp i(\ell_1 z_1 + kx - \omega t)$. Here T is the transmission coefficient and ℓ_1 is defined by the equation $\ell_1^2 = (\omega/v_1)^2 - k^2$, where v_1 is the sound speed in the sediment half-space. In order to satisfy the Summerfeld radiation condition ℓ_1 is taken as the root of ℓ_1^2 that lies in the first quadrant of the complex plane.

We can now calculate R, and T if desired, by requiring that the sound pressure (equal to $\rho(\partial\phi/\partial t)$, where ρ is the density) and the vertical component of particle velocity (equal to $\partial\phi/\partial z$) be continuous across the interface at $z_1 = 0$. Solving these two equations for R results in the familiar Rayleigh reflection coefficient.

$$R = (\rho_1 \ell_0 - \rho_0 \ell_1)/(\rho_1 \ell_0 + \rho_0 \ell_1) \quad ,$$

where ρ_0 and ρ_1 are the density in the water half-space and in the sediment half-space respectively.

If sediment sound speed is greater than the water sound speed then there will be no bottom loss, i.e. mod(R) = 1, for grazing angles less than or equal to the critical angle γ_{0C} which is defined by the equation $\cos \gamma_{0C} = v_0/v_1$. As γ_0 varies from 0 to γ_{0C} the phase shift changes from -180° to 0° as shown in Fig. 5 where we have plotted the modulus of R, the phase shift (i.e. the argument of R), and bottom-loss (i.e. - 20 $\log_{10}$ [mod(R)]) as a function of grazing angle. The example corresponds to coarse sand from the continental terrace in Hamilton's tables (Hamilton, 1974a). The value of v_1/v_0 is 1.201, corresponding to a critical angle of 33.6°, and the value of ρ_1/ρ_0 is 2.034.

If the sediment sound speed is less than the water sound speed then the losses are much higher for the small grazing angles. At the angle of intromission γ_{0I}, which is defined by the equation

$$\cos^2\gamma_0 = [(\rho_0 v_0)^2 - (\rho_1 v_1)^2]/[(\rho_0 v_1)^2 - (\rho_1 v_1)^2]$$

R is zero, or all sound energy is transmitted into the sediment half-space. The phase shift is -180° for $\gamma_0 < \gamma_{0I}$ shifting abruptly to 0° for $\gamma_0 > \gamma_{0I}$. Fry and Raitt (Fry and Raitt, 1961) measured this phase shift for deep sea Pacific sediments and by using known values of the density were able to determine the sound speed of the near bottom sediments.

Figure 6 shows the values of mod(R), phase shift, and bottom loss for low speed bottom corresponding to silty-clay from a continental terrace. The sediment-water sound speed ratio is 0.994 and the sediment-water density ratio is 1.421. These set the angle of intermission at 6.3°.

The effect of sediment attenuation can be introduced into the model (Mackenzie, 1960) by modifying the equation for ℓ_1^2 as follows

$$\ell_1^2 = [(\omega/v_1) + i\alpha_1/8.686]^2 - k^2 \quad ,$$

where α_1 is the attenuation of the sound wave in the sediment in dB per unit length. In Fig. 7 we have plotted the bottom loss as a function of γ_0 for the case where the sediment sound speed is greater than the water speed for several values of α_1. Hamilton (1972, 1974) has derived a simple empirical formula that relates a to sediment porosity and frequency.

Figure 8 shows the effect of increasing absorption for the low speed bottom. The essential effect is the removal of the peak in the bottom loss curve at the angle of intermission.

B. Solid

The liquid model of the bottom may be used in crude calculations, however, we do know that sediments have rigidity and we must account for this in accurate calculations. An isotropic sediment layer can be described by three sediment parameters (as shown in Fig. 9), the density ρ and the two Lamé constants lambda and mu, (Ewing, Jardetsky, and Press, 1957). The density can be measured directly but lambda and mu are determined by the speed and attenuation of the compressional and shear waves that travel in the sediment. These are related by two equations (Bucker et. al., 1965)

$$(\lambda + 2\mu) = \rho(x_p^2 - y_p^2 - i\,2x_p\,y_p)/(x_p^2 + y_p^2)^2$$

$$\mu = \rho(x_s^2 - y_s^2 - i\,2x_s\,y_s)/(x_s^2 + y_s^2)^2 \quad .$$

Here λ and μ are the Lamé constants, ρ is the density, $x_p = 1.0/v_p$, $y_p = \alpha_p/(8.686\ \omega)$, $x_s = 1.0/v_s$, $y_s = \alpha_s/(8.686\ \omega)$, v_p and v_s are sound speeds of the compressional wave and the shear wave respectively, and α_p and α_s are the attenuation (in dB per unit length) of the compressional and shear waves. Given v_p, v_s, α_p and α_s we can solve directly for λ and μ. If we do not know α_s then we can use the v_p, v_s and α_p and the assumption of zero volume viscosity (i.e. $Im(\lambda) + (2/3)Im(\mu) = 0$) to solve for λ and μ. If we do not know either v_s or α_s then we assume zero volume viscosity and an estimate of the rigidity (we define rigidity = $r = Re(\mu)/Re(\lambda)$) and then solve for λ and μ. Reflection of a plane wave from a solid half-space is shown in Fig. 10. A plane compressional wave is incident on the interface at grazing angle γ_0. There is a reflected wave in the water and a compressional wave and a vertically polarized shear wave in the solid. Note that there has been a simple change in notation to conform with geophysical publications. Earlier we formulated the problem in terms of the horizontal wave number k and the vertical wave number ℓ. Now the problems use the horizontal phase velocity $c(c = \omega/k)$ and the parameter r_α which is equal to ℓ divided by k. To solve for the three unknowns, R, T_p, and T_s, we require the following three interface conditions: (i) continuity of pressure, (ii) continuity of vertical particle motion, and (iii) zero stress on the x direction on the solid by the water. Solution of the interface equations results in the well known expression for R

$$R = (q-1)/(q+1) ,$$

where

$$q = \rho_1 r_{\alpha 0} [(\gamma_1 - 1)^2 + \gamma_1 r_{\beta 1} r_{\alpha 1}]/(\rho_0 r_{\alpha 1}) .$$

Here ρ_0 and ρ_1 are the density of the water and the solid respectively and the other quantities are defined as

$$r_{\alpha 0} = [(c/v_0)^2 - 1]^{1/2} ,$$

$$r_{\alpha 1} = [\rho_1 c^2/(\lambda_1 + 2\mu_1) - 1]^{1/2} ,$$

$$r_{\beta 1} = [\rho_1 c^2/\mu_1 - 1]^{1/2} ,$$

$$\gamma_1 = 2\mu_1/(\rho_1 c^2) , \text{ and } c = \omega/k .$$

Roots are chosen so that $r_{\alpha 0}$, $r_{\alpha 1}$, and $r_{\beta 1}$ lie in the first quadrant of the complex plane.

In Fig. 11 we have plotted bottom loss, phase, and the modulus of R as a function of grazing angle. For the case shown the ratios ρ_1/ρ_0, v_{r1}/v_0, and v_{s1}/v_0 are 2.6, 4.46 and 2.57 respectively. The rigidity value, r, is equal to 1.0. For all practical purposes the bottom loss is essentially zero. There are two critical angles. The first, γ_{cs}, comes when the horizontal phase velocity is equal to the shear speed. There are no losses for grazing angles less than γ_{cs}. The second critical angle, γ_{cp}, occurs when the phase velocity is equal to the compressional sound speed.

C. Multi-Layer Liquid

We next want to consider multi-layered sediment models that can be used either to represent actual layering (e.g. it is not uncommon to find alternating layers of sand and silt in shallow water) or to account for

gradients. For the layered liquid case the solution is very simple. In Fig. 12 we have n sediment layers and a half-space labeled (n + 1). In each layer the potential function is the sum of an up- and a down-going plane wave (e.g. $\phi_n - A_n \exp(i \ell_n z_n) + B_n \exp(-i \ell_n z_n)$) and in the half-space the potential function represents a down-going wave ($\phi_{n+1} = \exp(i \ell_{n+1} z_{n+1})$). If we let P represent the pressure ($P = \rho\phi$) and Q the vertical component of particle velocity we can start at the interface between layer n and the half-space with the values of P and Q as shown at the top of Fig. 13. P, equal to $\rho\phi$, and Q, equal to $d\phi/dz$ are easily evaluated at the n/(n+1) interface where z_{n+1} is zero. Because P and Q are continuous functions they have the same values at the bottom of layer n (at $z_n = d_n$) that they have at the top of the half-space (at $z_{n+1} = 0$). Therefore we can calculate A_n and B_n as shown in Fig. 13 and from these calculate P and Q at the top of layer n (at $z_n = 0$). We continue working up the layers until we have values for A_0 and B_0 from which the value of R is obtained, $R = B_0/A_0$.

D. Multi-Layer Linear Gradient

We consider now another method for modeling the change of sediment properties with depth due to increasing compaction and temperature. In this approach we account for changes in sound speed and density by using single or multiple liquid layers where Airy functions can be used to represent the sound energy. This method has been used by Morris (Morris, 1970) and also by Hanna (Hanna, 1973) to explain low values of bottom loss at small grazing angles and low frequency. In this case we will use a somewhat different function χ as shown at the top of Fig. 14. The general wave equation for the case where there is variation in both sound speed

and density is shown on the second line (Brekhovskikh, 1960). Cap. K squared is defined on the third line. If cap. K squared can be represented as a linear function of depth then the potential function χ can be written as the sum of the Airy functions Ai and Bi. The argument of the Airy functions is defined in terms of the horizontal wave number k, the profile parameters K_0 and β and the depth z by the relation shown in the 6th line. To add the effect of absorption in the liquid an imaginary term $i\alpha/8.686$ is added to K_0 as shown on the bottom line.

A multi-layered model composed of linear K^2 and constant K (constant sound speed) layers is shown in Fig. 15. We can start at the bottom, and work up through the layers using the interface conditions that the pressure and the vertical component of particle velocity are continuous functions. In this case P, equal to the pressure, is $\sqrt{\rho}\chi$ and Q, equal to $-i\omega$ times the particle velocity, is $\rho^{-1}\, d(\sqrt{\rho}\chi)/dz$. Note that in Fig. 15 we have made layer 2 a constant K layer. The ability to mix linear and constant layers is necessary in a general program because as the gradient, β, goes to zero the argument of the Airy functions increases without limit. Thus depending on frequency, layer thickness, and computer word length there is a minimum gradient that can be used. Layers with gradients smaller than this must be represented by constant K layers.

Now that we have two models that account for gradients it will be instructive to see how they compare. To do this consider Fig. 16. On the left hand side our linear model has a sound speed that increases from 1500 m/sec at the water/sediment interface to 1800 m/sec at a sediment depth of 300 m which corresponds to an average sound speed

gradient equal to (1800 - 1500) m/sec ÷ 300 m, or 1 sec^{-1}. The constant K model is shown for two layers. The layers have the same thickness and the sound speed at the center of the layers (i.e. at 75 and 225 m) is set equal to the sound speed of the linear layer at that depth.

On the right hand side of Fig. 16 is a diagram that indicates the main physical events. Most of the energy either reflects at the surface or is refracted in the sediment because of the gradient. Morris (Morris, 1973) has used a ray description to calculate the energy in each path and compare the ray description with the wave model. Of course there are 2nd and higher order effects as indicated by the dashed arrows that are implicit in the wave model.

In Fig. 17 we show our first comparison of the two models. For the calculations we used a frequency of 100 Hz, a density ratio (ρ in sediment)/(ρ in water) equal to 2.0, and zero attenuation. The reflection coefficient was calculated for grazing angles from 0° to 20° which are of interest in sound propagation. With zero attenuation both models return all sound to the water for these grazing angles so the modulus of R is 1.0 or the bottom loss is zero. Figure 17 shows plots of phase, i.e. the argument of R, for different cases. The curve marked L is for the linear K^2 model, while the curves labeled 1, 3, or 10 correspond to 1, 3, or 10 constant K layers. The 10 layer case has a layer thickness of 30 m which is equal to 2 wavelengths in the water. For 30 layers (or a thickness of 0.67 λ_w) there is a maximum phase difference of 2.2° at a grazing angle of 3.5° which cannot be plotted on this scale. For 100 layers there is a maximum phase difference of 0.2°.

In Fig. 18 we are using the same models except that there is an attenuation of 0.05 dB/m in both models. As in the previous case the 10 layer model (thickness = 2 λ_{ω}) has a maximum difference of ~10° and the 30 layer model has essentially the phase as the linear model. It is interesting to note that the attenuation has slowed the phase change a considerable amount. This will have a noticeable effect on the wave theory propagation models where a shift in phase of 360° will add a new mode to the sound field. (Bucker, 1964).

To complete the comparison of the linear and constant layers, the bottom loss curves are shown in Fig. 19. The one layer case has much less bottom loss because the sound speed is equal to the sound speed of the linear model at 150 m depth which is 1629.6 m/sec and corresponds to a critical angle greater than 20°.

E. Multi-Layer Solid

There are several approaches to the problem of modeling the sediment layers when there are significant changes of the sediment properties with depth. Gupta (1966a, 1966b) has developed closed solutions for the case where the compressional and shear velocity varies linearly with depth while the density remains constant. More general variations can be treated with the propagator method developed by Gilbert and Backus (1966). One problem of the propagator method is loss of accuracy when sediment penetration of many wavelengths occurs. In the most recent programs at NUC we have chosen to model the variable sediment properties with many layers and to maintain accuracy by use of Knopoff's formulation (Knopoff, 1964).

The multi-layer solid model is substantially more difficult than the multi-layer liquid model for two reasons. First there are twice as many waves (shear waves as well as compressional waves) and twice as many interface conditions (continuity of horizontal components of stress and strain as well as continuity of vertical components of stress and strain). Second you cannot start at the bottom and work to the top. All of the layers have to be considered as a group. The situation is shown in Fig. 20. There are an up- and a down-going compressional wave in the water, an up- and a down-going compressional wave and an up- and a down-going shear wave in each solid layer, and down-going compressional and shear waves in the bottom half-space. We can arbitrarily set the coefficient $A_{n+1} = 1$, as shown, so that there are $4n + 3$ unknown coefficients (A_0, B_0, A_1, B_1, C_1,..., C_{n+1}), where n is the number of layers. There are also $4n + 3$ interface conditions. Three conditions at the first interface (continuity of vertical components of stress and strain and zero horizontal stress) and four conditions at all other interfaces (continuity of vertical and horizontal stress and strain). Since the interface conditions can be written as a set of linear homogeneous algebraic equations the solution can be done using standard matrix inversion algorithms. This is not a practical method of solution when n is large because we would have to invert a matrix of $(4n + 3)^2$ elements and because of loss of accuracy problems. The number of terms in the problem can be kept under control by using transfer matrices that transfer the stress and strain at one interface of a layer to the other interface. This method was developed by Thomson (1950). For the problem of sound transmission through plates and extended by Bucker,

Whitney, Yee, and Gardner (1965) to include wave attenuation for the problem of bottom reflection. A serious drawback of the transfer matrix method is that it also suffers from loss of accuracy problems.

Fortunately the accuracy problems can be solved using methods developed by the geophysicists for earthquake problems (Thrower, 1965; Dunkin, 1965; Watson, 1970; Schwab, 1970). This is discussed in Appendix B. The results are summarized in Fig. 21. For a layered structure of the same form that we have for the bottom reflection problem there are natural vibrations at frequencies corresponding to zeroes of a determinant, $|\Delta_R|$, called the Rayleigh determinant. The geophysicists have developed very fast and accurate methods for calculating $|\Delta_R|$. In Appendix B we show that the reflection coefficient can be written as $R = (\rho_1 r_{\alpha 0} |\Delta_R| - \rho_0 |\Delta_S|)/(\rho_1 r_{\alpha 0} |\Delta_R| + \rho_0 |\Delta_S|)$ where $|\Delta_S|$ is the same as $|\Delta_R|$ except for row 1. Thus we can use the sophisticated methods of the geophysicists to solve our problem. We do have to generalize the equations to account for attenuation which is neglected at earthquake frequencies.

Figure 22 is a plot of bottom loss for a model of 100 layers. The curve labeled L is for the liquid layer model (it is also the bottom loss curve for the linear model). The other curves are for a 100 layer solid model with different values of rigidity. For r = 0 the curve is quite similar to the liquid model except that there is slightly more loss due to some conversion of compressional waves into shear waves. As the rigidity increases there are lower losses than the liquid model at very small grazing, angles and higher losses than the liquid model at larger grazing angles. Most likely the propagation to long ranges would be better for the r = 0.1 curve than for the liquid model.

III. COMPARISON WITH EXPERIMENT

The U.S. Navy has been concerned about the operation of bottom bounce sonars over the last twenty years. It is therefore not surprising that there have been a large number of laboratory reports on bottom loss, many of which are classified.

At the Underwater Sound Laboratory in New London (now NUSC-NL) the research work has concentrated on problems associated with the SQS-26 sonar. Significant papers have been published by Karamargin (1962), Cole (1965), Menotti, Santaniello, and Schumacher (1965).

At the Naval Undersea Center at San Diego most of the work has centered on data collected during three FASOR (forward area sonar research) cruises. Data was collected in over 90 stretegic areas in the Western Pacific Ocean, in contiguous seas and basins, and in the Indian Ocean. Most of the journal reports have been written by Hamilton (on sediment properties, (Hamilton, 1974a, b) and by Bucker and Morris (on calculation of the plane wave reflection coefficient, (Bucker et.al., 1965; Morris, 1970, 1973)).

At the Applied Research Laboratory (Univ. of Texas) sediment properties have been measured by Hampton (1967) and bottom reflection calculations have been reported by Banard, Bardin, and Hempkins (1964). Also, Frev (1967) has published a bibliography on the reflection and scattering of sound from the ocean bottom.

At SACLANTCEN the work of Hastrup has been already cited. More recently there have been significant reports by Tuncay Akal (1972, 1974).

We will illustrate the agreement between experimental data and calculated values of bottom loss with some NUC data from the FASOR cruises. In

the first case, Fig. 23, data is from an abyssal hill province in the Northeast Pacific and the frequency is 1.6 kHz. Two calculated curves are shown, one with a gradient and one with constant sound speed. The gradient model provides a somewhat better fit but there is not a large difference between the two. In the next figure, Fig. 24, the frequency has been reduced to 200 Hz and it is clear that there is refracted energy responsible for the small values of bottom loss that is not included in the iso-speed model.

Our last example, Fig. 25, is from the Coral Sea. The frequency is 50 Hz. At the lower grazing angles we see some negative bottom losses in the experimental data. This could be due to an error in the assummed source level of the explosive charges or some inacurracy in the analysis. We feel that a more fundamental problem is in doing an analysis of 50 Hz bottom loss. At very low frequencies we are concerned with passive systems which process essentially CW signals. Also the received signal is made up of all possible paths that can travel from the source to the receiver. The performance of operational systems can be accurately simulated with a CW source. The measured results can then be compared to wave theory calculations involving plane wave reflection coefficients as discussed before. It should be easy to determine the sensitivity of the acoustic field to bottom interaction and the accuracy of the reflection coefficient. By introducing the bottom loss measurements with the explosive charges we have unnecessarily complicated our analysis problem.

IV. SUMMARY

We began this review with the ray theory equations and the problem of a bottom bounce sonar. As far as levels are concerned this problem is mostly solved. With a good description of the upper 10 m or so of sediments a reflection coefficient can be calculated, converted to bottom loss and used in a ray theory description of the sound field. There are probably cases where the bottom is so rough that this direct approach is not applicable, but in the data that we have worked with, it does.

Several models of varying complexity for calculating the plane wave bottom reflection coefficient have been discussed. The most general model is composed of an almost unlimited number of solid layers with attenuation and should represent any reasonably uniform sediment structure.

At lower frequencies (e.g. below 2 kHz) we begin to see an appreciable amount of energy that is refracted from the positive gradients in the sediments. The sediment parameters must be defined to a depth at least as deep as the refracting sound field. This requires several hundred meters of sediment data. Also at the lower frequencies the formalism of ray theory begins to break down as the bottom and direct wave fronts begin to interact. We suggest that at low frequencies the standard shot runs and bottom loss curves are not useful and that we should consider CW experiments where the total sound field is measured and compared to wave theory calculations that contain bottom interaction in the plane wave reflection coefficient.

V. REFERENCES

Tuncay Akal, "Acoustical Characteristics of the Sea Floor: Experimental Techniques and Some Examples from the Mediterranean Sea", in Physics of Sound in Marine Sediments, pp. 447-480, Ed. by Loyd Hampton, Plenum Press, New York (1974).

Tuncay Akal, "The Relationship Between the Physical Properties of Underwater Sediments that Affect Bottom Reflection", Marine Geology 13, 251-266 (1972).

G. R. Barnard, J. L. Bardin, and W. B. Hempkins, "Underwater Sound Reflection from Layered Media," J. Acoust. Soc. Am. 36, 2119-2123 (1964).

Leonid M. Brekhovskikh, Waves in Layered Media, p. 171, English Translation, Academic Press, New York (1960).

H. P. Bucker, "Normal Mode Propagation in Shallow Water," J. Acoust. Soc. Am. 36, 251-258 (1964).

H. P. Bucker, J. A. Whitney, G. S. Yee and R. R. Gardner, "Reflection of Low Frequency Sonar Signals from a Smooth Ocean Bottom," J. Acoust. Soc. Am. 37, 1037-1051 (1965).

H. P. Bucker, "Sound Propagation in a Channel with Lossy Boundaries," J. Acoust. Soc. Am. 48, 1187-1194 (1970).

B. F. Cole, "Marine Sediment Attenuation and Ocean Bottom Reflected Sound," J. Acoust. Soc. Am. 38, 291-297 (1965).

J. W. Dunkin, "Computation of Modal Solutions in Layered Elastic Media at High Frequencies," Bull. Seism. Soc. Am. 55, 335-358 (1965).

W. Maurice Ewing, Wenceslas S. Jardetsky and Frank Press, Elastic Waves in Layered Media, pp. 79-83, McGraw-Hill Book Co., New York (1957).

H. G. Frey, "Reflection and Scattering of Sound by the Ocean Boundaries: A Bibliography," Defense Research Lab, Acoust. Report No. 285.

John C. Fry and Russell W. Raitt, "Sound Velocities at the Surface of Deep Sea Sediments," J. Geophys. Res. 66, 589-597 (1961).

Freeman Gilbert and George E. Backus, "Propagator Matrices in Elastic Wave and Vibration Problems," Geophysics 31, 326-332 (1966).

Ravindra N. Gupta, "Reflection of Sound Waves from Transition Layers," J. Acoust. Soc. Am. 39, 255-260 (1966a).

Ravindra N. Gupta, "Reflection of Elastic Waves from a Linear Transition Layer," Bull. Seism. Soc. Am. 56, 511-526 (1966b).

E. L. Hamilton, "Compressional Wave Attenuation in Marine Sediments," Geophysics 37, 620-646 (1972).

E. L. Hamilton, "Prediction of Deep-Sea Sediment Properties: State of the Art," pp. 1-43 in Deep Sea Sediments, Physical and Mechanical Properties, Ed. by A. L. Interbitzen, Plenum Press (1974a).

E. L. Hamilton, "Geoacoustic Models of the Sea Floor," pp. 1-43, in Physics of Sound in Marine Sediments, Ed. by L. Hampton, Plenum Press, (1974b).

L. D. Hampton, "Acoustic Properties of Sediments," J. Acoust. Soc. Am. 42, 882-890 (1967).

K. V. Mackenzie, "Reflection of Sound from Coastal Bottoms," J. Acoust. Soc. Am. 32, 221-231 (1960).

F. R. Menotti, S. R. Santaniello and W. R. Schumacher, "Studies of Observed and Predicted Values of Bottom Reflectivity as a Function of Incident Angle," J. Acoust. Soc. Am. 68, 707-714 (1965).

Halcyon E. Morris, "Bottom Reflection Loss Model with a Velocity Gradient," J. Acoust. Soc. Am. 48, 1198-1202 (1970).

Halcyon E. Morris, "Ray and Wave Solutions for Bottom Reflection for Linear Sediment Layers," J. Acoust. Soc. Am. 53, 323(A) (1973).

C. B. Officer, Introduction to the Theory of Sound Transmission with Application to the Ocean, pp. 74-82, McGraw Hill Book Co., New York (1958).

Fred Schwab, "Surface-Wave Dispersion Computations: Knopoff's Method," Bull. Seism. Soc. Am. 60, 1491-1520 (1970).

W. T. Thomson, "Transmission of Elastic Waves Through a Stratified Solid Medium," J. Appl. Physics 21, 89-93 (1950).

E. N. Thrower, "The Computation of Dispersion of Elastic Waves in Layered Media," J. Sound Vib. 2, 210-226 (1965).

T. H. Watson, "A Note on Fast Computation of Rayleigh Wave Dispersion in the Multilayered Half-Space," Bull. Seism. Soc. Am. 60, 161-166 (1970).

$$\Psi = \sum_n A_n \exp(i\Theta_n)$$

$$A_n = |R| \left[\cos\gamma_s \, \delta\gamma_s / (r\,\delta h)\right]^{1/2}$$

$$\Theta_n = \int_0^r \frac{\omega}{v} d\ell + \mathrm{ARG}(R) - \frac{m\pi}{2}$$

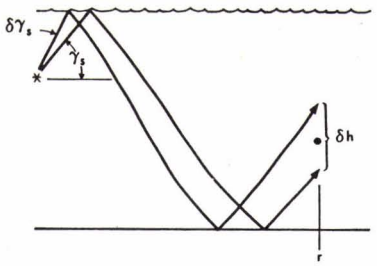

FIG. 1 RAY THEORY REPRESENTATION (HIGH FREQUENCY)

$$\Psi = \left(\frac{2\pi}{r}\right)^{1/2} \sum_n U_n(Z_o)\, U_n(Z)\, e^{ik_n r}$$

$$U = A\, f(Z) + B\, g(Z), \quad 0 \le Z \le Z_p$$

$$U = \exp\left[i\ell_b Z\right] + R \exp\left[i\ell_b (2Z_b - Z)\right]$$

$$(Z_p < Z < Z_b)$$

$$\ell_b^2 = (\omega/v_b)^2 - k^2$$

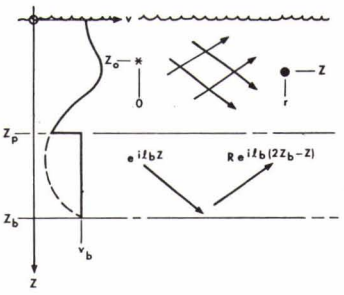

FIG. 2 WAVE THEORY REPRESENTATION (LOW FREQUENCY)

INTERFACE CONDITIONS

CONTINUITY OF PRESSURE (ρU)

CONTINUITY OF VERTICAL COMPONENT OF PARTICLE VELOCITY $\left(-\frac{\partial U}{\partial z}\right)$

SOLVE FOR A AND B AS $z_p \rightarrow z_b$

$$A = \exp(i\ell_b Z_b)\left[g'_b (1+R) - i\ell_b g_b (1-R)\right]/W.$$

$$B = \exp(i\ell_b Z_b)\left[i\ell_b f_b (1-R) - f'_b (1+R)\right]/W.$$

WHERE, $W = f_b g'_b - f'_b g_b$.

$f_b = f(Z_b)$, $g_b = g(Z_b)$, $f'_b = (df/dZ)_{Z_b}$, $g'_b = (df/dZ)_{Z_b}$

FIG. 3 INTRODUCTION OF R INTO WAVE SOLUTIONS

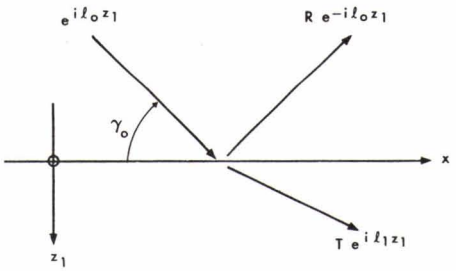

$$k = (\omega/v_o)\cos\gamma_o, \quad \ell = (\omega/v_o)\sin\gamma_o$$

$$\ell_1^2 = (\omega/v_1)^2 - k^2$$

$$R = (\rho_1 \ell_o - \rho_o \ell_1) / (\rho_1 \ell_o + \rho_o \ell_1)$$

FIG. 4 REFLECTION FROM LIQUID–LIQUID INTERFACE (RAYLEIGH MODEL)

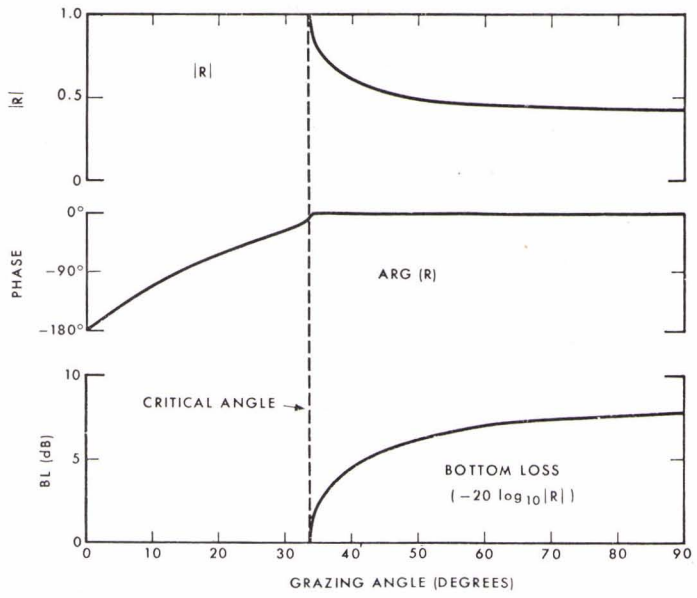

FIG. 5
RAYLEIGH MODEL ($v_1 > v_o$)

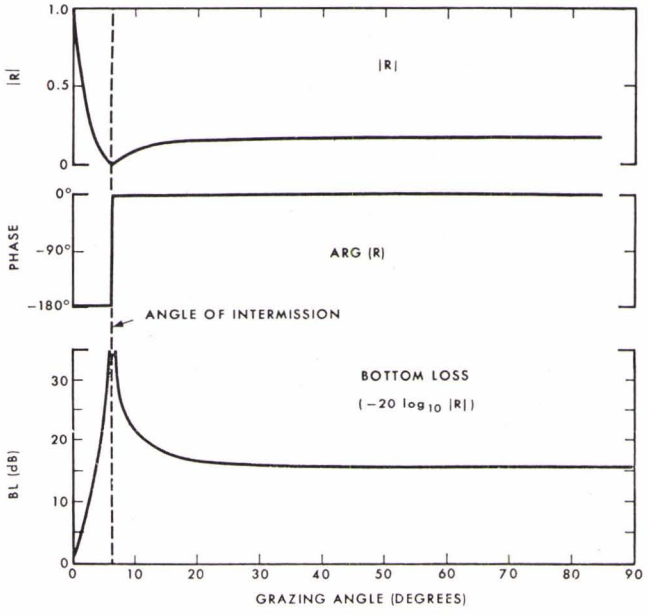

FIG. 6
RAYLEIGH MODEL ($v_1 < v_o$)

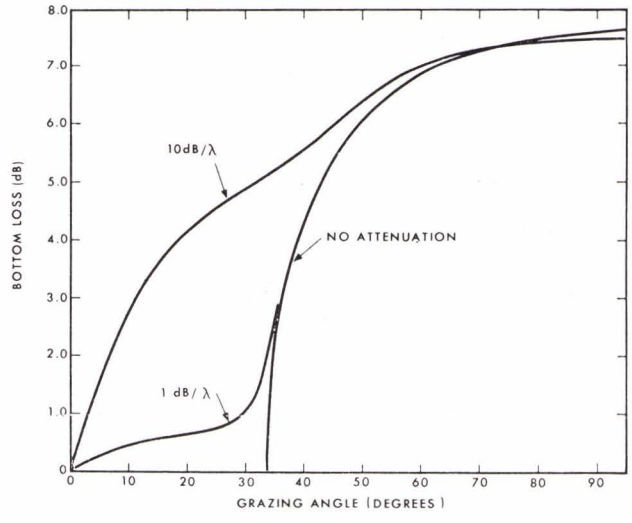

FIG. 7
RAYLEIGH MODEL ($v_1 > v_o$)
FOR 0, 1, 10 dB/λ ATTENUATION

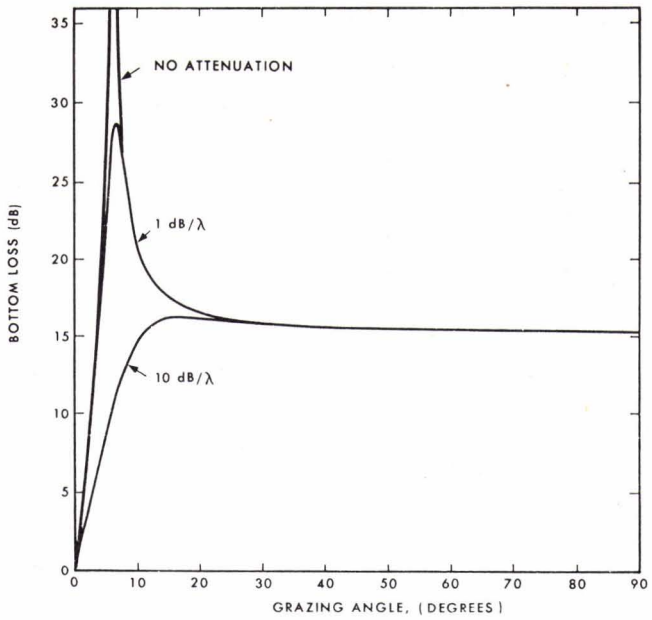

FIG. 8
RAYLEIGH MODEL ($v_1 < v_o$)
FOR 0, 1, 10 dB/λ ATTENUATION

SEDIMENT PARAMETERS ρ, $\underbrace{\lambda, \mu}_{\text{LAMÉ CONSTANTS}}$

ACOUSTIC PARAMETERS

v_p = SOUND SPEED (COMP. WAVE)

v_s = SOUND SPEED (SHEAR WAVE)

a_p = ATTEN., dB/UNIT LENGTH (COMP.)

a_s = ATTEN., dB/UNIT LENGTH (SHEAR)

CONSTITUTIVE EQUATIONS

$$\lambda + 2\mu = \rho(x_p^2 - y_p^2 - i2x_p y_p)/(x_p^2 + y_p^2)^2$$

$$\mu = \rho(x_s^2 - y_s^2 - i2x_s y_s)/(x_s^2 + y_s^2)^2$$

NOTATION

$x_p = 1/v_p$, $y_p = a_p/(8.686\omega)$

$x_s = 1/v_s$, $y_s = a_s/(8.686\omega)$

FIG. 9
SEDIMENT AND ACOUSTIC PARAMETERS FOR SOLID

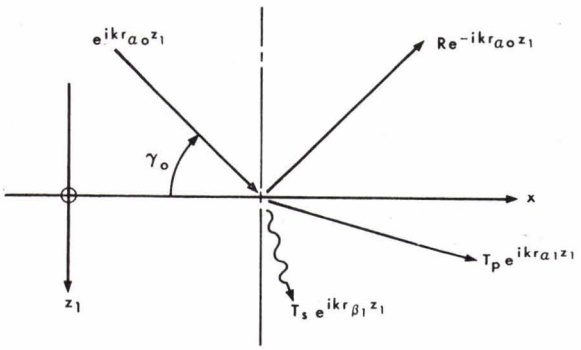

FIG. 10
REFLECTION FROM LIQUID–SOLID INTERFACE

$$R = (q-1)/(q+1)$$

WHERE $q = \rho_1 r_{ao}[(\gamma_1 - 1)^2 + \gamma_1 r_{\beta 1} r_{\alpha 1}]/(\rho_o r_{\alpha 1})$

$r_{ao} = \ell_o/k = [(c/v_o)^2 - 1]^{1/2}$

$r_{\alpha 1} = \ell_1/k = [\rho c^2/(\lambda + 2\mu) - 1]^{1/2}$

$r_{\beta 1} = [\rho c^2/\mu - 1]$

$\gamma_1 = 2\mu_1/(\rho_1 c^2)$

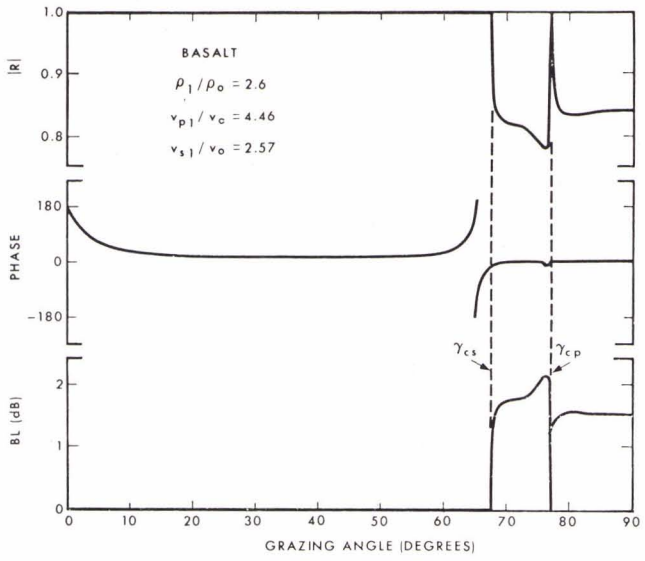

FIG. 11
REFLECTION FROM BASALT

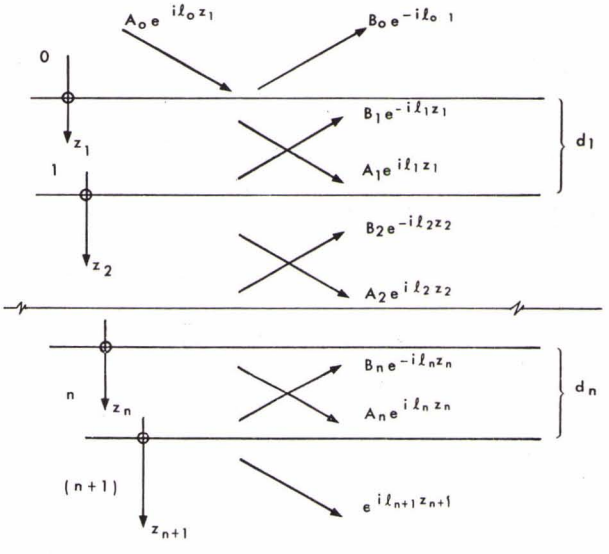

FIG. 12
MULTI-LAYER LIQUID MODEL

INTERFACE n/(n+1): $P = \rho\varphi = \rho_{n+1}$, $Q = (d\varphi/dz) = i\ell_{n+1}$

LAYER n:

$$A_n = \tfrac{1}{2}\exp(-i\ell_n d_n)\,[P/\rho_n + Q/(i\ell_n)]$$

$$B_n = \tfrac{1}{2}\exp(i\ell_n d_n)\,[P/\rho_n - Q/(i\ell_n)]$$

INTERFACE (n—1)/n:

$$P = \rho_n(A_n + B_n)$$

$$Q = i\ell_n(A_n - B_n)$$

CONTINUE UNTIL A_o & B_o ARE CALCULATED

REFLECTION COEFFICIENT: $R = B_o/A_o$

FIG. 13
CALCULATION OF R FOR MULTI-LAYER LIQUID

$$p = \sqrt{\rho}\,\chi$$

WAVE EQ. $\nabla^2 \chi + K^2 \chi = 0$

WHERE, $K^2 = (\omega/v)^2 + \frac{1}{2\rho}(d^2\rho/dz^2) - \frac{3}{4}\left[\frac{1}{\rho}(d\rho/dz)\right]^2$

IF $K^2 = K_o^2(1+\beta z)$

THEN $\chi = A \cdot Ai(\xi) + B\,Bi(\xi)$

WHERE $\xi = \frac{k^2 - K_o^2}{(K_o^2\beta)^{2/3}} - (K_o^2\beta)^{1/3} z$

TO ADD α (dB/UNIT LENGTH) ATTENUATION: $K_o \rightarrow K_o + i\frac{\alpha}{8.686}$

FIG. 14
WAVE SOLUTIONS FOR THE LINEAR MODEL

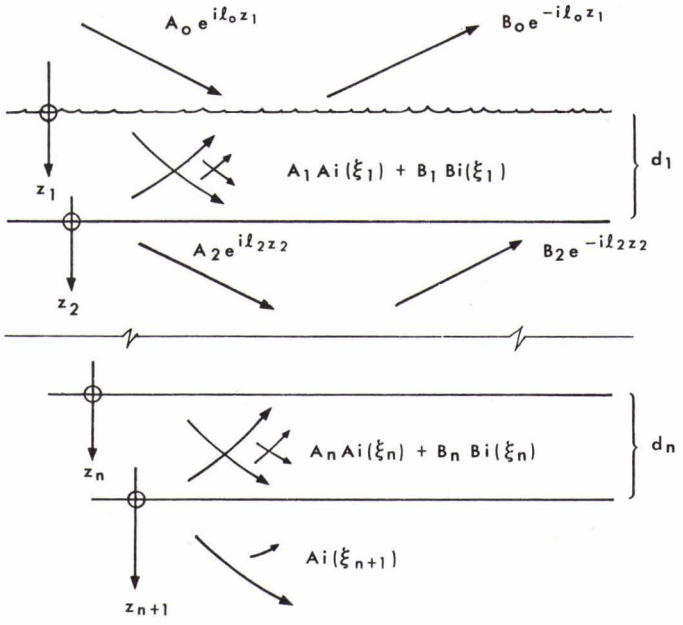

FIG. 15
MULTI-LAYER LINEAR LIQUID MODEL

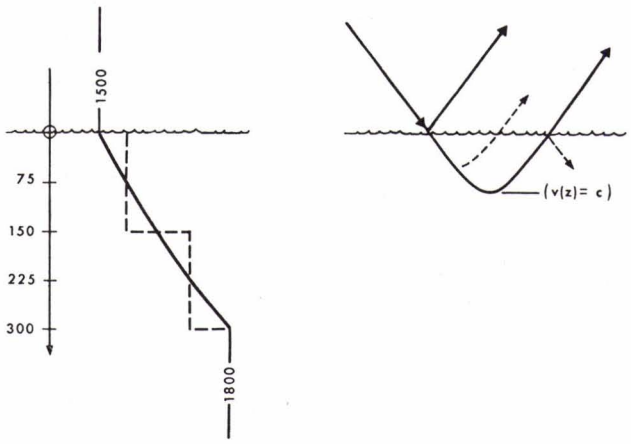

FIG. 16
LINEAR K^2 AND CONSTANT K LAYERS

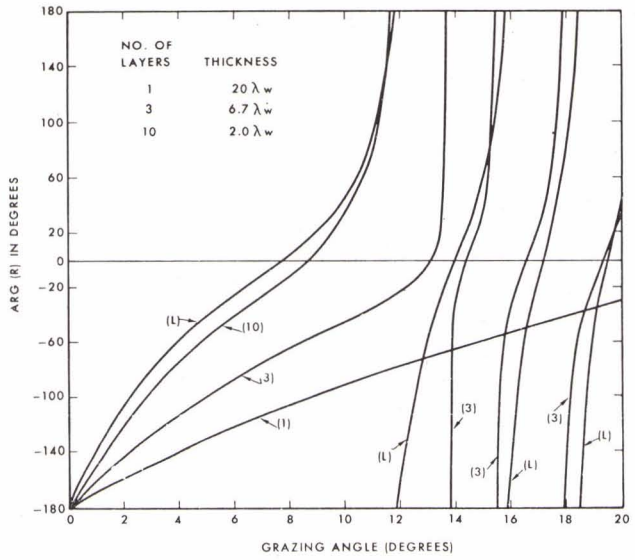

FIG. 17
PHASE COMPARISON FOR LINEAR K^2 AND CONSTANT K MODELS
(Zero Attenuation)

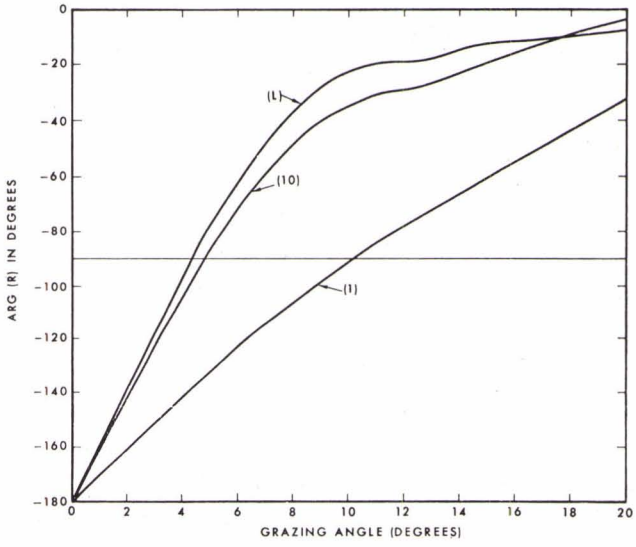

FIG. 18
PHASE COMPARISON FOR LINEAR K^2 AND CONSTANT K MODELS
(0.05 dB/m Attenuation)

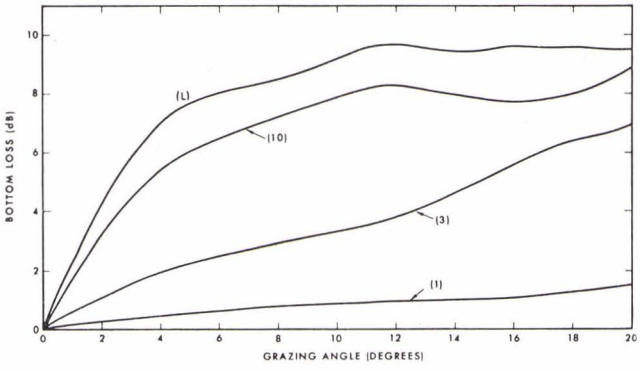

FIG. 19
BOTTOM LOSS COMPARISON FOR LINEAR K^2 AND CONSTANT K MODELS
(0.05 dB/m Attenuation)

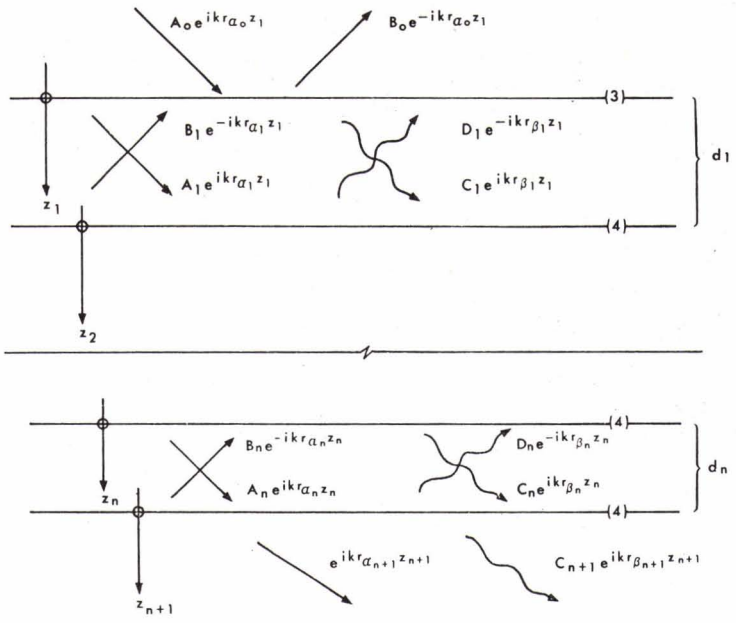

FIG. 20
MULTI-LAYER SOLID MODEL

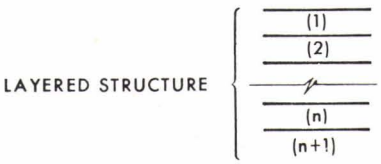

NATURAL VIBRATIONS (EARTHQUAKE WAVES) OCCUR AT ZERO'S OF RAYLEIGH DETERMINANT $|\Delta_R|$

WE CAN SHOW THAT $$R = \frac{\rho_1 r_{\alpha_o} |\Delta_R| - \rho_o |\Delta_S|}{\rho_1 r_{\alpha_o} |\Delta_R| + \rho_o |\Delta_S|}$$

WHERE Δ_S IS THE SAME AS Δ_R

EXCEPT FOR ROW 1

FIG. 21
REFLECTION COEFFICIENT FOR THE MULTI-LAYER SOLID MODEL

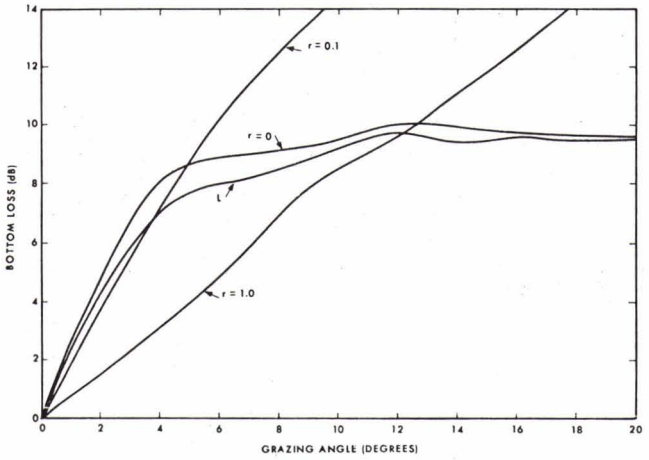

FIG. 22
COMPARISON OF MULTI-LAYER SOLID AND LIQUID MODELS

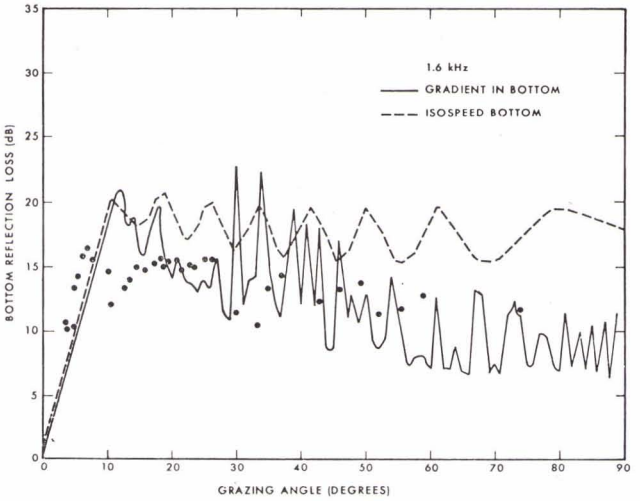

FIG. 23
COMPARISON OF GRADIENT AND NO GRADIENT MODELS WITH 1.6 kHz DATA

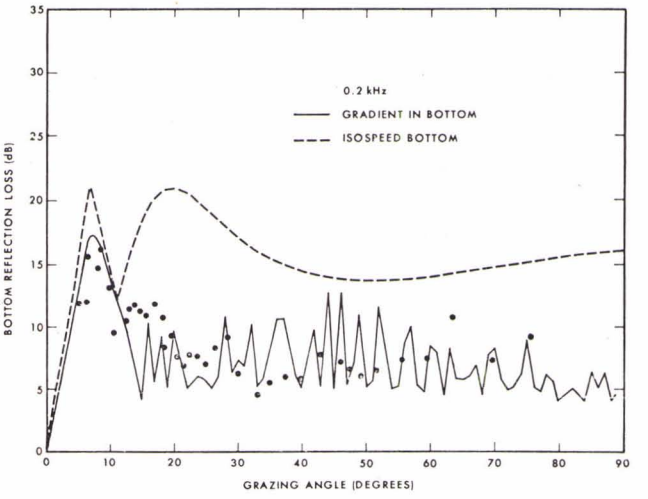

FIG. 24
COMPARISON OF GRADIENT AND NO GRADIENT MODELS WITH 0.2 kHz DATA

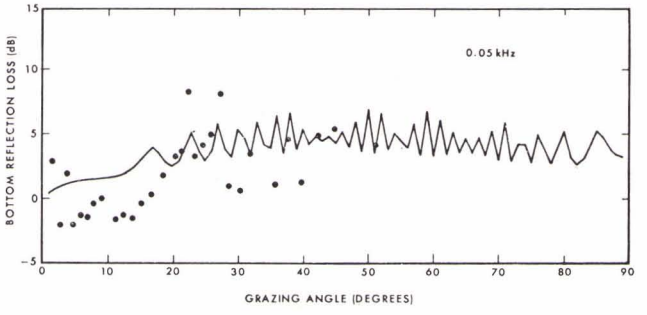

FIG. 25
COMPARISON OF GRADIENT MODEL WITH 0.05 kHz DATA

VII. APPENDICES

APPENDIX A: Formulation of the Sound Field Using the Plane Wave Reflection Coefficient R

The general form of the sound field can be written as a sum of cylindrical waves in the form (Bucker, 1970)

$$\psi = \int_0^\infty -2\, U(z_0)V(z)\, W^{-1}\, J_0(kr)\, kdk \qquad (z_0 \leq z \leq z_b)$$

where $W = U(z_0)V'(z_0) - U'(z_0)V(z_0)$.

The zero depth, source depth, receiver depth, and bottom depth are 0, z_0, z and z_b respectively. The zero depth may be set at the air-water interface or at some other convenient point. It represents the depth above which no sound is refracted or reflected to the receiver. The horizontal wave number is k, r is the horizontal distance between the source and receiver, J_0 is the Bessel function of the first kind of order zero, U is a solution of the z-separated part of the wave equation [i.e. $U'' = (k^2 - \omega^2/v^2(z))U$] that satisfies the boundary condition at z = 0, and v is a solution of the z-separated part of the wave equation [i.e. $V'' = (k^2 - \omega^2/v^2(z))V$] that satisfies the boundary condition at $z = z_b$. Formally our treatment will be restricted to $(z_0 \leq z \leq z_b)$, however, a similar development for $(0 \leq z \leq z_0)$ is easily derived.

It is easy to show that dW/dz is zero so that W is independent of depth. Also, we are free to specify the value of U and V at one depth. For convenience replace U and V by $\bar{U}$ and $\bar{V}$ where $\bar{U}(z_b) = \bar{V}(z_b) = 1$. It

follows then that in the limit $z_p \to z_b$ $W = W_{z_b} = [i \ell_b(1-R) - (1+R) \bar{U}'(z_b)]/(1+R)$. Therefore ψ can be expressed as

$$\psi = -2 \int_0^\infty \frac{(1+R)\, \bar{U}(z_0)\, \bar{V}(z)\, J_0(kr)\, kdk}{(i\ell_b - \bar{U}'_{z_b}) - R(i\ell_b + \bar{U}'_{z_b})} .$$

For the general sound speed profile it does not appear feasible to separate the direct sound paths from the bottom reflected paths. However, if the water has a constant sound speed then $\bar{U}(z) = \exp[i\ell(z_b - z)]$ and $\bar{V}(z) = [\exp - i\ell(z_b - z) + R \exp i\ell(z_b - z)]/(1+R)$. In this case it follows that

$$\psi = \underbrace{\int_0^\infty (i/\ell) e^{i\ell(z-z_0)} J_0(kr)\, kdk}_{\psi_D} + \underbrace{\int_0^\infty (i/\ell) R e^{i\ell(2z_b - z - z_0)} J_0(kr)\, kdk}_{\psi_R}$$

If the bottom reflected field ψ_R can be measured directly then we have

$$\psi_R = \int_0^\infty (i/\ell)\, R e^{i\ell(2z_b - z - z_0)} J_0(kr)\, kdk$$

and R can be determined experimentally by use of the Hankel Transform

$$R = \int_0^\infty \psi_R\, J_0(kr)\, rdr / [(i/\ell) \exp i\ell(2z_b - z - z_0)] .$$

This is not a practical procedure, however, because quadrature sampling would be required to determine the real and imaginary parts of ψ_R. That is Real $(\psi_R) = p_R \cos\phi$ and $\mathrm{Im}(\psi_R) = p_R \sin\phi$, where p_R is 1/2 the peak to peak pressure of the bottom reflected signal and ϕ is the phase. In any event when realistic profiles are considered it is not possible to separate the direct and bottom reflected paths at low frequencies.

APPENDIX B: Calculation of R for Many Solid Layers Using Knopoff's Method

The standard methods of solution (i.e. transfer matrices or matrix inversion) are not useable for the many solid layer model because of accuracy, computer storage, and computer run time problems. In this index we show how the fast and accurate methods developed in earth wave problems can be modified for calculation of R. In particular we will use the fast algorithm of Schwab (1970) which is based on Knopoff's formulation (Knopoff, 1964). The notation used is that of Haskell (1953).

Referring to Fig. 10 we choose the potential function for the up- and down-going compressional waves in the layer to be

$$\phi_n = \frac{1}{\omega} [i A_n \cos p_n + B_n \sin p_n] \exp[i(\omega t - kx)],$$

where $p_n = k r_{\alpha n} z_n$.

Also, we choose the potential function describing the up- and down-going shear waves to be

$$\Psi_n = \frac{1}{\omega} [C_n \sin q_n + i D_n \cos q_n] \exp[i(\omega t - kx)],$$

where $q_n = k r_{\beta n} z_n$.

The components of motion and stress in the n^{th} layer are therefore

$$c \dot{U}_n = A_n \cos p_n - i B_n \sin p_n + r_{\beta n} C_n \cos q_n - i r_{\beta n} D_n \sin q_n ,$$

$$c\dot{W}_n = -i\, r_\alpha A_n \sin p_n + r_\alpha B_n \cos p_n + i\, C_n \sin q_n - D_n \cos q_n \ ,$$

$$\sigma_n = \rho_n(\gamma_n - 1)\, A_n \cos p_n - i\, \rho_n(\gamma_n - 1)\, B_n \sin p_n$$

$$+ \rho_n \gamma_n r_{\beta n} C_n \cos q_n - i\, \rho_n \gamma_n r_{\beta n} D_n \sin q_n \ ,$$

$$\tau_n = i\, \rho_n \gamma_n r_{\alpha n} A_n \sin p_n - \rho_n \gamma_n r_{\alpha n} B_n \cos p_n$$

$$- i\, \rho_n(\gamma_n - 1)\, C_n \sin q_n + \rho_n(\gamma_n - 1)\, D_n \cos q_n \ .$$

In the above c is the horizontal phase velocity ($c = \omega/k$), $\dot{U}_n$ and $\dot{W}_n$ are the horizontal and vertical components of particle velocity, σ_n is the normal (vertical) stress, and τ_n is the tangential (horizontal) stress.

By separating ϕ_0 into an incident and reflected wave it is easy to show that the plane wave reflection coefficient R is given by

$$R = (A_0 - B_0)/A_0 + B_0) \ .$$

For convenience we set the value of $A_0 \equiv 1$. The three interface conditions at the water/sediment layer 1 interface can be written as

$$r_{\alpha 0} B_0 = r_{\alpha 1} B_1 - D_1 \qquad \text{(cont. of } \dot{W}\text{)}$$

$$-\rho_0 = \rho_1(\gamma_1 - 1)A_1 + \rho_1 \gamma_1 r_{\beta 1} C_1 \qquad \text{(cont. of } \sigma\text{)}$$

$$0 = -\rho_1 \gamma_1 r_{\alpha 1} B_1 + \rho_1(\gamma_1 - 1)\, D_1 \qquad \text{(cont. of } \tau\text{)}$$

Divide the last 2 above equations by ρ_1 and form the matrix of coefficients of B_0, A_1, B_1, C_1, D_1 (this is Knopoff's fast form).

B_0	A_1	B_1	C_1	D_1	
$r_{\alpha 0}$	0	$-r_{\alpha 1}$	0	1	$= 0$
0	$(\gamma_1 - 1)$	0	$\gamma_1\ r_{\beta 1}$	0	$= -\rho_0/\rho_1$
0	0	$-\gamma_1\ r_{\alpha 1}$	0	$(\gamma_1 - 1)$	$= 0$

Now modify the basis vectors so that the interface conditions can be within in the following matrix form

$$\begin{bmatrix} 1 & 0 & -1 & 0 & +1 \\ 0 & (\gamma_1-1) & 0 & \gamma_1 & 0 \\ 0 & 0 & -\gamma_1 & 0 & (\gamma_1-1) \end{bmatrix} \times \begin{bmatrix} B_0\ r_{\alpha 0} \\ A_1 \\ B_1\ r_{\alpha 1} \\ C_1\ r_{\beta 1} \\ D_1 \\ A_2 \end{bmatrix} = \begin{bmatrix} 0 \\ -\rho_0/\rho_1 \\ 0 \\ 0 \\ 0 \\ 0 \end{bmatrix}$$

Now solve for B_0 using Cramer's Rule

$$B_0\ r_{\alpha 0} = \frac{\begin{vmatrix} 0 & 0 & -1 & 0 & +1 \\ -\rho_0/\rho_1 & & & & \\ 0 & & \Delta_R & & \\ 0 & & & & \end{vmatrix}}{\begin{vmatrix} 1 & 0 & -1 & 0 & -1 \\ 0 & & & & \\ 0 & & \Delta_R & & \\ 0 & & & & \end{vmatrix}}$$

The elements inside the dashed areas designated Δ_R are the elements of the Rayleigh determinant. Fast and accurate methods are finding $|\Delta_R|$ have been developed (as mentioned before) because the zeroes of $|\Delta_R|$ determine the phase velocity of earthquake waves. Finally we can write

$$\frac{B_0\, r_{\alpha 0}}{(\rho_0/\rho_1)} = \frac{\begin{vmatrix} 0 & -1 & 0 & 1 \\ 0 & -\gamma_1 & 0 & (\gamma_1 - 1) \end{vmatrix}}{\begin{vmatrix} \gamma_1 - 1 & 0 & \gamma_1 & 0 \\ 0 & -\gamma_1 & 0 & (\gamma_1 - 1) \end{vmatrix}} \cdot = \frac{|\Delta_S|}{|\Delta_R|}$$

In the above $|\Delta_R|$ is the Rayleigh determinant and $|\Delta_S|$ is the same except for the first row. The fast methods developed for calculation of $|\Delta_R|$ can be used to evaluate $|\Delta_S|$. It follows then that the plane wave reflection coefficient can be written as

$$R = (\rho_1\, r_{\alpha 0}\, |\Delta_R| - \rho_0\, |\Delta_S|)/(\rho_1\, r_{\alpha 0}\, |\Delta_R| + \rho_0\, |\Delta_S|) \quad .$$

ACOUSTIC SCATTERING FROM ROUGH SURFACES

B. G. Hurdle, K. D. Flowers & J. A. DeSanto

Naval Research Laboratory
Washington, D.C. 20375

ABSTRACT

A review of scattering from the ocean bottom and ocean ice cover is given. Areas of deficiency are cited.

INTRODUCTION

NATO has an interest in acoustic scattering for several reasons. Among these are the support of navigation, communication, target detection, target classification, tracking, and fire control. In each of these operational functions, underwater scattering plays a major role in the degree of success that can be obtained. Antisubmarine warfare units whether they be active or passive are subjected to the environment of the ocean with a limited number of propagation paths over which the sound is transmitted. Scattering occurs when the paths intersect the rough boundaries and when discontinuities or inhomogeneities are encountered in the volume.

In practice all acoustic waves propagating in the ocean are scattered to some degree. There is less effective scattering at low frequencies and for propagation over certain paths. The frequency effect is caused by the relative size of the scatterers with respect to the wavelength of the sound. The path effect is

caused by the type, amount, and quantity of scatterers encountered.

Some deep water paths of interest to NATO are: RAP, SOFAR, surface duct, bottom bounce, and convergence zone forming types. In shallow water, wave guide type paths are, in general, the only propagation modes available. All of the paths involve volume scattering which is caused by inhomogeneities in the volume, such as, fish, internal wave fields, and random fluctuations of the physical parameters of the medium. Those paths concerned solely with volume scattering are: SOFAR and possibly convergence zone forming types. Surface duct paths have multiple interactions with the sea surface or ice cover and energy is continuously scattered out of the duct. Generally a sloping bottom and large topographic features are additional complications in this type of problem.

We discuss scattering from surfaces, specifically, from the bottom and ice cover, in more detail in subsequent sections.

SCATTERING FROM SURFACES

When acoustic waves intersect a rough surface, several effects are observed. These effects are a spatial redistribution of the scattered energy, a transmission of energy through the surface, frequency smearing of the signal, and time smearing of the signal. These effects will be discussed below for the specific surface types: sea bottom, and under ice. Since surface topography is common to both rough surfaces, we discuss its effect first.

Since it is impractical to measure precisely the topography of those scattering surfaces met in practice, it is required, in some way, to model these surfaces in order to do scattering problems.

Scattering theories based on these models, to be of use, must be verified by actual measurements or shown to predict known solutions adequately. Here, essentially, is the reason why surface scattering has remained a major unsolved problem; the complete lack of an exact, tractable solution for a realistic surface. Exact must be qualified with tractable since it is not difficult to write formally the exact solution [1-3] to the surface scattering problem. The real difficulty arises in its evaluation.

Scattering from rough surfaces can be treated either deterministically or statistically. Deterministic surfaces can be further divided into separable and nonseparable surfaces, where the category separable means that the surface fits into a natural coordinate scheme for which the solution of the Helmholtz equation is separable.[4] Examples of the separable type include the half plane, [2-5] rectangularly corrugated surfaces, [6-19] and sawtooth corrugations.[20-26] A classic example of the nonseparable type of surface is the sinusoidal surface. [27-43] In addition to surfaces which are geometrically rough, some authors [44-45] deal with a flat surface having a periodic impedance modulation.

The solution for the scattered velocity potential (or pressure) is often found by writing certain assumed forms of the fields with unknown (complex) amplitude coefficients in the various geometric regions of the problem. Continuity of pressure and velocity across the common boundaries yield linear equations relating the amplitude coefficients. These linear equations are usually solved by matrix

inversion [11,12,34,35,39] although in certain cases matrix inversion can be avoided. This is true if it is possible to relate the sets of linear equations to the residue series of integrals of certain meromorphic functions.[8,13-19] In this case, the amplitude coefficients are given in terms of the function. Other methods of solving linear equations are also employed. For example, continued fractions are used on the linear equations for a periodic impedance modulated surface.[45] If the surface is periodic, then it can be shown that the energy is scattered in discrete directions (grating effect) and the problem can be collapsed to a consideration of only a single period of the surface.[35]

Note, however, that the series expansions assumed must converge to the boundary conditions imposed on the surface. That all assumed expansions do not converge is well illustrated by the so-called Rayleigh hypothesis, i.e., that the field in the wells of a sinusoidal surface could be represented as a sum of upgoing plane waves combined with the single downgoing incident plane wave.[27,34-36] The Rayleigh hypothesis, for example, has been shown to be either true or false depending on whether $kb \leq 0.448$ or $kb > 0.448$ where the surface is given as $y = b \cos(kx)$.[46-48] The number 0.448 arises as the solution of a transcendental equation, which solution yields the singularities of the field expansion.

Solutions can be found using the Helmholtz integral formula, which simply yields an integral representation of the solution of the Helmholtz equation in terms of single and double layers

on the surface.[49-53] In addition to the known free space Green's function, both the velocity potential (or the pressure) and its normal derivative are required to be known on the surface. For a rigorous mathematical problem, only one of the two, either velocity potential or its normal derivative, can be specified.[3] An integral equation is then constructed for the surface value of the unspecified other quantity. Its solution is then substituted into the original Helmholtz integral formula to give, along with the assumed boundary value, an integral representation for the velocity potential (or pressure).

A mathematically rigorous variation of the procedure involves choosing a Green's function which itself satisfies a specified boundary condition and then writing Rayleigh-Sommerfeld integral formulas for the velocity potential.[54-56] Now only one surface value is involved, either velocity potential or its normal derivative (depending on which of the Rayleigh-Sommerfeld integral formulas one chooses), producing a mathematically rigorous problem. In this case the additional boundary condition assumption involves the specification of only one boundary value. Although the formulation of the problem is mathematically rigorous, the practical difficulty of specifying a boundary Green's function for arbitrary boundaries remains. The latter problem is as difficult as the original problem of calculating the velocity potential.

Other methods of solution are imaging, as has been applied to symmetrical bosses on a perfectly reflecting plane,[57-61] and generalized harmonic analysis [62-65] which may be applied to any surface.

We now consider approximate types of solutions, some of which have been comparatively reviewed.[66-68] The Helmholtz integral formula is an integral over the scattering surface and requires a knowledge of the field, ψ, and its normal derivative, $\frac{\partial \psi}{\partial n}$ everywhere on the surface. Since these two boundary conditions are not generally known, they are approximated by assuming that the surface is smooth enough to replace the field at a point by the field that would be present on the tangent plane at the point (Kirchhoff or geometrical acoustics approximation).[6,54-56,69-70] That is $\psi = (1 + V)\psi_i$ and $\frac{\partial \psi}{\partial n} = (1-V)\vec{n}\cdot\vec{k}_i\psi_i$, where V = local Fresnel reflection coefficient, ψ_i = incident field, and k_i = incident wave number. The scattered field is now completely specified; however, in general, the integration cannot be performed. Additional assumptions usually made are: V = constant, and the source and observation point removed to the Fraunhofer zone. The approximations made are: the surface is smooth, i.e., does not change appreciably within a wavelength, and the surface is completely illuminated (no shadowing). Surfaces that are shadowed are treated by making further assumptions and are discussed by several authors.[68-73]

The method of series expansion of the fields, where <u>allowable</u>, does not suffer from the restrictions noted in the Helmholtz formulation. <u>Allowable</u> refers to the necessity that the expansion in elementary solutions to the Helmholtz equation must converge to the boundary conditions imposed on the surface.[47,48] The problem encountered here is that infinite sets of equations must be solved for the expansion coefficients. The coefficients can,

for some surfaces, be determined exactly by various methods discussed above. However, these exact solutions are not easily evaluated and parameter dependencies are not obvious. In general, the approximations are: using finite sets of equations and proceeding by matrix inversion, [11,12,35,36,41] and using variational methods which choose coefficients such that the mean square error in the boundary conditions is minimized.[20]

If the roughness of the surface can be treated as small, various perturbation methods become available.[3,34,70] Mathematical techniques involving boundary perturbations and perturbations of the solutions of known canonical problems exist.[3] For example, the latter problem could consist of a surface with two scales of roughness.[14] The larger roughness part of the problem is canonical in the sense that the solution can be written down, whereas the smaller roughness induces small geometrical variations in the surface, and a corresponding variation in the scattered field.

Since the surfaces cannot realistically be measured, it is convenient to model them using statistical methods. This is done by considering random surfaces [6,77-84] or random point sets with given statistical properties.[85-90] Thus, when the statistical properties of the surface are determined, different moments of the scattered field can be calculated. Another approach is to consider smooth surfaces with random impedence [91-92] or smoothed boundary conditions.[93-95]

Although there exist many different statistical models of surface scattering in the literature, we attempt to classify and describe only a few.

A diagrammatic solution for scattering from single valued multivariate Gaussian surface has been derived.[96-98] Evaluation of the diagrams present numerical difficulties and only one first order diagram has been completed.[99]

There is a large amount of work which is based on the Helmholtz integral formula using the Kirchhoff approximation where both source and receiver are moved to the Fraunhofer zone.[6,69-70,78-84,100-102] The surface $z = \zeta(x,y)$ is then treated as a random variable and suitable moments of the field calculated. These models require knowledge of the joint probability distribution of any two surface points.

At least one model[103] addresses non Gaussian surface statistics whereas most others use Gaussian statistics for ease of evaluation.

One model[34] expands $\zeta(x,y)$ in a harmonic series with coefficients related to the surface power spectrum. This model requires the availability of the power spectrum of the surface and is extremely difficult to evaluate.

Two models, randomly spaced half planes,[104,105] and randomly spaced bosses on a plane,[60,61] are based on exact solutions where the spacing of elements has been randomized.

Models based on random facets,[106-108] and random point sets[85-89] have been developed. These incorporate such features as random spacings or slopes, random scattering strengths, and various directivity functions.

Some of these models have been used to describe experimental results with limited success. A basic problem here is the determination of the surface statistics and choice of parameters.

Surfaces with specified statistics have been constructed, one[109] physical and not yet used in an experiment, the other numerical[110] used in a computer experiment. Those models based on nonphysical surfaces[85-89 104,105] are especially difficult since there appears to be no way to relate the surface parameters to the parameters of the solution.

SCATTERING FROM THE SEA BOTTOM

The sea bottom, in general, has discontinuities, thereby limiting the use of the Kirchhoff approximation. In addition, in most places the bottom does not present a large impedance contrast. Thus the impedance of the bottom material and its distribution becomes extremely important in the description of the scattered field. Because of its remoteness, both the topography and impedance characteristics of the bottom are difficult to obtain.

The bottom, in places, is stratified and has been modeled[111-116] as such. In other places, however, the bottom composition is much more complicated and requires a statistical treatment. Existing models and detailed experimental data[117-124] on this aspect of the problem are insufficient. However, two collections, MGS and NAVADO, of data yield average acoustic scattering information for large ocean bottom regions. The scattering data are classified according to bottom characteristics. Frequency smearing of signals scattered from the bottom, due entirely to source-receiver motion, has not been measured. Further, rough surface time smearing and time smearing caused by penetration

into the bottom have not been adequately studied.

Measurement of the bottom relief and composition presents a major unsolved problem. Use of precision fathometers and various other acoustic devices aid in the determination of surface relief and sub-bottom reflectivity along a track, but have limited resolution. At least one paper[125] has dealt with the problem of measuring bottom surface statistics from scattering experiments. There are many papers[111-122, 126-129] presenting experimental data on scattering from the sea bottom for the backscatter and specular directions. Data for other directions are extremely limited.[111,117,130-133]

A recent Russian reference text[134] has nine chapters devoted to scattering and reflection from the ocean bottom and a bibliography through 1969.

SCATTERING FROM AN ICE COVER

The problem of predicting scattering from the under surface of an ice cover is extremely difficult because it is inaccessible, has extremes in roughness, has extensive entrapped air, and the ice cover itself is discontinuous. All of the problems encountered in sea bottom scattering are here. The great majority of our data on under ice scattering is obtained from multiple scattering in the forward direction during propagation experiments.

Wave motion on the ice has been detected and measured.[135-136] In the central Arctic this motion is very small and should have little effect on the acoustic scattering problems. However, in fringe Arctic regions it may be more important. Most of the

experimental scattering data from under ice have been for the backscatter case,[137-144] although at least one paper deals with specular reflection.[145] Recent transmission studies under ice[146-149] indicate that for sufficiently low frequencies the scattering loss becomes insignificant. There is very little knowledge about the acoustical properties of sea ice and even less is known about the surface topography necessary for scatter prediction. The method for measuring the latter using a submarine and obtaining related information is the subject of other papers.[150,151] Currently one of the hopes is that the measurement of characteristics of the upper surface by aircraft can be correlated with the roughness of below surface ice for acoustic purposes.

CONCLUDING REMARKS

Most theoretical treatments of scattering consider an incident plane wave or at least a locally plane wave. This choice is made in order to simplify the problem to manageable proportions. By assuming an incident plane wave, an approximation to the problem has been made. The fact that we are considering a linear problem and any incident wave may be represented by a suitable superposition of plane waves is in many instances not much comfort.

The assumption of an incident plane wave is a good approximation where the size of a scatterer is small compared to the acoustic wavelength. In the case of a surface, the projection of the effective insonified region normal to the incident direction should deviate from a wave front by a small amount compared to a wavelength.

More difficult theoretically is the addition of source and receiver directivities. Since directivity is a <u>far field</u> term

as derived in the free field it is more proper to refer to the difficulty as the finite size of sources and receivers in a non-free-field environment.

Scattering from realistic surfaces is approached by breaking down the allowable surfaces into three categories. The first category comprises those surfaces that have little roughness compared to an acoustic wavelength, second, those that have roughness comparable to a wavelength, and third, those that are very rough compared to an acoustic wavelength. The first and third of these have been worked on by numerous authors, while the second has been considered by only a few. Limited solutions exist for the smooth case, but no tractable results are available for the intermediate case, which is the case most often met in practice; the very rough case is approximated by the geometrical acoustics solution.

These are all surface relief type problems, if in addition the surface is penetrable, then several other complications enter the problem. Only relatively simple approximations have been made toward the solution of acoustic scattering from surfaces bounding inhomogeneous material.

Statistical scattering theories that have been developed do not predict the experimental results to a reasonable or required degree of accuracy. By parameter changes they can be brought into relatively close agreement, but, in general, the parameters cannot be associated with characteristics of the scatterers.

Adequate testing of the various approximations made in scattering theory has to be done. This will require experimentation under extremely well controlled and measured conditions.

It is proposed that the proper approach to solving problems of acoustic scattering from rough surfaces is one in which an appropriate field expansion is evaluated in conjunction with a controlled experiment. The authors feel that the ingredients for the solution lie in the theoretical diagrammatic expansions[97] and specified surface constructions.[109]

In 1968 the Russians assessed the understanding of and progress on scattering problems in the ocean as one of their major goals at the USSR Academy of Sciences and Sixth All Union Acoustic Conference.[152] As indicated by the magnitude of recent activities, the Russians are continuing to place a strong emphasis on ocean scattering problems.

REFERENCES

1. P. M. Morse and K. U. Ingard, Theoretical Acoustics (McGraw-Hill Book Co., New York, 1968).
2. B. B. Baker and E. T. Copson, The Mathematical Theory of Huygen's Principle (Clarendon Press, Oxford, 1953).
3. P. M. Morse and H. Feshback, Methods of Mathematical Physics (McGraw-Hill Book Co., New York, 1953), Pt. II., Pgs. 528-539.
4. P. Moon and D. E. Spencer, Field Theory Handbook (Springer-Verlag, Berlin, 1961).
5. I. Stakgold, Boundary Value Problems of Mathematical Physics (Macmillan Co., New York, 1967) Vols. I and II.
6. P. Beckmann and A. Spizzichino, The Scattering of Electromagnetic Waves from Rough Surfaces (Macmillan Co., New York, 1963).
7. J. F. Carlson and A. E. Heins, "The Reflection of an Electromagnetic Plane Wave by an Infinite Set of Plates, I and II," Quart. Appl. Math. 4, 313 (1947) and 5, 82 (1947).
8. F. Berz, "Reflection and Refraction of Microwaves at a Set of Parallel Metallic Plates," Proc. IEE (London), 98, 47 (1951), Pt. III.
9. E. A. N. Whitehead, "The Theory of Parallel-Plate Media for Microwave Lenses," Proc. IEE (London) 98, 133 (1951), Pt. III.
10. R. A. Hurd, "The Propagation of an Electromagnetic Wave Along an Infinite Corrugated Surface," Can. J.Phys. 32, 727 (1954).
11. L. N. Deryugin, "The Reflection of a Laterally Polarized Plane Wave from a Surface of Rectangular Corrugations," Radio Engineering 15, 2, 15-26 (1960).

12. L. N. Deryugin, "The Reflection of a Longitudinally Polarized Plane Wave from a Surface of Rectangular Corrugations," Radio Engineering 15, 5, 9-16 (1960).

13. J. A. DeSanto, "Scattering from a Periodic Corrugated Structure: Thin Comb with Soft Boundaries," J. Math. Phys. 12, 9 (Sept. 1971).

14. J. A. DeSanto, "Scattering from a Periodic Corrugated Structure: Thin Comb with Hard Boundaries," J. Math. Phys. 13, 3 (Mar. 1972).

15. J. A. DeSanto, "Scattering from a Periodic Corrugated Surface: Semi-Infinite Inhomogeneously Filled Plates with Soft Boundaries," NRL Rept. No. 7320, (November 1971).

16. J. A. DeSanto, "Scattering from a Periodic Corrugated Surface: Semi-Infinite Inhomogeneously Filled Plates with Hard Boundaries," NRL Rept. 7321, (November 1971).

17. J. A. DeSanto, "Scattering from a Periodic Corrugated Surface: Finite-Depth Inhomogeneously Filled Plates with Soft Boundaries," NRL Report 7375, (May 1972)

18. J. A. DeSanto, "Scattering from a Periodic Corrugated Surface: Finite-Depth Inhomogeneously Filled Plates with Hard Boundaries," NRL Rept. 7377, (May 1972).

19. R. Mittra and S. W. Lee, Analytical Techniques in the Theory of Guided Waves (Macmillan Co., New York, 1971).

20. W. C. Meecham and C. W. Peters, "Reflection of Plane-Polarized Electromagnetic Radiation from an Echelette Diffraction Grating," J. Appl. Phys. 28, 216 (1957).

21. Z. Szekeley, "The Scattered Field from a Sawtooth Corrugated Surface," Symposium on Microwave Optics - Part II, edited by B. S. Karasik (McGill University, Montreal, Canada, 1953), p. 329.

22. A. N. Leporski, "Scattering of Sound Waves by Sinusoidal and Saw-Tooth Surfaces," Soviet Phys. - Acoustics 2, 177 (1956).

23. T. Itoh and R. Mittra, "An Analytical Study of the Echelette Grating with Application to Open Resonators," IEEE Trans. MTT-17, 319 (1969).

24. A. D. Lapin, "The Scattering of a Plane Wave at a Serrated Surface," Soviet Phys. - Acoustics 9, 37 (1963).

25. R. D. Hatcher and J. H. Rohrbaugh, "Theory of the Echelette Grating - Part I," J. Opt. Soc. Am. 46, 104 (1956) and - Part II, J. Opt. Soc. Am. 48, 704 (1958).

26. R. D. Hatcher, J. H. Rohrbaugh, C. Prine, and W. G. Zoellner, "Theory of the Echelette Grating - Part III," J. Opt. Soc. Am. 48, 410 (1958).

27. Lord Rayleigh (J. W. Strutt) Theory of Sound (Dover, New York 1945).

28. B. A. Lippmann, "Note on the Theory of Gratings," J. Opt. Soc. Am. 43, 5, 408 (1953) (L).

29. H. S. Heaps, "Non-Specular Reflection of Sound from a Sinusoidal Surface," J. Acoust. Soc. Am. 27, 4, 698-705 (1955).

30. W. C. Meecham, "Variational Method for the Calculation of the Distribution Energy Reflected from a Periodic Surface," J. Appl. Phys. 27, 4, 361-367 (1956).

31. W. C. Meecham, "Fourier Transform Method for the Treatment of the Problem of the Reflection of Radiation from Irregular Surfaces," J. Acoust. Soc. Am. 28, 3, 370-377 (1956).

32. L. M. Brekhovskikh, "Diffraction of Waves by a Rough Surface, Parts I and II," (in Russian), Zh. Eksper. i Theor. Fiz. 23, 275-304 (1952).

33. T. O. LaCasce and P. Tamarkin, "Underwater Sound Reflection from a Corrugated Surface," J. Appl. Phys. 27, 2, 138-148 (1956).

34. S. O. Rice, "Reflection of Electromagnetic Waves from Slightly Rough Surfaces," Comm. Pure Appl. Math. 4, 351-378 (1951).

35. J. L. Uretsky, "Reflection of a Plane Sound Wave from a Sinusoidal Surface," J. Acoust. Soc. Am. 35, 8, 1293-1294 (1963)(L).

36. J. L. Uretsky, "Scattering of Plane Waves from Periodic Surfaces," Ann. Phys. (N.Y.) 33, 400-427(1965).

37. S. R. Murphy and G. E. Lord, "Scattering from a Sinusoidal Surface-A Direct Comparison of the Results of Marsh and Uretsky," J. Acoust. Soc. Am. 36, 8, 1598-1599 (1964)(L).

38. G. R. Barnard, C. W. Horton, M. K. Miller, and F. R. Spitznogle, "Underwater-Sound Reflection from a Pressure-Release Sinusoidal Surface," J. Acoust. Soc. Am. 39, 1162 (1966).

39. H. W. Marsh, "In Defense of Rayleigh's Scattering from Corrugated Surfaces," J. Acoust. Soc. Am. 35, 11, 1835-1836 (1963)(L).

40. K. A. Zaki and A. R. Neureuther, "Scattering from a Perfectly Conducting Surface with a Sinusoidal Height Profile: TE Polarization, " IEEE Trans. AP-19, 208 (1971).

41. T. B. A. Senior, "The Scattering of Electromagnetic Waves by a Corrugated Sheet," Can. J. Phys. 37, 787 (1959).

42. T. B. A. Senior and T. C. Tong, "Scattering by a Periodic Surface," Univ. of Mich. Radiation Lab Rept. No. 7 (Sept. 1970).

43. J. G. Parker, "Reflection of Plane Sound Waves from a Sinusoidal Surface," J. Acoust. Soc. Am. 29, 3, 377-380 (1957).

44. Y. P. Lysanov, "On the Scattering of Sound by a Nonuniform Surface," Soviet Physics-Acoustic 3, 45 (1958).

45. A. Hessel and A. A. Oliner, "A New Theory of Wood's Anomalies on Optical Gratings," Appl. Opt. 4, 1275(1965).

46. J. A. DeSanto, It is possible to show that the full amplitude of the plane waves scattered from a sinusoidal surface can be naturally written as the Rayleigh amplitude plus a sum of other terms.

47. R. F. Millar, "On the Rayleigh Assumption in Scattering by a Periodic Surface. I and II," Proc. Cam. Phil. Soc. 65, 773 (1969) and 69, 217 (1971).

48. R. L. Holford, "Scattering of Sound Waves at a Periodic Pressure-Release Surface: An Exact Solution," Bell Telephone Laboratories Report under Contract No. N00014-69-C-0074 (5 Mar. 1971).

49. B. Noble, "Integral Equation Perturbation Methods in Low Frequency Diffraction," in Electromagnetic Waves, edited by R. Langer (University of Wisconsin Press, Madison, Wisc., 1962).

50. G. Chertock, "Sound Radiation from Vibrating Surfaces," J. Acoust. Soc. Am. 36, 1305 (1964).

51. L. G. Copley, "Integral Formulation in Acoustic Radiation," J. Acoust. Soc. Am. 44, 28 (1968).

52. L. G. Copley and H. A. Schenck, "Vanishing of the Surface Pressure Contribution to the Helmholtz Integral," J. Acoust. Soc. Am. 44, 228 (1968).

53. H. A. Schenck, "An Improved Integral Formulation for Acoustic Radiation Problems," J. Acoust. Soc. Am. 44, 41 (1968).

54. E. Wolf and E. W. Marchand, "Comparison of the Kirchhoff and the Rayleigh-Sommerfeld Theories of Diffraction at an Aperture," J. Opt. Soc. Am. 54, 587 (1964).

55. N. Mukunda, "Consistency of Rayleigh's Diffraction Formulas with Kirchhoff's Boundary Conditions," J. Opt. Soc. Am. 52, 336 (1962).

56. J. W. Goodman, Introduction to Fourier Optics (McGraw-Hill, New York, 1968).

57. V. Twersky, "On the Non-Specular Reflection of Plane Waves of Sound," A. Acoust. Soc. Am. 22, 539-546 (1950).

58. V. Twersky, "On the Non-Specular Reflection of Sound from Planes with Absorbent Bosses," J. Acoust. Soc. Am. 23, 336-338 (1951a).

59. V. Twersky, "Reflection Coefficients for Certain Rough Surfaces," J. Appl. Phys. 24, 569-660 (1953).

60. V. Twersky, "On the Scattering and Reflection of Electromagnetic Waves by Rough Surfaces," Trans. I.R.E. AP-5, 81-90 (1957a).

61. V. Twersky, "On Scattering and Reflection of Sound by Rough Surfaces," J. Acoust. Soc. Am. 29, 209-225 (1957b).

62. H. W. Marsh, "Exact Solution of Wave Scattering by Irregular Surfaces," J. Acoust. Soc. Am. 33, 330-333 (1961).

63. H. W. Marsh, M. Schulkin, and S. G. Kneale, "Scattering of Underwater Sound by the Sea Surface," J. Acoust. Soc. Am. 33, 3, 334-340 (1961).

64. H. W. Marsh, "Non-Specular Scattering of Underwater Sound by the Sea-Surface," in Underwater Acoustics, edited by V. M. Albers (Plenum Press, New York, 1962), Lecture 11, pp. 193-197.

65. H. W. Marsh, "Sound Reflection and Scattering from the Sea Surface," J. Acoust. Soc. Am. 35, 2, 240-244 (1963).

66. L. Fortuin, "Reflection and Scattering at the Sea Surface," J. Acoust. Soc. Am. 47, 1209-1228 (1970).

67. A. B. Shmelev, "Wave Scattering by Statistically Uneven Surfaces," Sov. Phys. Upsek 15, 173 (1972).

68. H. Trinkaus, "Fundamental Approximations for the Scattering of Acoustic Waves from a Rough Surface," Saclantcen Memorandum SM-15 (1 Aug. 1973)

69. C. Eckart, "Scattering of Sound from the Sea Surface," J. Acoust. Soc. Am. 25, 566-570 (1953).

70. W. C. Meecham, "On the Use of the Kirchhoff Approximation for the Solution of Reflection Problems," J. Rat. Mech Anal. 5, 323 (1956).

71. P. Beckmann, "Shadowing of Random Rough Surfaces," Trans. IEEE Antennas Propagation 13, 384-388 (1965).

72. R. J. Wagner, "Shadowing of Randomly Rough Surfaces," J. Acoust. Soc. Am. 41, 138-147 (1967).

73. P. J. Lynch and R. J. Wagner, "Rough-Surface Scattering: Shadowing, Multiple Scatter, and Energy Conservation," J. Math. Phys. 11, 3032 (1970).

74. B. G. Smith, "Geometrical Shadowing of a Random Rough Surface," Trans. IEEE Antennas Propagation 15, 668-671 (1967).

75. K. E. Hawker and P. J. Welton, "Shadowing of Randomly Rough Surfaces," J. Acoust. Soc. Am. 45(A), 295 (1969).

76. R. R. Gardner, "Acoustic Backscattering from a Rough Surface at Extremely Low Grazing Angles," Ph.D. Dissertation, University of California, San Diego (1970).

77. B. F. Kur'yanov, "The Scattering of Sound at a Rough Surface with Two Types of Irregularity," Soviet Physics - Acoustics 8, 3, 252-257 (1963).

78. M. A. Isakovich, "The Scattering of Waves from a Statistically Rough Surface," (in Russian), Zhurn. Eksp. Theor. Fiz. 23, 305-314 (1952).

79. W. S. Ament, "Toward a Theory of Reflection by a Rough Surface," Proc. I.R.E. 41, 142-146 (1953).

80. C. W. Horton and T. G. Muir, "Theoretical Studies on the Scattering of Acoustical Waves from a Rough Surface," J. Acoust. Soc. Am. 41, 627-634 (1967).

81. H. Davies, "The Reflection of Electromagnetic Waves from a Rough Surface," Proc. I.E.E., Pt. III, 101, 209-214 (1954). Discussion on above paper, Proc. I.E.E., Pt. III, 102.

82. J. Feinstein, "Some Stochastic Problems in Wave Propagation," Part I. Trans. I.R.E. AP-2, 23-30 (1954).

83. J. G. Parker, "Reflection of Plane Sound Waves from an Irregular Surface," J. Acoust. Soc. Am. 28, 4, 672-680 (1956).

84. Yu P. Lysanov, "Theory of the Scattering of Waves at Periodically Uneven Surfaces," Soviet Physics - Acoustics 4, 1, 1-10 (1958).

85. L. M. Spetner and I. Katz, "Two Statistical Models for Radar Terrain Return," Trans. I.R.E. AP-8, 242-246 (1960).

86. M. A. Spizzichino, "La Reflexion des ondes electromagnetiques par une surface irreguliere," Research Rept. No. 549 T, Centre National d'Etudes des Telecommunications, 4.11.1959 (1959).

87. F. Du Castel and A. Spizzichino, "Reflection en milieu Inhomogene," (Reflexions partielles dans l'atmosphere et propagation a grande distance, 3 eme partie). Ann Tele-comm. 14, 33-40 (1959).

88. D. Middleton, "A Statistical Theory of Reverberation and Similar First-Order Scattered Fields - Part I: Waveforms of the General Process," IEEE Trans. IT-13, 3, 372-392 (1967).

89. D. Middleton, "A Statistical Theory of Reverberation and Similar First-Order Scattered Fields - Part II: Moments, Spectra, and Special Distributions," IEEE Trans. IT-13, 3, 393-414 (1967).

90. S. M. Karp, R. M. Gagliardi, I. S. Reed, "Radiation Models Using Discrete Radiator Ensembles," Proc. IEEE 56, 1704 (1968).

91. K. Sobczyk, "Reflection of Scalar Wave from a Plane with Random Impedance", Acta Physica Polonica A44, 581 (1973).

92. W. A. Kuperman, "Sound Propagation in Shallow Water, II", Saclantcen Conf. Proc. 14, Edited by O. F. Hastrup, O. V. Olesen 15 Nov. 1974.

93. M. S. Howe, "Contributions to the Theory of Scattering by Randomly Irregular Surfaces," Proc. R. Soc. London A337, 413(1974).

94. A. R. Wenzel, "Smoothed boundary conditions for Randomly Rough Surfaces," J. Math. Phys. 15, 317 (1974).

95. V. D. Freilikher, I. M. Fuks, "Attenuation of the Mean Field in a Waveguide at the Critical Frequency," Radiophysics and Quantum Electronics 13, 96-99 (1970).

96. G. G. Zipfel, "Scattering of Scalar Waves From a Random Irregular Interface," J. Math. Phys. 15, 101 (1974).

97. G. G. Zipfel, J. A. DeSanto, "Scattering of a Scalar Wave from a Random Rough Surface: A Diagrammatic Approach," J. Math. Phys. 13, 1903 (1972).

98. J. A. DeSanto, "Scattering from a Random Rough Surface: Diagram Methods for Elastic Media", J. Math. Phys. 14, 1566 (1973).

99. J. A. DeSanto, O. Shisha, "Numerical Solution of a Singular Integral Equation in Random Rough Surface Scattering Theory", J. Comp. Phys. 15, 286 (1974).

100. M. L. Boyd, R. L. Deavenport, "Forward and Specular Scattering From a Rough Surface: Theory and Experiment", JASA 53, 791 (1973).

101. C. S. Clay, H. Medwin, W. M. Wright, "Specularly Scattered Sound and the Probability density function of a rough surface", JASA 53, 1678 (1973).

102. H. Medwin, J. D. Hagy, "Helmholtz-Kirchhoff Theory for Sound Transmission through a Statistically Rough Plane Interface Between Dissimilar Fluids," JASA 51, 1083 (1971).

103. P. Beckmann, "Scattering by Non-Gaussian Surfaces," IEEE Trans. AP-21, 169 (1973).

104. W. S. Ament, "Forward and Back-Scattering by Certain Rough Surfaces", Trans. I.R.E. AP-4, 369-373 (1956).

105. W. S. Ament, "Reciprocity and Scattering by Certain Rough Surfaces," Trans. I.R.E. AP-8, 167-174 (1960).

106. L. S. Ornstein and A. Van Der Berg, "Reflectivity of Corrugated Surfaces," Physica 4, 1181 (1937).

107. P. Beckmann, "A New Approach to the Problem of Reflection from a Rough Surface," Acta Techn. CSAV 2, 311-355 (1957).

108. R. B. Patterson, "Model of a Rough Boundary as a Backscatter of Wave Radiation", J. Acoust. Soc. Am. 36, 1150-1153 (1964).

109. L. S. Schuetz and G. G. Zipfel, "Theory and Construction of Multivariate Gaussian Surfaces," J. Acoust. Soc. Am., Vol. 56, No. 1, 99-109 (1974).

110. J. C. Novarini and J. W. Caruthers, "Numerical Modeling of Randomly Rough Surfaces with Application to Sea Surfaces," Texas A&M University, Dept. of Oceanography, Ref. No. 71-13-T (1971).

111. G. R. Barnard, J. L. Bardin, and W. B. Hempkins, "Underwater Sound Reflection from Layered Media," J. Acoust. Soc. Am. 36, 2119 (1964).

112. H. P. Bucker, J. A. Whitney, G. S. Yee, and R. R. Gardner, "Reflection of Low-Frequency Sonar Signals from a Smooth Ocean Bottom," J. Acoust. Soc. Am. 37, 1037 (1965).

113. B. F. Cole, "Marine Sediment Attenuation and Ocean-Bottom Reflected Sound," J. Acoust. Soc. Am. 38, 291 (1965).

114. A. H. Nuttall and B. F. Cron, "Signal-Waveform Distortion Caused by Reflection off Lossy-Layered Bottoms," J. Acoust. Soc. Am. 40, 1094 (1966).

115. R. S. Winokur and J. Bohn, "Sound Reflection from a Low Velocity Bottom," J. Acoust. Soc. Am. 44, 1130 (1968).

116. H. C. Morris, "Bottom-Reflection-Loss Model with a Velocity Gradient," J. Acoust. Soc. Am. 48, 1198 (1970).

117. A. W. Nolle, et al., "Acoustic Properties of Water-Filled Sands," J. Acoust. Soc. Am. 35, 1394-1408 (1963).

118. J. L. Jones, C. B. Leslie, and L. E. Barton, "Acoustic Characteristics of Underwater Bottoms," J. Acoust. Soc. Am. 36, 154 (1964).

119. C. M. McKinney and C. D. Anderson, "Measurements of Back-scattering of Sound from the Ocean Bottom," J. Acoust. Soc. Am. 36, 158 (1964).

120. H. M. Merklinger, "Bottom Reverberation Measured with Explosive Charges Fired Deep in the Ocean," J. Acoust. Soc. Am. 44 508 (1968).

121. R. B. Patterson, "Relationships between Acoustic Backscatter and Geological Characteristics of the Deep Ocean Floor," J. Acoust. Soc. Am. 46, 756 (1969).

122. D. R. Horn, B. M. Horn, M. N. Delach, and M. Ewing, "Prediction of Sonic Properties of Deep Sea Cores from the Hatteras Abyssal Plane and Environs," Lamont-Doherty Technical Report No. 1 (NAVSHIPS Contract N00024-69-1184 of Nov. 1969).

123. Yu. Yu. Zhitkovskii, "Relationship between the Reflection and Scattering of Sound by the Ocean Bottom," Acoustics Institute, Acad. Sci., Moscow, Vol. 18, No. 4 533-6 (1972).

124. V. I. Volovov, "Fluctuation Frequency of the Envelopes of Sound Signals Reflected from the Ocean Bottom," Acoustics Institute, Acad. Sci., Moscow, Vol. 17, No. 3 466-7 (1971).

125. E. Y. T. Kuo, "Wave Scattering and Transmission at Irregular Surfaces," J. Acoust. Soc. Am. 36, 2135-2142 (1964).

126. F. R. Menotti, S. R. Santaniello, and W. R. Schumacher, "Studies of Observed and Predicted Values of Bottom Reflectivity as a Function of Incident Angle," J. Acoust. Soc. Am. 38, 707 (1965).

127. J. P. Buckley and R. J. Urick, "Backscattering from the Deep Sea Bed at Small Grazing Angles," J. Acoust. Soc. Am. 44 (L), 648 (1968).

128. K. D. Flowers and B. G. Hurdle, "Monostatic Scattering from the Ocean Bottom," J. Acoust. Soc. Am. Vol. 51, No. 3, 1109-1111 (1972).

129. C. S. Clay, "Scattering and Reflection of Acoustic Waves at the Bottom and Surface of the Ocean," University of Wisconsin, Final Report, No. 74-1 (1974).

130. R. J. Urich, "The Backscattering of Sound from a Harbor Bottom," J. Acoust. Soc. Am. 26, 231 (1954).

131. B. G. Hurdle, K. D. Flowers, and K. P. Thompson, "Bistatic Acoustic Scattering from the Ocean Bottom," NRL Rept. No. 7285 (1971).

132. B. G. Hurdle, K. D. Flowers, and K. P. Thompson, "Three-Dimensional Scattered Fields from the Ocean Bottom," NRL Rept. No. 7325 (1971).

133. P. B. Schmidt, "Monostatic and Bistatic Backscattering Measurements from the Deep Ocean Bottom," J. Acoust. Soc. Am. Vol 50, No. 1, 326-31 (1971).

134. L. M. Brekhovskikh, "Acoustics of the Ocean," U.S. Joint Publications Research Service, No. 64008-1, (1975).

135. K. Hunkins, "Seismic Studies of Sea Ice," J. Geophys. Res. 65, 3459 (1960).

136. K. Hunkins, "Waves on the Arctic Ocean," J. Geophys. Res. 67, 2477 (1962).

137. R. H. Mellen, "Underwater Acoustic Scattering from Arctic Ice," J. Acoust. Soc. Am. 40 (L) 1200 (1966).

138. R. P. Chapman, "Backscattering Strengths of Sea Ice," J. Acoust. Soc. Am. 39 (L), 1191 (1966).

139. J. R. Brown and D. W. Brown, "Reverberation under Arctic Sea-Ice," J. Acoust. Soc. Am. 40, 399 (1966).

140. J. R. Brown, "Reverberation Under Arctic Ice," J. Acoust. Soc. Am. 36 (L) 601 (1964).

141. A. R. Milne, "Underwater Backscattering Strengths of Arctic Pack Ice," J. Acoust. Soc. Am. 36, 1551 (1964).

142. R. P. Chapman and H. D. Scott, "Backscattering Strength of Young Sea Ice," J. Acoust. Soc. Am. 36 (L), 2417 (1964).

143. R. H. Mellen and H. W. Marsh, "Underwater Sound Reverberation in the Arctic Ocean," J. Acoust. Soc. Am. 35, 1645 (1963).

144. W. B. Birch, "Under-Ice Reverberation Modeling by Means of Multiple Regression," Program of the 84th Meeting of the Acoustical Society of America (1972).

145. M. P. Langleben, "Reflection of Sound at the Water-Sea Ice Interface," J. Geophys. Res. 75, 5243 (1970).

146. D. I. Diachok, "Effects of Sea-Ice Ridge Characteristics on Under Ice Reflection Loss in Arctic and Sub-arctic Waters," Proceedings of the Satellite Symposium on Underwater Acoustics (1974).

147. Diachok, D. I. and Kozo, T. L., "Measured Effects of Ice Roughness on Under-Ice Transmission Loss," Program of the 84th Meeting of the Acoustical Society of America (1972).

148. T. J. Tulko and Lindsay, R. B., "Comparison of Under-Ice and Open Water Transmission Loss Measurements in Baffin Bay," Program of the 84th Meeting of the Acoustical Society of America (1972).

149. S. K. Numrich, "Low-Frequency Sound Propagated in the Marginal Ice Zone of the Greenland Sea," JASA, Vol. 56, 550 (1974).

150. R. E. Francois, "The Unmanned Arctic Research Submersible System," Technol. Soc. U. Vol. 7, No. 1 46-8 (1973).

151. W. Lyon, "Ocean and Sea Ice Research in the Arctic Ocean via Submarine," Trans. N.Y. Acad. Sci. 23, 662-674 (1961).

152. L. M. Brekhovskikh, "Some Problems of Oceanic Acoustics," Atmos. Oceanic Phys. 4, 12, 1291-1304 (1968).

DISCUSSION

DISCUSSION ON SESSION 4

Reported by R.I. Tait

DIACHOK

Has the model described by SANTANIELLO been related to actual data?

SANTANIELLO

No

McCOY

There is a problem in relating the sound speed to the porosity of the bottom. The presence of voids would invalidate any model, and texts on cores are unsatisfactory as the results depend on how the lab experiment was carried out.

HAMILTON

This is really a two-part problem. Empirical relationships between sound speed and some easily defined property such as porosity are needed, and if care is taken in collecting samples with a minimum of disturbance the variance can be reduced and good results achieved.

McCOY

A sample from the bottom will yield a particular grain size while another (adjacent) area will give a different result. How does one cope with this?

HAMILTON

This is not really a problem: several samples can be taken and the spread is not so bad.

HURDLE

We really require in-situ measurements of both sound speed and attenuation from deep sea drilling; this is for the future. HURDLE then drew attention to some recent work on "in situ" attenuation measurements. Some inconclusive discussion followed on the effect of pressure on attenuation in sediments.

R.B. WILLIAMS

With reference to HURDLE's paper: the small number of reflecting surfaces involved implies that there was no gaussian distribution of reflection points. How can this be modelled? The fact that the signals are reflected from highlights only gives a high correlation and changes the picture.

HURDLE

I agree that the models do not allow for this situation. It is difficult to say how it arises - it must be related to topography.

McCOY

How sensitive is acoustic scattering to the statistical parameters of the scattering surface?
In the discussion that followed there was some disagreement. SCHNEIDER described some work with a ray-tracing model that allowed for different surface-distribution functions. The output as a function of sea state gave good agreement with measurements and the use on different scattering functions in the model gave similar results. However, other models were quoted (DeSANTO, TRINKAUS?) in which surface scattering was found to be sensitive to non-gaussian statistics.

DIACHOK

How important is it to take into account the non-linear sound-speed gradient in sediments?

HURDLE

It is well established that the gradients are non-linear and this should be considered if deep propagation is involved.

INITIAL DISTRIBUTION

	Copies
MINISTRIES OF DEFENCE	
MOD Belgium	1
DND Canada	10
CHOD Denmark	8
MOD France	8
MOD Germany	15
MOD Greece	11
MOD Italy	10
MOD Netherlands	12
CHOD Norway	10
MOD Portugal	5
MOD Turkey	5
MOD U.K.	16
SECDEF U.S.	60
NATO AUTHORITIES	
Defence Planning Committee	3
NAMILCOM	2
SACLANT	10
SACLANTREPEUR	1
CINCWESTLANT/COMOCEANLANT	1
COMIBERLANT	1
CINCEASTLANT	1
COMSUBACLANT	1
COMCANLANT	1
COMMAIREASTLANT	1
COMNORLANT	1
SACEUR	2
CINCNORTH	1
CINCSOUTH	1
COMNAVSOUTH	1
COMSTRIKFORSOUTH	1
COMEDCENT	1
COMSUBMED	1
COMMARAIRMED	1
CINCHAN	1

	Copies
SCNR FOR SACLANTCEN	
SCNR Belgium	1
SCNR Canada	1
SCNR Denmark	1
SCNR Germany	1
SCNR Greece	1
SCNR Italy	1
SCNR Netherlands	1
SCNR Norway	1
SCNR Portugal	1
SCNR Turkey	1
SCNR U.K.	1
SCNR U.S.	2
NATIONAL LIAISON OFFICERS	
NLO Denmark	1
NLO Italy	1
NLO U.K.	1
NLO U.S.	1
NLR TO SACLANT	
NLR Belgium	1
NLR Canada	1
NLR Germany	1
NLR Greece	1
NLR Italy	1
NLR Norway	1
NLR Portugal	1
NLR Turkey	1
ESRO/ELDO Doc. Service	1
ATTENDEES	110